AD NUMBER
ADA801176
CLASSIFICATION CHANGES
TO: **unclassified**
FROM: **confidential**
LIMITATION CHANGES
TO: **Approved for public release; distribution is unlimited.**
FROM: **Distribution authorized to DoD only; Administrative/Operational Use; 28 OCT 1948. Other requests shall be referred to National Aeronautics and Space Administration, Washington, DC. Pre-dates formal DoD distribution statements. Treat as DoD only.**
AUTHORITY
NASA TR Server website; NASA TR Server website

COPY NO. 1

CONFIDENTIAL

NATIONAL ADVISORY COMMITTEE FOR AERONAUTICS

NACA CONFERENCE ON TURBOJET-ENGINE THRUST-AUGMENTATION RESEARCH

A COMPILATION OF THE PAPERS PRESENTED BY NACA STAFF MEMBERS

Lewis Flight Propulsion Laboratory
Cleveland, Ohio

October 28, 1948

NACA

CONFIDENTIAL

NACA CONFERENCE

ON TURBOJET-ENGINE THRUST-AUGMENTATION RESEARCH

A COMPILATION OF THE PAPERS PRESENTED

BY NACA STAFF MEMBERS

Lewis Flight Propulsion Laboratory
Cleveland, Ohio

October 28, 1948

CONTENTS

Page

INTRODUCTION v

LIST OF CONFEREES vii

TECHNICAL DISCUSSIONS:

ANALYSIS OF EFFECT OF TAIL-PIPE-BURNER DESIGN PARAMETERS ON THRUST AUGMENTATION. By EUGENE J. MANGANIELLO 1

EXPERIMENTAL INVESTIGATION OF TAIL-PIPE-BURNER DESIGN VARIABLES. By ALFRED W. YOUNG 13

PERFORMANCE CHARACTERISTICS OF SEVERAL TAIL-PIPE BURNERS. By WILLIAM A. FLEMING and HARRY W. DOWMAN 23

COOLING OF TAIL-PIPE BURNERS. By WILLIAM K. KOFFEL and NEWELL D. SANDERS 34

ANALYSIS OF WATER-INJECTION METHODS OF THRUST AUGMENTATION By E. CLINTON WILCOX 45

EXPERIMENTAL INVESTIGATION OF THRUST AUGMENTATION BY WATER-ALCOHOL INJECTION. By BRUCE T. LUNDIN 56

INVESTIGATION OF BLEEDOFF METHOD OF THRUST AUGMENTATION. By DAVID S. GABRIEL and WILLIAM L. JONES 69

COMPARISON OF VARIOUS METHODS OF THRUST AUGMENTATION. By ELDON W. HALL 77

The authors are members of the staff of the NACA Lewis laboratory at Cleveland, Ohio.

[redacted]

INTRODUCTION

The conference on Turbojet-Engine Thrust-Augmentation Research was organized by the NACA to present in summarized form the results of the latest experimental and analytical investigations conducted at the Lewis Flight Propulsion Laboratory on methods of augmenting the thrust of turbojet engines.

The technical discussions are reproduced herewith in the same form in which they were presented. The original presentations in this record are considered as complementary to, rather than substitutes for, the Committee's system of complete and formal reports.

A list of the conferees is included.

NATIONAL ADVISORY COMMITTEE
FOR AERONAUTICS

[redacted]

[redacted]

LIST OF CONFEREES

The following conferees were registered at the NACA conference on Turbojet-Engine Thrust-Augmentation Research, Lewis Flight Propulsion Laboratory, Cleveland, Ohio, October 28, 1948:

Ahern, Raleigh	AMC, U. S. Air Force
Ahola, Maj. T. A.	AMC, U. S. Air Force
Angell, P. T.	Thompson Products
Appold, Lt. Col. N. C.	Hq., U. S. Air Force
Ashley, Lt. Col. P. H.	Naval Operations, Guided Missiles
Atkinson, A. S.	Bureau of Aeronautics, Dept. of Navy
Auyer, E. L.	General Electric
Baker, John	Solar Aircraft
Barker, J. H.	Westinghouse Electric
Bartlett, P. M.	Bureau of Aeronautics, Dept. of Navy
Beer, Dr. A. C.	Applied Physics Laboratory, Johns Hopkins University
Bennett, M. A.	AMC, U. S. Air Force
Bevans, Dr. Rowland S.	Massachusetts Institute of Technology
Bevins, J. E.	Eclipse-Pioneer Div., Bendix Aviation
Bodemuller, R.	AMC, U. S. Air Force
Boden, Dr. R. H.	University of Michigan
Borden, D. M.	Chrysler
Brown, W. H.	Pratt & Whitney Aircraft Div., United Aircraft
Brown, W. M.	AMC, U. S. Air Force
Bunyan, F. J.	Pierce Aviation
Burhana, Lt. Col. Howard	AMC, U. S. Air Force
Bush, W.	Republic Aviation
Chandler, M. E.	Chandler Evans, Div. Niles-Bement-Pond
Chapman, C. E.	Consolidated Vultee
*Chenoweth, Opie	AMC, U. S. Air Force
Christensen, Maj. J. E.	AMC, U. S. Air Force
Clauser, M. U.	Douglas Aircraft
Cleveland, F. A.	Lockheed Aircraft
Cohn, Benedict	Boeing Aircraft
Cole, R. W.	Wright Aeronautical
Collins, Whitney	Continental Aviation & Engineering

*Member of NACA Subcommittee on Propulsion Systems.

[redacted]

Couter, D. H.	Lear
Coyle, J. B.	AMC, U. S. Air Force
Davis, Lt. Col. W. A.	AMC, U. S. Air Force
Dietz, R. O., Jr.	NACA
Douglas, W. A.	Northrop Aircraft
Dowman, Harry W.	NACA
Engelberger, J. F.	Manning, Maxwell & Moore
Feijer, A. A.	Packard Aircraft Engine Div., Packard Motor Car
Fisher, R. E.	Marquardt Aircraft
Fisher, W. G.	AMC, U. S. Air Force
Fleming, William A.	NACA
Floor, Urban	Woodward Governor
Foster, R. B.	Bell Aircraft
Foy, E. G.	Curtiss-Wright
Frithsen, Capt. H. R.	AMC, U. S. Air Force
Gabriel, David S.	NACA
Gist, W. B.	Westinghouse Electric
Glodeck, Edward	Research & Development Board
Goff, Maj. C.	AMC, U. S. Air Force
Hall, Eldon W.	NACA
Harkelroad, Lt. Comdr. N. E.	Bureau of Aeronautics, Dept. of Navy
Harvey, Lt. Col. J. A.	AMC, U. S. Air Force
Hartman, E. P.	NACA
Hildestad, H. L.	Westinghouse Electric
Holbrook, G. E.	Allison Div., General Motors
Hopkins, Lt. Comdr. L. A.	Naval Air Materiel Center
Hughes, W.	AMC, U. S. Air Force
Jackson, Lt. Col. C. E.	AMC, U. S. Air Force
Johnson, Lt. Col. O. B.	Hq., U. S. Air Force
Jonas, Julius	Northrop Aircraft
Jones, William L.	NACA
Judd, F.	Republic Aviation
Karanik, John	Grumman Aircraft Engineering
Keeffe, Lt. Col. H. M.	AMC, U. S. Air Force
*Keenan, Prof. J. H.	Massachusetts Institute of Technology
Kemper, Carlton	NACA

*Member of NACA Subcommittee on Propulsion Systems.

King, J. Austin	Ranger Aircraft Engines Div., Fairchild Engine & Airplane
Klauber, P. M.	Solar Aircraft
Kloer, A. F.	Pierce Aviation
Koch, L. L.	AMC, U. S. Air Force
Koffel, William K.	NACA
Kuzmitz, F. V.	Bendix Aviation, Bendix Products Div.
Lafaye, W. P.	Bureau of Aeronautics, Dept. of Navy
Laffoon, C. M.	Ryan Aeronautical
Lancaster, O. E.	Dept. of Navy
Laucher, R. G.	McDonnell Aircraft
Luecht, Prof. John W.	University of Michigan
Lundin, Bruce T.	NACA
Manganiello, Eugene J.	NACA
Martins, C. M.	AMC, U. S. Air Force
Masi, F.	Naval Air Materiel Center
McCarthy, J. S.	McDonnell Aircraft
McGrath, D. M.	Eclipse-Pioneer Div., Bendix Aviation
McVeigh, J. R.	Continential Aviation & Engineering
Michaels, C. M.	AMC, U. S. Air Force
Michaels, Lt. Comdr. W. C.	Naval Operations, Guided Missiles
Mock, F. C.	Bendix Aviation, Bendix Products Div.
Montgomery, Maj. E. H.	Hq., U. S. Air Force
Moore, J. W.	G. M. Giannini
Moore, V.	Wright Aeronautical
Morrisson, R.	United Aircraft
Mullaney, Robert	Grumman Aircraft Engineering
Norton, M. T.	Westinghouse Electric
*O'Donnell, W. J.	Republic Aviation
Parkinson, Prof.	Syracuse University
Patton, J. R.	Office Naval Research
Petry, E. C.	Minneapolis-Honeywell
Phelan, A. J.	Northrup Aircraft
*Pinkel, Benjamin	NACA
Pinnes, R. W.	De Laval Steam Turbine
Piry, Marcel	Ranger Aircraft Engines Div., Fairchild Engine & Airplane
Pitt, P. A.	Solar Aircraft
*Pratt, P. W.	Pratt & Whitney Aircraft Div., United Aircraft

*Member of NACA Subcommittee on Propulsion Systems.

Reinhardt, T. F.	Bell Aircraft
Rennels, Maj. F. L.	Hq., U. S. Air Force
Rethman, Maj. V. C.	AMC Liaison Officer, Cleveland
Rifner, Frank	AMC, U. S. Air Force
Rock, E. A.	Boeing Aircraft
Rothrock, A. M.	NACA
*Rubert, Dr. K. F.	NACA
Rumph, L. B.	Curtiss-Wright
Sanders, Newell D.	NACA
Schwartz, I. R.	Bristol
Scott, Maj. O. M.	AMC, U. S. Air Force
Sforzini, R. A.	Packard Aircraft Engine Div., Packard Motor Car
Sharp, Edward R.	NACA
Sheets, Dr. H. E.	Goodyear Aircraft
*Shoemaker, J. M.	Chance Vought Aircraft Div., United Aircraft
Shoenhair, Comdr. J. L.	Office of Naval Research
Silk, Lt. Col. J.	AMC, U. S. Air Force
Silverstein, Abe	NACA
Simmers, Richard	Naval Air Missile Test Center
Sowers, Lt. Col. L. M.	Hq., U. S. Air Force
Stanger, W. E.	General Electric
*Stoeckly, E. E.	General Electric
Stressen-Reuter, J. H.	Holley Carburetor
Tauson, Peter	Frederic Flader
Taylor, J. E.	AMC, U. S. Air Force
Thoren, T. R.	Thompson Products
Todd, Donald	NACA
Towle, H. C.	Republic Aviation
Townsend, S. J. C.	Chance Vought Aircraft Div., United Aircraft
Trussell, J. I.	Glenn L. Martin
Van Pelt, W. R.	AMC, U. S. Air Force
Walsh, Richard	AMC, U. S. Air Force
Way, Stewart	Westinghouse Electric
Weise, C. A.	Douglas Aircraft
Weiss, L. A.	Lear
Wetzler, J. M.	Allison Div., General Motors
Wheeler, W. L.	North American Aviation

*Member of NACA Subcommittee on Propulsion Systems.

White, Ralph S.	Civil Aeronautics Administration
Whitehead, W. J.	Woodward Governor
Wilcox, E. Clinton	NACA
Williams, Prof. G. C.	Massachusetts Institute of Technology
Wolfe, E. A.	AMC, U. S. Air Force
Wright, A. M.	Chandler Evans, Div. Niles-Bement-Pond
Young, Alfred W.	NACA
Yust, V. E.	Shell Oil, Wood River Research Laboratory
*Zucrow, Dr. Maurice J.	Purdue University

*Member of NACA Subcommittee on Propulsion Systems.

ANALYSIS OF EFFECT OF TAIL-PIPE-BURNER DESIGN PARAMETERS ON THRUST AUGMENTATION

By Eugene J. Manganiello

Lewis Flight Propulsion Laboratory

INTRODUCTION

The tail-pipe-burning method of thrust augmentation for turbojet engines consists of introducing and burning fuel between the turbine and the exhaust nozzle of the engine. The increased temperature of the exhaust gases results in increased jet velocity and hence increased thrust. Tail-pipe burning, or afterburning or reheat, as it is sometimes designated, is not only an augmentation device for improving the take-off and high-speed performance of aircraft, but also the complete configuration may be considered as a distinct engine type for flight at supersonic speeds.

A theoretical analysis of tail-pipe burning is reported in reference 1 wherein generalized charts are presented that permit convenient estimation of tail-pipe-burning performance for various design and operating conditions. In this paper, results of the investigation of reference 1 are reviewed and extended with particular attention to the effect of burner design parameters on augmented and normal engine performance. Consideration is also given to the correlation of tail-pipe-burner blow-out limits with flight operating conditions.

METHODS

Schematic diagrams of normal and tail-pipe-burning engine configurations are shown in figure 1. The two engines are the same except, of course, for their tail pipes. In the normal configuration (fig. 1(a)), the turbine-outlet gas is diffused slightly to the exhaust-cone-exit plane and flows to the jet nozzle through a simple tail pipe of a length dictated by the airplane installation.

In the tail-pipe-burner configuration (fig. (1(b)), the turbine-outlet gas is diffused to the burner-inlet plane where fuel is injected. In some designs fuel is injected at various positions in the diffuser. Flame holders are located downstream of the fuel-injection nozzles to furnish the stagnation regions and the turbulence necessary for combustion, and a suitable length of

tail pipe is provided to permit completion of combustion before reaching the exhaust nozzle.

The tail-pipe-burner-inlet velocities must be sufficiently low to avoid excessive pressure losses and to insure satisfactory combustion. Accordingly, the system requires more diffusion and a tail pipe of greater area than the normal engine. The exhaust nozzle must also be larger than that of the normal engine because of the increased gas volume associated with the higher temperature and must be adjustable (either two-position or continuously variable) in order to provide for operation under both normal and augmented conditions.

Calculations were made to investigate the effect on engine performance of the following tail-pipe-burner and engine design parameters:

1. Diffuser efficiency η_d, considered herein as adiabatic efficiency on energy basis between turbine-outlet and burner-inlet stations, $\dfrac{\frac{R\gamma}{\gamma-1} t_t \left[\left(\frac{p_b}{p_t}\right)^{\frac{\gamma-1}{\gamma}} - 1\right]}{\frac{1}{2}(V_t^2 - V_b^2)}$

2. Burner-inlet velocity V_b

3. Burner drag coefficient C_D, defined as total frictional pressure drop across tail-pipe burner divided by burner-inlet dynamic head

4. Burner-outlet gas temperature T_b

5. Exhaust-nozzle velocity coefficient C_V, defined as ratio of actual to theoretical jet velocity and equal to square root of exhaust-nozzle efficiency (on energy basis)

6. Turbine-outlet velocity V_t

7. Turbine-outlet pressure or engine compressor pressure ratio

The additional symbols used herein are:

p static pressure

R gas constant

t static temperature

γ ratio of specific heats

Subscripts:

b burner inlet

t turbine outlet

The effects of these design parameters were calculated for a range of flight Mach numbers at sea level and 35,000 feet altitude.

The engine assumptions used in the calculations are:

Compressor pressure ratio at sea level and flight Mach number of zero (At other flight conditions the pressure ratio was varied to meet the condition of constant rotative speed, that is, constant work input per pound of air; for example, at sea level and a Mach number of 2, the pressure ratio is 2.4.) . . . 4

Compressor polytropic efficiency, $\frac{\gamma-1}{\gamma} \frac{\log\left(\frac{P_2}{P_1}\right)}{\log\left(\frac{T_2}{T_1}\right)}$ 0.80

Turbine polytropic efficiency, $\frac{\gamma}{\gamma-1} \frac{\log\left(\frac{T_t}{T_4}\right)}{\log\left(\frac{P_t}{P_4}\right)}$ 0.85

Turbine-outlet temperature corresponding to turbine-inlet temperature of 1960° R, °R 1650

Combustion efficiency 0.96

Primary combustion-chamber pressure drop divided by combustion-chamber-inlet pressure 0.03

Exhaust-nozzle velocity coefficient (normal engine) 0.975

Engine inlet-diffuser polytropic efficiency,

$$\frac{\gamma-1}{1} \frac{\log\left(\frac{P_1}{P_0}\right)}{\log\left(1 + \frac{\gamma-1}{2} M^2\right)}:$$

Flight Mach number up to 1 (For flight Mach numbers above 1, the diffuser efficiency was reduced 0.1 per unit increase in Mach number; for example, at a Mach number of 2, the efficiency was 0.75.) 0.85

The additional symbols are:

M Mach number

P total pressure

T total temperature

Subscripts:

0 free stream

1 compressor inlet

2 compressor outlet

4 turbine inlet

The foregoing assumptions are, for the most part, fairly conservative and represent an average of the performance of various present-day engines. The inlet-diffuser efficiency values, which are representative of the performance of convergent-divergent-type diffusers, are conservative compared to values currently being obtained experimentally with other types of supersonic diffuser.

The performance of the normal engine for the different flight conditions was calculated by step-by-step methods and the performance of the tail-pipe-burner configuration was calculated from the normal engine performance by the methods of reference 1. Dissociation was taken into account in the calculations of fuel consumption for the tail-pipe-burner configuration, and the combustion efficiency was assumed to be 0.96 as for the primary engine combustion chamber. The normal engine was assumed to have no tail-pipe pressure losses; that is, the exhaust-nozzle-inlet total pressure was taken equal to the turbine-outlet total pressure. Inasmuch as the calculations were made for constant turbine-outlet temperature it is implicitly assumed that the exhaust-nozzle area is adjusted to the proper value at all operating conditions.

The data and calculations involved in the correlation of tail-pipe-burner blow-out limits are based upon the results of experimental investigations with a current turbojet engine and tail-pipe burner.

RESULTS AND DISCUSSION

The effects of design parameters on augmented and normal engine performance are presented in figures 2 to 9 and the information pertaining to blow-out limits is given in figures 10 and 11.

Augmented and Normal Engine Performance

Gas temperature and inlet velocity. - The ratio of augmented to normal thrust is plotted in figure 2 against tail-pipe-exit gas temperature for a range of burner-inlet velocities from 200 to 750 feet per second. The results in figure 2(a) are for sea-level altitude, flight Mach number of zero, turbine-outlet velocity of 750 feet per second, diffuser efficiency of 80 percent, burner drag coefficient of 1, and exhaust-nozzle velocity coefficient of 0.975, which is the same as that assumed for the normal engine. The normal thrust used as the basis of augmented ratio is that calculated for the engine with a normal or conventional tail pipe.

The augmented thrust ratio increases with increase in tail-pipe gas temperature as a result of the accompanying increase in jet velocity and decreases with increase in burner-inlet velocity because of increased friction and momentum pressure drop across the burner. At a gas temperature of 3600° R and a burner-inlet velocity of 400 feet per second, the augmented thrust is 1.45 times the normal thrust. At the same temperature but at an inlet velocity of 700 feet per second, the augmented thrust ratio is reduced to 1.2. At high burner-inlet velocities (700 and 750 ft/sec), the maximum augmentation is limited to the end points of the curves because of thermal choking, which limits the maximum temperature that can be realized without affecting the engine operating conditions.

The effect of the tail-pipe burner on engine performance for the condition of no afterburning is shown by the results at tail-pipe gas temperature equal to turbine-outlet temperature, that is, 1650° R. At a burner-inlet velocity of 400 feet per second, the augmented thrust is about 97 percent of the normal engine thrust, and at an inlet velocity of 700 feet per second, the thrust is reduced to 93 percent of the normal engine thrust. These losses are a result of the diffuser inefficiency and the friction drag of the burner and correspond to total-pressure-loss ratios $\frac{\Delta P}{P_b}$ of 0.04 and 0.085 at 400 and 700 feet per second, respectively. These losses in normal thrust and those indicated in subsequent curves are higher than would be obtained in practice for the same design

conditions because they are based on zero pressure loss in the normal engine tail cone and tail pipe.

Thus low burner-inlet velocity is not only desirable for obtaining high thrust augmentation but also for minimizing the loss of normal or nonaugmented thrust. In addition, low velocity is required for satisfactory combustion efficiency and stability as is discussed in the second and third papers of this series.

The effects of tail-pipe gas temperature and burner-inlet velocity are illustrated in figure 2(b) for altitude of 35,000 feet and flight Mach number of 1.50. Again the ratio of augmented to normal thrust is plotted against tail-pipe gas temperature for a range of burner-inlet velocities. The values of the design parameters are the same as in figure 2(a); but the normal engine thrust used as the base for the augmented ratio is changed to the value corresponding to the new flight conditions. Effects similar to those illustrated in figure 2(a) are obtained, however change in inlet velocity results in only about half as much percentage change in the augmented thrust ratio as occurs at sea level and zero flight Mach number. The smaller effects are due to the fact that at a higher pressure ratio across the exhaust nozzle (as exists at the high Mach number condition) a given percentage change in pressure loss produces a smaller change in thrust than at a lower pressure ratio across the nozzle. The higher values of augmentation indicated are due to the higher flight Mach number and not the higher altitude as is illustrated in a subsequent figure of this paper.

Turbine-outlet velocity and diffuser efficiency. - In figure 3, augmented-to-normal thrust ratio is plotted against turbine-outlet velocity for a tail-pipe gas temperature of 3800° R and diffuser efficiencies of 100, 80, and 60 percent. A similar set of curves is included for a gas temperature of 1650° R in order to illustrate the performance at nonburning conditions. These results are for sea-level altitude, zero flight Mach number, burner-inlet velocity of 400 feet per second, drag coefficient of 1, and exhaust-nozzle velocity coefficient of 0.975.

For a diffuser efficiency of 100 percent, both the augmented and normal thrust remain constant with change in turbine-outlet velocity; but for the more realistic values of diffuser efficiency, the performance decreases progressively with increased turbine-outlet velocity and decreased diffuser efficiency. For example, at a diffuser efficiency of 80 percent, the augmented thrust ratio decreases from about 1.48 at 800 feet per second to 1.43 at 1200 feet per second for the afterburning condition and from

0.97 to 0.95 for the nonburning condition. With a diffuser efficiency of 60 percent, the adverse effects of increased turbine-outlet velocity are greater.

The curves of figure 3 illustrate the desirability of designing the turbojet engine with a low turbine-outlet velocity in order to realize high augmentation and to minimize penalties during nonburning operation. Alternatively, if the engine has a high turbine-outlet velocity, the designer should make every effort to obtain a high diffuser efficiency.

Burner drag coefficient. - In figure 4 the augmented-to-normal thrust ratio is plotted against burner drag coefficient for burner-inlet velocities of 200, 400, and 600 feet per second, and for tail-pipe gas temperatures of 3800° (augmented condition) and 1650° R (nonburning condition). These curves are for sea-level altitude, zero flight Mach number, turbine-outlet velocity of 750 feet per second, diffuser efficiency of 80 percent, and exhaust-nozzle velocity coefficient of 0.975.

As might be expected the ratio of augmented to normal thrust is not appreciably affected by increase in burner drag at low burner-inlet velocities. At the higher inlet velocities, however, the adverse effects of high drag coefficient are of significant magnitude; for example, at 600 feet per second, an increase in drag coefficient from 0.5 to 2 reduces the augmented-to-normal thrust ratio from 1.39 to 1.23 for the 3800° R gas temperature condition and from 0.98 to 0.89 for the nonburning condition. At 400 feet per second, which may be considered a desirable design value for burner-inlet velocity, the loss in performance with increase in drag coefficient is about 40 percent as much as at 600 feet per second. Although low burner drag is advantageous for obtaining maximum thrust, some drag is necessary for satisfactory combustion as is discussed in the second and third papers of this series.

Nozzle velocity coefficient. - In figure 5 the ratio of augmented to normal thrust is plotted against nozzle velocity coefficient for sea-level altitude, tail-pipe gas temperatures of 3800° and 1650° R, and flight Mach numbers of 0, 0.75, and 1.50. For these calculations, the turbine-outlet velocity was 750 feet per second; diffuser efficiency, 80 percent; burner-inlet velocity, 400 feet per second; and drag coefficient, 1. The variation in nozzle velocity coefficient applies only to the tail-pipe-burner configuration, that is, the normal engine thrust used as the base of the augmented ratio is calculated for a constant value of the coefficient of 0.975.

The augmented-to-normal thrust ratio decreases linearly with decrease in nozzle velocity coefficient, the decrease being greater at the high than at the low flight Mach numbers. For example, decrease in nozzle coefficient from 0.975 to 0.850 for the augmented condition results in a 13 percent reduction in thrust ratio at 0 Mach number and 23 percent reduction at 1.50 Mach number. For the nonburning condition, the thrust reductions are 13 percent at 0 Mach number and 42 percent at 1:50 Mach number. The percentage decrease in high-speed thrust accompanying decrease in nozzle velocity coefficient is thrust of greater magnitude for the nonaugmented than for the augmented condition. This situation is aggravated by the fact that variable-area exhaust nozzles are more difficult to design for high velocity coefficient in the closed position corresponding to nonburning operation than in the open position corresponding to tail-pipe-burning operation.

Flight conditions. - The effect of flight Mach number on tail-pipe-burning performance has already been partially indicated, however, in order to give a more complete and direct representation of the effects of flight operating conditions, figure 6 has been prepared wherein the ratio of augmented to normal thrust is plotted against flight Mach number for altitudes of sea level and 35,000 feet. The tail-pipe design parameters are the reference values used in preceeding figures. Included for references are curves of the thrust of the normal engine configuration divided by the thrust obtained at sea-level altitude and zero Mach number; a subscript 0 has been used to indicate that the base thrust is for the sea-level, zero Mach number condition.

The somewhat wavy curve of sea-level normal thrust is the result of the combined effects of changing air flow, pressure ratio, propulsive efficiency, and inlet-diffuser efficiency that accompany change in flight Mach number. If a higher inlet-diffuser efficiency had been assumed, the decrease in thrust at high Mach number would not have occurred until a higher flight speed. The 35,000-foot curve is lower than the sea-level curve because of the decreased air density at altitude. It does not fall off as rapidly as the sea-level curve at the high Mach numbers because of the lower air temperature and the consequently higher permissible heat addition before the turbine.

The augmented-to-normal thrust ratio increases considerably with increase in Mach number but is not appreciably affected by altitude up to Mach numbers of about 1.0. At higher Mach numbers, the sea-level augmentation is greater than the high altitude augmentation, attaining a value 4 times the normal thrust at a Mach number of 2.0 compared with a value of 2.7 times the normal thrust

at 35,000 feet altitude. A large portion of this reduction is due to the decrease in normal thrust for the sea-level high-speed condition.

The corresponding specific fuel consumptions are shown in figure 7 plotted against Mach number for sea level and 35,000 foot altitudes. The normal fuel consumption increases rapidly with increased flight Mach number, varying from 1.1 pounds per hour per pound of thrust at sea level and 0 Mach number to 2.6 pounds per hour per pound of thrust at 2.0 Mach number. The normal consumption is from 9 to 30 percent lower at the 35,000-foot-altitude condition than at sea level because of the lower atmospheric air temperature. The total fuel consumption for the augmented condition at sea level varies from about 2.5 times the corresponding normal fuel consumption at 0 Mach number to 1.25 times the normal consumption at 2.0 Mach number. At an altitude of 35,000 feet, the augmented consumption is about 17 percent lower than at sea level and, at a Mach number of 2.0, is 1.5 times the corresponding normal consumption.

Pressure ratio. - The effect of change in engine compressor pressure ratio is illustrated in figure 8 where the ratio of augmented to normal thrust is plotted against flight Mach number at the 35,000-foot-altitude condition for design pressure ratios of 4 and 8. The engine with the design pressure ratio of 4 is the reference engine used for all previous calculations. The other engine is assumed to have the same component efficiencies and design conditions as the reference engine except for the higher pressure ratio. Similar to the reference engine, the design pressure ratio of 8 pertains to the sea-level, zero Mach number condition. At the 35,000-foot-altitude condition in figure 8, the actual pressure ratio varies from 5.3 at Mach number of 2.0 to 12.4 at Mach number of 0. The corresponding pressure ratios for the reference engine are between 3.0 and 5.6. The tail-pipe-burner conditions are the same as those used in figure 7.

Included for reference is the normal thrust of each engine divided by the normal thrust of the engine with a pressure ratio of 4 at the sea-level, zero Mach number condition, designated by the subscripts 0, 4. The high-pressure engine develops more than 100-percent-higher normal thrust than the low-pressure engine at 0 Mach number and about 60 percent more at 2.0 Mach number. The augmented-to-normal thrust ratio of the high-pressure engine is only between 6 and 11 percent higher than that of the low-pressure engine; however, the actual augmented thrust is much greater because of the higher normal thrust.

The corresponding specific fuel consumptions of the two engines are compared in figure 9. For the normal engine configuration, the high-pressure engine shows a 15-percent-lower fuel consumption than the low-pressure engine at 0 Mach number and a few-percent-lower consumption at 2.0 Mach number. For the augmented condition the high-pressure engine provides about 8-percent-lower fuel consumption than the low-pressure engine at 0 Mach number and slightly higher consumption at 2.0 Mach number. Thus from figures 8 and 9 it appears that higher pressure ratio engines than those in current use are advantageous both for normal and tail-pipe-burning operation for the range of flight Mach numbers considered.

Altitude Limits

The discussion thus far has dealt with the thrust and fuel consumption of tail-pipe burners. Another important performance criterion is the combustion stability or blow-out limits of the burner, which determine the maximum altitude at which the burner will operate. Such information cannot be readily predicted from analysis but must be obtained experimentally in altitude test chambers, altitude tunnels, or in flight. Analysis can, however, provide methods for generalizing the blow-out data and thus reduce the amount of testing required to establish the altitude limits.

Experience with turbojet and ram-jet engine combustion chambers indicated that the combustion blow-out of a given configuration and fuel-air ratio is affected by combustion-chamber-inlet velocity, inlet temperature, and inlet pressure. Tail-pipe-burner blow-out should be affected by the same parameters; accordingly, figure 10 illustrates the variation of tail-pipe-burner-inlet temperature, velocity, and static pressure with flight Mach number and altitude for a current turbojet engine operating at rated engine speed.

Over the range of flight Mach number and altitude, the burner-inlet or turbine-outlet temperature is held constant at the maximum permissible value by varying either the exhaust-nozzle area or the burner fuel flow. The corresponding burner-inlet velocities are substantially constant with flight Mach number but decrease with increased altitude, the change being smaller at high altitudes. Between 20,000 and 40,000 feet, burner-inlet velocity decreases about 6 to 10 percent. This variation is characteristic of the particular engine under consideration. Other engines for which data have been obtained at the Lewis laboratory indicate an even smaller change in burner-inlet velocity with flight conditions and in some cases the change with altitude is in the opposite direction to that shown in figure 10.

The burner-inlet pressure increases with increase in flight Mach number and decreases with increase in altitude. At a Mach number of 1.0, the pressure at 20,000 feet is double that at 40,000 feet. Thus the variation of inlet pressure with flight operating conditions is considerably greater than the variation of the other inlet conditions. It might then be expected that altitude blow-out data for constant engine speed could be correlated simply with burner-inlet pressure.

Such a correlation is illustrated in figure 11 for a typical tail-pipe burner on the same engine used in figure 10, again operating at rated engine speed and constant turbine-outlet temperature. Lines of constant burner-inlet pressure as obtained from normal engine-performance characteristics are plotted on coordinates of flight Mach number and altitude. Each line in figure 11 represents the combinations of altitude and Mach number at which the particular pressure is obtained in the tail pipe. The data points represent experimentally determined blow-out limits for the specific tail-pipe burner; for example, at a Mach number of 0.3, blow-out occurred at 32,000 feet altitude, and at a Mach number of 0.97, blow-out occurred at an altitude of 41,000 feet.

Higher altitude limits than these have been obtained with other tail-pipe burners; however, the data for this particular burner serve to illustrate general trends. Because blow-out is sensitive to small differences in operational technique, the data do not delineate a definite curve of altitude limit but indicate a band of altitude (5000 to 8000 ft wide) in which blow-out may occur. Similar bands of blow-out limits are generally obtained in testing other burners.

The data tend to fall within a band of constant pressure lines, in this case between 20 and 25 inches of mercury. It thus appears that if the altitude blow-out limit for a tail-pipe burner is obtained at one flight Mach number, the limits for other Mach numbers can be predicted from a knowledge of flight operating characteristics of the engine. Tail-pipe fuel-air ratio has considerable effect on altitude limits; in these tests the fuel-air ratio did not, however, have to be varied appreciably to maintain constant turbine-outlet temperature over the range of flight operating conditions. Similar data will have to be obtained with other engines and other tail-pipe burners before this method can be unreservedly accepted.

SUMMARY OF RESULTS

This theoretical investigation indicated the desirability of designing tail-pipe burners with low burner-inlet velocity, low burner drag, high diffuser efficiency, and high exhaust-nozzle velocity coefficient. These design criteria are considered essential not only for obtaining high augmentation, but also for minimizing the loss in normal engine performance during non-burning operation. Low turbine-outlet velocity was shown as a favorable engine design characteristic for tail-pipe-burning application, and higher pressure ratios than those currently used appeared to be advantageous for flight Mach numbers up to at least 2.0. Thrust augmentation increased considerably with increased flight Mach number but it was not appreciably affected by altitude except at Mach numbers above 1 where augmentation decreases with increased altitude. The total specific fuel consumption during tail-pipe-burning operation is about 2.5 times the normal consumption at sea level and 0 flight Mach number but was only 1.5 times the normal consumption at 35,000 feet altitude and a Mach number of 2.0.

REFERENCE

1. Bohanon, H. R., and Wilcox, E. C.: Theoretical Investigation of Thrust Augmentation of Turbojet Engines by Tail-Pipe Burning. NACA RM No. E6L02, 1947.

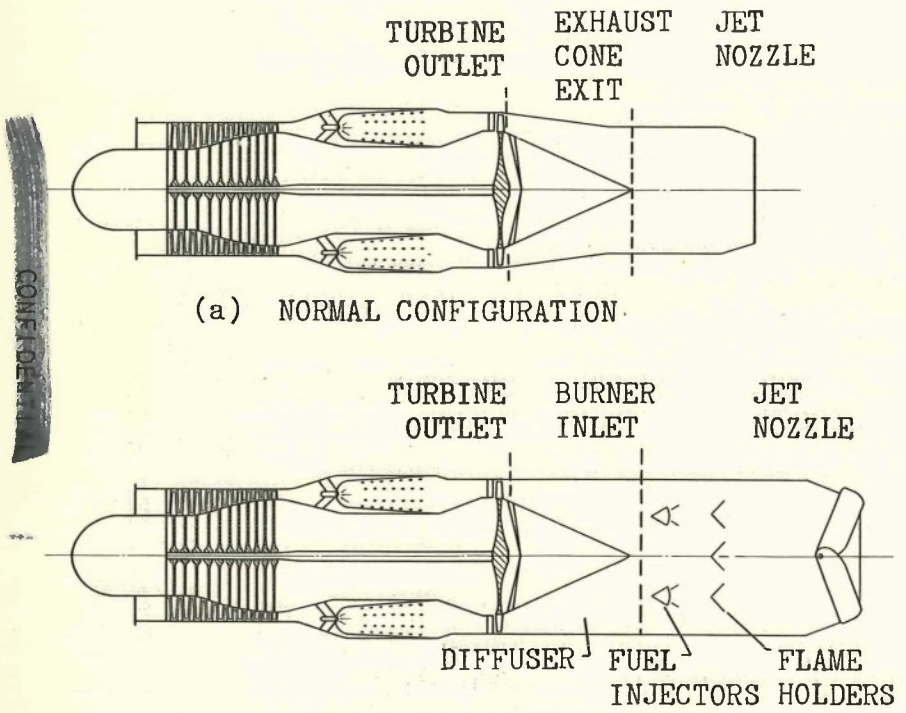

Figure 1. Normal and tail-pipe-burner engine configuration.

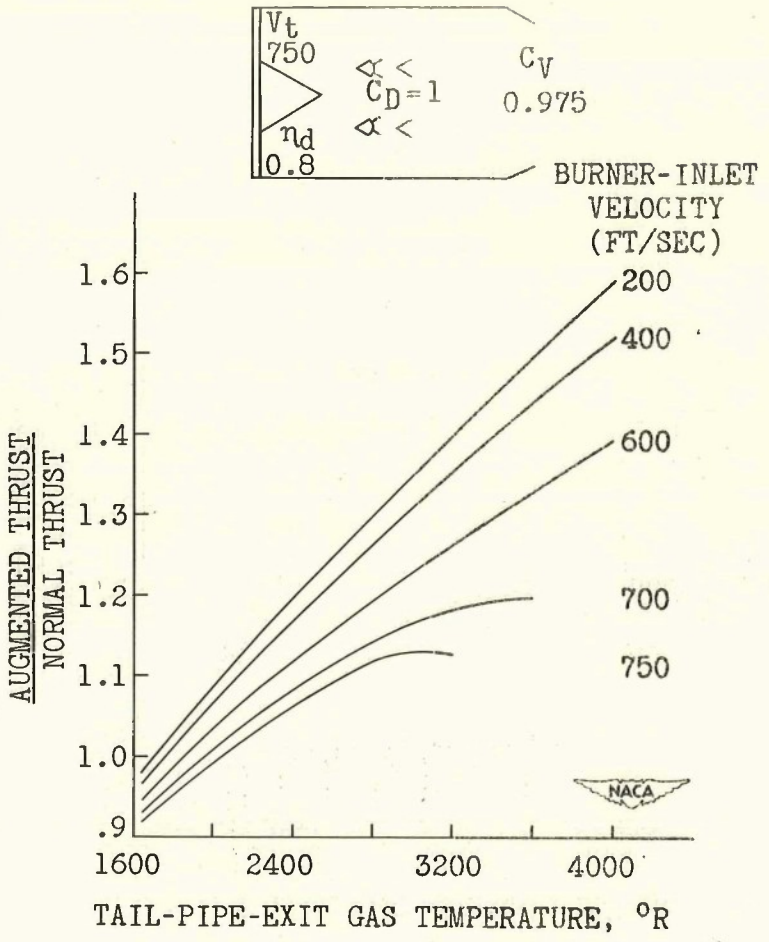

(a) Altitude, sea level; flight Mach number, 0.

Figure 2. - Effect of tail-pipe-exit gas temperature and burner-inlet velocity on augmentation.

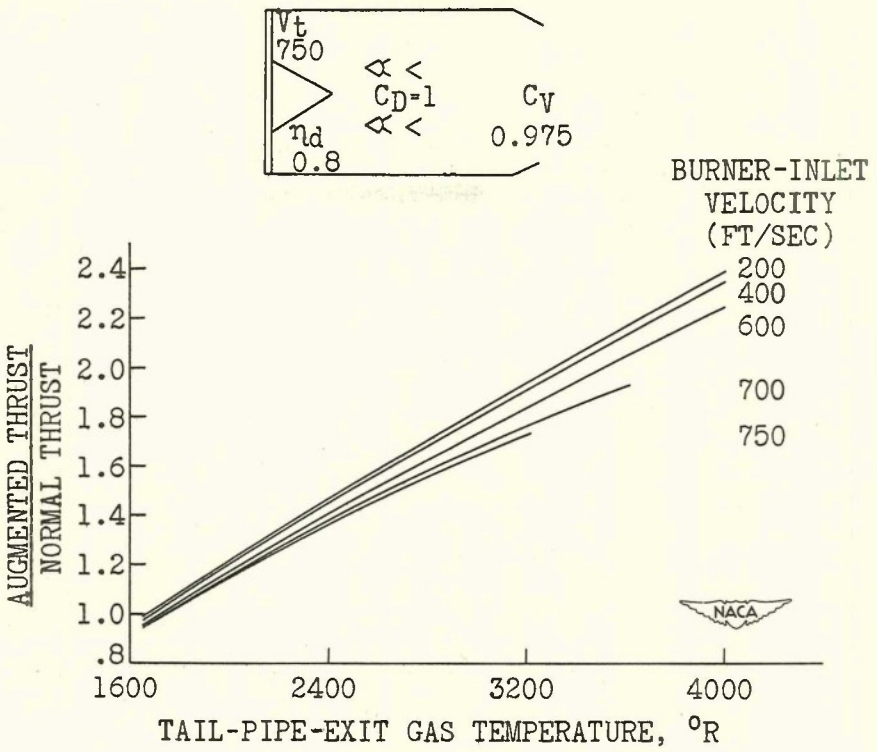

(b) Altitude, 35,000 feet; flight Mach number, 1.50.

Figure 2. - Concluded. Effect of tail-pipe-exit gas temperature and burner-inlet velocity on augmentation.

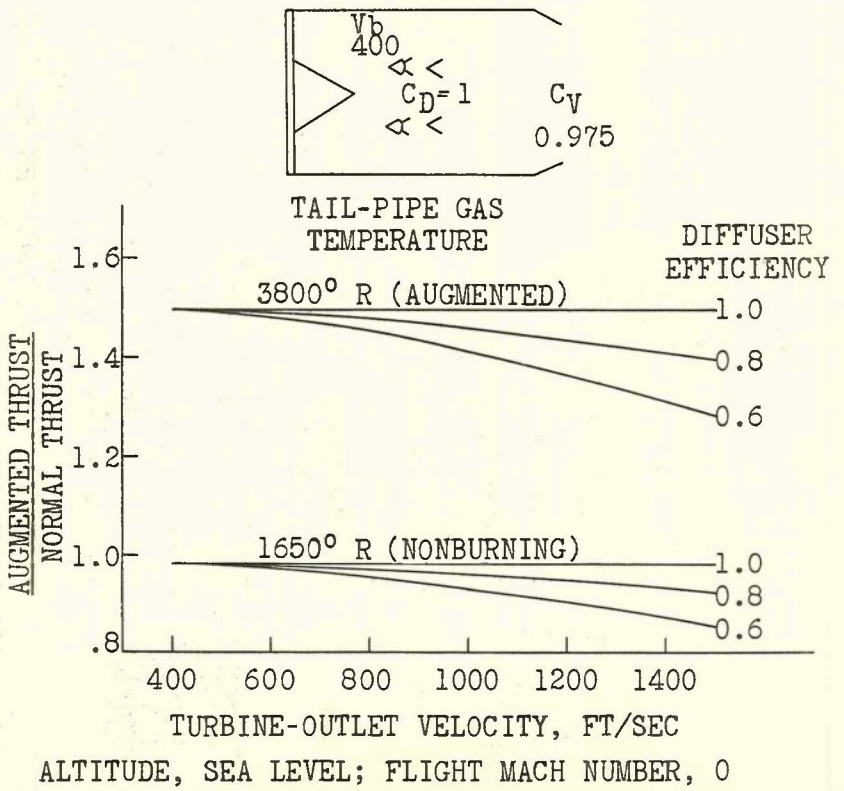

Figure 3. - Effect of turbine-outlet velocity and diffuser efficiency on augmentation.

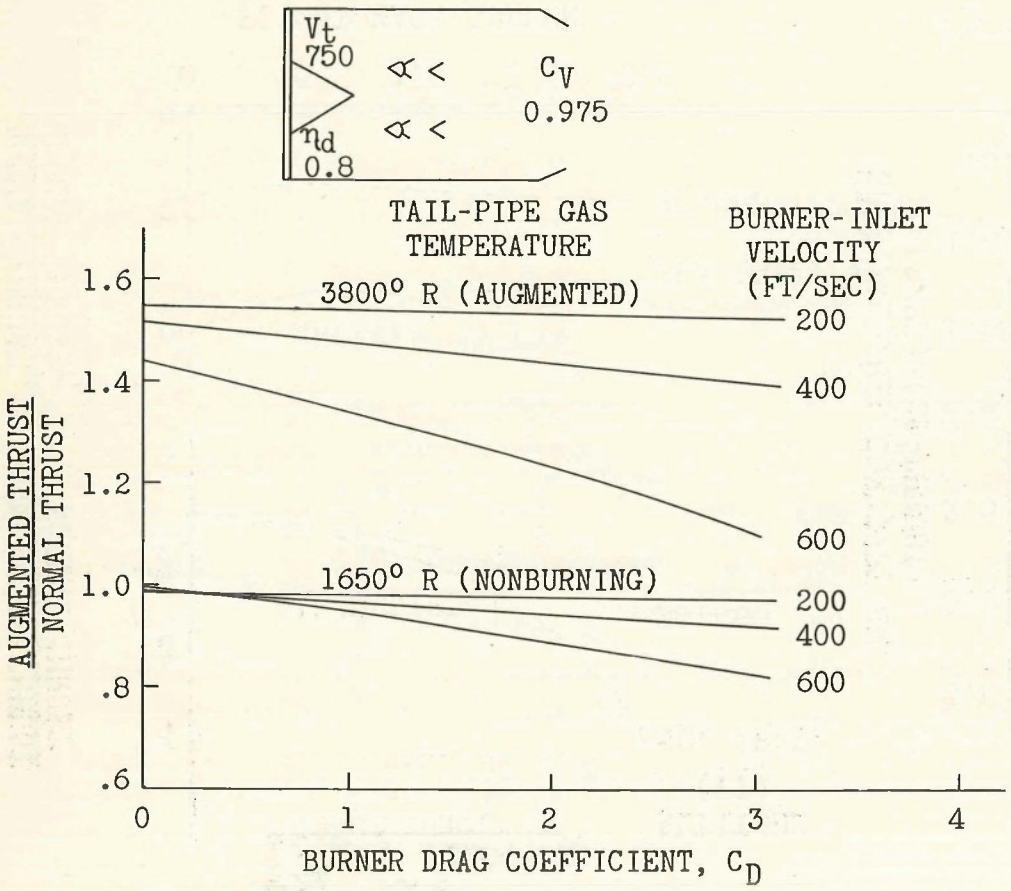

Figure 4. - Effect of burner drag and burner-inlet velocity on augmentation.

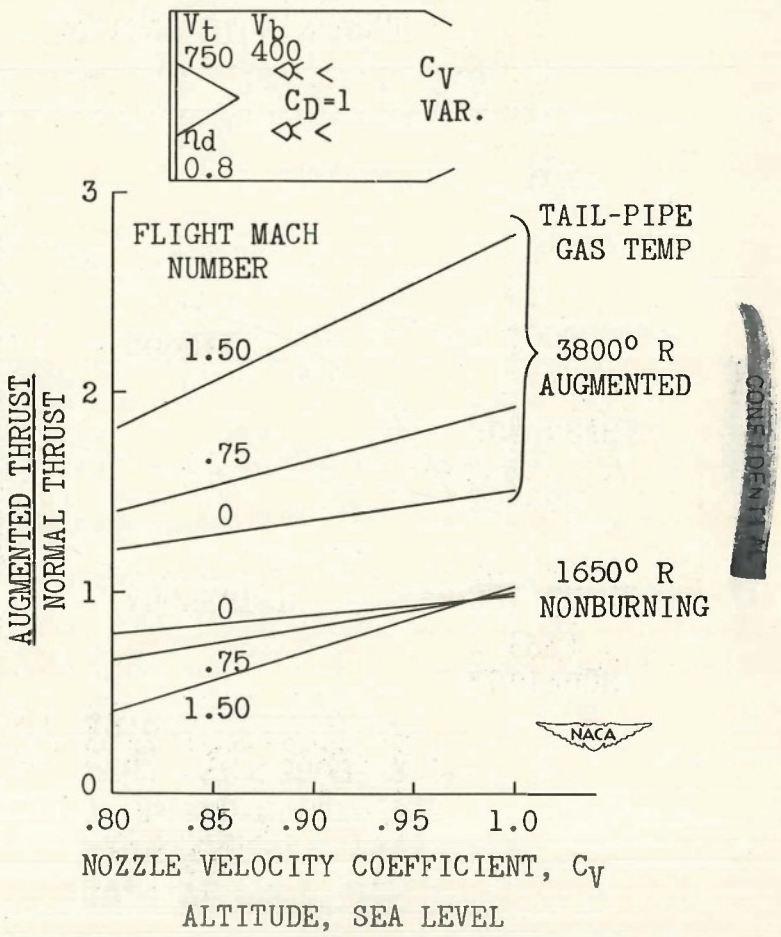

Figure 5. - Effect of tail-pipe-burner nozzle velocity coefficient on augmentation.

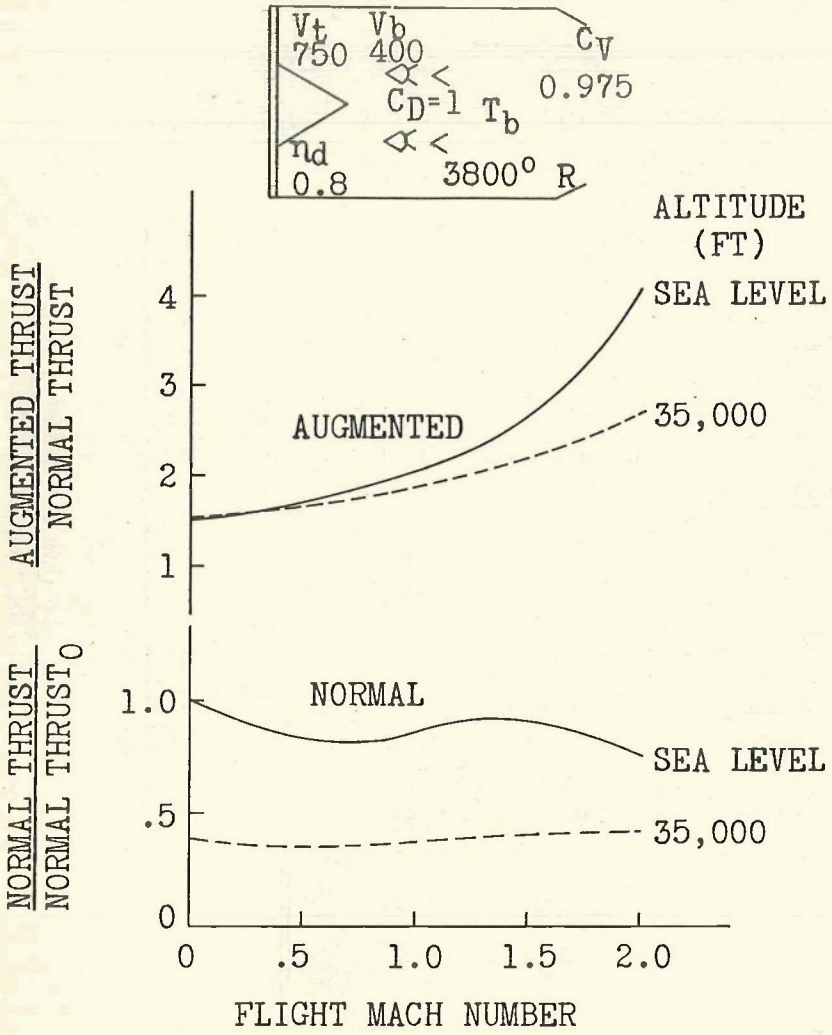

Figure 6. - Effect of flight conditions on augmentation.

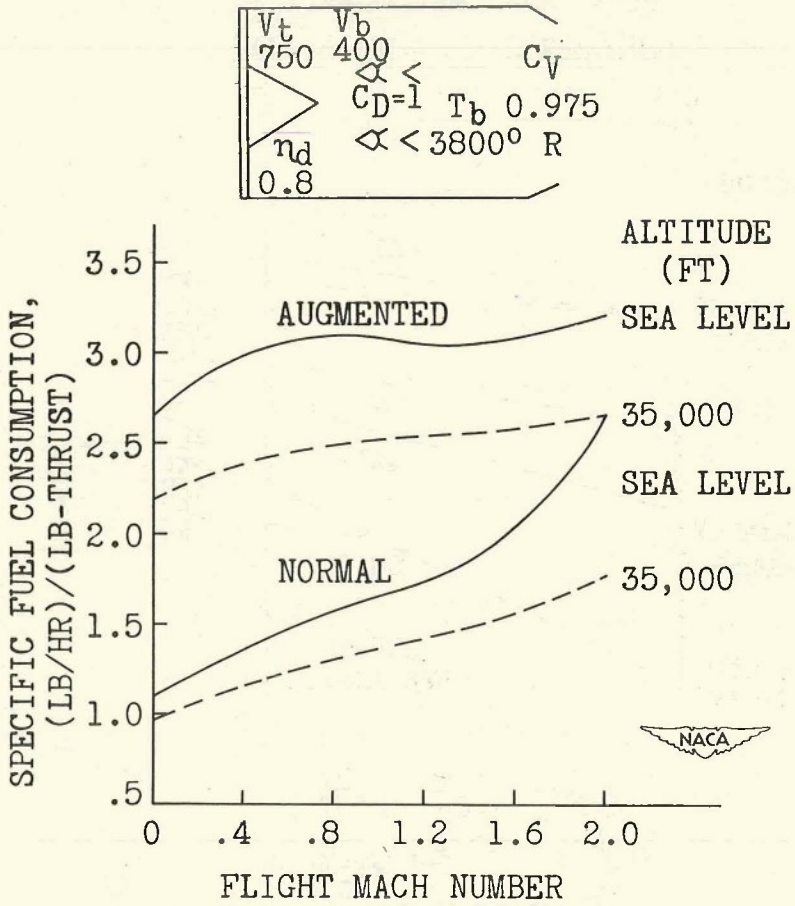

Figure 7. - Effect of flight conditions on fuel consumption.

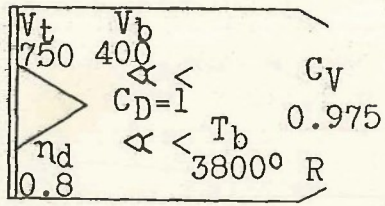

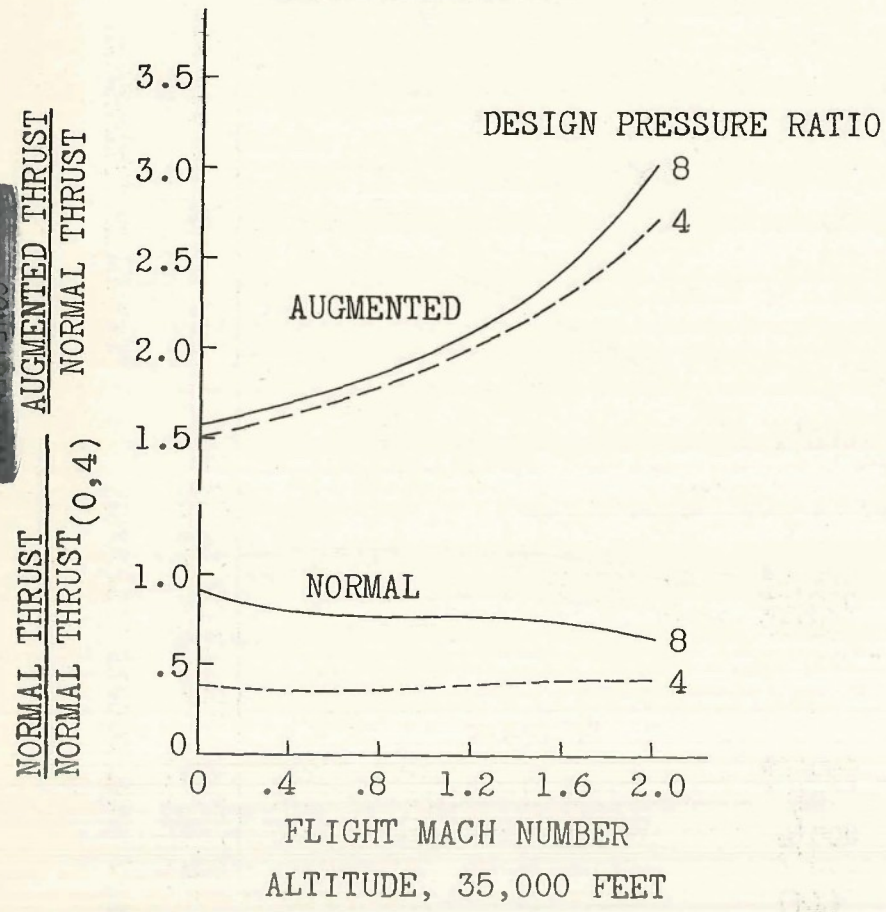

Figure 8. - Effect of compressor pressure rstio on augmentetion.

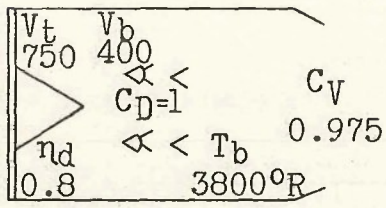

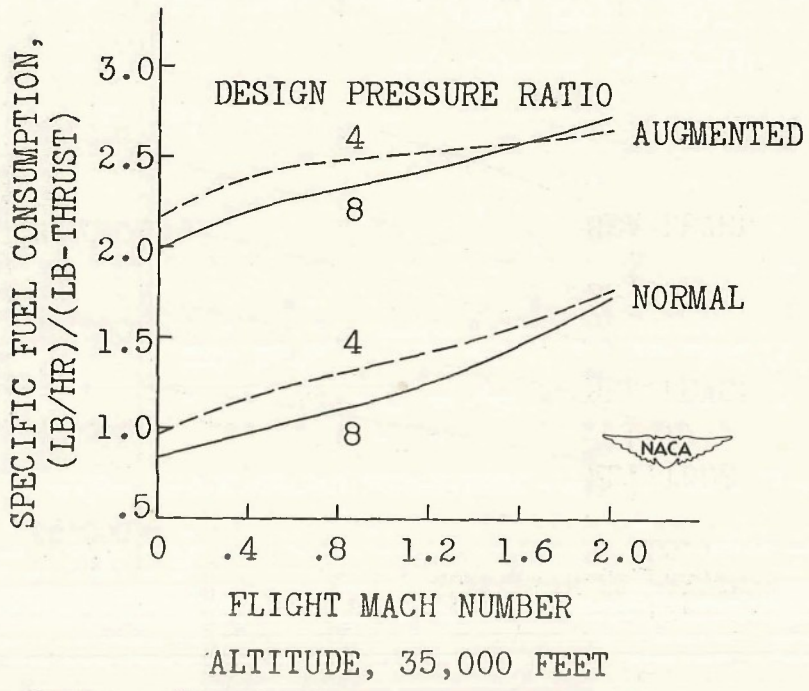

Figure 9. - Effect of compressor pressure rstio on fuel consumption.

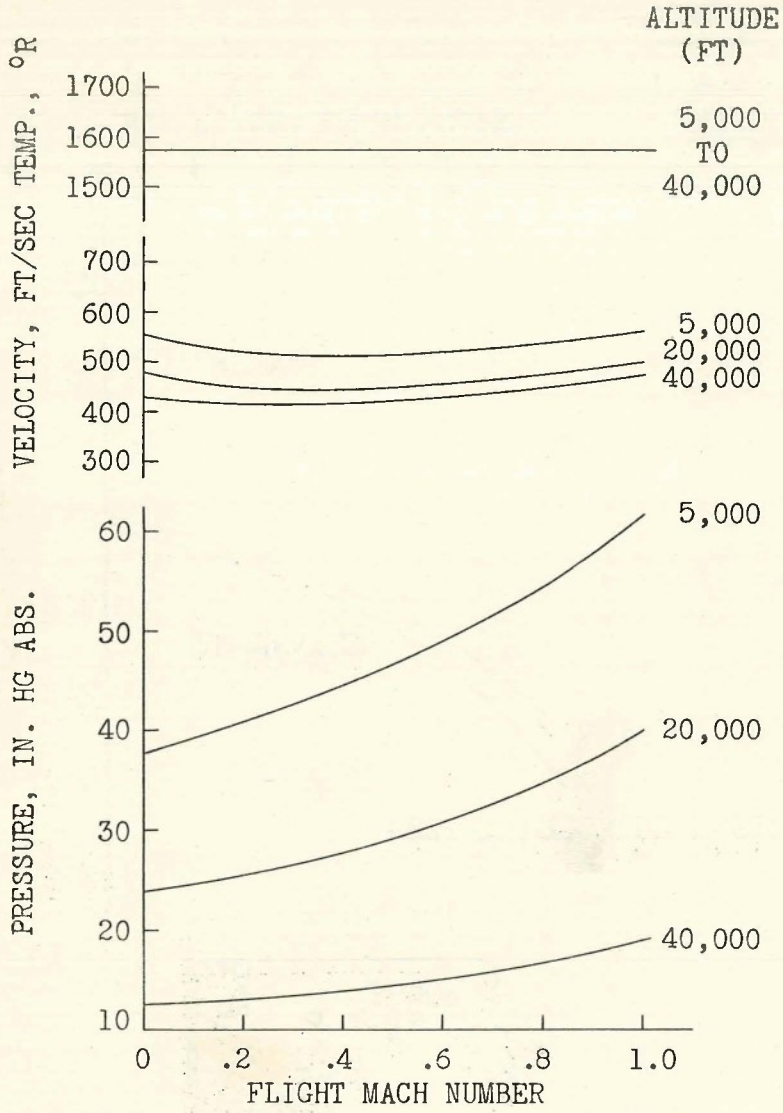

Figure 10. - Tail-pipe-burner conditions for turbojet engine.

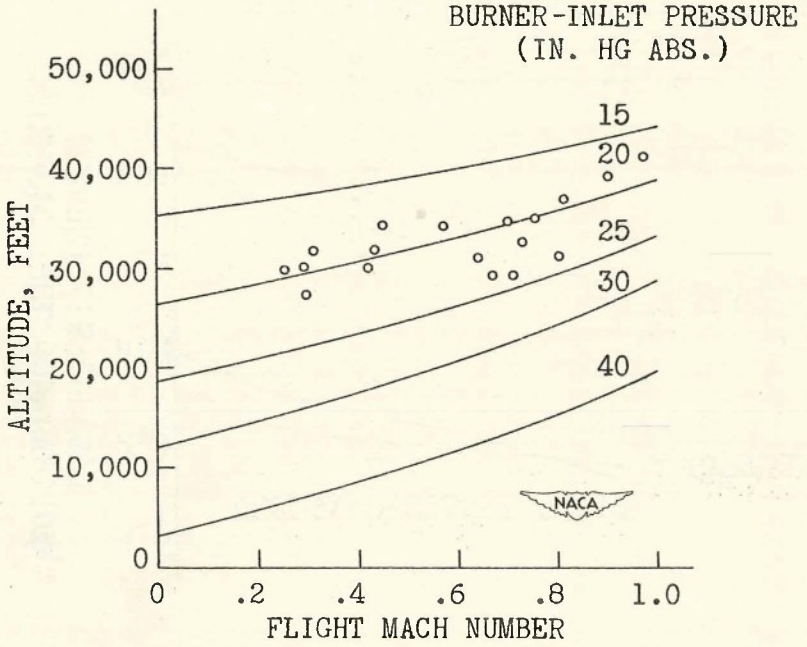

BLOW-OUT LIMITS OF A CURRENT TAIL-PIPE BURNER
RATED RPM - CONSTANT TURBINE-OUTLET
TEMPERATURE

Figure 11. - Blow-out limits of a typical tail-pipe burner.

EXPERIMENTAL INVESTIGATION OF TAIL-PIPE-BURNER DESIGN VARIABLES

By Alfred W. Young

Lewis Flight Propulsion Laboratory

INTRODUCTION

Designers of tail-pipe burners for turbojet engines have been handicapped by a lack of specific information that would help in the selection of suitable burner diameter and length, flame-holder type and size, diffuser shape, exhaust nozzle, fuel system, and ignition system. During the past $2\frac{1}{2}$ years, several experimental investigations of tail-pipe burning have been conducted at the NACA Lewis laboratory with three engine types and dozens of tail-pipe-burner configurations. Many of these burner configurations demonstrated the progressive effect of changing a single design variable. Most of the configurations were investigated over a wide range of simulated altitudes and flight speeds. Data selected to show the effect of several design variables on the operating characteristics of tail-pipe burners are presented.

TAIL-PIPE-BURNER REQUIREMENTS

The requirements that must be considered in designing a tail-pipe burner for a given application are:

1. Maximum thrust
2. Maximum operable range
3. High combustion efficiency
4. Minimum weight
5. Minimum size
6. Low internal losses
7. Adequate shell cooling
8. Satisfactory control

Each of these requirements conflicts with some of the others. Maximum thrust, operable range, and combustion efficiency are obtained when burning is made easy, that is, when the velocity of the gas entering the combustion chamber is low, when there are suitable sheltered regions where the flame can seat, and when the combustion

chamber is long enough that combustion can be completed before the mixture leaves the exhaust nozzle. Minimum weight and size may be obtained by reducing the diameter, which will increase the gas velocity, or by reducing the length, which may not give all the gas sufficient time to burn inside the combustion chamber. Low internal losses may be obtained with optimum diffuser design, low gas velocities, and the smallest possible flame holder. Provision for cooling requires additional weight and results in some performance loss. Control, the last requirement, necessitates a satisfactory variable-area exhaust nozzle, which will be heavier than the fixed-area conical exhaust nozzle and possibly not quite as efficient.

DESIGN VARIABLES

The design variables considered in this paper are flame-holder design, burner-inlet velocity, combustion-chamber length, fuel distribution, diffuser design, variable-area exhaust nozzles, and ignition systems. Tail-pipe cooling is discussed in the fourth paper of this series.

Flame Holders

The flame holder shown in figure 1 was used in early tail-pipe-burning experiments at the NACA Lewis laboratory (reference 1). This design proved effective in ram jets. The flame holder consists of V-shaped gutters arranged in horizontal and vertical rows to form a grid. The gutters are $1\frac{3}{4}$ inches wide across the open downstream ends and are spaced 4 inches apart on centers. This size and spacing of gutter elements proved more satisfactory in ram jets than a size and spacing of twice this scale or one-half this scale. The flame holder blocked one-half the cross-sectional area of the combustion chamber and caused a pressure drop of 1.25 times the velocity head of the approaching gas. Although the V-shaped gutter-grid flame holder was very effective, too much pressure drop was produced, the flame propagated near the combustion-chamber wall would aggravate the tail-pipe cooling problem, and the central portion would be burned out if the rear of the diffuser inner cone were used as a pilot flame seat.

The flame holder shown in figure 2 is one ring made of a closed half-round section. This semitorodial flame holder blocks about

19 percent of the combustion-chamber area and is reasonably satisfactory, except at high altitudes or with high gas velocities.

A two-ring V-gutter flame holder that blocks about 23 percent of the combustion-chamber area is shown in figure 3. The two rings provide adequate coverage of the combustion-chamber area and also avoid flame seating on the wall. Flame from a large pilot at the rear of the diffuser inner cone passes through the hole in the center of the flame holder. The two-ring V-gutter flame holder is one of the better designs investigated and permits altitude operation except at extremely high gas velocities.

The "lockwasher-type" flame holder in figure 4 was constructed of V-gutter elements and was designed to cover the same general area as the two-ring V-gutter flame holder, and to offer a maximum perimeter from which the flames could start. The flame holder blocked 28 percent of the combustion-chamber area. The lockwasher flame holder was not quite as effective as a two-ring V-gutter flame holder with the same blocked area.

The arrangement in figure 5 is most advantageous from the standpoint of having low internal losses. The blunt end of the inner cone serves as the flame holder for a large pilot flame, which is relied upon to spread throughout the combustion chamber. Such an arrangement resulted in low combustion efficiencies and was unsuitable for high altitude operation, and it might be adequate where thrust augmentation is needed only at take-off. This type of burner is sometimes subject to rough burning, which has been known to shake the tail pipe hard enough to open its seams.

The flame holder in figure 6 is intended to produce burning in five stages, with each ring after the first partly submerged in flame from the proceding ring. This flame holder requires cooling, which is accomplished by fuel that is supplied through the mounting tubes and distributed to the rings by the longitudinal tubes. The fuel is sprayed through small holes in the front of each ring. The five-stage flame holder operates only at very low fuel-air ratios. It was belatedly realized that the blocking effect of the small forward rings, augmented by the pressure drop due to burning, forced the air flow toward the outside of the combustion chamber and thus increased the gas velocity in the region where it was already highest. Flame would not seat on the outer rings.

In figure 7 is the five-stage flame holder rebuilt to place the large ring forward, where its blocking effect tends to provide a more uniform velocity distribution in the tail pipe. Flame

holders of this type provided reasonably satisfactory performance, but were subject to local overheating, coking of the fuel, and cracking of the metal tubing.

The combustion efficiency obtained with three types of flame holder is shown in figure 8 as a function of tail-pipe fuel-air ratio. The data shown were obtained at rated engine speed with a tail pipe having a burner-inlet velocity of approximately 420 feet per second and a fixed-area exhaust nozzle. A higher combustion efficiency was reached with the two-ring V-gutter flame holder than with either the three-stage flame holder or the large pilot alone at altitudes of 25,000 and 45,000 feet. The peak combustion efficiency decreased, however, from 0.89 at 25,000 feet to 0.59 at 45,000 feet. The three-stage flame holder, which comprised only three rings but was otherwise similar to the flame holder of figure 7, reached a peak combustion efficiency of 0.85 at 25,000 feet and 0.49 at 40,000 feet. When no flame holder other than the blunt end of the diffuser inner cone (that is, large pilot) was used, the burner operated satisfactorily at 25,000 feet with a peak combustion efficiency of 0.69, but at 45,000 feet the flame was weak and the combustion efficiency dropped to 0.12. Flame holders that provide little blockage are generally quite satisfactory under most favorable conditions, but they are most sensitive to the adverse effects of high altitude or high burner-inlet velocity.

Of all the flame holders used in tail-pipe burners at the Lewis laboratory, those using V-gutter sections proved to be the most generally satisfactory. V-gutters measuring $1\frac{1}{2}$ to 2 inches across the legs of the V permitted somewhat wider operating ranges than those made either smaller or larger. The effect of the shape of the V was investigated by operating a tail-pipe burner with three two-ring V-gutter flame holders that were identical except for the included angle of the V. As shown in figure 9, included angles of 20°, 35°, and 50° were used, but the width across the legs of the V was kept constant at $1\frac{3}{4}$ inches and each of the flame holders blocked 30 percent of the combustion-chamber area. A fixed-area conical exhaust nozzle was used. At an altitude of 25,000 feet, the variation in gutter angle had little effect on combustion efficiency and the best angle appeared to be between 30° and 40°. At 45,000 feet, the best angle was about 30°; the combustion efficiency dropped seriously with the flame holder having a 50° gutter angle.

Burner-Inlet Velocity

It is recognized that high burner-inlet velocities are detrimental, but some uncertainty has existed concerning what velocities might be called high and how serious their effects are. In order to investigate the effect of burner-inlet velocity, three tail-pipe combustion chambers having different diameters were used on one engine. Each of these combustion chambers was 4 feet long and was fitted with a two-ring V-gutter flame holder providing 28-percent blockage. The same fixed-area conical exhaust nozzle was used on each tail pipe.

In figure 10 the symbols indicate the maximum altitudes at which stable operation was obtained with each combustion chamber. The two larger combustion chambers with inlet velocities of 490 and 533 feet per second operated at an altitude of 50,000 feet at a simulated flight Mach number of 0.2. The smallest combustion chamber with an inlet velocity of 601 feet per second was limited to an altitude of 35,000 feet at the same flight Mach number. Combustion blow-out occurred at altitudes slightly higher than 35,000 and 50,000 feet. Lines of constant turbine-outlet pressure have been drawn through the data points of figure 10 to indicate the maximum altitudes at which stable operation could be expected at higher flight speeds.

The combustion efficiency obtained with the same series of combustion chambers is shown in figure 11 for three altitudes at rated engine speed and limiting turbine-outlet temperature. At 25,000 feet, the burner-inlet velocities for the three combustion chambers ranged from 470 to 605 feet per second, and the combustion efficiencies remained near 0.80. There is no apparent explanation for the slight drop in combustion efficiency at the lower velocities, which is inconsistent with the other data. At 35,000 feet, the combustion efficiency dropped from 0.76 at a burner-inlet velocity of 463 feet per second to 0.69 at a velocity of 525 feet per second. At 45,000 feet, the combustion efficiency dropped from 0.55 at a burner-inlet velocity of 490 feet per second to 0.40 at a velocity of 550 feet per second. With the smallest combustion chamber, which had an inlet velocity of 605 feet per second at 25,000 feet, the combustion efficiency dropped so much at 35,000 feet that limiting turbine-outlet temperature could not be obtained.

Combustion-Chamber Length

The effect of combustion-chamber length (fig. 12) was investigated by using lengths of 2, 4, and 6 feet in otherwise identical

burner configurations. A two-ring V-gutter flame holder that blocked 30 percent of the combustion-chamber area was used. At an altitude of 25,000 feet, an increase in combustion-chamber length from 2 to 4 feet raised the peak combustion efficiency from 0.70 to 0.81, but a further increase in length to 6 feet had only a negligible effect. At 45,000 feet, the combustion efficiency was only 0.12 with the 2-foot combustion chamber and each successive increase in length cuased a marked improvement, until with a length of 6 feet a peak efficiency of 0.56 was reached. At 45,000 feet, the 6-foot combustion chamber was the only one that would permit limiting turbine-outlet temperatures to be reached.

The effect of a single variable, such as combustion-chamber length, would be reduced if other variables were chosen to be more favorable for combustion. That is, with a lower burner-inlet velocity, a larger flame holder, and a better fuel distribution system, the effect of changing the combustion-chamber length could be expected to be less than that shown in figure 12.

Fuel Distribution

The importance of fuel distribution is shown in figure 13 with two different fuel systems used in the same tail pipe (reference 2). In the multiple-nozzle fuel system, 80 percent of the fuel was sprayed downstream through 18 nozzles located in a circle just upstream of the flame holder and 20 percent was sprayed radially outward through 12 nozzles mounted in the surface of the diffuser inner cone. At an altitude of 25,000 feet, the peak combustion efficiency was 0.76 at a tail-pipe fuel-air ratio of 0.025 and was considerably less at other fuel-air ratios.

In the spray-bar fuel system, all the fuel was injected through eight spray bars mounted in the diffuser annulus $35\frac{1}{2}$ inches upstream of the flame holder. Four pairs of 0.040-inch holes were drilled in each spray bar. With this configuration a peak combustion efficiency of 0.96 was reached at a tail-pipe fuel-air ratio of 0.025 and the efficiency dropped only to 0.80 at a fuel-air ratio of 0.06.

The superior performance of the spray-bar fuel system is attributed to the better coverage of the air stream afforded by the spray bars and to the distance between the spray bars and the flame holder, which permitted sufficient mixing of the fuel and air. Experience with other tail-pipe burners using similar fuel spray bars has shown

that the holes should be located to take account of the velocity distribution of the tail-pipe gas and that the central region should be relatively rich to provide a strong stabilizing flame at the rear of the diffuser inner cone. The high combustion efficiency obtained with the spray-bar fuel system in figure 13 is attributed to the combination of a good fuel system with other favorable design variables. It should be noted that the burner-inlet velocity was low, ranging from 420 to 460 feet per second, and the flame holder provided 32-percent blockage.

Diffuser Design

The hot gas leaving the turbine must be slowed down before it enters the tail-pipe combustion chamber. The diffuser-design problem is aggrevated by the uneven velocity profile at the turbine outlet. A typical velocity profile, taken in a standard tail cone about 10 inches from the turbine wheel, is shown in figure 14. A steep velocity gradient exists and the highest velocity is near the outside wall.

In figure 15 are shown the lines of two diffusers that were used with the same tail-pipe burner as well as the lines of the standard engine tail cone. In the tail-pipe-burner diffuser with the long inner cone, the rate of change of area was approximately uniform. The short inner cone of the other diffuser followed the same contour to the point where the area ratio was 1.4. After this point the short cone gave a much more rapid area change than the long cone.

The difference in the losses produced by the two diffusers can be determined from the curves of over-all tail-pipe total-pressure-loss ratio given in figure 15. The curves (fig. 15) are for the nonburning condition, where the exhaust nozzle was small enough to produce limiting turbine-outlet temperatures at rated engine speed. The tail pipe having the short inner cone has a loss that is greater than that of the pipe with the long inner cone by about 0.5 percent of the total pressure.

The design of the diffuser with the short inner cone is shown to be better than that of the standard engine tail cone by the fact that the losses in the tail pipe with the short inner cone but no flame holder were about the same as those in the standard tail cone. That is, the losses incurred in slowing down the gas plus the friction losses in the long combustion chamber were no more than the friction losses in the standard tail cone. These results indicate that careful diffuser design is effective in minimizing tail-pipe burner pressure losses and that improvement in the dosign of the standard engine tail cone is needed.

Variable-Area Exhaust Nozzles

One of the items needed for control of a tail-pipe burner is a good variable-area exhaust nozzle. The clamshell type is probably the most promising, and certainly the one on which the most effort has been expended. The two most improtant considerations in designing a clamshell nozzle are efficiency in producing thrust and durability. High efficiency can be obtained by eliminating leakage and using the best possible shape.

Two clamshell nozzles of different shape are shown in figures 16 and 17. The fixed-area inner shell of nozzle A has its exit opening in one plane and would be a desirable nozzle. As the outer shells move together, however, the shape of the opening is changed until in the closed position the opening is no longer, even approximately, in a single plane. Gases are discharged at the sides of this opening with a large component normal to the main thrust axis. The movable shells of nozzle B have been shaped to keep the exit opening approximately planar regardless of size.

Clamshell nozzles A and B and a series of fixed-area conical exhaust nozzles were tested on the same engine to determine their comparative performance (reference 3). The results are presented in figure 18 in which the variation of corrected jet thrust with corrected fuel consumption is shown for a single corrected engine speed (rated value). Nozzle A in the closed position, where the corrected fuel flow was 3340 pounds per hour, produced about 7 percent less thrust than an equivalent conical nozzle at the same fuel consumption. Nozzle B produced within 1 percent of the thrust of the conical nozzles.

Clamshell nozzles on tail-pipe burners have shown a tendency to overheat, warp, and jam. Some progress has been made in cooling them and reasonably satisfactory results have been obtained. Nozzle B withstood 40 minutes of tail-pipe burner operation without damage. However, it is too early to say that any given design is completely suitable for tail-pipe burners.

Ignition Systems

Igniting the mixture in the tail pipe proved to be a troublesome problem. Many arrangements of spark plugs and pilot fuel nozzles were used, two of which are shown in figure 19. One of the schemes consisted of a small ram jet located upstream of the main flame holder. The ram jet has its own inlet diffuser, fuel nozzle,

spark plug, flame holder, and jet nozzle, and was supposed to send a jet of flame downstream to the main flame holder. It was completely unreliable.

The second scheme consisted of a pilot fuel nozzle in the center of a depression in the end of the diffuser inner cone and a spark plug near by. Except at high altitudes this pilot was effective when the spark plug would operate, but it was difficult to maintain high voltage insulation inside the tail pipe. The pilot fuel nozzles invariably melted, but this did not matter when the main fuel was introduced upstream of the pilot.

The stand-by method of starting the tail-pipe burner was a rapid acceleration of the engine, which sent flame back through the tail pipe. This method is quite effective, but is not recommended operating practive because of the danger of overheating the turbine. A modification of the practice of accelerating the engine proved to be by far the most satisfactory scheme for lighting the tail-pipe fuel. In this scheme (fig. 19), the tail-pipe fuel pump must first be operating and producing a higher pressure than that in the engine fuel manifold. A line from the tail-pipe fuel pump is brought to the line supplying one of the engine combustion chambers. A solenoid valve and two check valves are installed as shown in figure 19. The tail-pipe fuel is ignited by opening the solenoid valve for a fraction of a second. The momentary rich mixture produced in one combustion chamber sends flame downstream to the tail pipe. This scheme is positive in operation and produced over 200 starts on one engine with no sign of damage to the engine.

SUMMARY OF RESULTS

The results of research on tail-pipe-burner design variables are briefly summarized as follows:

1. Flame holders providing little blockage were found to be adequate for low altitude operation, but at high altitudes a blocked area of about 30 percent of the combustion-chamber area was found to be desirable.

2. Ring-type V-gutter flame holders have proved satisfactory. The best operating characteristics were obtained when the included angle of the V-gutter elements was about 30° and the width across the opening of the V was $1\frac{1}{2}$ to 2 inches.

3. Burner-inlet velocity is the variable that is most likely to establish the value of a tail-pipe burner. Satisfactory operation up to an altitude of about 25,000 feet was obtained with burners having inlet velocities as high as 600 feet per second, but lower velocities were required at high altitudes; and every advantage was found to lie with burners having inlet velocities in the range from 400 to 450 feet per second.

4. In burners indentical except for combustion-chamber length, a length of 4 feet was found to be sufficient to provide the best performance at altitudes up to 25,000 feet, whereas at an altitude of 45,000 feet a combustion-chamber length of 6 feet was not enough to develop the maximum combustion efficiency.

5. The highest combustion efficiencies were obtained when the fuel was injected as far as possible upstream of the flame holder and when the fuel distribution was made to match the air-flow distribution as closely as practicable.

6. Tail-pipe pressure losses have been reduced by careful diffuser design, but the data are not sufficient to establish an optimum diffuser design.

7. A variable-area exhaust nozzle can be designed to be nearly as efficiency as a fixed-area conical nozzle, but variable-area nozzles have not yet been thoroughly proved in tail-pipe-burner operation.

8. Dependable methods for starting a tail-pipe burner were available.

REFERENCES

1. Fleming, W. A., and Dietz, R. O.: Altitude-Wind-Tunnel Investigations of Thrust Augmentation of a Turbojet Engine. I - Performance with Tail-Pipe Burning. NACA RM No. E6I20, 1946.

2. Fleming, William A., and Wallner, Lewis E.: Altitude-Wind-Tunnel Investigation of Tail-Pipe Burning with a Westinghouse X24C-4B Axial-Flow Turbojet Engine. NACA RM No. E8J25e, 1948.

3. Lundin, Bruce T.: Investigation of Several Clamshell-Type Adjustable-Area Exhaust Nozzles for Turbojet Engines. NACA RM (to be pub.).

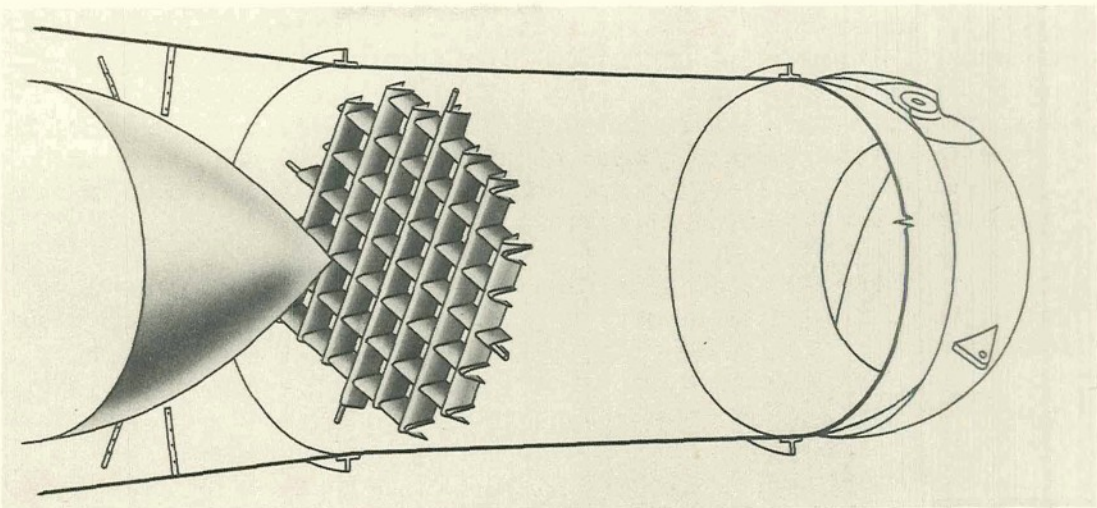

Figure 1. - V-shaped gutter-grid flame holder.

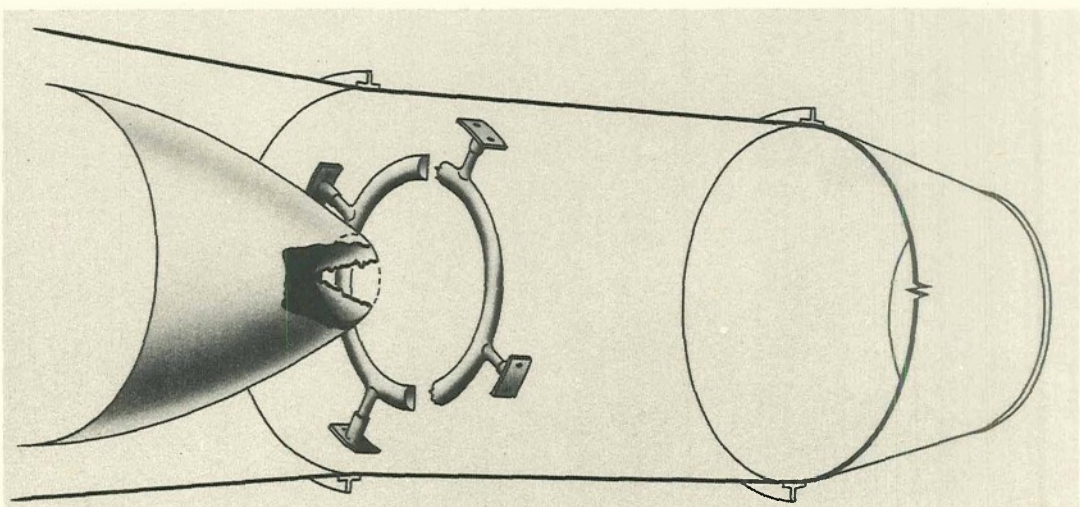

Figure 2. - Semitoroidal flame holder.

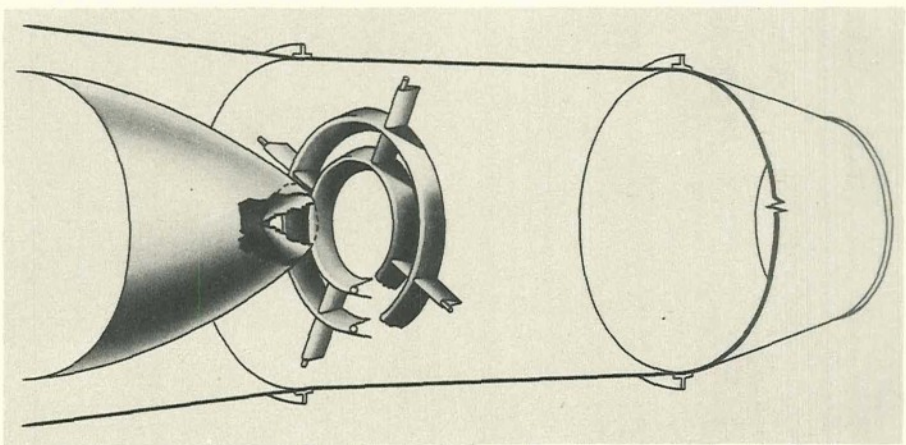

Figure 3. - Two-ring V-gutter flame holder.

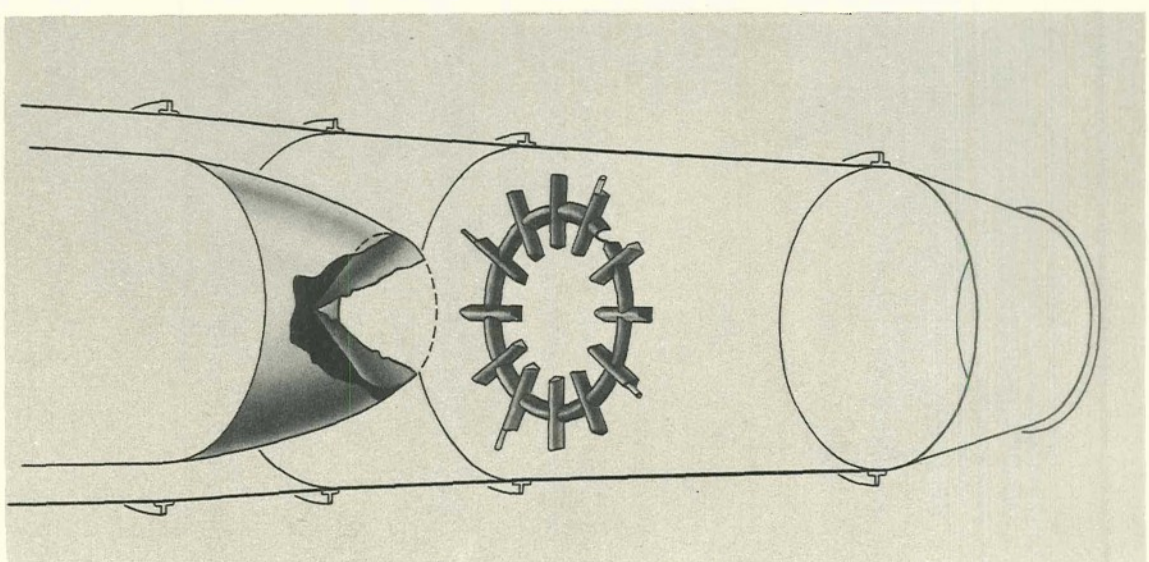

Figure 4. - Lockwasher flame holder.

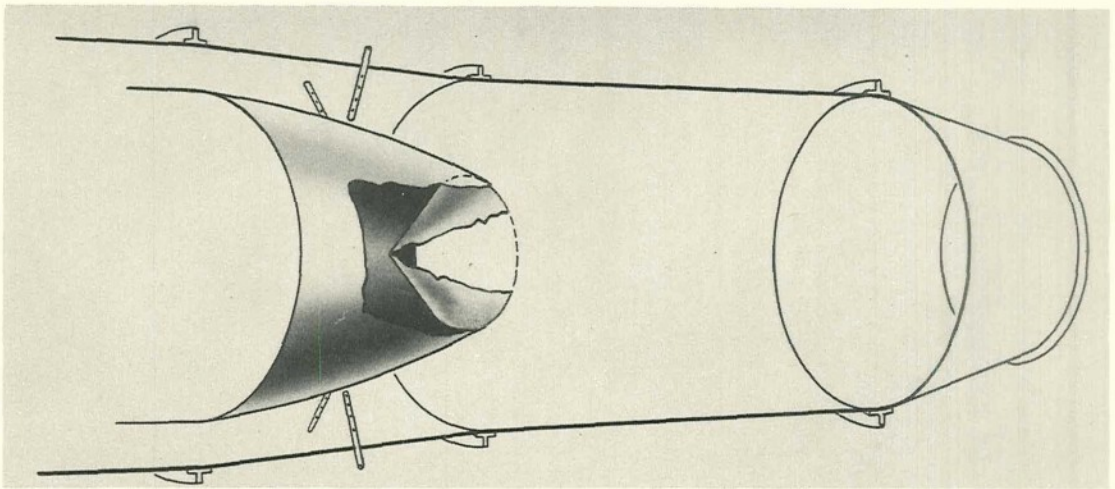

Figure 5. - Large pilot in blunt end of inner cone.

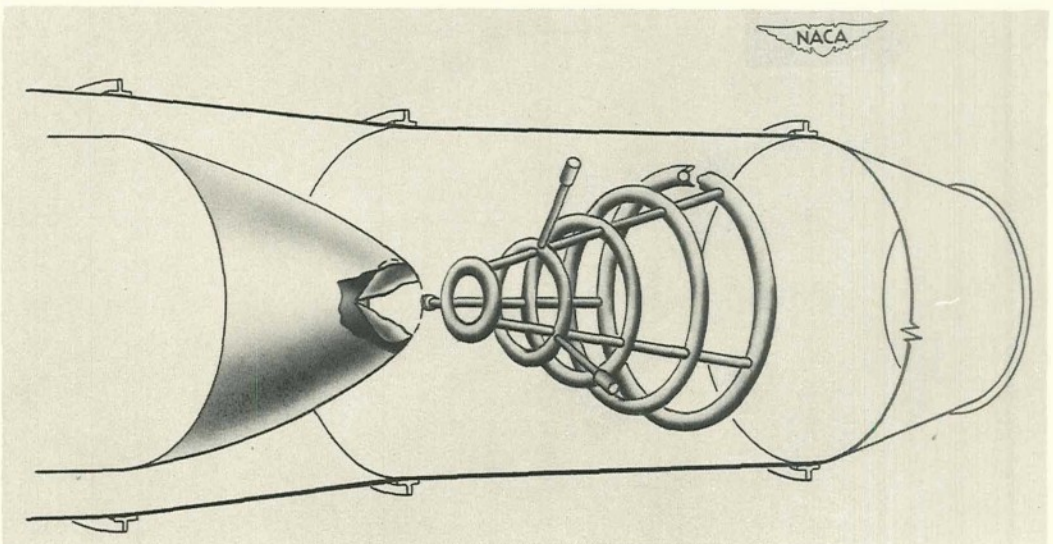

Figure 6. - Five-stage flame holder.

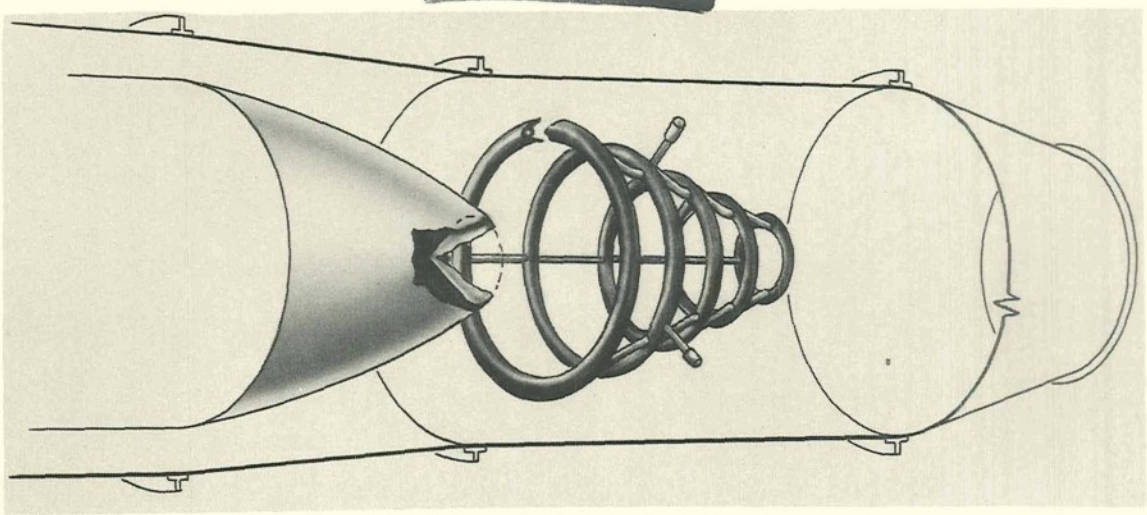

Figure 7. - Modified five-stage flame holder.

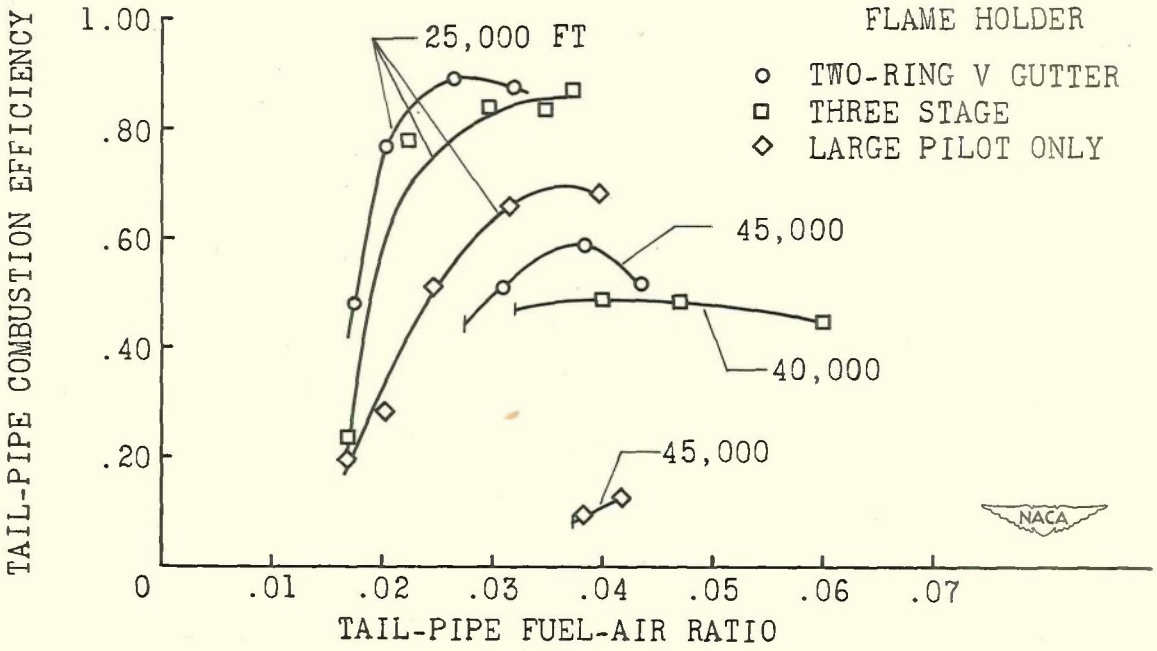

Figure 8. - Tail-pipe combustion efficiency for three flame-holder configurations. Exhaust-nozzle area constant; rated engine speed.

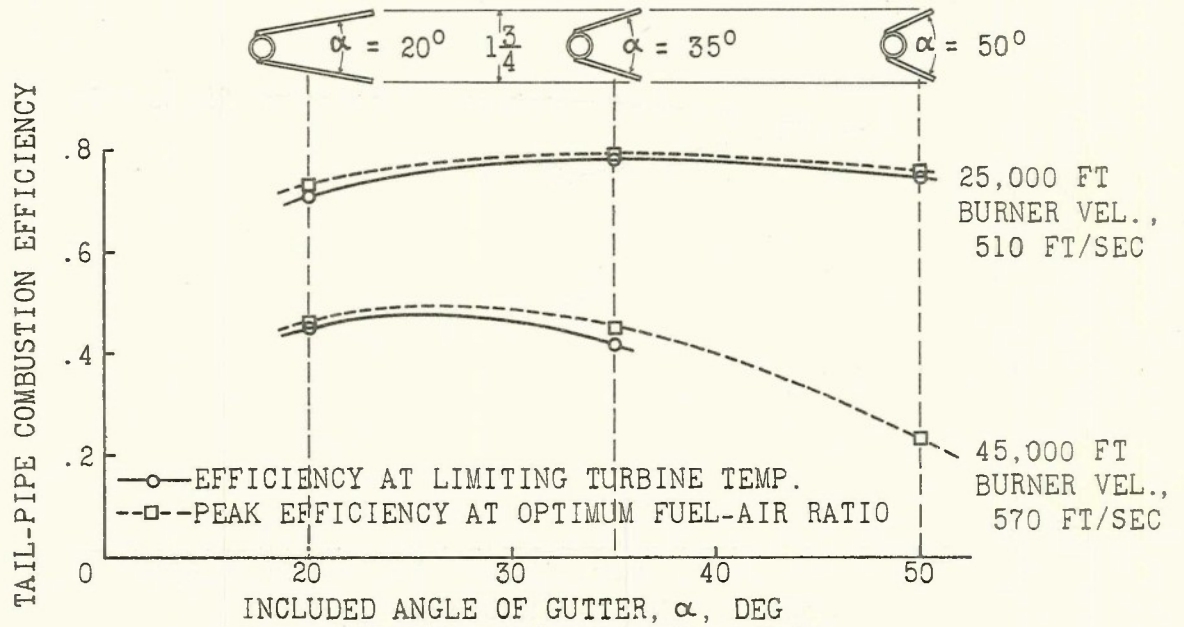

Figure 9. - Effect of flame-holder gutter angle on tail-pipe combustion efficiency. Rated engine speed.

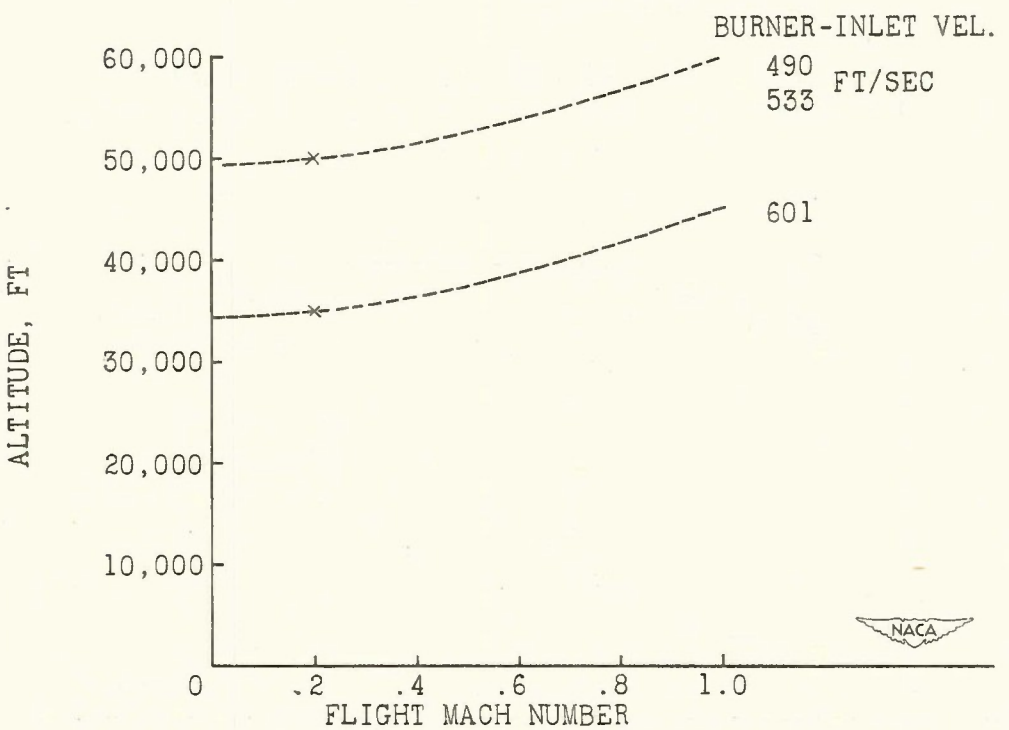

Figure 10. - Effect of burner-inlet velocity on altitude limits. Rated engine speed.

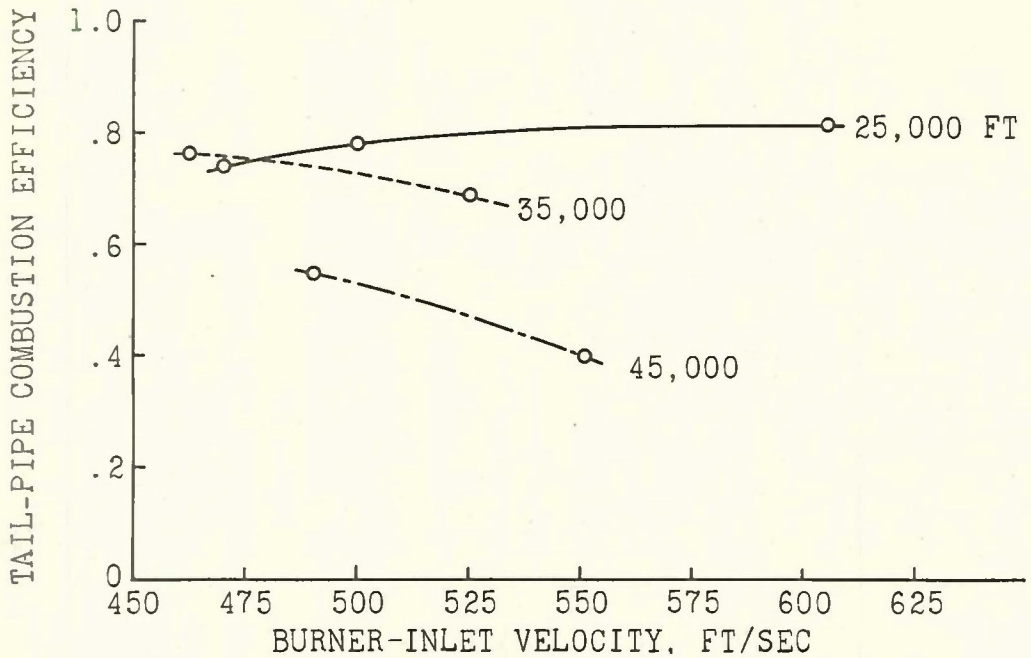

Figure 11. - Effect of burner-inlet velocity on tail-pipe combustion efficiency. Rated engine speed; limiting turbine-outlet temperature.

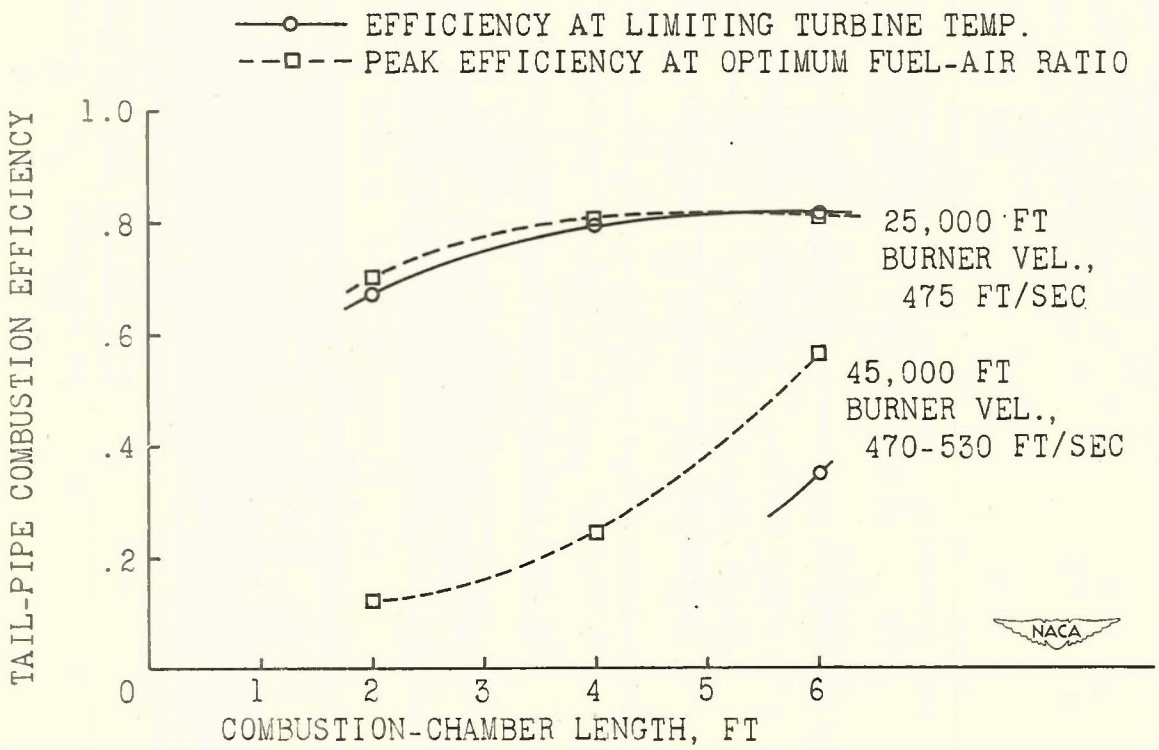

Figure 12. - Effect of combustion-chamber length on tail-pipe combustion efficiency. Rated engine speed.

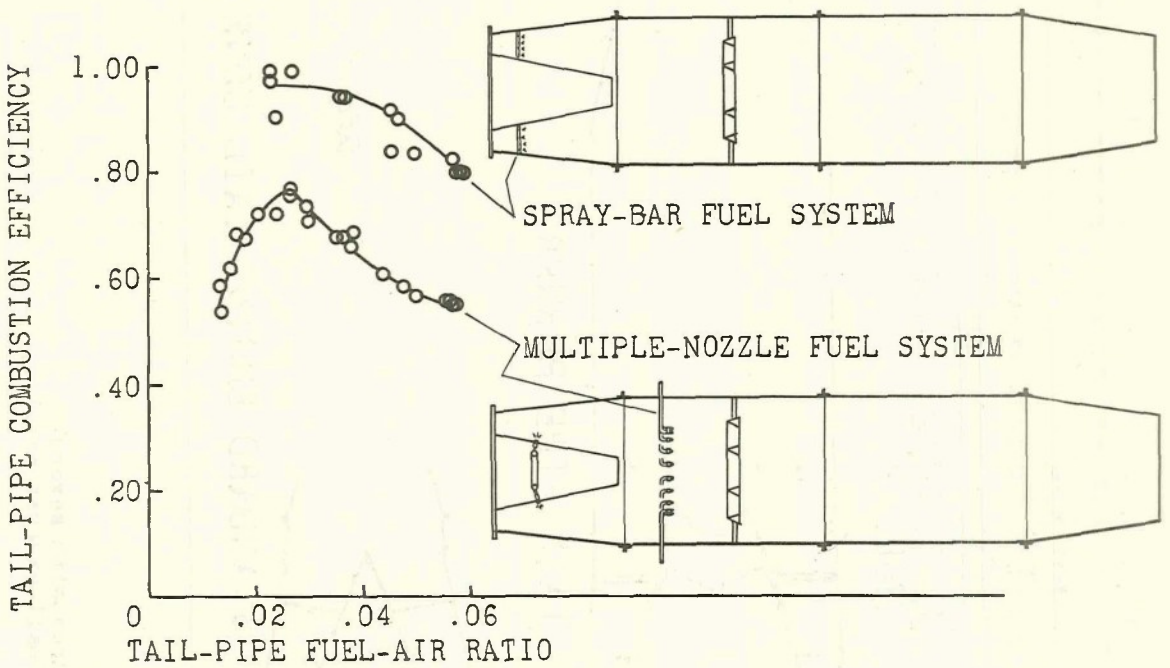

Figure 13. - Tail-pipe combustion efficiency for two fuel systems. Burner-inlet velocity, 420 to 460 feet per second.

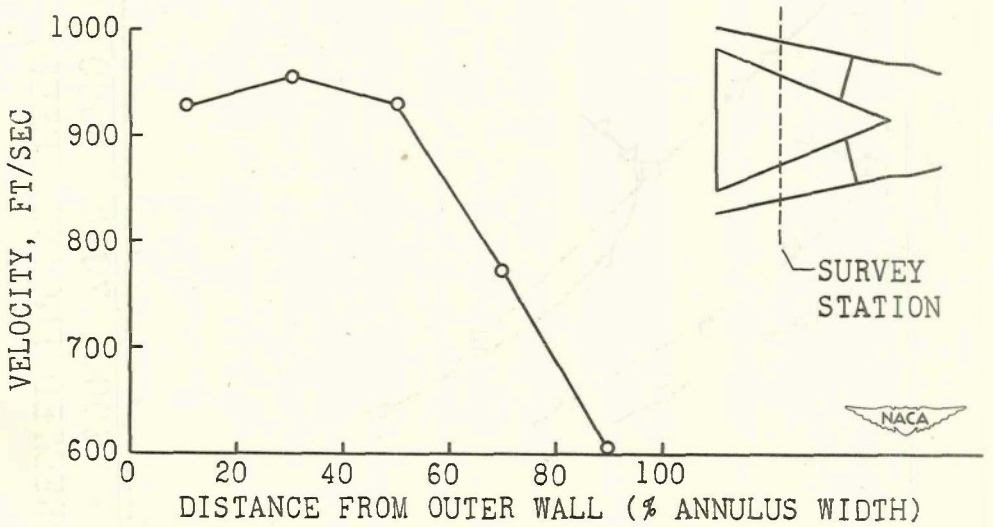

Figure 14. - Typical velocity profile near turbine outlet. Altitude, 5000 feet; rated engine speed.

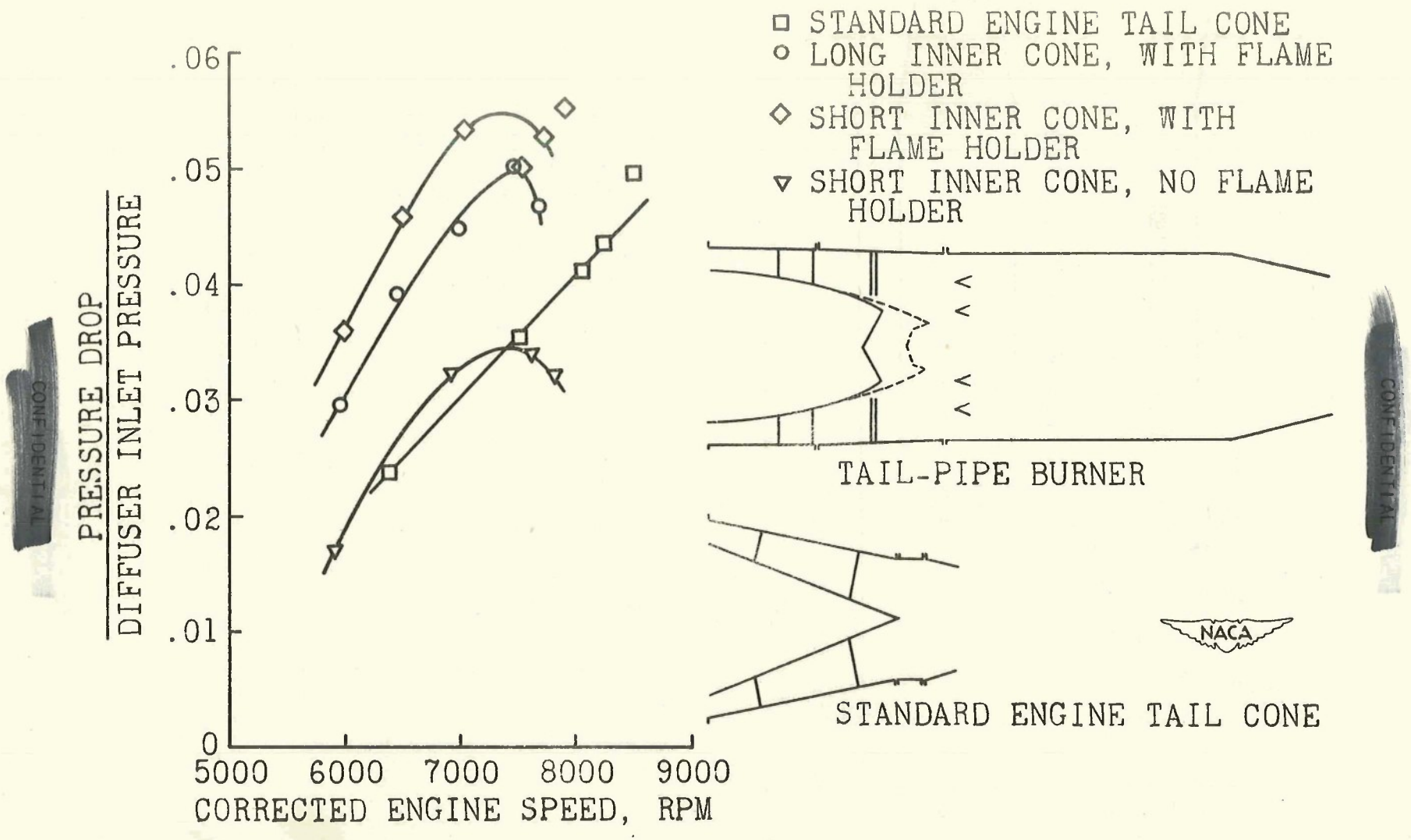

Figure 15. - Tail-pipe total-pressure losses with several diffusers without tail-pipe burning. Small exhaust nozzle.

OPEN

CLOSED

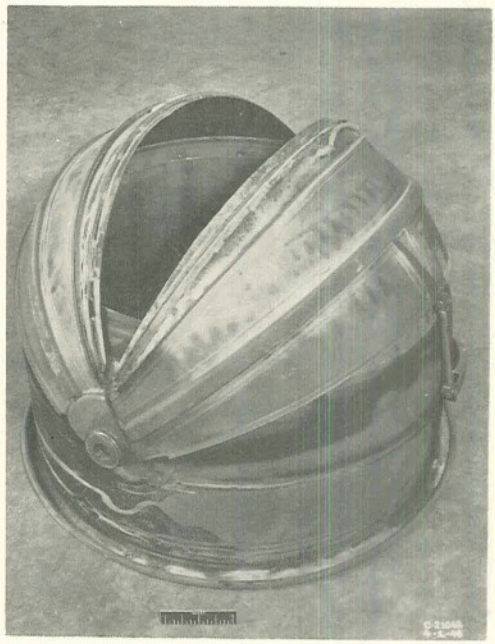

Figure 16. - Clamshell nozzle A.

OPEN

CLOSED

Figure 17. - Clamshell nozzle B.

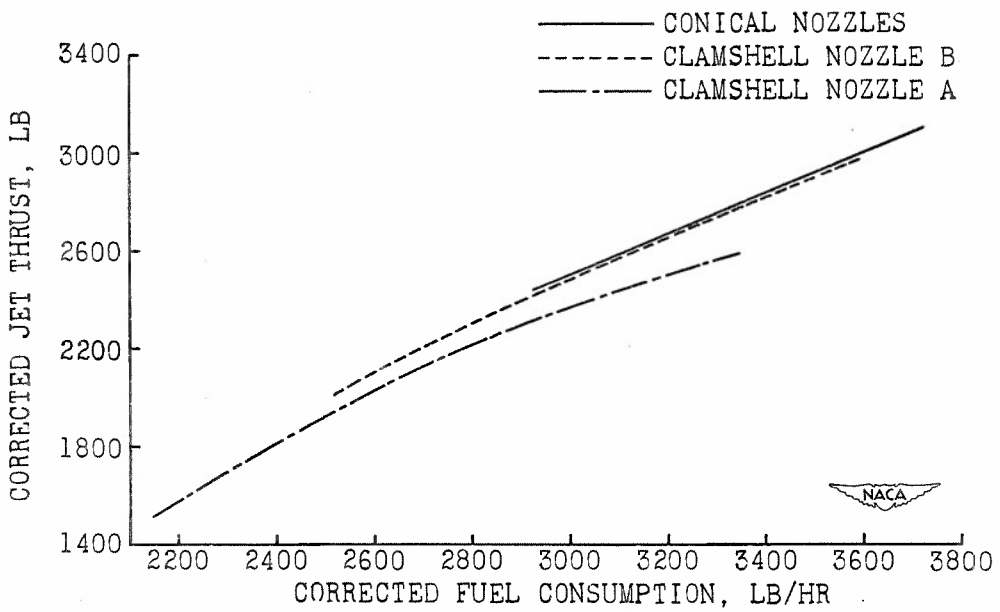

Figure 18. - Performance of exhaust nozzles. Corrected engine speed, 7700 rpm.

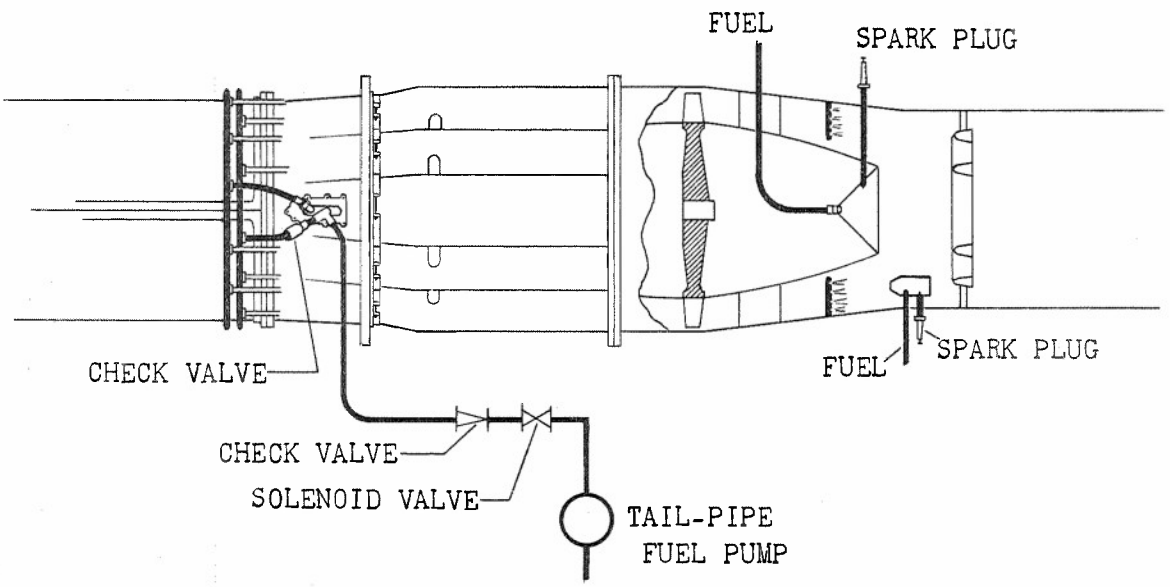

Figure 19. - Tail-pipe ignition systems.

PERFORMANCE CHARACTERISTICS OF SEVERAL TAIL-PIPE BURNERS

By William A. Fleming and Harry W. Dowman

Lewis Flight Propulsion Laboratory

INTRODUCTION

Performance theoretically calculated for tail-pipe burning and experimental results indicating the effect of the various design considerations on burner characteristics at altitude are discussed in the two preceding papers of this series. Included in this paper are experimental results that show the performance and the operable range of several tail-pipe burners at altitude conditions.

A considerable amount of data was obtained for a large number of different tail-pipe-burner configurations with the J34 engine, the J35 engine, and an experimental version of the J47 engine. Some of the more recent tail-pipe burning results for four of these burners are presented. Thrust performance, burner-outlet temperatures, specific fuel consumptions, combustion efficiencies, the operable ranges of tail-pipe fuel-air ratio, and burner-inlet pressure, temperature, and velocity are shown for a range of flight conditions.

TAIL-PIPE-BURNER INSTALLATIONS

Four tail-pipe burners are considered. Burners A and B were installed on a J34 engine, burner C on a J35 engine, and burner D on an experimental version of the J47 engine.

Burner A. - Burner A (fig. 1), which was installed on a J34 engine, was attached to the standard engine tail cone and has an over-all length of about $8\frac{1}{2}$ feet. The gas leaving the turbine is diffused to a 23-inch-diameter section where the flame holder is installed. The combustion chamber is a 40-inch conical section that tapers from 23 inches in diameter at the flame holder to $18\frac{7}{16}$ inches at the outlet.

The flame holder consists of two semicircular-gutter-type rings joined with four radial struts of similar construction. This flame holder blocks approximately 25 percent of the cross-sectional area of the tail pipe. Both the rings and the radial struts of the flame

holder are provided with small slots on the upstream face. Fuel is injected through five circular tubes located immediately upstream of the flame holder. Two of these tubes, which are alined with the two flame-holder rings, inject the fuel through several small orifices in a downstream direction through the slots of the flame holder. Fuel is injected from the other three tubes through small orifices in an upstream direction.

A two-position variable-area exhaust nozzle was used on the burner, which in the closed position has a projected elliptical area equivalent to a circular diameter of $15\frac{3}{8}$ inches. During tail-pipe burner operation, this nozzle was in the wide-open position and the throat area was provided by the outlet of the combustion chamber.

A shroud was installed around the burner through which air flowed to cool the burner shell during operation.

Burner B. - Burner B (fig. 2), which was also installed on a J34 engine, has an over-all length, including the diffuser section, of about 10 feet and a maximum diameter of $25\frac{3}{4}$ inches. The exhaust gas was diffused to the combustion chamber, which is $25\frac{3}{4}$ inches in diameter and 6 feet long. A flame holder was installed 18 inches downstream of the front flange of the combustion chamber, thus giving a burning length of $4\frac{1}{2}$ feet upstream of the fixed-area conical exhaust nozzle. The exhaust nozzle is $19\frac{1}{2}$ inches in diameter at the outlet.

Fuel is injected $4\frac{1}{2}$ inches downstream of the turbine through eight streamlined spray tubes; this arrangement gives a mixing length for the fuel of $35\frac{1}{2}$ inches between the fuel injector and the flame holder. Each spray tube has four pairs of impinging jets through which the fuel is sprayed into the diffuser. The downstream end of the inner cone was cut off where it was 5 inches in diameter with the blunt end covered by a disk, thereby profiding a turbulent region for the purpose of seating a stabilizing flame in the center of the tail pipe.

A two-ring V-gutter flame holder that blocks 32 percent of the burner cross-sectional area was installed. The mean diameters of the outer and inner gutters are 17 and 10 inches, respectively; the included angle of the gutters is 30°; and the distance across the open end of the gutters is $1\frac{3}{4}$ inches.

The burner shell was cooled only by the flow of low-velocity air over the outside of the burner.

Burner C. - Burner C (fig. 3), which was installed on a J35 engine, has an over-all length, including the diffuser section, of about 9 feet and a maximum diameter of 29 inches. The exhaust gas was diffused to the combustion chamber, which is 29 inches in diameter and 4 feet long. The flame holder was located at the upstream end of the combustion chamber, giving a 4-foot burning length between the flame holder and the fixed-area conical exhaust nozzle. The outlet diameter of the exhaust nozzle is $20\frac{1}{8}$ inches.

Fuel was injected in the diffuser through 12 streamlined spray tubes installed 14 inches upstream of the flame holder. Each tube had four pairs of small orifices that injected fuel from opposite sides of the tubes into the gas stream normal to the direction of flow. The downstream end of the inner cone was cut off where it was $8\frac{1}{2}$ inches in diameter and a concave dome was installed that provided a turbulent region for the purpose of seating a stablizing flame in the center of the pipe.

A two-ring V-gutter flame holder similar to the one used in burner B blocked 29 percent of the burner cross-sectional area. The mean diameters of the outer and inner flame-holder rings are $21\frac{1}{4}$ and $9\frac{7}{8}$ inches, respectively; the included angle of the gutters is 35°; and the distance across the open ends of the gutters is $1\frac{1}{2}$ inches.

A cooling liner extended the full length of the combustion chamber, and a $\frac{1}{2}$-inch radial gap was provided between the liner and the outer shell through which flowed part of the exhaust gas at approximately turbine-outlet temperature.

Burner D. - Burner D (fig. 4), which was installed on the experimental version of the J47 engine, has an over-all length, including the diffuser section, of about 9 feet and a maximum diameter of 32 inches. The exhaust gas was diffused to the 32-inch-diameter combustion chamber, which is 4 feet in length. The flame holder was installed at the forward end of the combustion chamber, thereby giving a 4-foot burning length upstream of the fixed-area conical exhaust nozzle. The diameter at the outlet of the exhaust nozzle is $25\frac{1}{4}$ inches.

Fuel was injected in the diffuser 14 inches upstream of the flame holder through 12 stream lined spray tubes similar to those used in burner C. Each tube had four pairs of orifices that injected fuel from opposite sides of the tubes into the gas stream normal to the direction of flow. The downstream end of the inner cone was cut off where it was 14 inches in diameter and a concave dome was installed that provided a large turbulent region for the purpose of seating a stabilizing flame in the center of the pipe.

The flame holder was a two-ring V-gutter flame holder, similar to those used in burners B and C, and blocked 32 percent of the burner cross-sectional area. The mean diameters of the outer and inner flame-holder rings are 23 and 14 inches, respectively; the included angle of the gutters is 35°; and the distance across the open end of the gutters is $1\frac{13}{16}$ inches.

A cooling liner, similar to that used in burner C, extended the full length of the combustion chamber and 12 inches into the exhaust nozzle. A $\frac{1}{2}$-inch radial air gap was provided between the liner and the outer shell through which part of the exhaust gas flowed.

TAIL-PIPE-BURNER PERFORMANCE

Burner A. - Performance data obtained with burner A over a range of flight Mach numbers at an altitude of 20,000 feet are presented in figures 5 and 6. These data were obtained at maximum engine speed with a turbine-outlet temperature of approximately 1600° R. The burner-inlet velocity varied from 440 to 480 feet per second for these conditions. The augmented thrust was obtained with the tail-pipe burner installed and the normal thrust was obtained with the standard engine tail pipe.

With tail-pipe burning (fig. 5), the ratio of augmented thrust to normal thrust increased from a value of 1.27 at a flight Mach number of 0.25 to 1.84 at a flight Mach number of 0.85. When the tail-pipe burner was inoperative, the thrust obtainable at limiting turbine-outlet temperatures was 4 percent less than that available with the standard engine tail pipe at the same operating conditions.

The specific fuel consumption with and without tail-pipe burning is shown in figure 6. With tail-pipe burning the specific fuel consumption decreased rapidly as the flight Mach number was raised, varying from a value of about 3.25 at a flight Mach number

of 0.25 to a value of 2.10 at a flight Mach number of 0.85. The specific fuel consumption with the standard engine tail pipe and exhaust nozzle was 1.40 at a flight Mach number of 0.85.

The operable range of tail-pipe fuel-air ratios at an altitude of 20,000 feet is shown in figure 7. Tail-pipe fuel-air ratio is defined as the ratio of tail-pipe fuel flow to the unburned air flow entering the tail pipe. The maximum operable tail-pipe fuel-air ratio was limited by turbine-outlet temperature and the minimum fuel-air ratio by lean combustion blow-out. At a flight Mach number of 0.85 at an altitude of 20,000 feet, it was possible to operate burner A between tail-pipe fuel-air ratios of 0.0395 and 0.0486. The maximum operable fuel-air ratio is significant only for the exhaust nozzle used with burner A. With a larger outlet area, the burner could have been operated at higher tail-pipe fuel-air ratios.

The altitude limits of operation at maximum engine speed and turbine-outlet temperature of about 1625° R are shown in figure 8. At each flight Mach number, a band of uncertain operation amounting to about 8000 feet in altitude was encountered within which combustion blow-out occurred. Altitudes at which the engine could be operated without encountering combustion blow-out varied from 24,600 feet at a Mach number of 0.25 to 34,200 feet at a Mach number of 1.0. Over the entire range of flight conditions, this limit of combustion blow-out occurred at an approximately constant burner-inlet pressure.

Burner B. - Performance data obtained with burner B are presented in figures 9 and 10 for a range of flight Mach numbers at an altitude of 25,000 feet (reference 1). These data were obtained at maximum engine speed and the turbine-outlet temperature with tail-pipe burning was 1650° R, whereas the turbine-outlet temperature with the standard engine tail pipe varied from 1650° R at a flight Mach number of 0.25 to 1620° R at a flight Mach number of 0.72. The burner-inlet velocity was approximately 455 feet per second for these conditions.

The ratio of augmented thrust to normal thrust (fig. 9) increased from a value of 1.31 at a flight Mach number of 0.25 to 1.73 at a flight Mach number of 0.72. The burner-outlet temperature increased slightly with flight Mach number, reaching a value of 3470° R at a flight Mach number of 0.72. This temperature corresponds to a burner temperature rise of 1820° R and to an over-all fuel-air ratio of 0.052, where the over-all fuel-air ratio is defined as the engine fuel plus tail-pipe fuel divided by the total air flow.

The specific fuel consumption with and without tail-pipe burning (fig. 10) varied only slightly over the flight conditions investigated. At a flight Mach number of 0.72, the specific fuel consumption was 2.55 with tail-pipe burning compared with 1.19 with the standard engine tail pipe.

The tail-pipe combustion efficiency is presented in figure 11 as a function of tail-pipe fuel-air ratio. As mentioned previously, tail-pipe fuel-air ratio is defined as the ratio of tail-pipe fuel flow to unburned air flow entering the tail pipe. Because the tail-pipe fuel-air ratio was varied by changing the tail-pipe fuel flow with a fixed-area exhaust nozzle, the conditions at the burner inlet also changed.

Variations in burner-inlet total temperature, total pressure, and velocity with tail-pipe fuel-air ratio are also shown in figure 11. For the range of fuel-air ratios investigated, the total temperature, the total pressure, and the burner-inlet velocity increased with fuel-air ratio. As the tail-pipe fuel-air ratio was raised, the combustion efficiency dropped from a peak value of 0.96 at a tail-pipe fuel-air ratio of 0.025 to a value of 0.86 at limiting turbine-outlet temperature of 1650° R and tail-pipe fuel-air ratio of 0.050, the condition for which thrust and specific fuel consumption data are presented in figures 9 and 10. The increase in burner-inlet pressure accompanying the change in flight Mach number from 0.26 to 0.84 had no apparent effect on the tail-pipe combustion efficiency. The primary factor affecting combustion efficiency is believed to be the fuel distribution in the tail-pipe burner, because at a given fuel-air ratio changes in burner-inlet pressure had no apparent effect on combustion efficiency.

The operable range of tail-pipe fuel-air ratios at an altitude of 25,000 feet is shown in figure 12 as a function of flight Mach number. The maximum fuel-air ratio was limited by turbine-outlet temperature and the minimum fuel-air ratio by lean combustion blow-out. At a flight Mach number of 0.72, stable burner operation was possible at tail-pipe fuel-air ratios between 0.024 and 0.053. The minimum operable fuel-air ratio for burner B was somewhat lower than that for burner A, which was 0.041 at a Mach number of 0.72. The maximum fuel-air ratio is significant only for the size exhaust nozzle used.

Burner C. - Performance data for burner C at an altitude of 25,000 feet over a range of flight Mach numbers are presented in figures 13 and 14. These data were obtained at maximum engine speed

and at turbine-outlet temperature (both with and without tail-pipe burning) of 1600° R. The burner-inlet velocity was about 415 feet per second for these flight conditions.

The ratio of augmented thrust to normal thrust with tail-pipe burning (fig. 13) increased from 1.41 at a flight Mach number of 0.27 to 1.74 at a flight Mach number of 0.92. The burner-outlet temperature increased slightly with flight Mach number, reaching a value of 3150° R at a flight Mach number of 0.92. This temperature corresponds to a burner temperature rise of 1750° R with an overall fuel-air ratio of 0.475. The net thrust obtained at limiting turbine-outlet temperature with the tail-pipe burner inoperative is shown to be about 1 percent less than the thrust obtainable with the standard engine tail pipe. This small loss in thrust results from the fact that the ratio of total-pressure loss between the turbine outlet and exhaust-nozzle outlet to the turbine-outlet total pressure is only slightly higher for the tail-pipe burner (0.025) than with the standard tail pipe (0.010) at the same turbine-outlet conditions. Neither value includes the pressure loss across the exhaust-nozzle outlet.

The specific fuel consumptions with and without tail-pipe burning increased only slightly with flight Mach number (fig. 14). At a flight Mach number of 0.92, the specific fuel consumption was 2.21 with tail-pipe burning compared with 1.26 with the standard engine. The specific fuel consumption with tail-pipe burning was slightly lower for burner C than for burner B. However, burner B, as shown subsequently, was operated at a higher tail-pipe fuel-air ratio and thus a greater percentage of the total fuel flow was being burned in the low-efficiency part of the engine plus tail-pipe-burner cycle.

Tail-pipe combustion efficiency is presented as a function of tail-pipe fuel-air ratio for a range of flight Mach numbers at an altitude of 25,000 feet (fig. 15) and for a range of altitudes at a flight Mach number of 0.27 (fig. 16). These data were also obtained with a fixed-area exhaust nozzle, and therefore, the variations in burner-inlet total temperature, total pressure, and velocity are shown in the figures. The burner-inlet temperature and pressure increased with tail-pipe fuel-air ratio, whereas the burner-inlet velocity remained substantially constant between 410 and 420 feet per second. At a given fuel-air ratio, the burner-inlet temperature remained approximately constant with changes in altitude and flight Mach number. Combustion efficiency increased rapidly with tail-pipe fuel-air ratio, reaching a peak at a fuel-air ratio of about 0.030. The combustion efficiency dropped off slightly at higher fuel-air ratios.

Over the range of flight Mach numbers investigated, changes in tail-pipe pressure due to variations in flight Mach number (fig. 15) or in altitude up to 35,000 feet (fig. 16) had no effect on the combustion efficiency. Increasing the altitude from 35,000 to 45,000 feet at a flight Mach number of 0.27 did result in a decrease in combustion efficiency amounting to about 0.10 at a turbine-outlet temperature of 1600° R. The trend of these combustion efficiency data with fuel-air ratio up to an altitude of 35,000 feet is again attributed to the fuel distribution in the tail-pipe burner because changing the pressure at a given fuel-air ratio within the range of pressure investigated had no effect on the combustion efficiency. With this particular burner-inlet velocity and fuel distribution, the critical burner-inlet pressure is reached between altitudes of 35,000 and 45,000 feet at a flight Mach number of 0.27, where the pressure then becomes a principle variable affecting the combustion efficiency.

The operable range of tail-pipe fuel-air ratios is shown in figure 17 as a function of altitude at a flight Mach number of 0.27. The maximum operable fuel-air ratio was limited by turbine-outlet temperature, whereas the minimum fuel-air ratio was limited by lean combustion blow-out. At each altitude, combustion blow-out was encountered within the range of fuel-air ratios shown in figure 17 as the region of uncertain operation. The region of uncertain operation occurred at higher tail-pipe fuel-air ratios as the altitude was increased. At an altitude of 45,000 feet and a flight Mach number of 0.27, operation was possible at tail-pipe fuel-air ratios between 0.029 and 0.040; however, the maximum fuel-air ratio is significant only for the size exhaust nozzle used.

Burner D. - Performance data obtained with burner D are presented in figures 18 and 19 for an altitude of 25,000 feet and a range of flight Mach numbers. These data were obtained at maximum engine speed and the turbine-outlet temperature was 1675° R both with and without tail-pipe burning.

The ratio of augmented to normal thrust increased from 1.34 at a flight Mach number of 0.22 to 1.78 at a flight Mach number of 0.82 (fig. 18). Burner-outlet temperatures increased from 2975° to 3525° R with this increase in flight Mach number. The large increase in temperature is mainly attributed to an increase in engine component efficiency as the flight Mach number was raised. The burner-outlet temperature of 3525° R corresponds to a burner temperature rise of 1850° R with an over-all fuel-air ratio of 0.053. The total-pressure-loss ratio measured across the tail-pipe burner when it

was inoperative (0.050 to 0.055) was slightly more than that measured across the standard engine tail pipe (0.045) at the same turbine-outlet conditions. As a result, the net thrust obtainable at limiting turbine-outlet temperatures with the burner inoperative was 0.5 to 1 percent less than that obtainable with the standard engine tail pipe.

The specific fuel consumption with tail-pipe burning (fig. 19) increased slightly up to a flight Mach number of about 0.45 and then decreased slightly at higher Mach numbers. The increase in specific fuel consumption at low flight Mach numbers is attributed to the corresponding increase in tail-pipe fuel-air ratio with no change in tail-pipe combustion efficiency. The decrease in specific fuel consumption at flight Mach numbers above 0.50 is attributed to the fact that the combustion efficiency is increased. This increase in combustion efficiency had a greater effect than the further increase in tail-pipe fuel-air ratio. At a flight Mach number of 0.81, the specific fuel consumption was 2.49 with tail-pipe burning compared with 1.38 with the standard engine tail pipe.

Tail-pipe combustion efficiency is presented as a function of tail-pipe fuel-air ratio for a range of flight Mach numbers at an altitude of 25,000 feet (fig. 20) and for a range of altitudes at a flight Mach number of 0.22 (fig. 21). The variations in burner-inlet total pressure, total temperature, and velocity as a function of tail-pipe fuel-air ratio are also shown in these figures. At a given fuel-air ratio, changes in flight Mach number had no effect on burner-inlet velocities, although increases in altitude raised the burner-inlet velocity. The combustion efficiency increased rapidly with fuel-air ratio and reached a maximum value at a fuel-air ratio of about 0.035 with the exception of the data obtained at 45,000 feet altitude where operation was erratic. For the range of fuel-air ratios investigated, the combustion efficiency remained essentially constant above a fuel-air ratio of 0.035.

The data in figure 20 show that the variations in burner-inlet pressure, accompanying changes in flight Mach number for the range of burner-inlet velocities from 460 to 515 feet per second, had a definite effect on the tail-pipe combustion efficiency. Raising the flight Mach number from 0.27 to 0.52, which represents a change in tail-pipe pressure of 15 percent, had no apparent effect on the combustion efficiency. A further increase in flight Mach number, however, from 0.52 to 0.81, which corresponds to a rise in tail-pipe pressure of about 30 percent, raised the peak combustion efficiency from 0.80 to 0.90.

Increasing the altitude from 15,000 to 35,000 feet resulted in uniform reductions in peak combustion efficiency from 0.85 to 0.76 (fig. 21), which accompanied a decrease in pressure and a slight increase in velocity. Between 35,000 and 45,000 feet, a critical region was encountered with the result that operation was somewhat erratic at 45,000 feet with considerably lower combustion efficiency. At a given tail-pipe fuel-air ratio (fig. 21), operation was possible in two regions of tail-pipe combustion efficiency at 45,000 feet altitude. In the higher region of combustion efficiency, it was observed through a periscope that the flame was seated on the entire flame holder. When the lower combustion efficiencies were encountered, however, observation through a periscope revealed that the flame on the outer ring of the flame holder had blown out.

The fuel distribution with burner D was quite similar to that of burner C and, although the diffuser inner cone was shorter and was larger in diameter at the downstream end, the primary difference between the two burners was an increase in burner-inlet velocity from about 415 feet per second with burner C to a range of 460 to 515 feet per second with burner D.

The operable range of tail-pipe fuel-air ratios is presented as a function of altitude at a flight Mach number of 0.20 in figure 22. The maximum operable tail-pipe fuel-air ratio was limited by turbine-outlet temperature and the minimum operable fuel-air ratio was limited by lean combustion blow-out. As with burner C, combustion blow-out occurred over a range of fuel-air ratios at each altitude. This range of combustion blow-out is indicated as the region of uncertain operation. The region of uncertain operation occurred at higher tail-pipe fuel-air ratios as the altitude was increased to 35,000 feet. The data obtained were insufficient to completely determine the region of uncertain operation at 45,000 feet. The rapid reduction in maximum tail-pipe fuel-air ratio at altitudes up to 35,000 feet is attributed to lowered engine component efficiency at the high altitudes. Operation at a somewhat higher fuel-air ratio at 45,000 feet than was possible at 35,000 feet is attributed to the large drop in combustion efficiency between these two altitudes, which, as a result, required a considerably higher tail-pipe fuel-air ratio at 45,000 feet in order to obtain limiting turbine-outlet temperature. At 35,000 feet, operation was possible between tail-pipe fuel-air ratios of 0.031 and 0.038. The minimum fuel-air ratio was slightly higher than that with burner C, 0.026 at 35,000 feet. The maximum fuel-air ratio is significant only for the size exhaust nozzle used.

SUMMARY OF RESULTS

The data presented herein showed that at an altitude of 25,000 feet and a flight Mach number of 0.85 it was possible to obtain thrust gains with tail-pipe burning amounting to about 0.80 of the normal thrust. The data also showed that up to 35,000 feet altitude it was possible to maintain the tail-pipe combustion efficiencies in the region of 0.85 with burner-outlet temperatures of about 3500° R. Burner-inlet velocity was shown to be a principle factor in maintaining the combustion efficiency approximately constant over a wide range of flight conditions.

With a burner having an inlet velocity of 415 feet per second, the combustion efficiency was unaffected by changes in flight Mach number up to 0.92 at 25,000 feet altitude and changes in altitude up to 35,000 feet at a flight Mach number 0.27. With a burner having an inlet velocity of about 460 to 515 feet per second, however, increasing the burner-inlet pressure by raising the flight Mach number from 0.52 to 0.81 at 25,000 feet altitude increased the peak combustion efficiency from 0.80 to 0.90. Increases in burner-inlet velocity were also shown to raise the tail-pipe fuel-air ratio at which lean blow-out of the burner occurred at all altitudes.

REFERENCE

1. Fleming, William A., and Wallner, Lewis A.: Altitude-Wind-Tunnel Investigation of Tail-Pipe Burning with a Westinghouse X24C-4B Axial-Flow Turbojet Engine. NACA RM No. E8J25e, 1948.

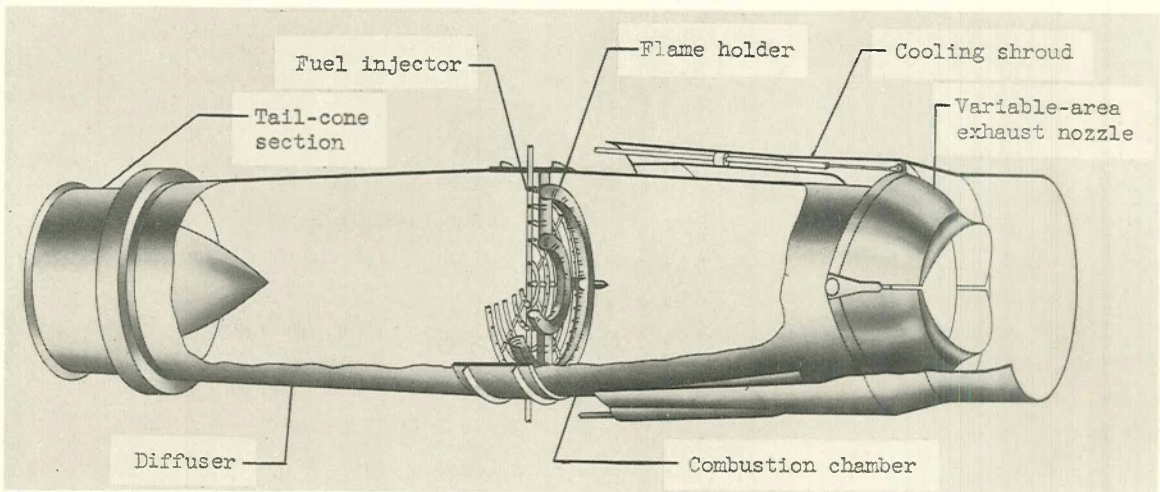

Figure 1. - Burner A.

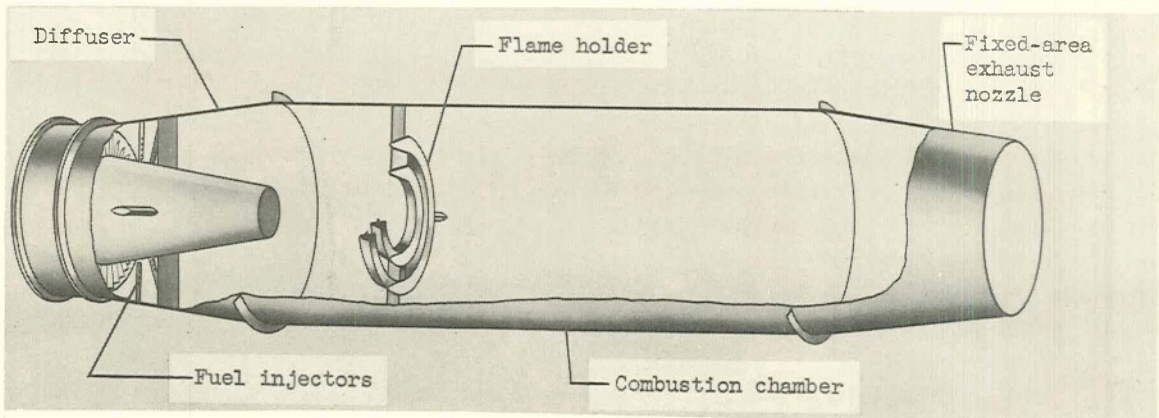

Figure 2. - Burner B.

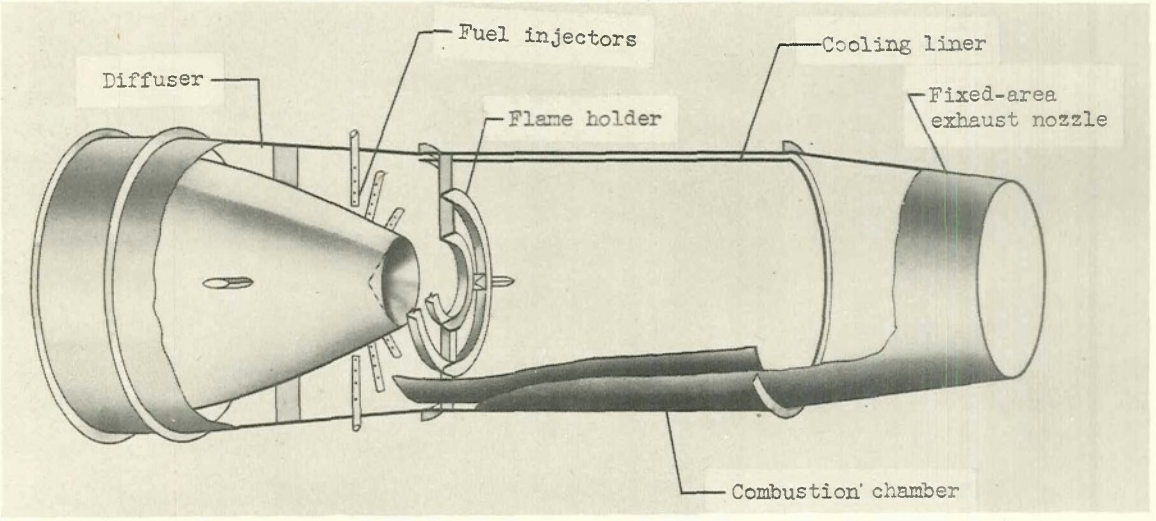

Figure 3. - Burner C.

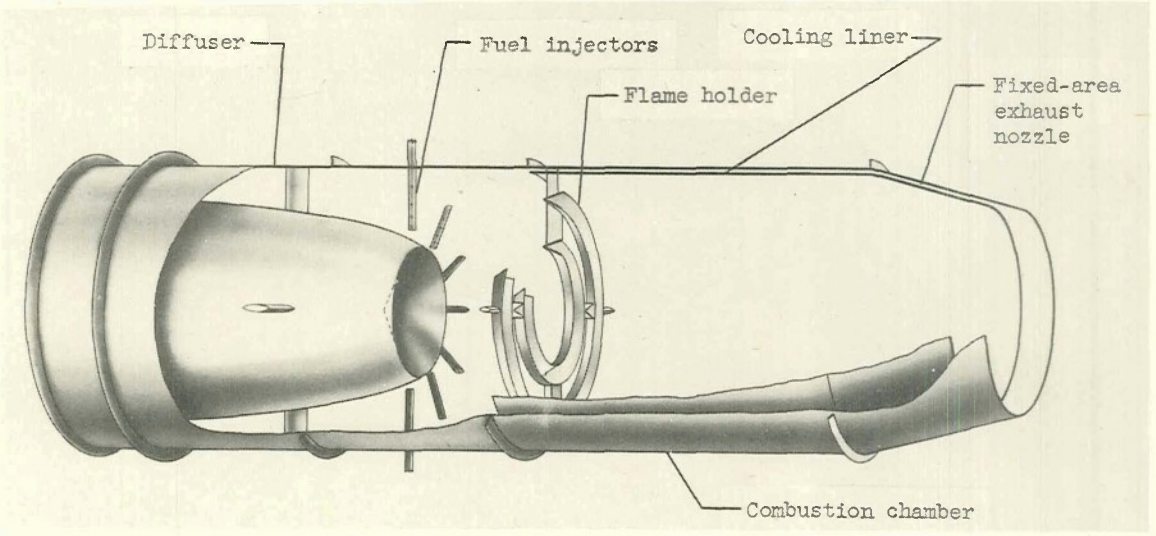

Figure 4. - Burner D.

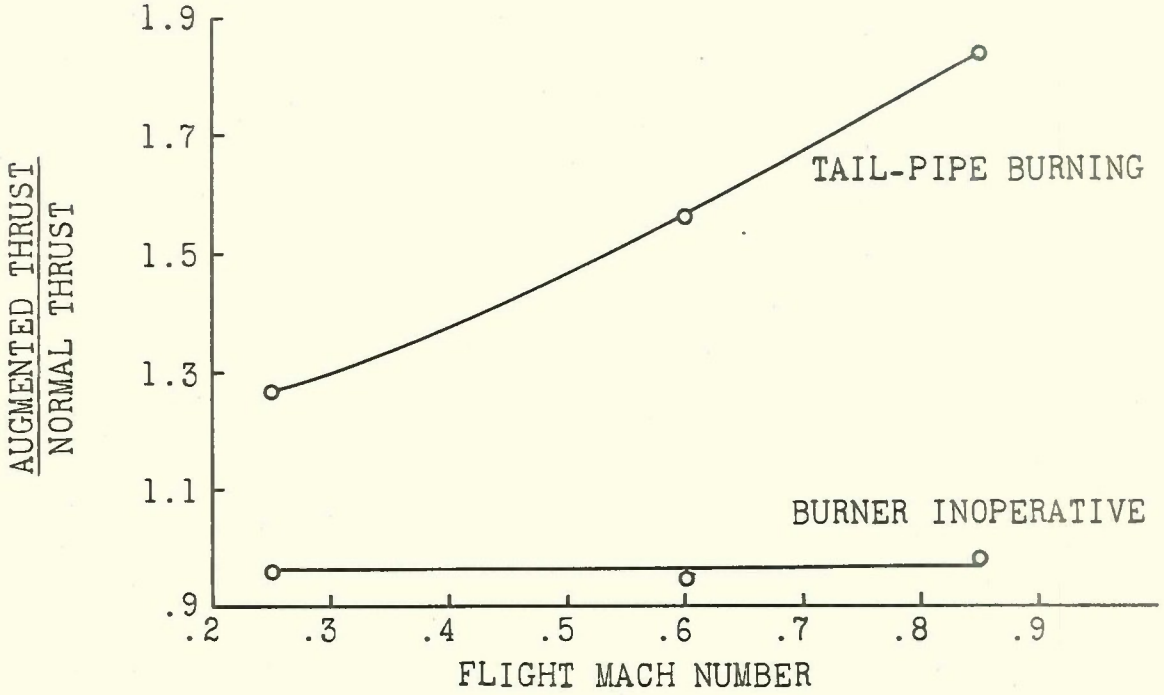

Figure 5. - Thrust performance for burner A. J34 engine; altitude, 20,000 feet; burner-inlet velocity, 440 to 480 feet per second; turbine-outlet temperature, 1600° R.

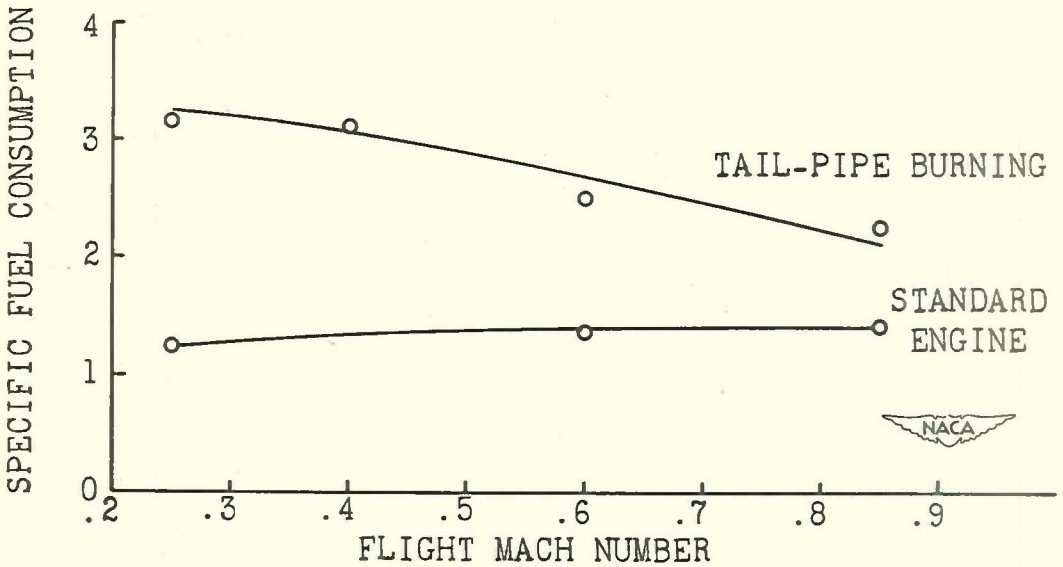

Figure 6. - Comparison of specific fuel consumption for J34 engine with standard tail pipe and with burner A. Altitude, 20,000 feet; burner-inlet velocity, 440 to 480 feet per second; turbine-outlet temperature, 1600° R.

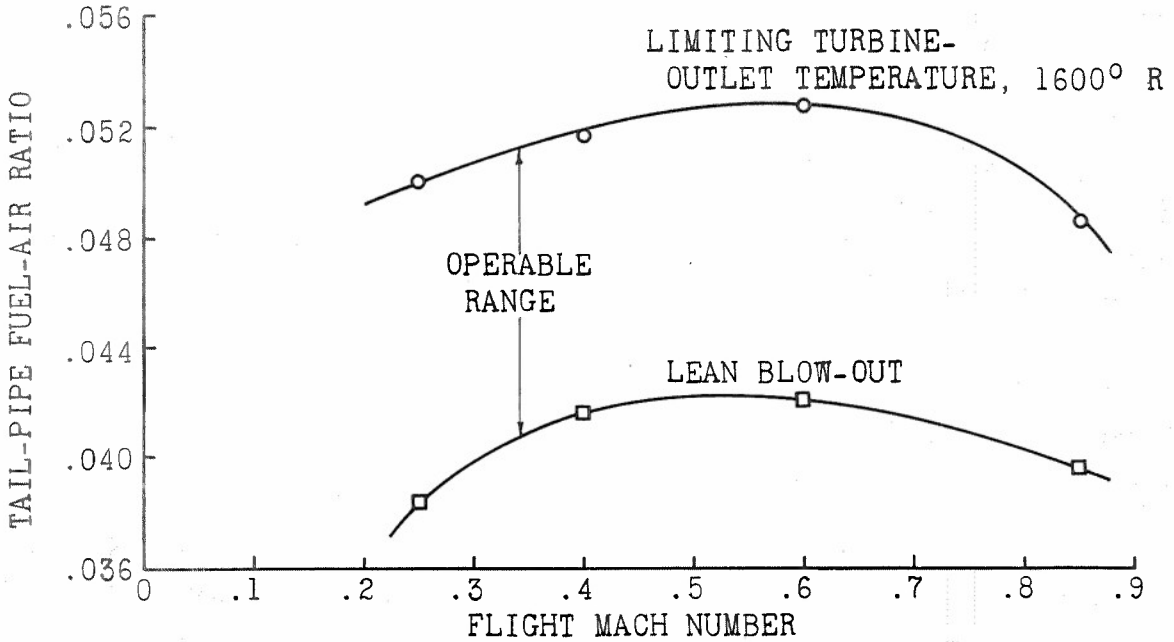

Figure 7. - Operable range of tail-pipe fuel-air ratios for burner A. J34 engine; altitude, 20,000 feet; burner-inlet velocity, 440 to 480 feet per second.

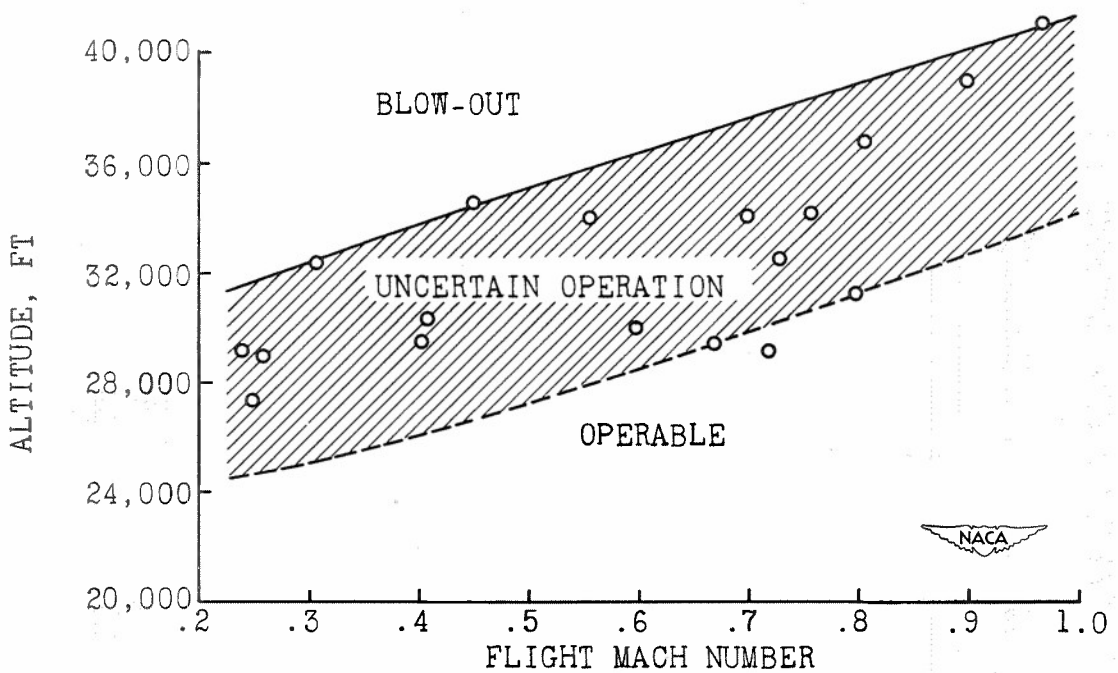

Figure 8. - Altitude limits of operation for burner A. J34 engine; burner-inlet velocity, 350 to 500 feet per second; turbine-outlet temperature, 1625° R.

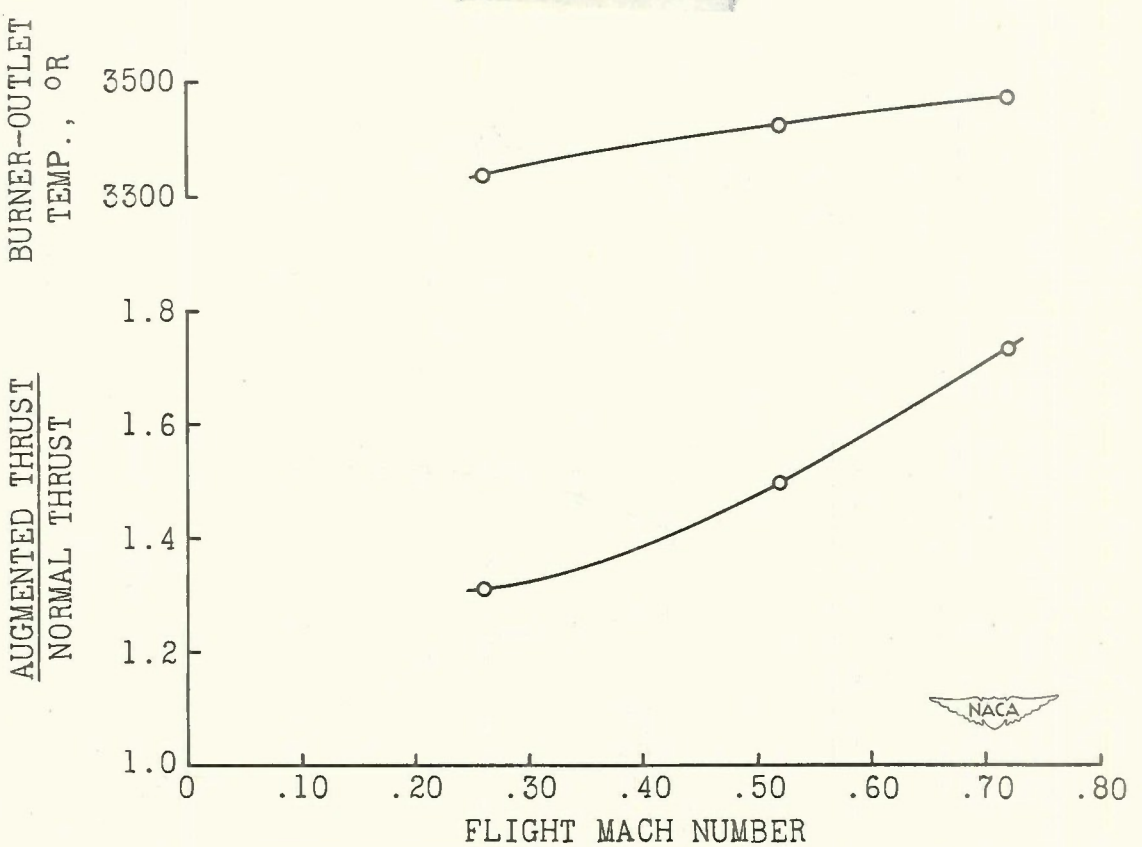

Figure 9. - Thrust performance and burner-outlet temperature for burner B. J34 engine; altitude, 25,000 feet; burner-inlet velocity, 455 feet per second; turbine-outlet temperature, 1650° R.

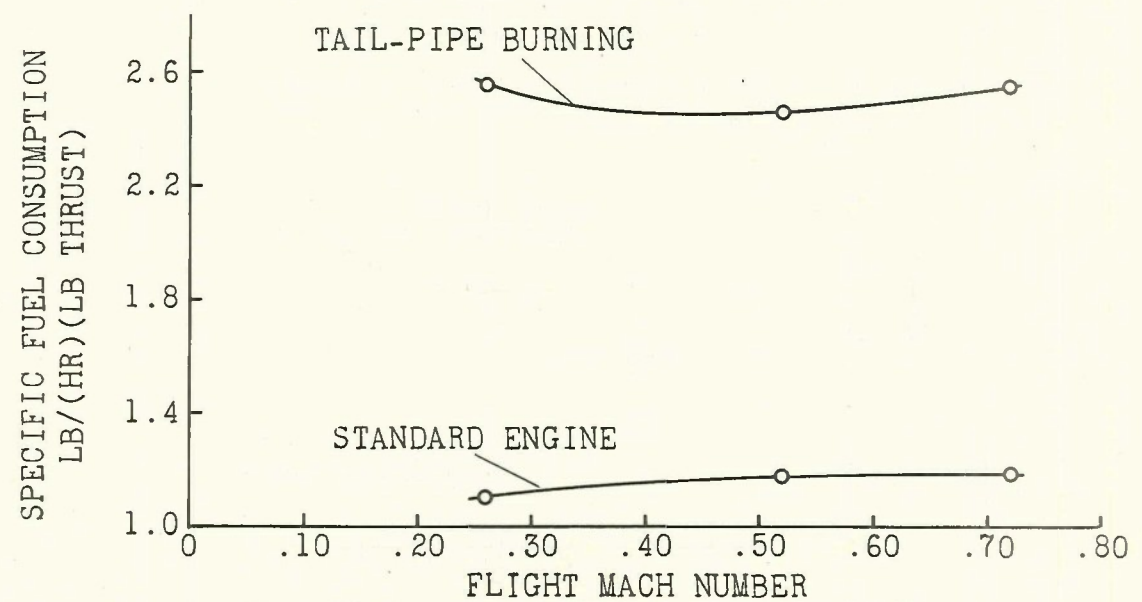

Figure 10. - Comparison of specific fuel consumption for J34 engine with standard tail pipe and with burner B. Altitude, 25,000 feet; burner-inlet velocity, 455 feet per second; turbine-outlet temperature, approximately 1650° R.

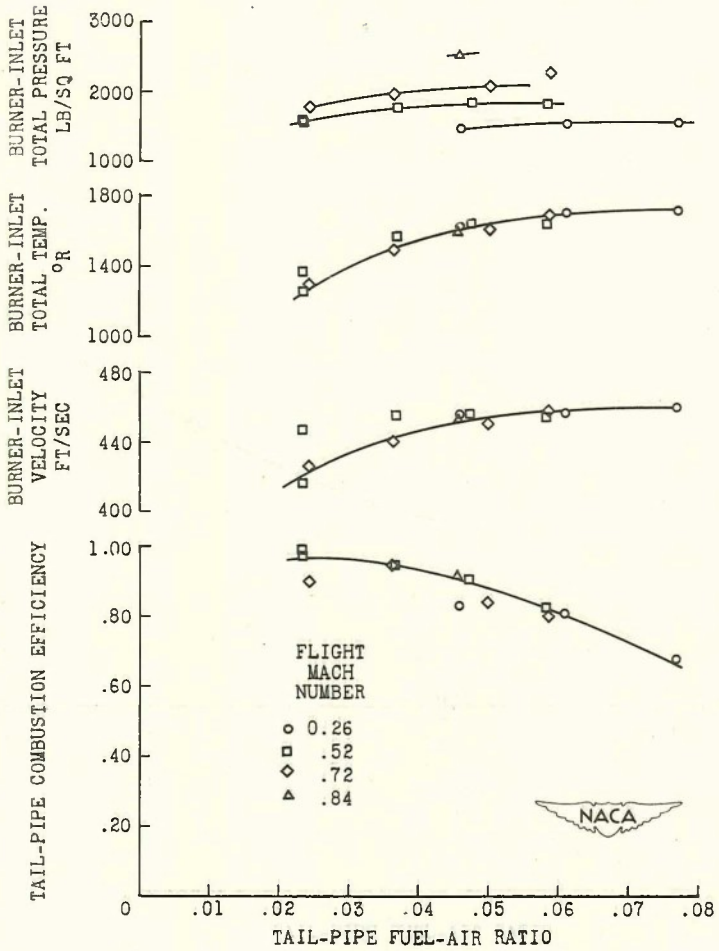

Figure 11. - Variation of combustion efficiency, burner-inlet total temperature, total pressure, and velocity with tail-pipe fuel-air ratio for burner B. J34 engine; altitude, 25,000 feet.

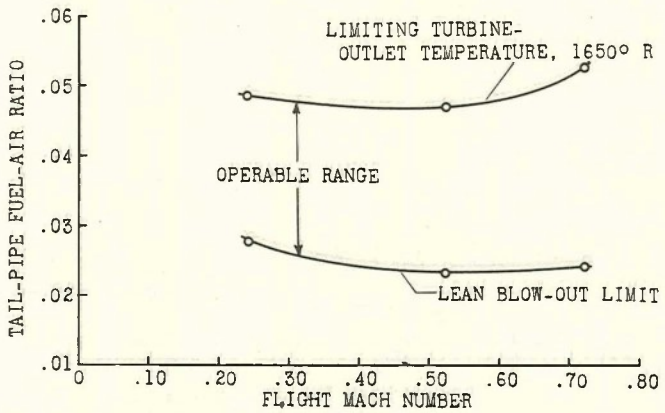

Figure 12. - Operable range of tail-pipe fuel-air ratios for burner B. J34 engine; altitude, 25,000 feet; burner-inlet velocity, 420 to 460 feet per second.

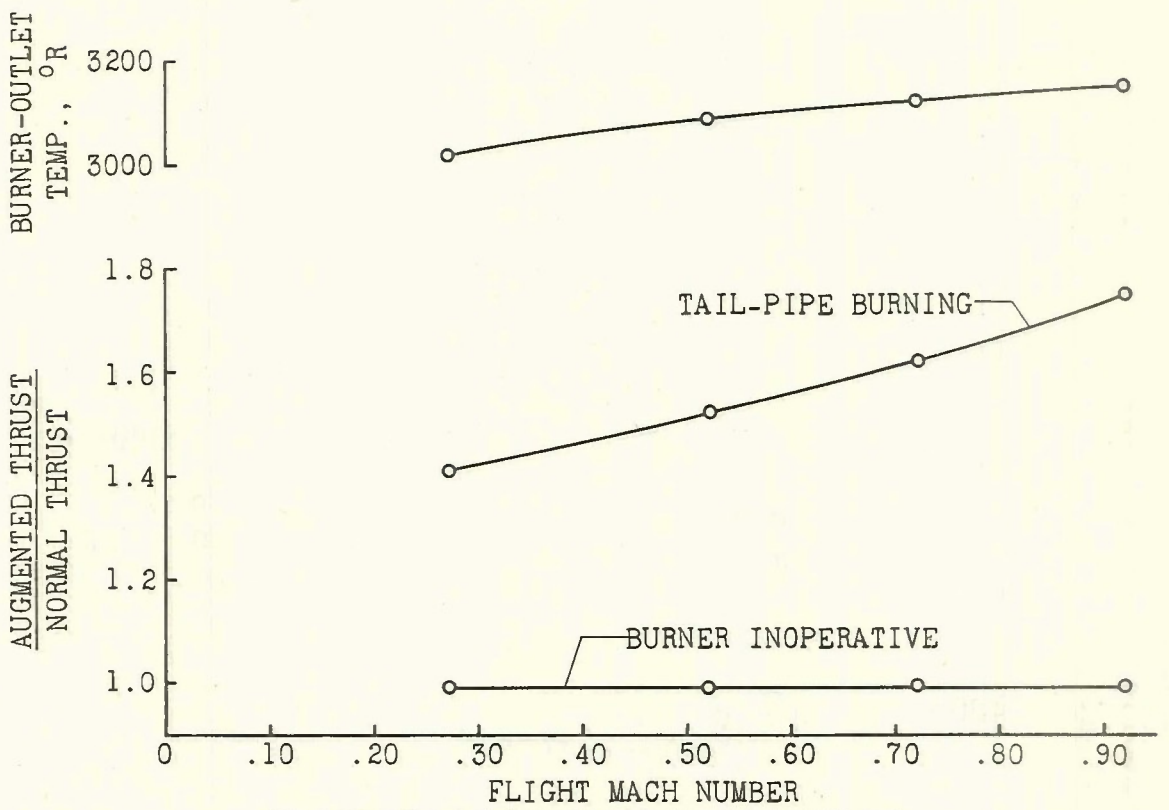

Figure 13. - Thrust performance and burner-outlet temperature for burner C. J35 engine; altitude, 25,000 feet; burner-inlet velocity, 415 feet per second; turbine-outlet temperature, 1600° R.

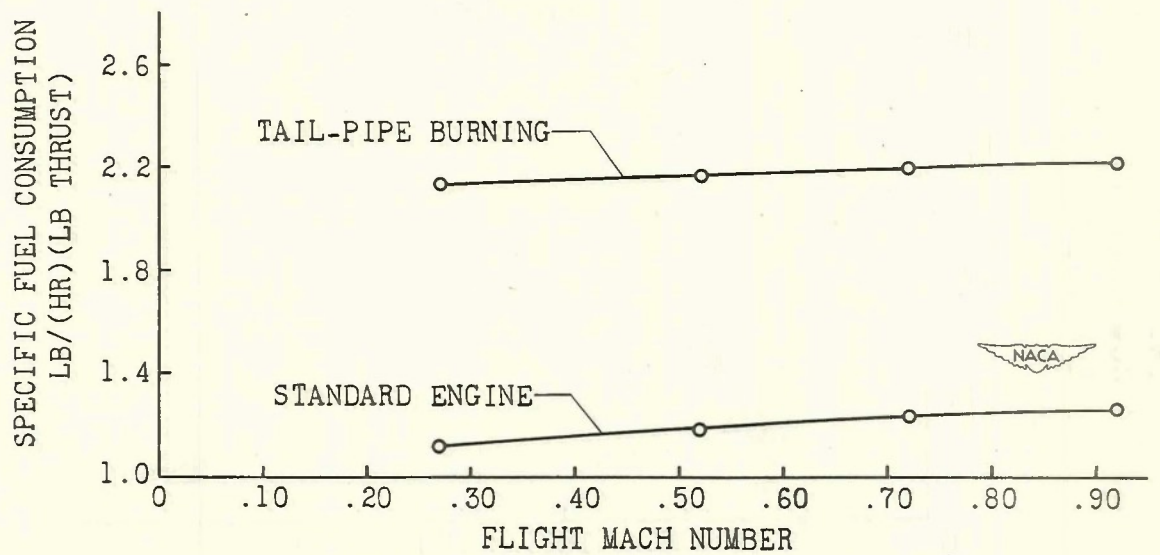

Figure 14. - Comparison of specific fuel consumption for J35 engine with standard tail pipe and with burner C. Altitude, 25,000 feet; burner-inlet velocity, 415 feet per second; turbine-outlet temperature, 1600° R.

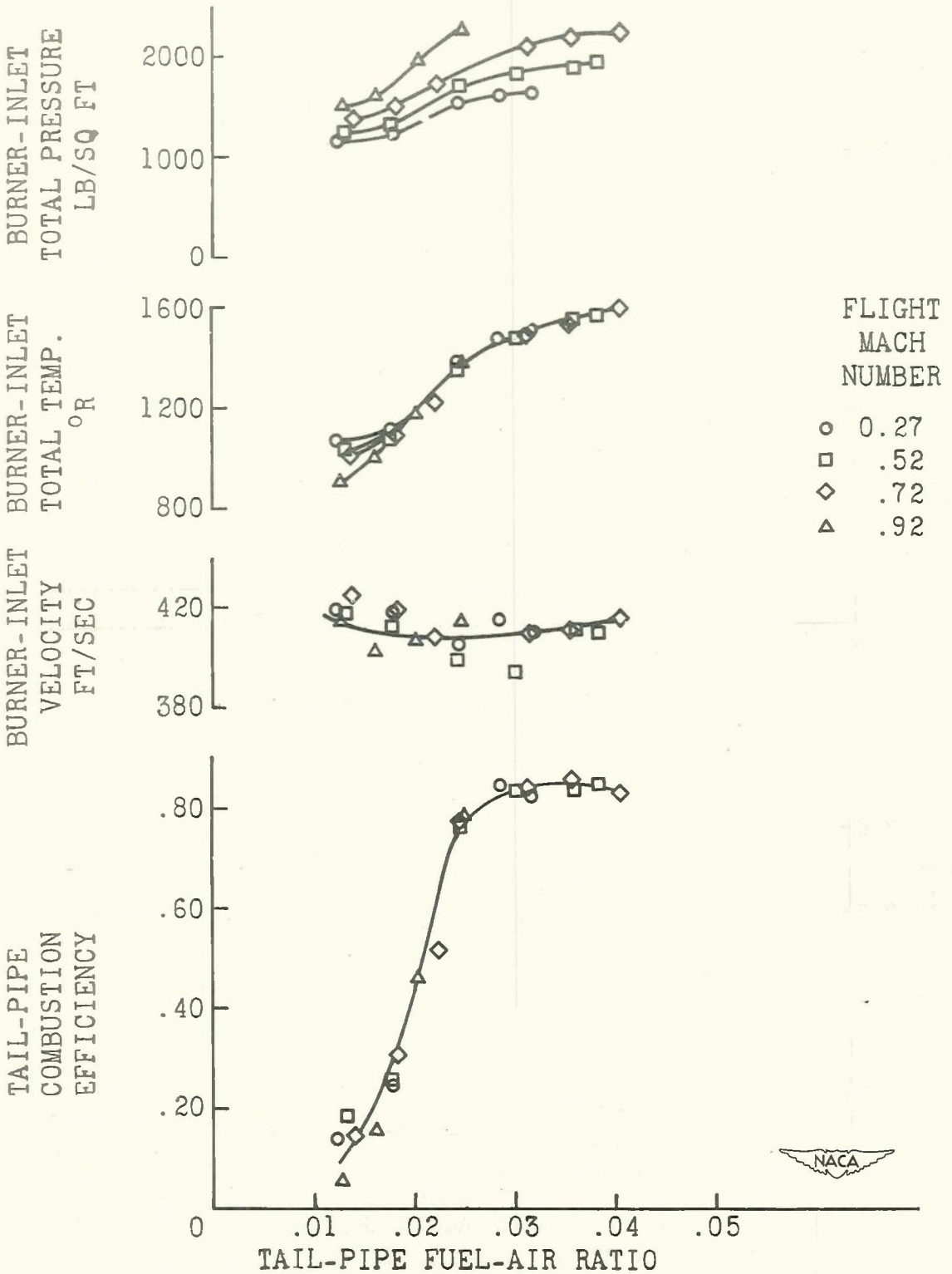

Figure 15. - Variation of combustion efficiency, burner-inlet total temperature, total pressure, and velocity with tail-pipe fuel-air ratio for burner C at altitude of 25,000 feet. J35 engine.

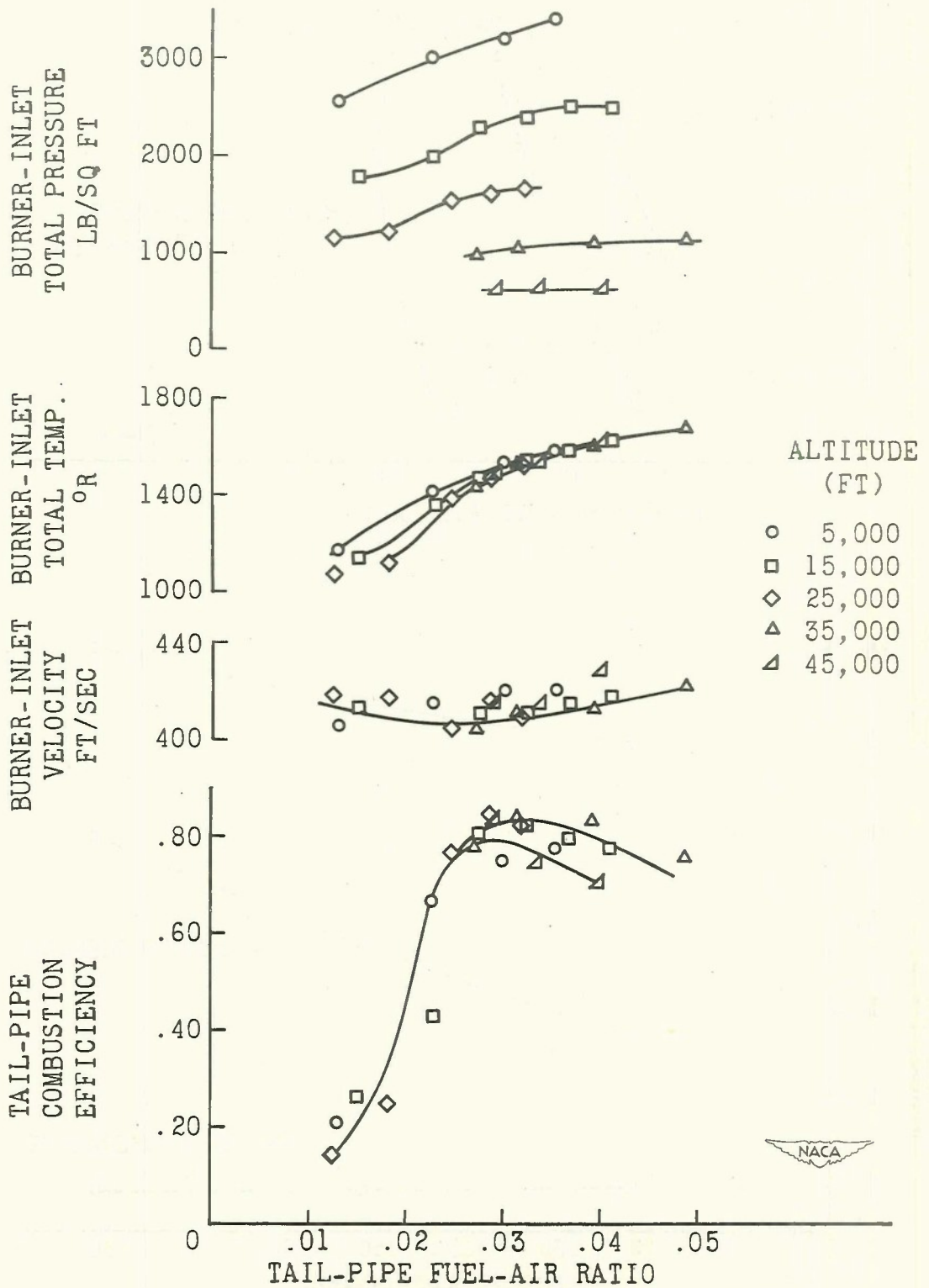

Figure 16. - Variation of combustion efficiency, burner-inlet total temperature, total pressure, and velocity with tail-pipe fuel-air ratio for burner C at Mach number of 0.27. J35 engine.

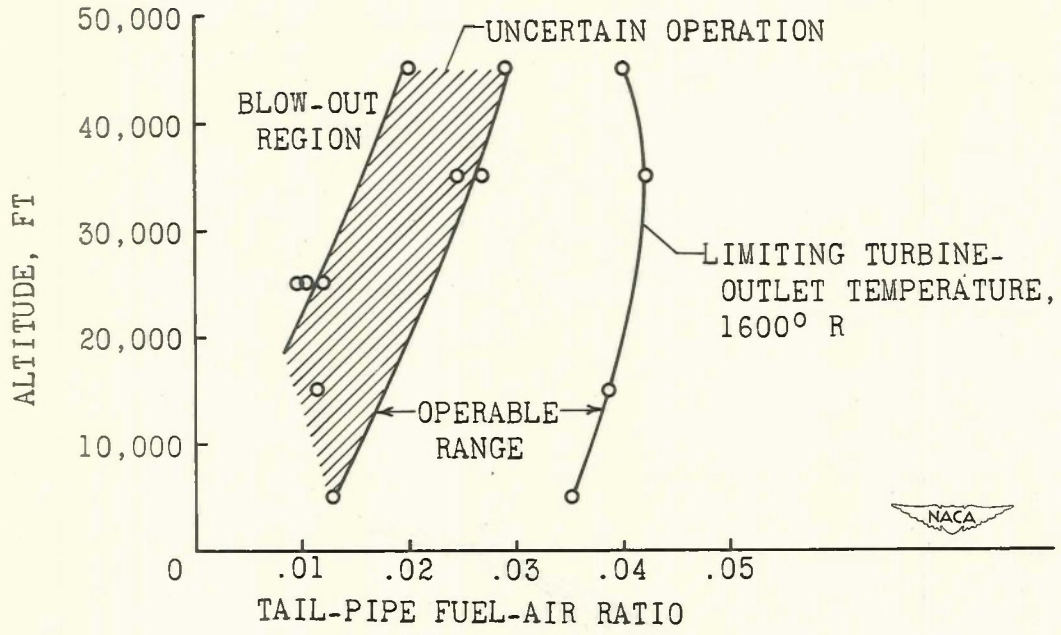

Figure 17. - Operable range of tail-pipe fuel-air ratios for burner C. J35 engine; Mach number, 0.27; burner-inlet velocity, 415 feet per second.

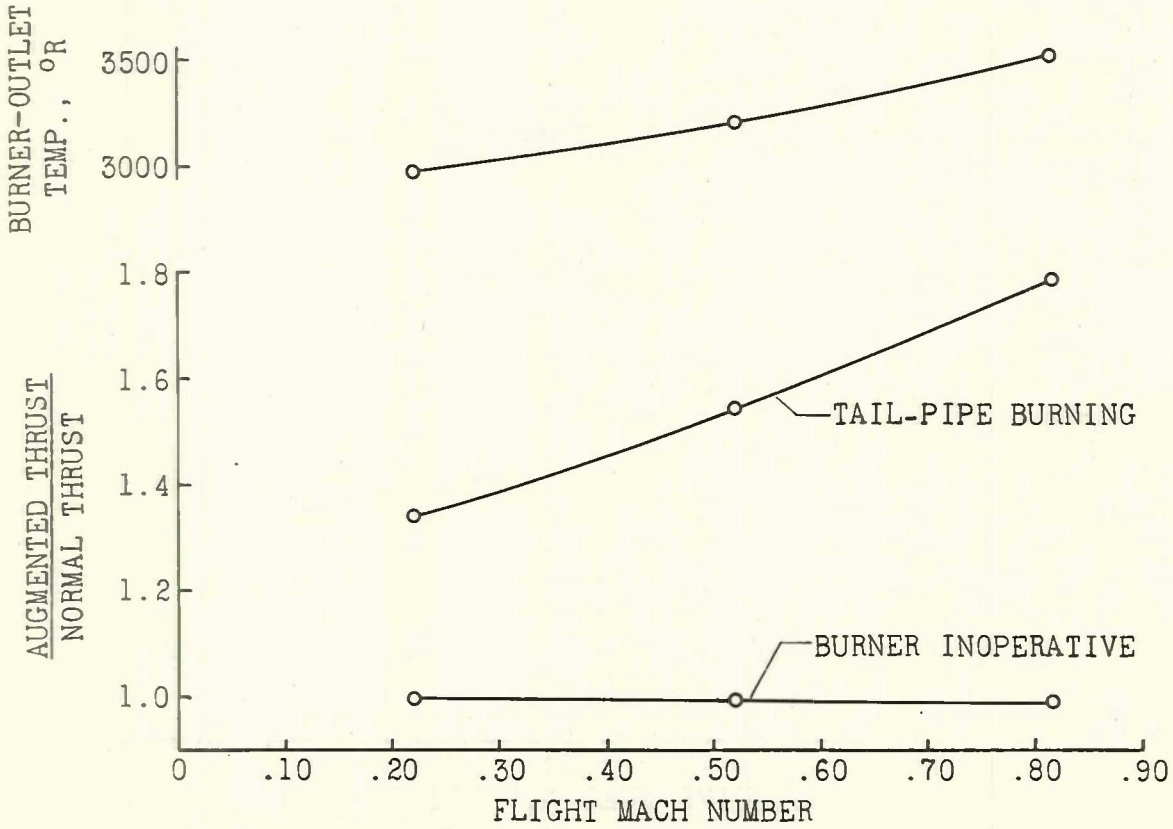

Figure 18. - Thrust performance and burner-outlet temperature for burner D. J47 engine; altitude, 25,000 feet; burner-inlet temperature, 465 feet per second; turbine-outlet temperature, 1675° R.

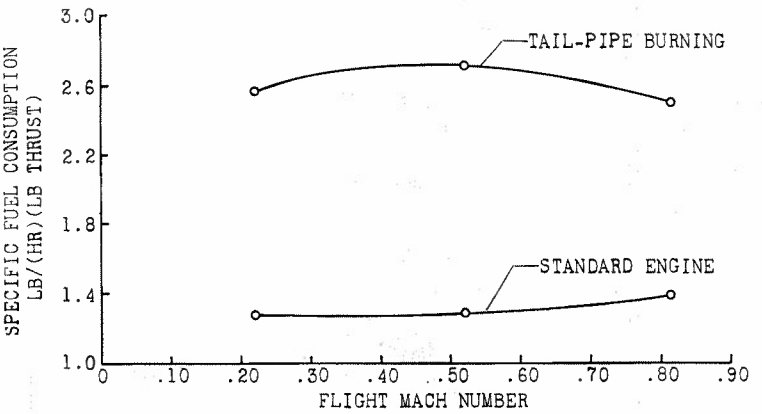

Figure 19. - Comparison of specific fuel consumption for J47 engine with standard tail pipe and with burner D. Altitude, 25,000 feet; burner-inlet velocity, 465 feet per second; turbine-outlet temperature, 1675° R.

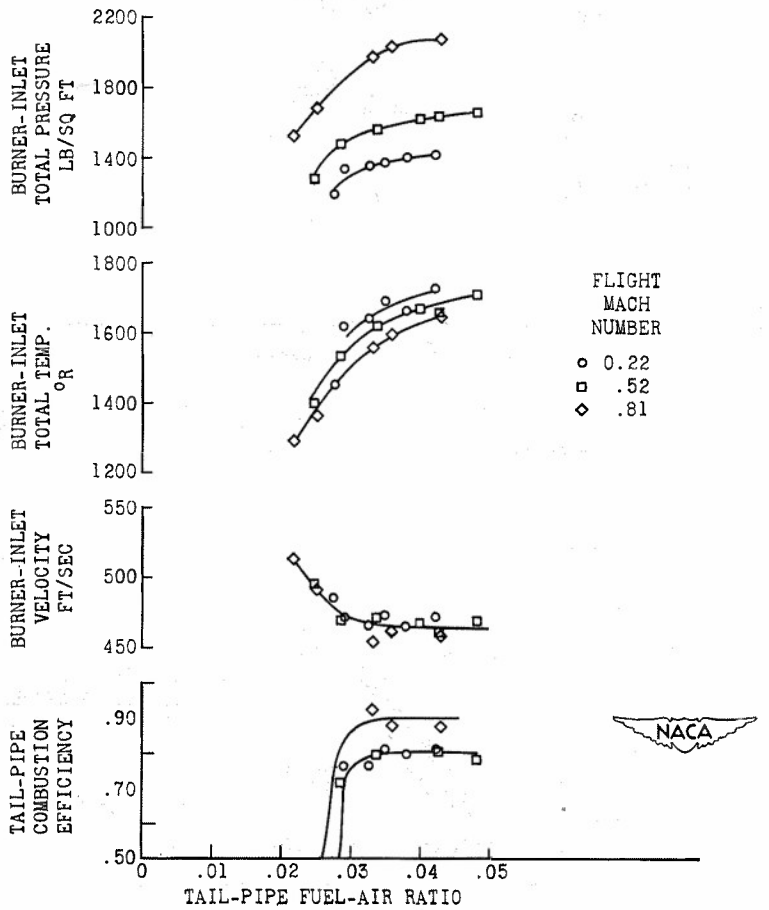

Figure 20. - Variation of combustion efficiency, burner-inlet total temperature, total pressure, and velocity with tail-pipe fuel-air ratio for burner D at altitude of 25,000 feet. J47 engine.

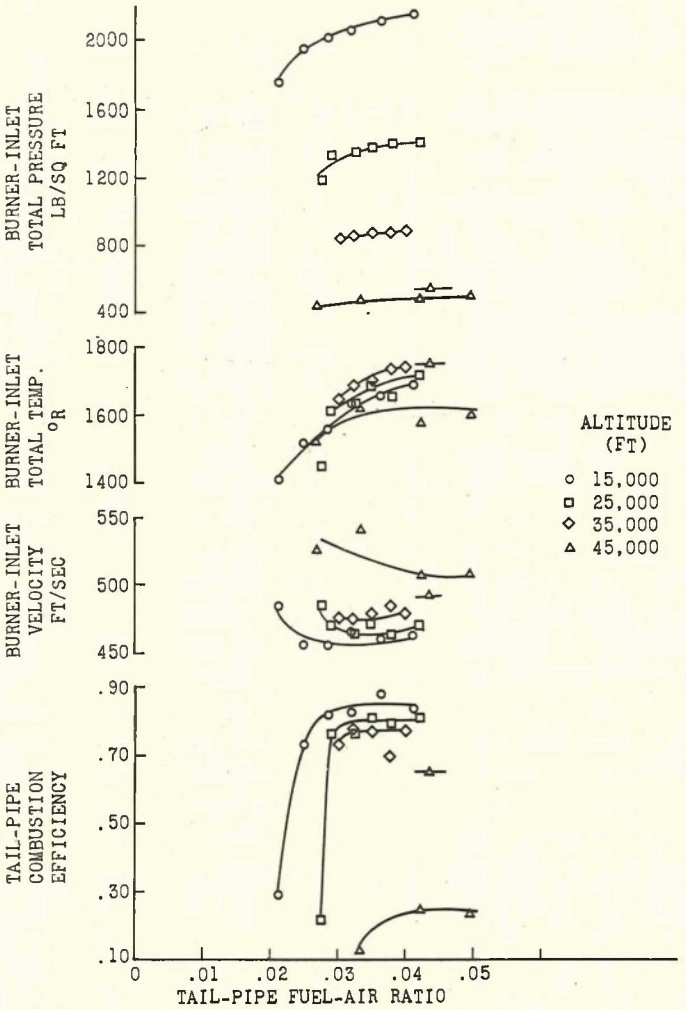

Figure 21. - Variation of combustion efficiency, burner-inlet total temperature, total pressure, and velocity with tail-pipe fuel-air ratio for burner D at Mach number of 0.22. J47 engine.

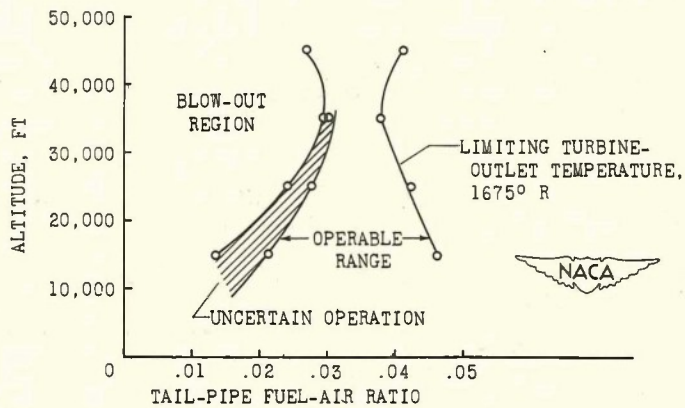

Figure 22. - Operable range of tail-pipe fuel-air ratios for burner D. J47 engine; Mach number, 0.20; burner-inlet velocity, 460 to 515 feet per second.

COOLING OF TAIL-PIPE BURNERS

By William K. Koffel
and Newell D. Sanders

Lewis Flight Propulsion Laboratory

INTRODUCTION

Combustion temperatures of 3000° to 4000° R reached in tail-pipe burners make cooling necessary to prevent destruction of the burner shell and to avoid overheating the surrounding aircraft structure. The high-temperature alloys currently used in tail-pipe-burner construction have maximum allowable temperatures of about 2000° to 2200° R and airplane structures of aluminum alloys are limited to temperatures of about 660° to 760° R by strength considerations.

This paper presents some preliminary results of an analytical and experimental investigation of several methods for tail-pipe-burner cooling in progress at the NACA Lewis laboratory. A general method for computing the maximum wall temperature of cooling systems utilizing annular cooling passages is also given and applied to a system in which some of the turbine-outlet gas is used as the cooling fluid.

METHODS OF COOLING

Tail-pipe burner cooled by stratification of combustion. - The simplest means of tail-pipe-burner cooling is by stratification of combustion in order to preserve a relatively cool layer of gas between the hot combustion zone and the burner shell. This stratification can be accomplished with an annular-type flame holder having radial clearance from the shell sufficient to prevent impingement of the turbulent wake of burning gases on the shell. Cooling by stratification is present in varying degrees in all tail-pipe burners. Figure 1 illustrates the cooling of a thin shell combustion chamber by a combination of internal stratification and external convection and radiation to the free stream.

An experimental tail-pipe burner utilizing stratification plus external cooling by free convection and radiation to the surroundings was tried on a J35 engine in a sea-level static

test stand. The cylindrical shell of the experimental burner, which is constructed of $\frac{1}{16}$-inch-thick Inconel, has an internal diameter of $25\frac{3}{4}$ inches. The annular flame holder used in this burner has a semicircular cross section 2 inches wide at the downstream side and a mean diameter of 16 inches, leaving $3\frac{7}{8}$ inches of radial clearance to the shell. (See fig. 2 of second paper in this series.) The combustion zone extended 72 inches downstream of the flame holder to the exhaust-nozzle outlet; however, measurements of shell temperatures 48 and 72 inches downstream of the flame holder were nearly equal and were the highest shell temperatures measured.

Temperature of the shell measured 48 inches downstream from the flame holder and the average temperature of the turbine-outlet gas are shown in figure 2 as a function of the final combustion temperature. These data were obtained at rated engine speed and an average mass velocity of 18.8 pounds per second per square foot of burner flow area. The turbine-outlet temperature increased as the combustion temperature increased to 3000° R. At higher combustion temperatures, the turbine-outlet temperature was held at about 1715° R by increasing the flow area of the variable-area exhaust nozzle. The shell temperature followed the same trend as the turbine-outlet gases and the highest shell temperature measured was about 1650° R at a final combustion temperature of 3500° R.

The same tail-pipe burner with a modified diffuser was operated on a J34 engine in the altitude wind tunnel where external cooling by free convection and radiation was approximately the same as in the static test-stand installation. The downstream end of the shell was streaked with hot spots, which may have resulted from the lower velocity in the tail pipe for the smaller engine, and consequently the lower velocity gave sufficient time for the flame to reach the shell.

Visual observations of the same tail-pipe burner and original diffuser on another J35 engine in the altitude wind tunnel indicated that cooling was less effective, combustion efficiency was lower, and operational characteristics were poorer at altitude than at sea-level static conditions. The combustion efficiency and operational characteristics at altitude were improved by replacing the original annular flame holder with a two-ring V-gutter flame holder having a radial clearance of 4-1/16 inches and located 14 inches upstream of the position of the annular flame holder. The nozzle end of the tail-pipe burner was severely overheated and burned, indicating inadequate stratification.

These experiences illustrate that the stratification method of cooling is adversely affected by the requirements for service at high altitudes. The need for greater burner length, low velocities, and different flame-holder design for the high-altitude condition increases the difficulty of maintaining the cool layer of gas next to the shell for operation at low altitude.

Tail-pipe burner cooled by liquids. - Another method of cooling is shown in figure 3 in which a helical cooling coil encircles the burner shell. The use of fuel as a coolant was tried in several experimental tail-pipe burners and ram-jet burners. Although preheating and vaporizing the fuel as it passed through the cooling coil improved combustion efficiency, the quantity of fuel required for combustion was insufficient to hold the shell temperature at values where fuel cracking and coking do not occur. Fuel cooling was also subject to vapor lock and to consequent hot spots that, together with the high-temperature gradients in the shell between coils, caused buckling and rupture of welds.

The use of coolants other than fuel is more or less precluded by the necessity for the addition of plumbing, pumps, and a heat exchanger.

Tail-pipe burner cooled by turbine gases. - Another method of cooling conveys a portion of the high-pressure gases from the turbine outlet through an annular passage formed between an internal liner and the shell to insure a layer of relatively cool gases next to the shell (fig. 4). The internal liner assumes a temperature between the cooling-gas temperature and the combustion-gas temperature. Although the liner may be hotter than a shell cooled by stratification of combustion, low stresses make high temperatures in the liner less serious than high temperatures in the stressed shell. The advantages of this system are the built-in supply of high-pressure cooling gases that provide cooling under take-off conditions and the greater freedom in selecting flame holders for improved performance at high altitudes. One disadvantage is the small difference between the allowable temperature of the liner and the temperature of the cooling gases. This small difference limits the length of liner that may be adequately cooled.

An uninsulated tail-pipe burner with internal liner was used extensively in the investigations reported in the second and third papers of this series. A view of the upstream end of an experimental burner with an internal liner is shown in figure 5. This burner has a diameter of 32 inches and a length of 4 feet plus an exhaust

nozzle. The liner is 0.040-inch-thick Inconel and forms an annular passage $\frac{1}{2}$-inch high. Many schemes for supporting the liner were tried. The interlocking channels shown in figure 5 proved most successful in permitting freedom for thermal expansion and in supporting the liner against the pressure difference across it. Adequate cooling was provided over a wide range of operating conditions. More than 20 hours of operation with tail-pipe burning have been accumulated on one liner of this type with only minor distortions.

A tail-pipe burner similar to the one shown in figure 5 but having a shell diameter of 29 inches, a liner $\frac{1}{16}$-inch thick, and a two-ring V-gutter flame holder with a radial clearance of $3\frac{3}{4}$ inches was tested on a J35 engine. Temperatures of the liner, the cooling gas, and the shell measured 48 inches downstream of the flame holder are plotted against mass velocity in figure 6. The data were obtained at approximately rated turbine speed for an average mass ratio of cooling gas to combustion gas of 0.066 and an average final combustion temperature of 2860° R. The mass velocity was varied by changing the altitude and flight Mach number. At a mass velocity of 15.5 which corresponds to an altitude of 5000 feet and a flight Mach number of 0.27, the temperature of the liner and the shell were 2120° and 1430° R, respectively. This shell temperature is 160° colder and the liner temperature is 530° hotter than the shell temperature of 1590° R (fig. 2), corresponding to a final combustion temperature of 2860° R and a mass velocity of 18.8, which was obtained in sea-level static tests of the thin shell cooled by stratification of the combustion gases.

As altitude increased, the temperatures (fig. 6) of the liner and the shell decreased until an altitude of about 25,000 feet was reached. Between altitudes of 25,000 and 45,000 feet, the temperatures were approximately constant with a liner temperature of 1730° R and a shell temperature of 1250° R.

Tail-pipe burner cooled by air. - Another method for tail-pipe cooling utilizes an external cooling passage through which atmospheric air flows. One possible arrangement of such a system is shown in figure 7. Boundary-layer air enters flush-type inlets and flows through an annular passage formed by a shroud enclosing the shell. Air might also be rammed from the free stream. Neither of these configurations cool under static conditions; however, an ejector can be used at the exit to pump cooling air under static conditions.

An experimental tail-pipe burner (fig. 1 of the third paper in this series) having a shrouded passage about 1 inch in height, a burner length of about 40 inches, and a two-ring semicircular gutter-type flame holder was operated on a J34 engine at simulated altitudes of 5000 to 30,000 feet and Mach numbers of 0.22 to 1.0. The maximum shell temperatures measured about 12 inches upstream of the exhaust-nozzle outlet ranged from 1410° to 1630° R over a range of tail-pipe fuel-air ratios from 0.05 to 0.04 with the highest temperature occurring at the high flight Mach numbers. The temperature of the turbine-outlet gases was approximately constant at 1580° R. Cooling air without ram pressure was pumped through the cooling shroud by the ejector action of the exhaust gases, but no measurements were made of the mass flow of cooling air or the pressure drop across the annular cooling passage.

One obstacle in applying the external shroud is the difficulty of obtaining an unobstructed passage enclosing the shell because of flanges, nozzle actuators, and burner supports.

Tail-pipe burner cooled by turbine gases and by air. - Because the shell temperatures of the internal liner are too high for the adjacent aircraft structure, the combination of internal liner and external shroud (fig. 8) appears very practicable. In event of damage to the liner, the double annular passage may be safer than the insulated shell with internal liner. It is difficult, however, to design unobstructed internal and external passages.

Both analytical and experimental work is being continued toward the solution of problems connected with the methods of cooling that have been discussed.

METHOD OF COMPUTING TEMPERATURES

A method of computing the maximum temperature of the wall separating an annular cooling passage from the burner combustion zone is presented (reference 1). The method is applicable to configurations using turbine-outlet gases with an internal liner for cooling (fig. 4) or to configurations using atmospheric air with an external shroud (fig. 7).

The temperature at any point on the wall can be calculated by a simple heat balance if the convective and radiant heat-transfer coefficients on both sides of the wall are known and if the effective combustion-gas and cooling-air temperatures adjacent to the point are known. The first step in the analysis is therefore the estimation of these coefficients and temperatures.

In the cooling-air passage, the convective heat-transfer coefficients can be estimated from the usual heat-transfer formulas applicable to flow in long passages. The magnitude of radiation can be found from formulas for radiation between two infinite cylinders.

The selection of convective heat-transfer coefficients between combustion gases and the wall is difficult because of large unknown velocity and temperature gradients and because of the unknown effects resulting from turbulence introduced by the flame holder and turbine. For the purpose of analysis, heat-transfer coefficients equal to those obtained with fully developed turbulent flow in long pipes have been used.

Radiation between combustion gases and the wall is also difficult to estimate because radiation from luminous flames may be ten times greater than radiation from nonluminous gases and because of the unknown degree of luminosity of the flames. Under certain operating conditions, the combustion in some types of tail-pipe burner is practically nonluminous, whereas other burners or other flight conditions give luminous flames. For the purpose of this analysis, the radiant heat-transfer coefficients were assumed to be double the coefficients for nonluminous gases.

In addition to the heat-transfer coefficients, the temperature of the combustion gases must be known. The experimental temperature profiles have not been measured and instrumentation for their direct measurement is troublesome and uncertain. The longitudinal distribution of the bulk temperature can be determined from the static-pressure measurements along the burner and the usual one-dimensional relations for momentum pressure loss. The variation of bulk combustion temperature rise with burner length for two length-diameter ratios is shown in figure 9. These data were obtained from static-pressure measurements on a ram-jet burner having a diameter of 20 inches. The rate of temperature rise is rapid in the first half of the burner and decreases as combustion nears completion. Trial calculations, made by the method being presented, of the maximum wall temperature using the temperature distribution of figure 9 and a linear rise in combustion temperature indicated small differences in the maximum wall temperature. In the remainder of the analysis, the bulk temperature was assumed to rise linearly with combustion-chamber length.

The cooling-air temperature is a function of the initial gas temperature and the gain in temperature while traveling through the cooling passage. This gain in temperature is unknown and must be

calculated by integrating the heat transfer from the combustion gases to the cooling air along the length of the passage. The differential equation relating cooling-air temperature rise to the independent variables cannot be integrated to obtain an algbraic equation because the heat-transfer coefficients vary with temperature along the length of the burner. Consequently, numerical methods must be applied. One numerical method is described in the next section of this paper.

Procedure and assumptions. - The initial procedure is to solve heat balances across the dividing wall step-by-step along the length of the burner and cooling passage until the maximum temperatures of the wall and of the cooling air are obtained. A recapitulation of assumptions previously given and statements of additional assumptions are:

1. The convective heat-transfer coefficient corresponds to fully developed turbulent flow in a long pipe.

2. The radiant heat-transfer coefficient between the combustion gas and the liner is twice the radiant heat-transfer coefficient for nonluminous gases based on complete combustion of a stoichiometric mixture of kerosene ($C_{12}H_{26}$) and air. (On the basis of assumptions 1 and 2, the convective and radiant heat-transfer coefficients are found to be approximately equal at the outlet.)

3. The bulk total temperature of the combustion gases increases linearly with burner length.

4. No heat flows through the outside wall of the annular passage, and the temperature of the outside wall equals the local temperature of the cooling gas in the passage. (This assumption is conservative and is equivalent to the insulated configuration of fig. 4.)

The step-by-step process is used in a systematic study of the effects on the maximum temperature of the dividing wall of the 8 independent variables: passage height b, passage length l, burner diameter D, mass velocity of combustion gas $\rho_g V_g$, ratio of mass velocity of cooling air to mass velocity of combustion gas $\frac{\rho_a V_a}{\rho_g V_g}$, final combustion-gas temperature $T_{g,2}$, inlet combustion-gas temperature $T_{g,1}$, and inlet cooling-air temperature $T_{a,1}$.

Empirical equation for cooling-air temperature. - Because of the large number of variables, many step-by-step solutions would be required to cover all possible combinations. The labor of calculations could be greatly reduced if an equation relating cooling-gas temperature to the independent variables could be found. It was stated earlier that direct derivation of such an equation is not possible because the differential equation for cooling-air temperature cannot be solved except by numerical methods. An alternate approach is to select an approximate empirical equation that fits the results of a number of step-by-step solutions. The development of such an approximate equation generalizing the results of the step-by-step process is discussed in succeeding paragraphs.

The symbols used in this analysis are:

b	height of cooling passage, ft
c_p	specific heat at constant pressure, Btu/(lb)(°R)
D	diameter, ft
H	heat-transfer coefficient, Btu/(hr)(sq ft)(°R)
K	constant
l	length, ft
m,n,p,q,r	exponents
T	total temperature, °R
t_w	wall temperature, °R
U	effective over-all heat-transfer coefficient, Btu/(hr)(sq ft)(°R)
V	velocity, ft/sec
ρ	density, lb/cu ft

Subscripts:

a	cooling air or gas
g	combustion gas

1 inlet

2 outlet

The form of the empirical equation should be similar to the exact equation for the systems shown in figures 4 and 7 with the simplifying assumption that the over-all heat-transfer coefficient U is constant and the gas properties are constant. With the use of this simplifying assumption, a solution of the differential equation is obtained, which shows that the performance of a parallel-flow heat exchanger can be expressed in terms of three dimensionless ratios:

$$\frac{T_{a,2} - T_{a,1}}{T_{g,2} - T_{g,1}} = f\left[\frac{T_{g,1} - T_{a,1}}{T_{g,2} - T_{g,1}} \frac{b}{l} \frac{\rho_a V_a c_{p,a}}{U}\right] \qquad (1)$$

where f indicates a functional relation. This function is not given here because ot its complexity but is plotted in figure 10. Dimensional analysis shows that the parameter $\frac{b}{l} \frac{\rho_a V_a c_{p,a}}{U}$ is a function of the Reynolds number of the combustion chamber, the Reynolds number in the cooling passage, and, because radiation is important, the temperature of the combustion gas. The results of the dimensional analysis leads to the empirical equation

$$\frac{b}{l} \frac{\rho_a V_a c_{p,a}}{U} = K \frac{b^m}{l} (\rho_g V_g)^n \left(\frac{\rho_a V_a}{\rho_g V_g}\right)^p T_{g,2}^q D^r \qquad (2)$$

Equation (2) in combination with figure 10 gives a trial form of the desired empirical relation. The next step is to fit the empirical relation to the results of the step-by-step calculations. This fitting can be accomplished by selecting proper values of the constant K, and the five exponents m, n, p, q, and r.

The method for selecting the values of the exponents is illustrated by the selection of p. From the results of step-by-step calculations in which $\frac{\rho_a V_a}{\rho_g V_g}$ is varied and all other quantities are held constant, values of $\frac{T_{a,2} - T_{a,1}}{T_{g,2} - T_{g,1}}$ are obtained. The value of $\frac{T_{g,1} - T_{a,1}}{T_{g,2} - T_{g,1}}$ is found from the initial conditions. Figure 10 is

then used to find the values of $\frac{b}{l}\frac{\rho_a V_a c_{p,a}}{U}$. These values of $\frac{b}{l}\frac{\rho_a V_a c_{p,a}}{U}$ are then plotted against $\frac{\rho_a V_a}{\rho_g V_g}$ on logarithmic coordinates as shown in figure 11. The data fall on a straight line and the slope of the line is the exponent p.

If the trial form of the equation is correct, the value of the exponent p should be independent of the values of the variables. the constancy of p is checked by plotting $\frac{b}{l}\frac{\rho_a V_a c_{p,a}}{U}$ against $\frac{\rho_a V_a}{\rho_g V_g}$ for a wide range of the variables b, l, ρ_g, T_g, and D. All curves are parallel and consequently the value of p is constant.

A similar procedure was employed in determining the values of all the other exponents. These exponents are also independent of the values of the variables. Equation (2) can therefore be rewritten

$$\frac{b}{l}\frac{\rho_a V_a c_{p,a}}{U} = 53\,\frac{b^{1.23}}{l}\,(\rho_g V_g)^{0.282}\left(\frac{\rho_a V_a}{\rho_g V_g}\right)^{0.89} T_{g,2}^{0.082} \qquad (3)$$

Equation (3) and figure 10 give the desired empirical relation between outlet cooling-air temperature and the independent variables.

Calculation of wall temperature. - The maximum temperature of the dividing wall t_w can be calculated from the equation

$$t_{w,2} = \frac{H_{g,2}T_{g,2} + H_{a,2}T_{a,2}}{H_{g,2} + H_{a,2}} \qquad (4)$$

which is derived from a heat balance at the outlet. The local coefficient $H_{g,2}$ at the outlet is the sum of the local convective and radiant heat-transfer coefficients from the combustion gases to the wall and $H_{a,2}$ is the sum of the local convective and radiant heat-transfer coefficients from the shell to the cooling air calculated by use of the initial assumptions.

Comparison of calculated and experimental temperatures. - Experimentally determined temperatures are compared in figure 12 with theoretical temperatures calculated from equation (3) and figure 10.

Experimental data in figures 12 and 6 were obtained from the same tail-pipe configuration. Because the empirical equation is for an insulated burner and the experimental burner was uninsulated, the outlet cooling-gas temperature computed from the equation (3) and figure 10 was reduced by an amount equivalent to the heat losses through the uninsulated shell. Figure 12 shows the cooling-gas temperature and the maximum liner temperature plotted as a function of final combustion temperature.

The theoretical cooling-gas temperatures are about 50° to 100° R higher than the measured gas temperatures. The theoretical liner temperatures are about 200° to 270° R higher than the measured temperatures. The analysis appears to give conservative temperatures for the cooling gas and liner; however, the degree of conservatism cannot be stated positively for other configurations.

SUMMARY

Experience with various methods of tail-pipe burner cooling were discussed. Several appear promising and experimental and analytical work is continuing to evaluate which is best.

A generalized analysis for determining the maximum wall temperature of a burner cooled by air or gases flowing through a surrounding annular passage was presented. Application of this analysis to a full-scale tail-pipe burner having an internal liner cooled with turbine-outlet gas appeared to give conservative results when compared with experimental temperatures. The generalized analysis should prove useful in correlating experimental data and, in spite of the approximations involved, will prove a valuable means of comparing several methods of cooling with annular passages.

REFERENCE

1. Koffel, William K.: An analytical Method for Determining the Maximum Shell Temperature of a Combustion Chamber Having a Shrouded Cooling Passage. NACA RM (to be pub.).

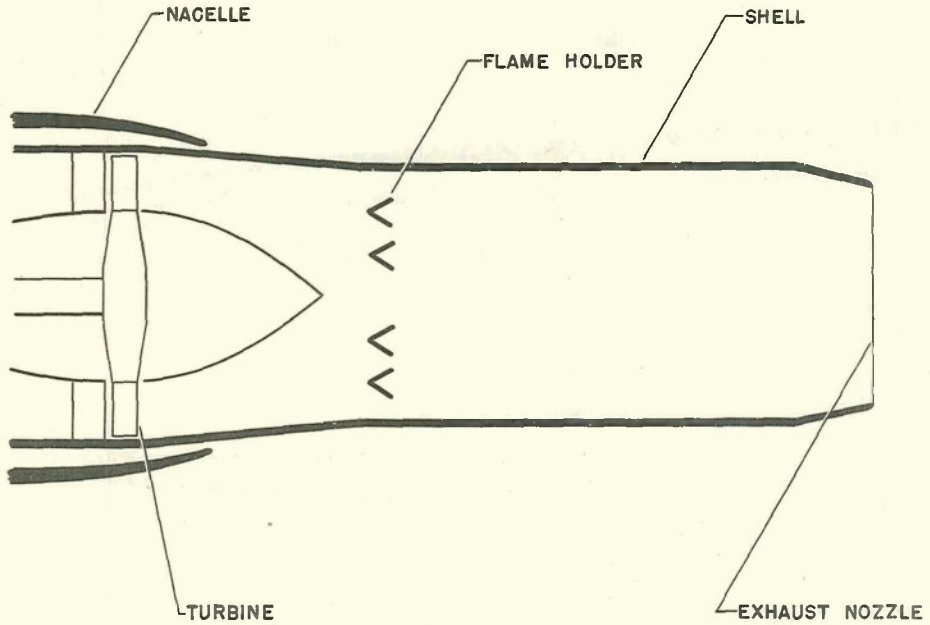

Figure 1. - Shell cooled internally by stratification of combustion and externally by convection and radiation to free stream.

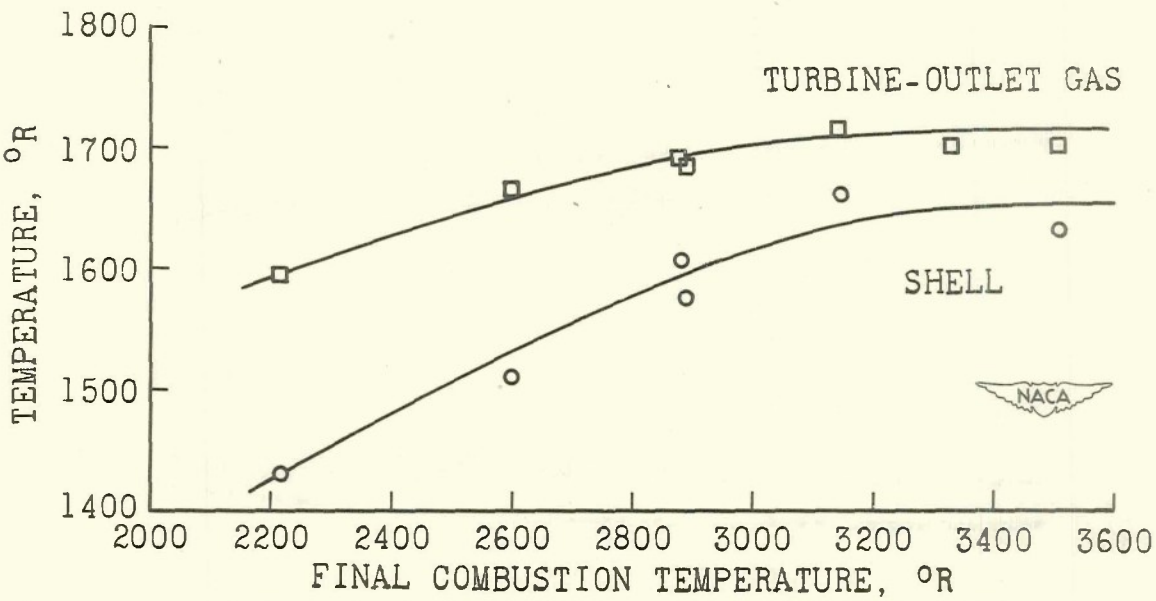

Figure 2. - Variation of maximum shell temperature and turbine-outlet gas temperature with final combustion temperature. Sea-level static tests of tail-pipe burning on J35 engine.

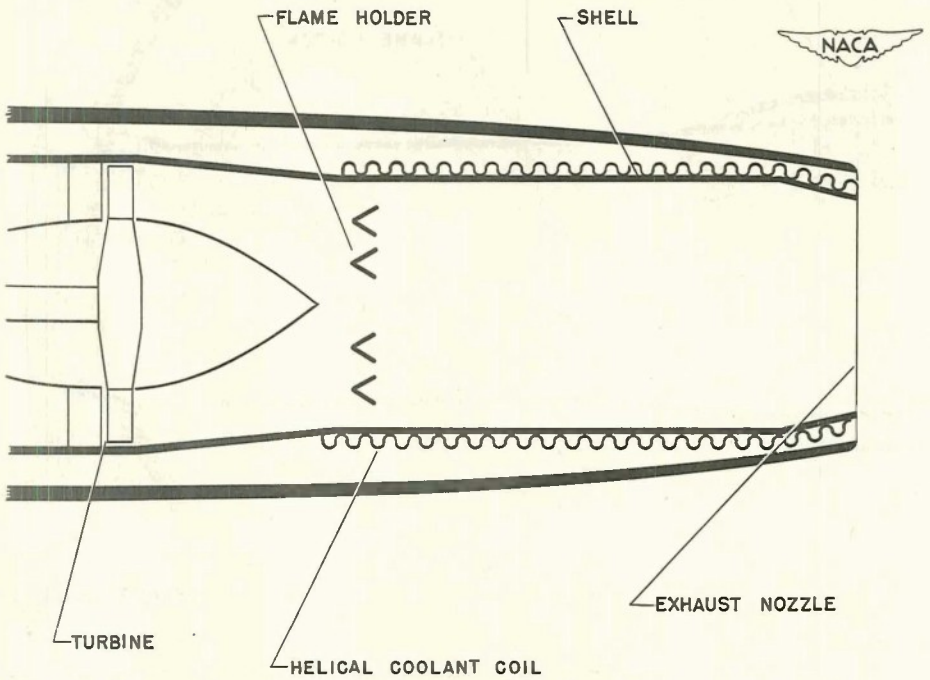

Figure 3. - Tail-pipe burner cooled by liquids.

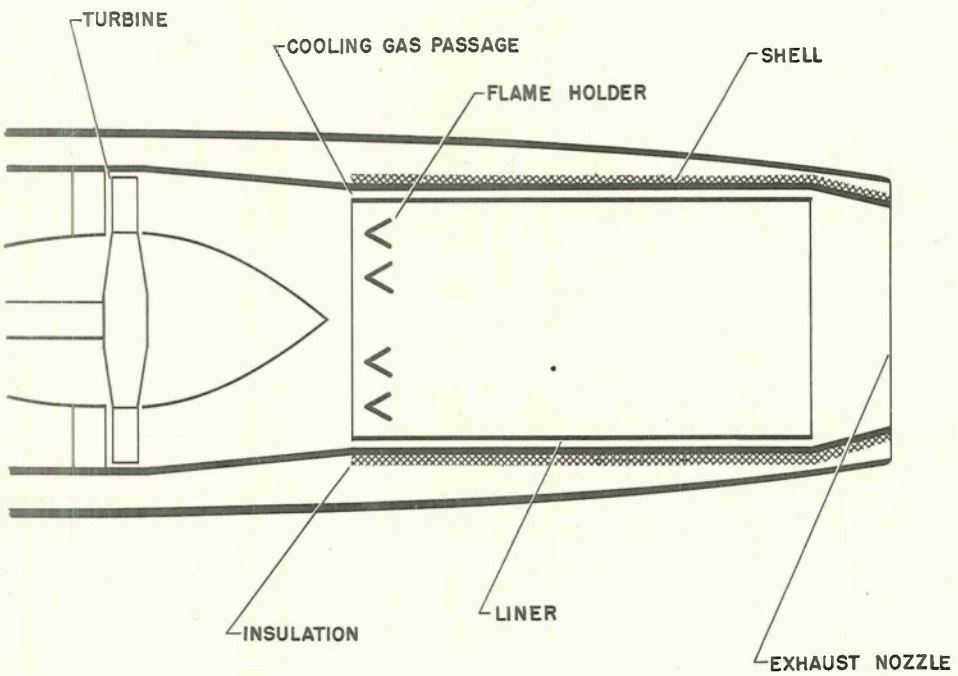

Figure 4. - Tail-pipe burner cooled by turbine-outlet gas flowing through an annular cooling passage.

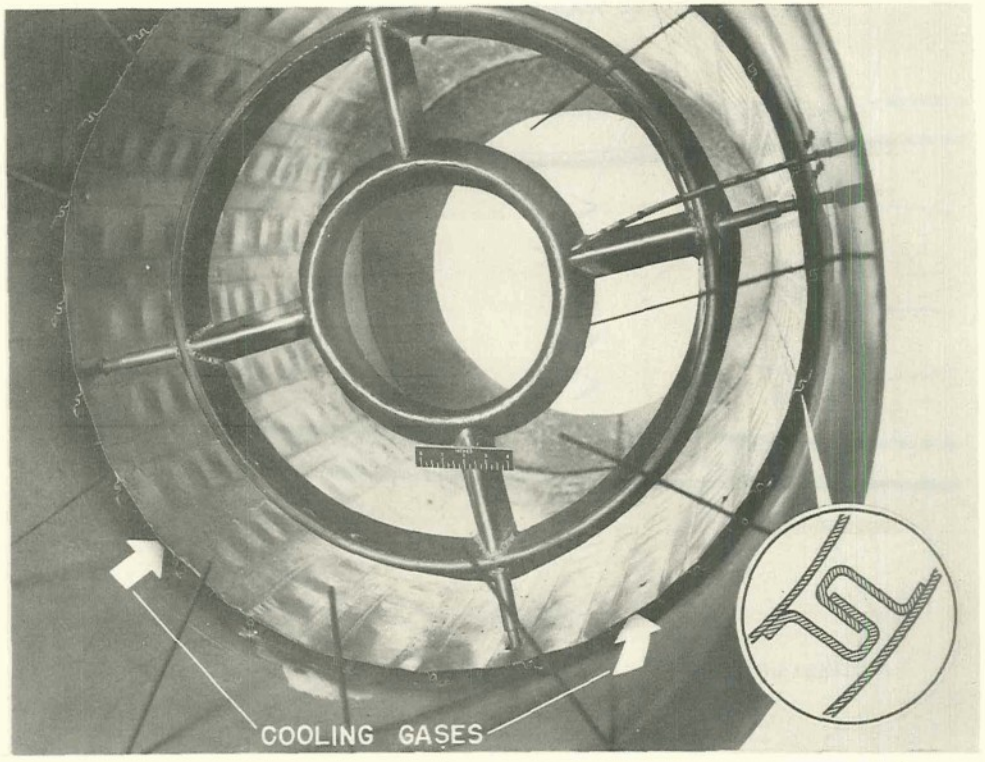

Figure 5. - Experimental tail-pipe burner with internal liner cooled by turbine-outlet gas.

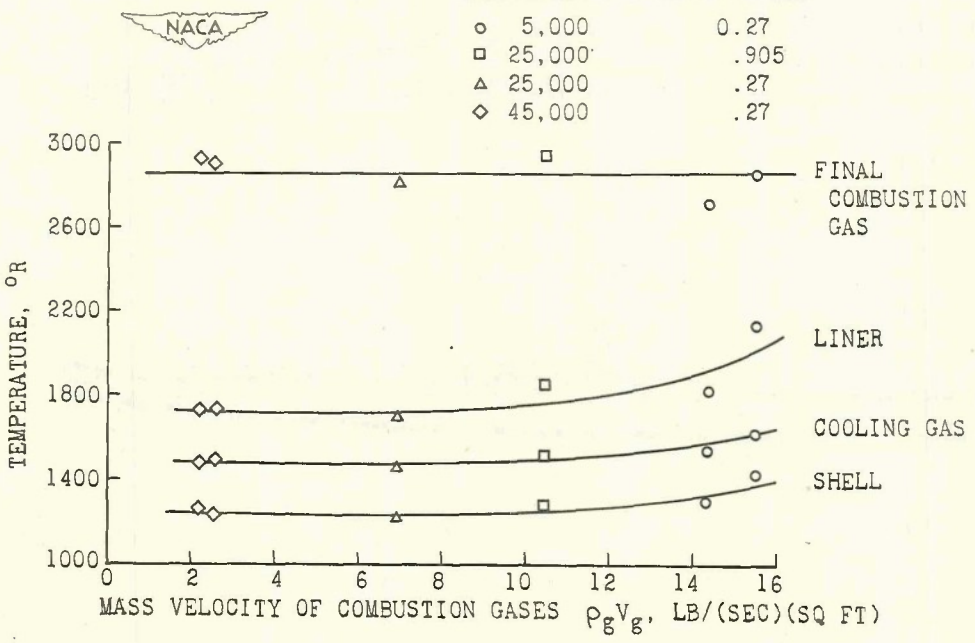

Figure 6. - Variation of temperatures at burner outlet with mass velocity of combustion gas. Altitude-wind-tunnel investigation of tail-pipe burning on J35 engine.

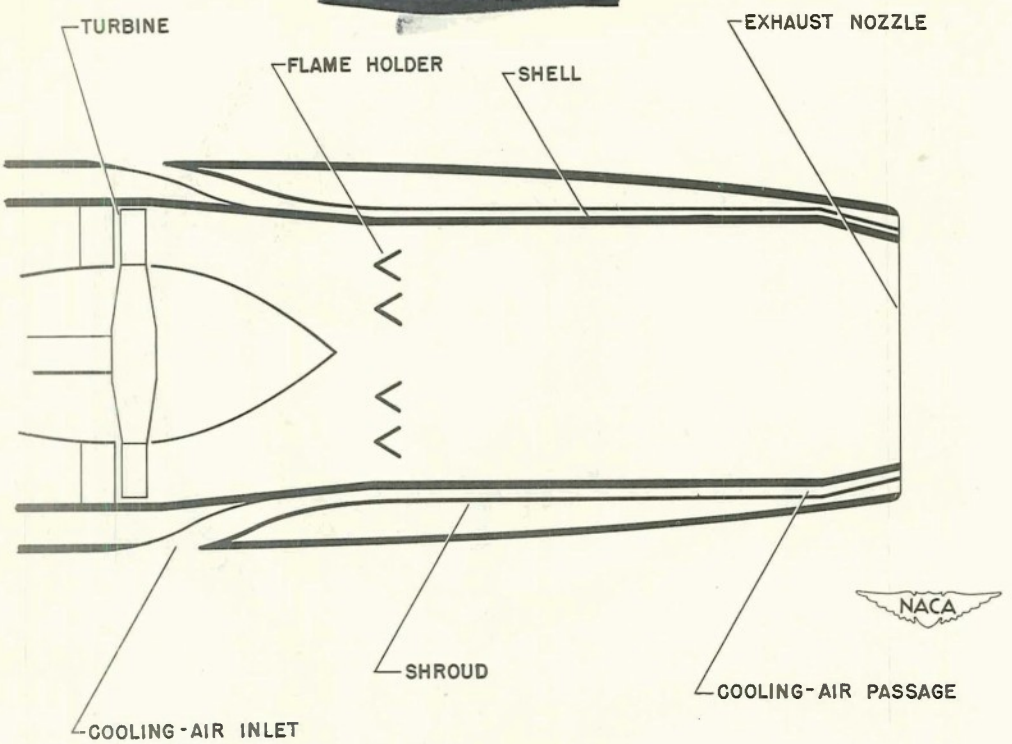

Figure 7. - Tail-pipe burner cooled by air flowing through an external shroud.

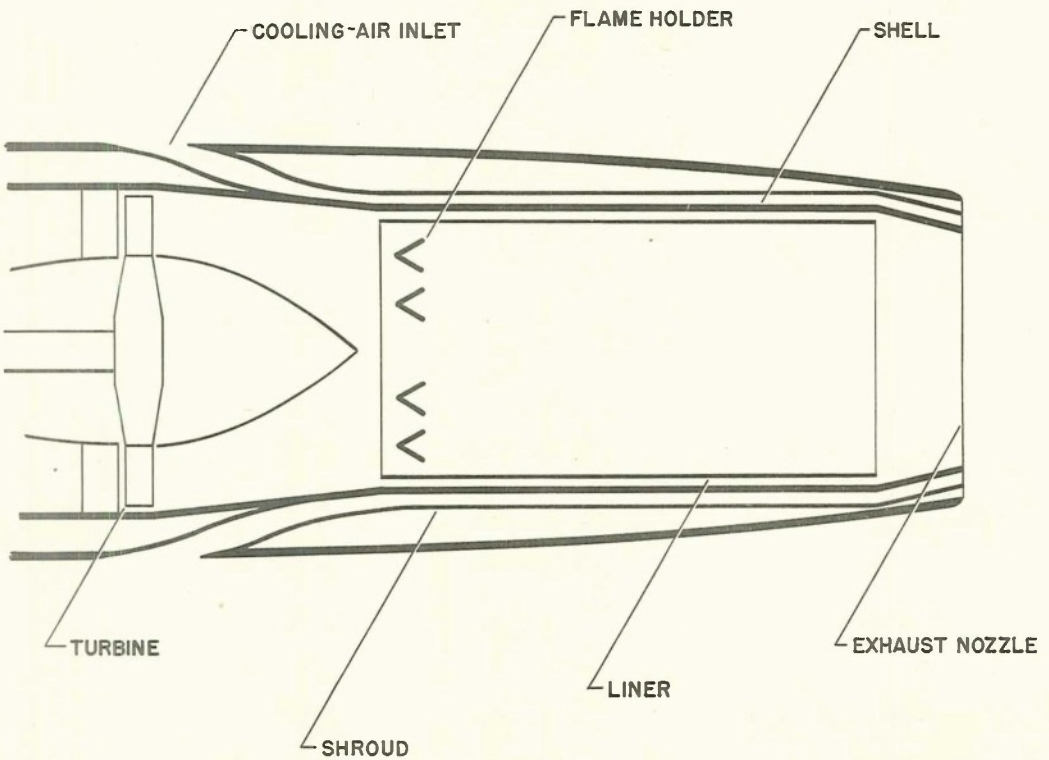

Figure 8. - Tail-pipe burner cooled by air flowing through external shroud and by turbine-outlet gas flowing through internal liner.

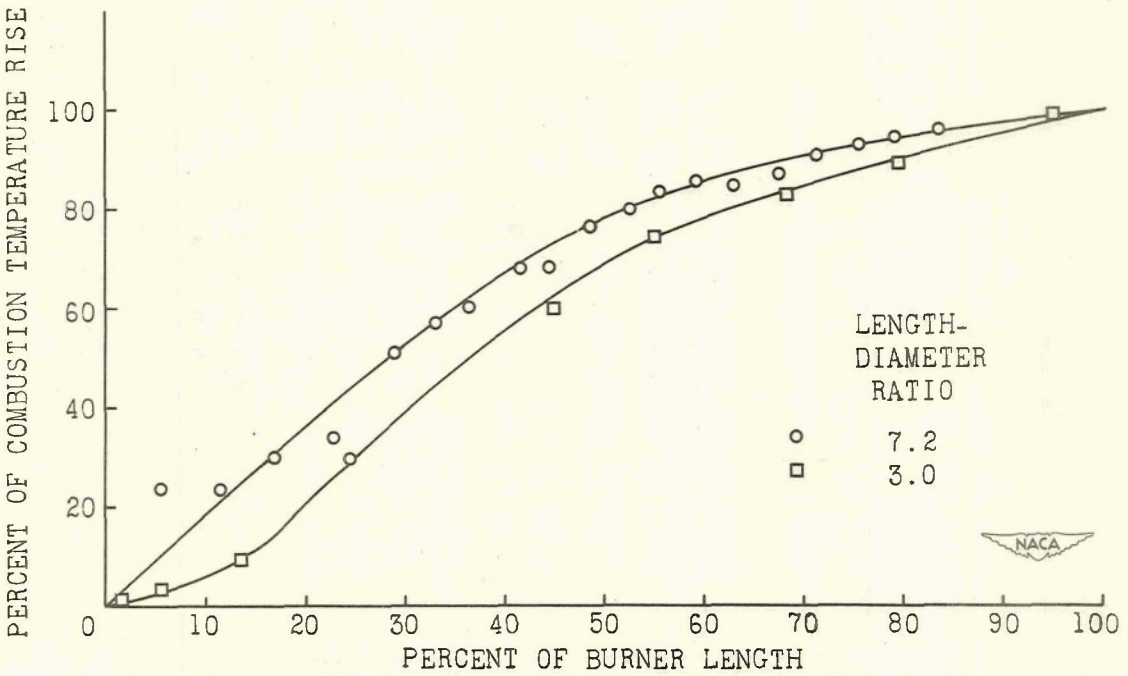

Figure 9. - Variation of combustion-gas bulk total temperature with percent of burner length.

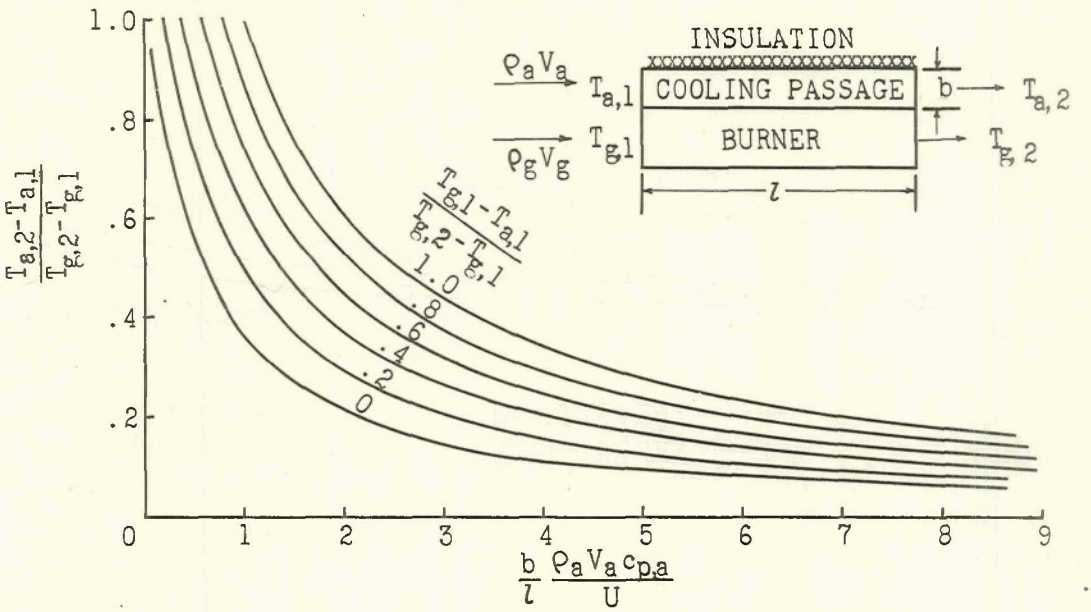

Figure 10. - Performance characteristics of parallel-flow heat exchanger having linear rise in combustion temperature and constant over-all heat-transfer coefficient.

$$\frac{b}{l}\frac{\rho_a V_a c_{p,a}}{U} = K\left(\frac{b}{l}\right)^m (\rho_g V_g)^n \left(\frac{\rho_a V_a}{\rho_g V_g}\right)^p T_{g,2}{}^q D^r$$

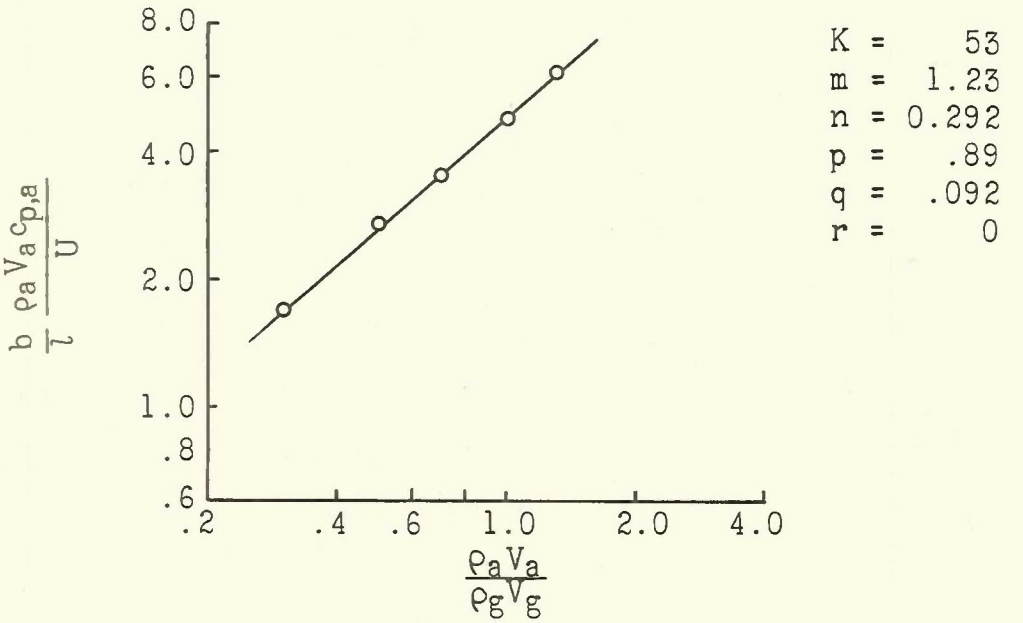

Figure 11. - Determination of the exponent p in empirical equation (3).

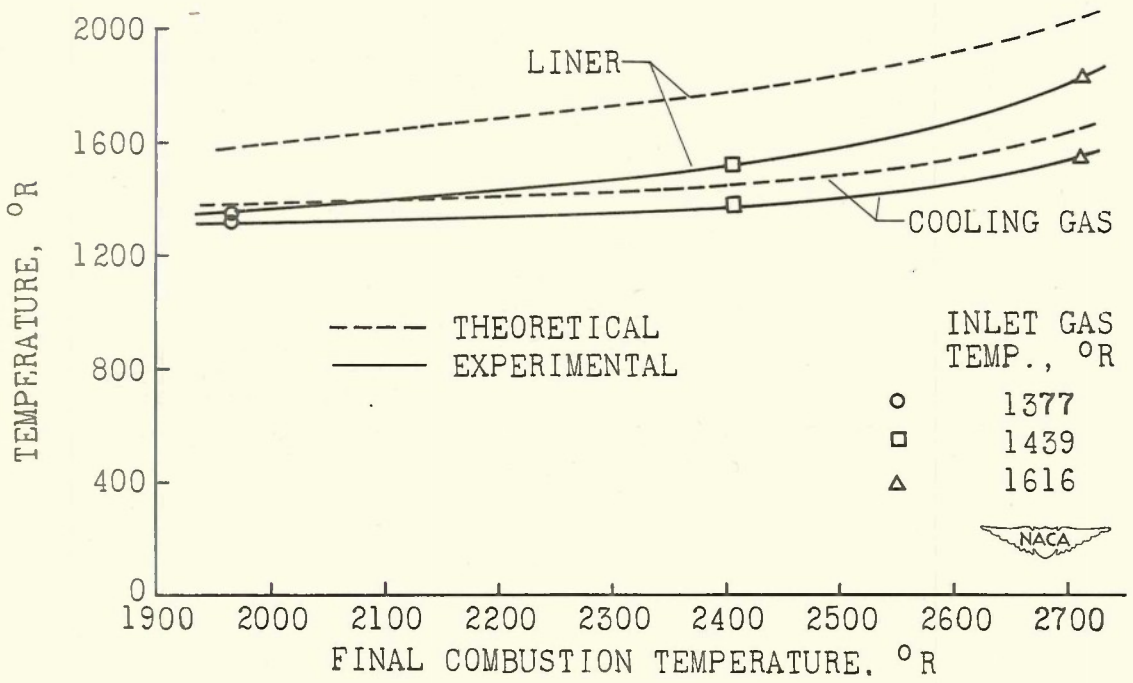

Figure 12. - Comparison of theoretical and experimental temperatures.

ANALYSIS OF WATER-INJECTION METHODS OF THRUST AUGMENTATION

By E. Clinton Wilcox

Lewis Flight Propulsion Laboratory

INTRODUCTION

One of the simplest methods of augmenting the thrust of a turbojet engine is the injection of a volatile liquid into the compressor inlet. Evaporation of this liquid extracts heat from the inlet air, and it is theoretically possible to cool the inlet air to the saturation temperature of the final mixture before it enters the engine compressor. When liquid in excess of that required to saturate the inlet air is injected at the compressor inlet, further cooling is obtained by additional evaporation during the mechanical compression process. The temperature of the fluid is therefore reduced and for a constant work input per unit of air-liquid mixture corresponding to a constant compressor speed, a higher compressor pressure ratio is obtained. This increased pressure ratio is reflected throughout the engine, and the engine mass flow and the exhaust-jet velocity are increased, both factors increasing the thrust produced by the engine.

Altering a turbojet engine for thrust augmentation by the water-injection method makes it necessary to provide an injection system at the compressor inlet, additional tanks, and, if maximum gains in thrust are to be realized, a variable-area exhaust nozzle. Thrust augmentation by injecting a volatile liquid at the compressor inlet is a method that can be readily applied to any engine already in use and has the advantage of not introducing any thrust loss when the augmentation scheme is inoperative.

Experimental investigations of the effect of the injection of water and water-alcohol mixtures on the performance of several different turbojet engines are presented in references 1 to 3 and are discussed in the next paper of this series. Water, because of its favorable thermodynamic properties, widespread availability, and ease of handling, is a desirable substance for inlet injection with the addition of alcohol for the prevention of freezing during low-temperature operation.

Another method for utilizing water injection to provide thrust augmentation is injection in the engine combustion chambers.

Injecting water in the engine combustion chambers tends to decrease the air flow through the compressor because the total flow through the engine is fixed for a given turbine-inlet temperature and pressure. For a constant compressor work input per pound of air, less turbine work is required because of the decreased compressor air flow, and this decrease results in a decreased pressure ratio across the turbine. The decreased pressure ratio across the turbine increases the pressure ratio across the exhaust nozzle and provides a greater jet velocity and hence greater thrust. Depending on the characteristics of the particular compressor under consideration, the decreased air flow may result in an increased engine pressure ratio. The change in thermodynamic properties of the working fluid due to the addition of water also tends to increase the engine thrust to some extent.

In the present paper, the results of a theoretical investigation of the effect on turbojet-engine performance of the injection of water at the compressor inlet of the engine are presented. Compressor-inlet injection is considered in two parts: (1) the case where sufficient water is injected to saturate the compressor-inlet air and (2) the case where sufficient water is injected at the compressor inlet to saturate the air at some point during the mechanical compression process.

The performance of a turbojet engine utilizing combustion-chamber injection is also considered and compared with the performance of compressor-inlet and -outlet saturation. For the present analysis the change in compressor pressure ratio resulting from change in air flow was not considered for the case of augmentation by injection of water into the combustion chamber.

RESULTS AND DISCUSSION

Saturation at Compressor Inlet

In order to determine the thrust augmentation resulting from compressor-inlet saturation, it is necessary to calculate saturation temperatures resulting from various initial temperatures, pressures, and water contents. A psychrometric chart was therefore developed to enable calculation of these saturation temperatures. A simplified version of this chart is presented in figure 1. Enthalpy in Btu per pound of air is plotted against temperature in degrees Fahrenheit for various values of the ratio of relative humidity to δ, where δ is the ratio of static pressure at the point of interest to standard sea-level static pressure. From theoretical considerations it was found that the introduction of the factor δ in this manner would

generalize the values of relative humidity appearing on the familiar psychrometric chart for any pressure. Lines of constant water-air ratio are also included. Inasmuch as the temperatures encountered at the compressor inlet of a turbojet engine at high flight Mach numbers are considerably higher than those appearing on the usual psychrometric chart, which are generally limited to about 120° F, the temperature range covered by the present chart has been extended to 700° F by means of the thermodynamic data for air and water contained in references 4 and 5.

In order to illustrate the use of this chart the following example is presented: Air at an initial temperature of 600° F with a pressure of twice standard sea-level static pressure and with an initial water content corresponding to a water-air ratio of 0.005 is assumed. Saturation always occurs, by definition, at a value of relative humidity of 100 percent and the ratio of relative humidity divided by δ at saturation for these particular conditions is therefore 0.5. Enter figure 1 at the original temperature, for this case 600° F, follow this temperature line to the water-air-ratio line representing the original water-air ratio of 0.005, go across a constant-enthalpy line to the value of relative humidity divided by δ for saturation, which is 0.5. This value determines the saturation temperature, which for this example is 156° F. Thus, for this particular example, the air can be cooled 444° F by saturation.

The amount of water that must be evaporated to saturate the air can also be determined directly from the chart. For the saturated condition (fig. 1), the water-air ratio is 0.105 and for the initial condition, 0.005. In order to saturate the air, the difference or 0.100 pound of water per pound of air must therefore be evaporated for this particular example.

For a given pressure, the ratio of relative humidity to δ for saturation remains constant, and as can be seen from figure 1 these curves of constant ratio of relative humidity to δ, over a wide range in the vicinity of 1, are approximately vertical, indicating a constant saturation temperature. Therefore, as the starting temperature is increased, the amount of cooling possible increases.

Increasing the pressure decreases the ratio of relative humidity to δ for saturation. From figure 1 it can be seen that decreasing the value of relative humidity divided by δ results in an increased saturation temperature; thus, for a given initial temperature increasing the pressure reduces somewhat the cooling possible from saturation.

In figure 2 the effect of flight conditions on the amount of cooling that can be obtained by saturating the compressor-inlet air

to a turbojet engine is presented. The data shown in this figure are for an inlet-diffuser efficiency of 0.80 and an atmospheric relative humidity of 50 percent. Compressor-inlet stagnation pressure and temperature are shown as functions of flight Mach number for altitudes of sea level and 35,000 feet. Also shown as dashed lines are the temperatures resulting after constant-pressure saturation. The water-air ratios necessary to produce saturation are shown in the uppermost curves. As the flight Mach number is increased, the amount of cooling possible increases as indicated by the increasing difference between the solid and dashed curves. For sea-level altitude the cooling possible increases from 10° at a Mach number of 0 to 155° at a Mach number of 1.5. The increased cooling at the higher Mach numbers is a result of the increased temperature prior to saturation; the increased pressure encountered at the higher Mach numbers would tend to decrease the cooling possible as was pointed out in the discussion of figure 1. The cooling obtained for a given Mach number at an altitude of 35,000 feet is less than that obtained at sea level because of the decreased temperatures at high altitude. The water-air ratio required to produce saturation increases as the Mach number increases and decreases with increased altitude.

With the use of data presented in figure 1, the thrust augmentation resulting from compressor-inlet saturation was determined for a representative turbojet engine. The following values for efficiencies and design constants were assumed: compressor efficiency, 0.80; turbine efficiency, 0.85; exhaust-nozzle efficiency, 0.951 inlet-diffuser efficiencies of 1.00, 0.85, 0.80, and 0.75 for flight Mach numbers of 0, 1.0, 1.5, and 2.0, respectively; a loss in total pressure in the engine combustion chambers of 3 percent of the combustion-chamber-inlet total pressure; and a tail-pipe gas temperature of 1650° R. The compressor was assumed to have a sea-level static-pressure ratio of 4.32; at other flight conditions the pressure ratio was varied to meet the conditions of constant work input (constant rotative speed).

These assumed design variables were maintained constant for all conditions except where it was desired to show the effect of inlet-diffuser efficiency and compressor pressure ratio. For these cases the inlet-diffuser efficiency and compressor pressure ratio were varied systematically.

In figure 3 the ratio of augmented to normal thrust is shown as a function of flight Mach number for inlet-diffuser efficiencies of 0.60, 0.80, and 1.00 and for altitudes of sea level and 35,000 feet. The relative humidity of the ambient air is assumed to be 50 percent. For each point on the curve sufficient water has been injected in the compressor inlet to saturate the air. The ratio

of augmented to normal thrust increases rapidly with increased Mach number. For sea-level altitude and an inlet-diffuser efficiency of 0.80, the ratio of augmented to normal thrust increases from 1.03 at a flight Mach number of 0 to 2.16 at a flight Mach number of 2.0. At a flight Mach number of 2.0, the ratio of augmented to normal thrust is decreased to 1.48 with increase in altitude to 35,000 feet. This decrease in thrust augmentation is due to the lower temperatures associated with high-altitude operation. For a given flight Mach number, the ratio of augmented to normal thrust increases as the inlet-diffuser efficiency decreases. This effect occurs because of the increased cooling possible at the decreased pressure attending lower diffuser efficiency. Although the ratio of augmented to normal thrust is increased, a low inlet-diffuser efficiency is not a virtue since it reduces the entire performance level of the engine.

The cooling possible from inlet saturation and hence the augmentation is influenced by atmospheric relative humidity. In figure 4, the ratio of augmented to normal thrust is shown as a function of flight Mach number for atmospheric relative humidities of 0, 50, and 100 percent. These curves are for sea-level altitude and an inlet-diffuser efficiency of 0.80. For each point on the curves sufficient water has been injected to saturate the compressor-inlet air. The relative humidity of the atmosphere has a comparatively slight effect on the ratio of augmented to normal thrust, with the maximum change in performance occurring at low Mach numbers and the effect decreasing as the Mach number is increased.

Saturation at Some Point during Mechanical Compression

The previous discussion has been concerned with cases where only sufficient water to saturate the compressor-inlet air has been injected; the problem where sufficient water is injected to saturate the air at some point during the mechanical compression process is now considered. In order to calculate compressor performance when water is evaporating during the compression process, a Mollier diagram was prepared specifically for this application. A simplified version of this diagram is presented in figure 5.

Every point on the diagram pertains to a saturated mixture of air and water vapor and was determined from the thermodynamic properties of air and water contained in references 4 and 5. Enthalpy in Btu per pound of air is shown as a function of entropy in Btu per pound of air per degree Rankine for various temperatures much as in the familiar Mollier diagram for steam. Constant-pressure lines appear as approximately straight lines having a positive slope and

lines of constant water-air ratio appear as negatively sloping straight lines. The zero of enthalpy and entropy have been arbitrarily chosen at a temperature of 59° F and a pressure of 14.7 pounds per square inch.

In order to utilize this chart to calculate compressor performance it is necessary to know the actual and isentropic works of compression. The actual work can be found as the product of the compressor tip speed squared and the compressor slip factor, and the isentropic work can be calculated as the product of the actual work of compression and the compressor efficiency.

The following example is presented to illustrate the use of this chart: Initially saturated air at a temperature of 59° F having a pressure of 14.7 pounds per square inch is assumed. It is further assumed that sufficient water is injected to saturate the air at the compressor outlet and that the compressor has an efficiency of 0.80 and imparts a work of 80 Btu per pound of air passing through it. This actual work and compressor efficiency correspond to an isentropic work input of 64 Btu per pound of air. Enter the chart at a temperature of 59° F and a pressure of 14.7 pounds per square inch as indicated by point 1 on figure 5. Increase the enthalpy at constant entropy by an amount equal to the ideal work of compression, for this particular example 64 Btu per pound of air as indicated by point 2 (fig. 5). The pressure at point 2 is the actual pressure at the compressor outlet. Follow along the constant-pressure line (point 2 to poing 3) until the enthalpy is equal to the enthalpy at point 1 plus the actual compressor work, for this case 80 Btu per pound of air as indicated by point 3. The conditions at point 3 represent the actual conditions at the compressor outlet and for the present example the temperature is 170° F and the pressure 70 pounds per square inch. The value of water-air ratio can also be read from the chart, and for this example is 0.058. The water-air ratio at the compressor-inlet conditions is 0.011 so that for the present example the difference or 0.047 pound of water per pound of air are evaporated in passing through the compressor.

The chart only applied for saturated mixtures and if there is insufficient water to saturate the air at the compressor outlet, the compressor performance is calculated by assuming the process to consist of the following two steps:

1. Compression as previously described to the point where saturation occurs

2. Adiabatic compression of a gas mixture consisting of air and water vapor, which can be calculated using familiar thermodynamic relations

In order to illustrate a case of this type, the compressor previously described was again assumed: a compressor efficiency of 0.80, and an actual compressor work input of 80 Btu per pound of air passing through it. For this case it is assumed that water is evaporating only during one-half of the actual compressor work input. The pressure and temperature after all the water is evaporated can be determined from the Mollier diagram (fig. 5) as previously described but using 40 and 32 instead of 80 and 64 Btu per pound of air for the actual and isentropic work input, respectively. For this case, the pressure is 33.5 pounds per square inch and the temperature is 120° F. The remaining work input of 40 Btu per pound of air is done on a mixture of air and water vapor. The temperature rise for this part of the process can be determined from the specific heat of the mixture and the remaining work input. For the remaining compression process the temperature rise is calculated to be 161° F. The temperature after compression is the sum of the temperature after the initial stage and the temperature rise during the second stage or 281° F. From the compressor efficiency, the pressure after the first stage, the temperatures before and after the second stage of compression, and the ratio of specific heats for the air-water mixture, the final pressure can be found. For this particular example the compressor-outlet pressure is found to be 68 pounds per square inch.

If it is desired to calculate the compressor performance for a given water-air ratio, the procedure is similar to that previously described except a trial-and-error solution is involved.

To date it has been impossible to obtain close agreement between theoretical and experimental results for saturation at some point during the mechanical compression process because the effect of water injection on the performance of each component, particularly the compressor of the turbojet engine, is not understood. Also it is not known to what extent the actual process, both before and during the compression process, follows the thermodynamic equilibrium for air and water. Correction factors must therefore be introduced to reconcile theoretical and experimental data. These correction factors seem to vary with different engines and because of the limited amount of data available no general corrections are recommended at the present time.

For the investigation of the thrust augmentation resulting when water evaporates during the compression process, the Mollier diagram (fig. 5) was used to calculate compressor performance for the turbojet engine having the assumed design characteristics previously given. In calculating the following results, the compressor

efficiency was altered with varying water-air ratio to bring agreement between calculated sea-level static performance and experimental sea-level static performance for one particular engine. These values of compressor efficiency were then used in calculating performance at other flight conditions.

In figure 6 the ratio of augmented to normal thrust is shown as a function of water-air ratio for sea-level Mach numbers of 0, 0.85, and 1.50, and for Mach numbers of 0.85 and 1.50 at an altitude of 35,000 feet. The ratio of augmented to normal thrust increases as the water-air ratio and the flight Mach number are increased and decreases as the altitude is increased. The condition of compressor-outlet saturation is indicated by the circles, and the condition of compressor-inlet saturation is indicated by the crosses (fig. 6). At sea level and a flight Mach number of 1.50, the ratio of augmented to normal thrust is 1.56 for compressor-inlet saturation and 2.01 for compressor-outlet saturation. At sea level and a flight Mach number of 0, the ratio of augmented to normal thrust for compressor-outlet saturation decreases to 1.33. For a flight Mach number of 1.5, increasing the altitude from sea level to 35,000 feet decreases the ratio of augmented to normal thrust for compressor-outlet saturation from 2.01 to 1.63.

The effect of atmospheric temperature and relative humidity on thrust augmentation resulting from compressor-outlet saturation are shown in figure 7. The ratio of augmented to normal thrust is shown as a function of atmospheric temperature for values of atmospheric relative humidity of 0 and 100 percent. The curves presented are for sea level and for flight Mach numbers of 0 and 0.85, and for each point on the curves sufficient water has been injected to saturate the compressor-outlet air. The augmentation for an atmospheric relative humidity of 0 percent is always greater than that for an atmospheric relative humidity of 100 percent. For a relative humidity of 0 percent, the augmentation increases as the atmospheric temperature increases; whereas for an atmospheric relative humidity of 100 percent, the thrust augmentation is approximately constant for a Mach number of zero, and for a flight Mach number of 0.85 augmentation increases slightly and then decreases as the atmospheric temperature increases. The conditions of 100-percent atmospheric relative humidity and high atmospheric temperatures are not ones that would usually be encountered under actual atmospheric conditions.

The effect of normal engine compressor pressure ratio on thrust augmentation is shown in figure 8 at sea level and zero flight Mach number. In this particular figure, the turbine-inlet temperature rather than the turbine-outlet temperature has been maintained constant

because if the turbine-outlet temperature were maintained constant, the turbine-inlet temperature at the higher compressor pressure ratios would have been considerably higher than current turbine materials allow. For each point on the curve sufficient water has been injected to saturate the compressor-outlet air. It can be seen that the thrust augmentation increases approximately linearly with increased compressor pressure ratio. An augmented thrust of 1.31 times the normal thrust is obtained for a compressor pressure ratio of 4, and this ratio increases to 1.7 at a compressor pressure ratio of 10.

Also shown in figure 8 is the ratio of total liquid (water plus fuel) to normal fuel as a function of normal compressor pressure ratio. This ratio also increases as the compressor pressure ratio is increased and thus the higher thrust augmentation obtained at the higher compressor pressure ratios are obtained at the expanse of increased ratio of total liquid to normal fuel. The increased liquid consumptions at the high compressor pressure ratios are a result of the high water-air ratios required to saturate the air.

Injection in Engine Combustion Chambers

For the augmentation method consisting of water injection in the engine combustion chambers, performance was calculated for the same turbojet engine as previously described and is shown in figure 9. The ratio of augmented to normal thrust and the ratio of total liquid to normal fuel are shown as functions of sea-level Mach number for water-air ratios of 0.08 and 0.2. Both the ratio of augmented to normal thrust and the ratio of total liquid to normal fuel increase as the flight Mach number and the water-air ratio are increased. For a water-air ratio of 0.20, increasing the flight Mach number from 0 to 2.0 increases the ratio of augmented to normal thrust from 1.18 to 2.25. The ratio of total liquid to normal fuel increases from about 11 at a Mach number of 0 to 15 at a flight Mach number of 2.0.

Comparison of Water-Injection Methods

In figure 10 the ratio of augmented to normal thrust and the ratio of total liquid (water plus fuel) to normal fuel as functions of flight Mach number for compressor-inlet and compressor-outlet saturation are superimposed on the curves of figure 9 to obtain a comparison. Compressor-outlet saturation provides the greatest thrust increase at all flight Mach numbers. At a Mach number of 0, compressor-outlet saturation provides a ratio of augmented to normal thrust twice

that produced by combustion-chamber injection for a water-air ratio of 0.20. At a Mach number of 2.0, the ratio of augmented to normal thrust produced by outlet saturation is approximately 35 percent greater than that for combustion-chamber injection. For all flight Mach numbers, the ratio of total liquid to normal fuel for compressor-outlet saturation is less than or equal to that for combustion-chamber injection (water-air ratio 0.20). This difference in ratio of total liquid to normal fuel decreases as the flight Mach number increases. The ratio of augmented to normal thrust for compressor-inlet saturation is less than that for combustion-chamber injection (water-air ratio 0.20) at low Mach numbers and the ratios are approximately equal at high Mach numbers. For all flight Mach numbers, the ratio of total liquid to normal fuel for compressor-inlet saturation is considerably lower than that for combustion-chamber injection (water-air ratio 0.20).

SUMMARY OF RESULTS

The theoretical investigation of water-injection methods for thrust augmentation has shown that the injection of sufficient water at the compressor inlet to saturate the compressor-outlet air provided up to approximately 30-percent increase in thrust for sea-level static conditions and up to 100-percent increase at sea level and a Mach number of 1.50. At sea level and a Mach number of 1.50, compressor-inlet saturation provided approximately 60-percent increase in thrust. For all flight Mach numbers, compressor-outlet saturation provided greater thrust increase than combustion-chamber injection (water-air ratio 0.20) at equal or lower liquid consumptions. Increasing altitude decreases the thrust increase produced by water injection.

REFERENCES

1. Jones, William L., and Dowman, Harry W.: Experimental Investigation of Thrust Augmentation of a 1600-Pound Thrust Centrifugal-Flow-Type Turbojet Engine by Injection of Refrigerants at Compressor Inlets. NACA RM No. E7G23, 1947.

2. Dietz, Robert O., and Fleming, William A.: Altitude-Wind-Tunnel Investigation of Thrust Augmentation of a Turbojet Engine. II - Performance with Water Injection at Compressor Inlet. NACA RM No. E7C12, 1947.

3. Jones, William L., and Engelman, Helmuth W.: Experimental Investigation of Thrust Augmentation of 4000-Pound-Thrust Centrifugal-Flow-Type Turbojet Engine by Injection of Water and Alcohol at Compressor Inlets. NACA RM No. E7J19, 1948.

4. Keenan, Joseph H., and Kaye, Joseph: Thermodynamic Properties of Air. John Wiley & Sons, Inc., 1945.

5. Keenan, Joseph H., and Keyes, Frederick G.: Thermodynamic Properties of Steam. John Wiley & Sons, Inc., 1936.

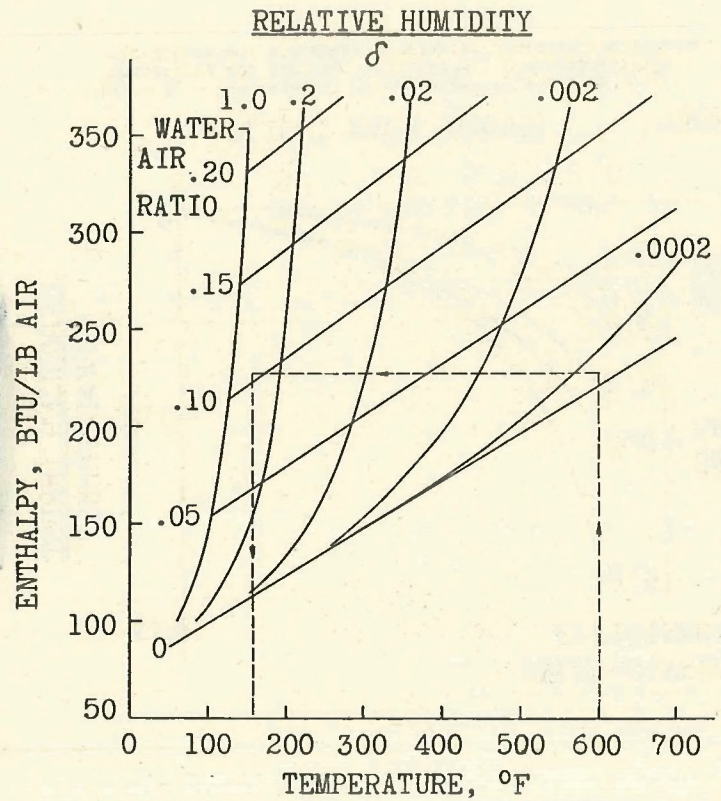

Figure 1. - Psychrometric chart.

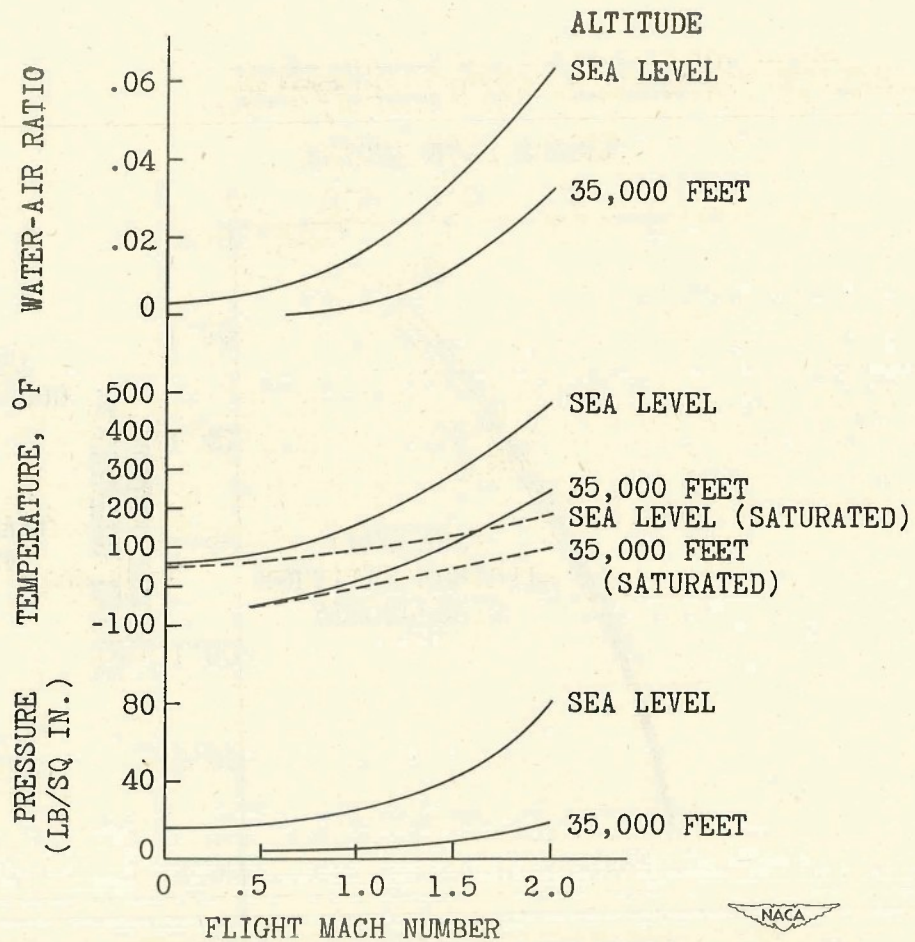

Figure 2. - Effect of flight conditions on cooling possible from saturation. Inlet-diffuser efficiency, 0.80; atmospheric relative humidity, 50 percent.

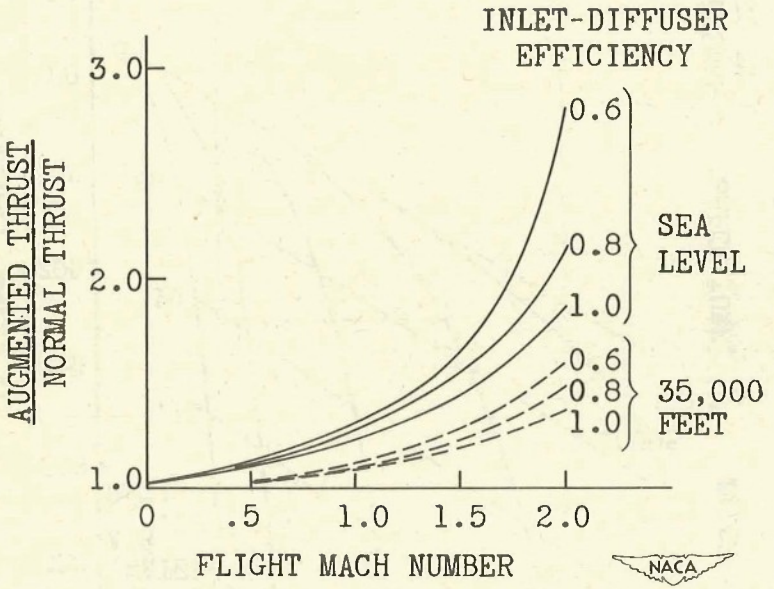

Figure 3. - Variation of thrust augmentation with flight conditions and diffuser efficiency. Compressor-inlet air saturated; atmospheric relative humidity, 50 percent.

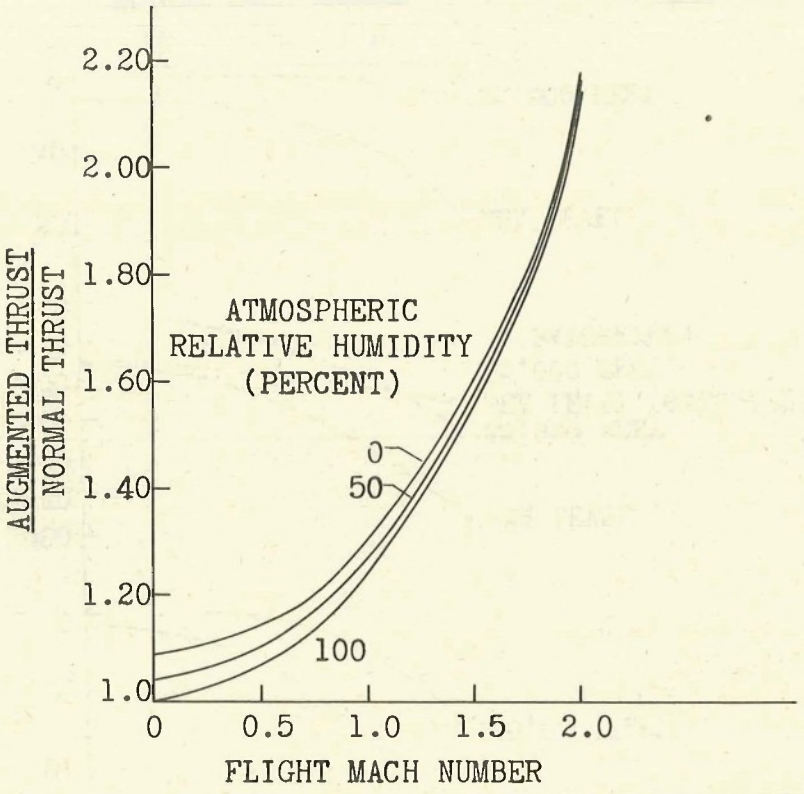

Figure 4. - Variation of thrust augmentation with flight conditions and atmospheric relative humidity. Altitude, sea level; inlet-diffuser efficiency, 0.80; compressor-inlet air saturated.

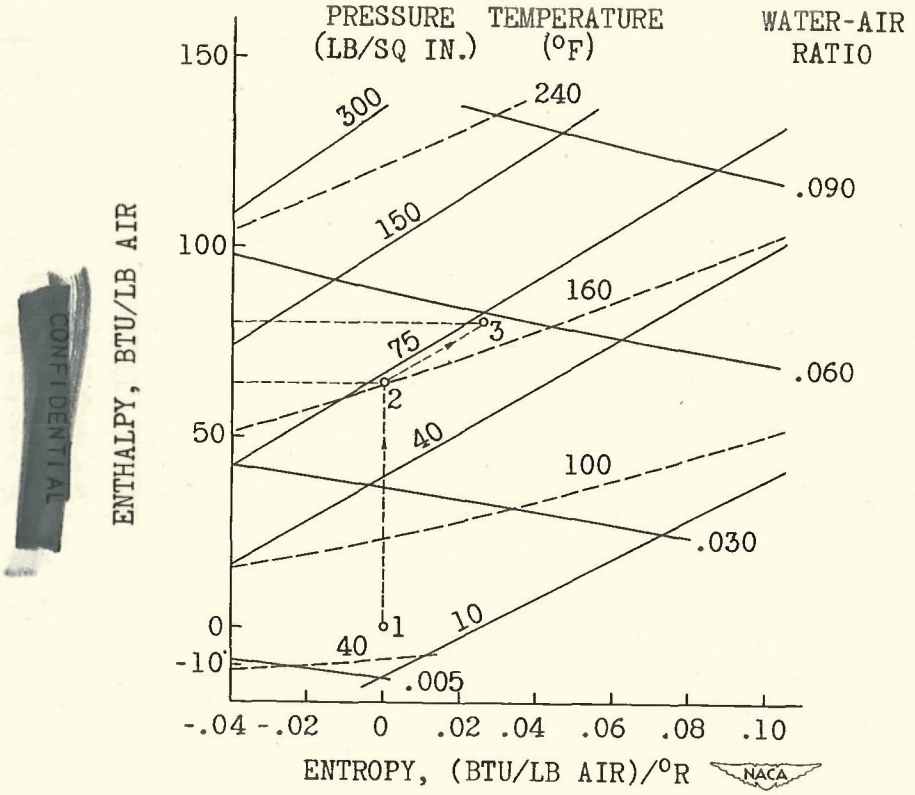

Figure 5. - Mollier diagram.

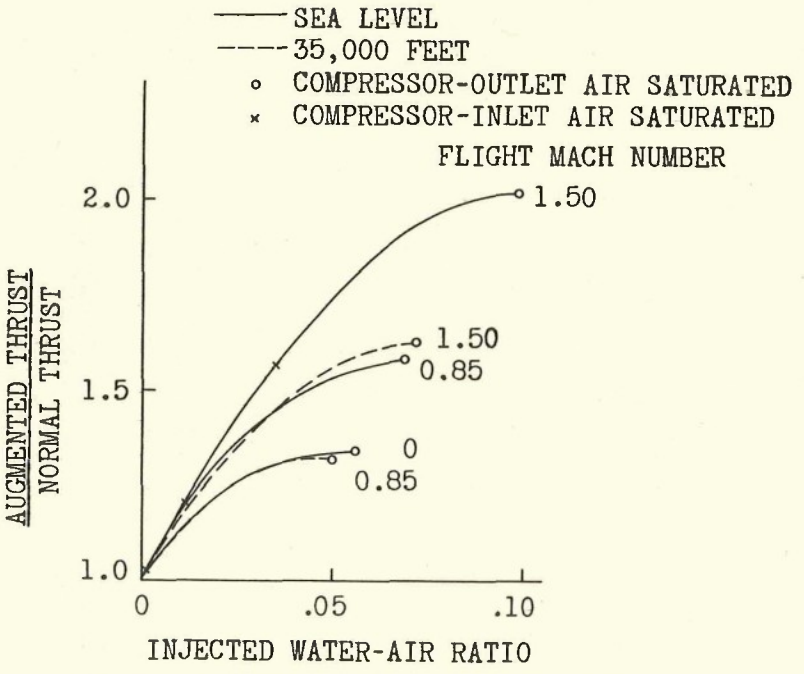

Figure 6. - Effect of flight conditions and water air ratio on thrust augmentation. Atmospheric relative humidity, 50 percent.

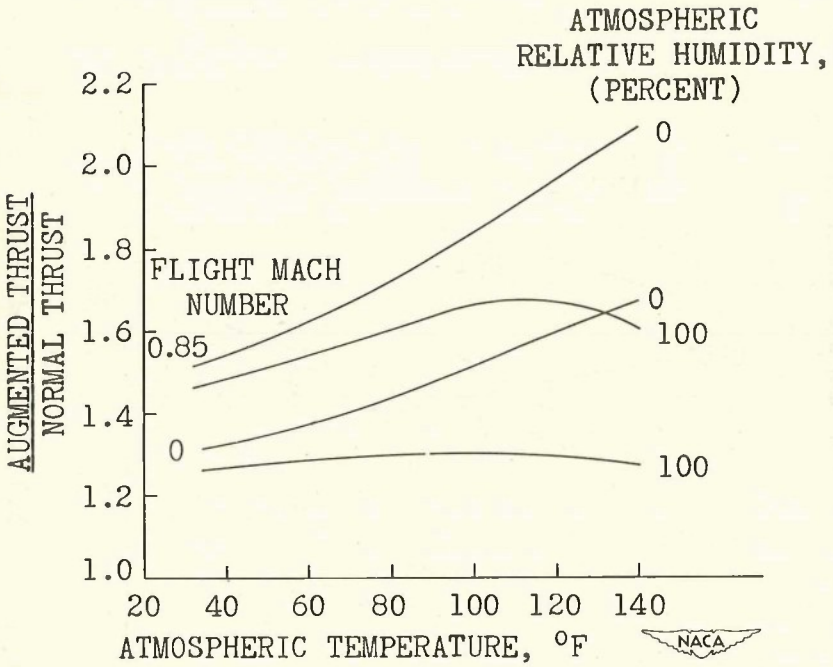

Figure 7. - Variation of thrust augmentation with atmoapheric temperature and ralativa humidity. Altitude, sea level; compraseor-outlet air saturated.

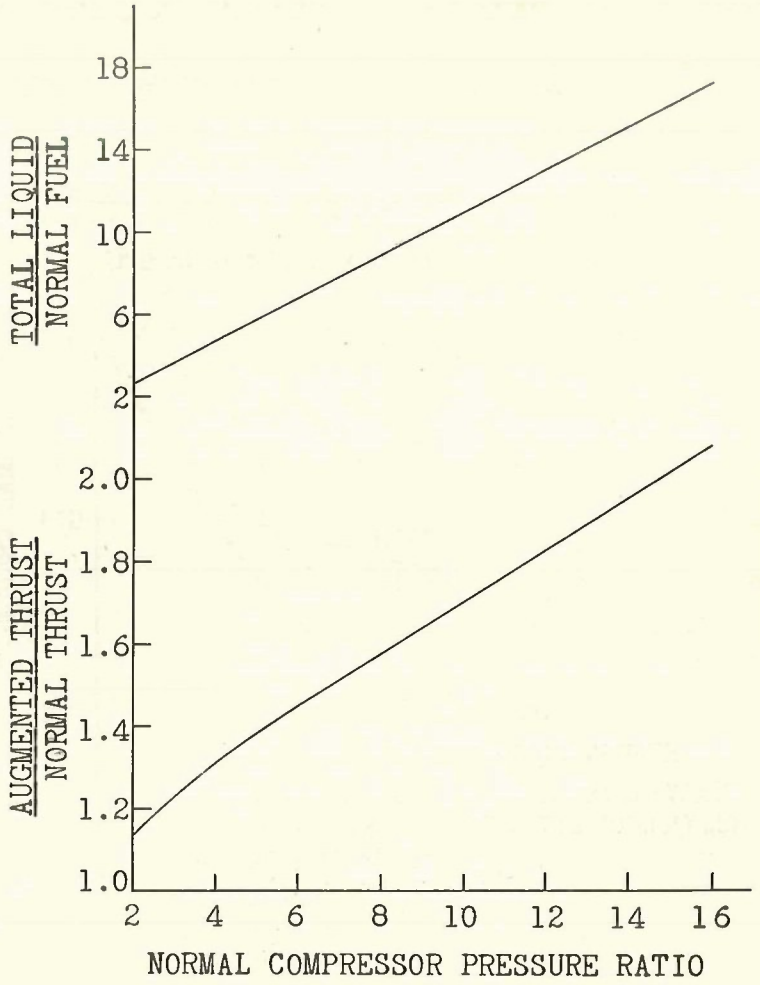

Figure 8. - Effect of compressor prassure ratio on thruat augmentation and on ratio of total liquid to normal fuel. Altitude, asa level; flight Mach number, 0; compreseor-outlet air saturated; atmospheric relative humidity, 50 percent.

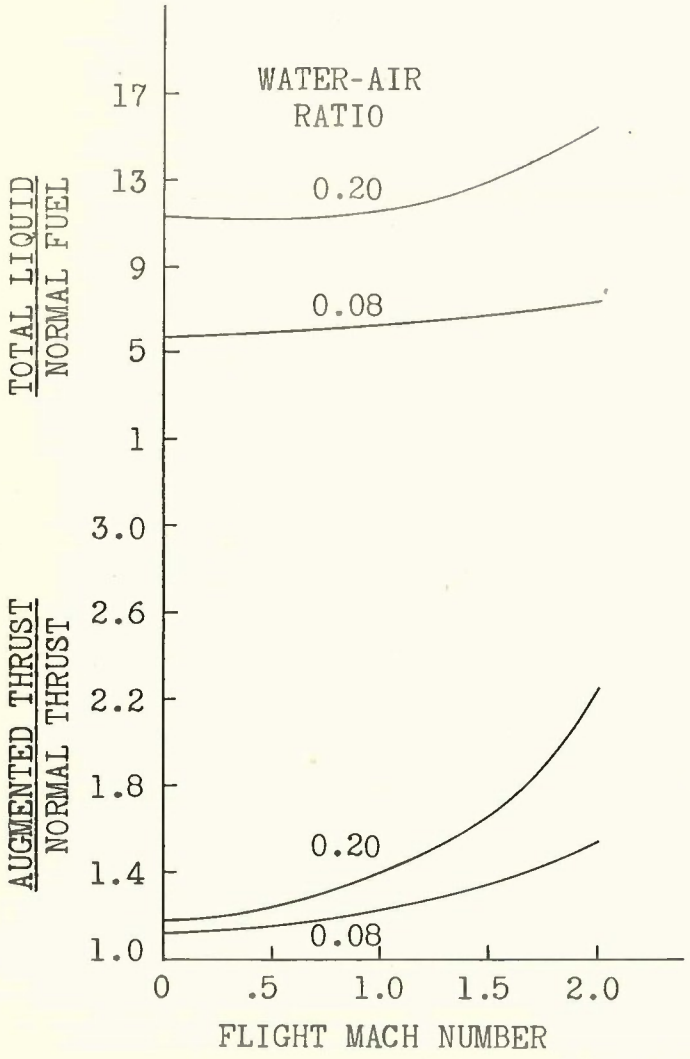

Figure 9. - Augmentation and totel liquid comeumption for combuetion-chember injection. Altitude, eea level: atmoepheric reletiva humidity, 50 percent.

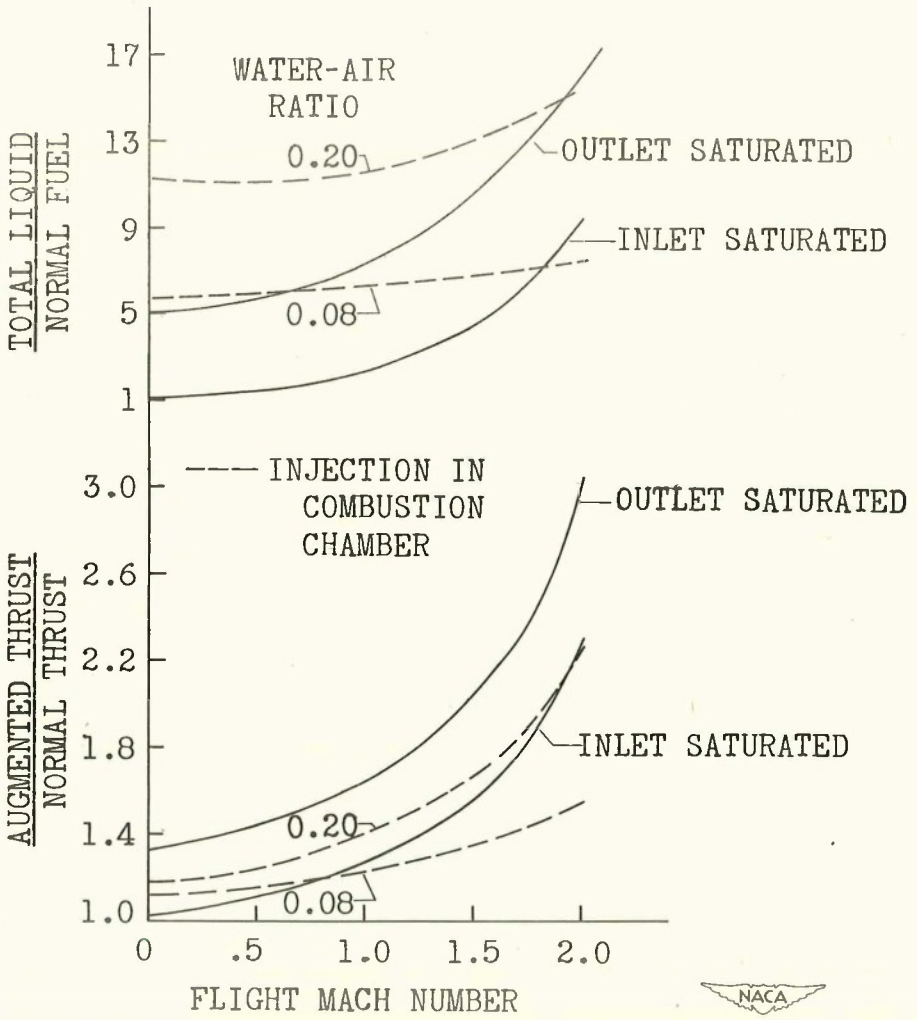

Figure 10. - Comparieon of compreeeor-inlat and -outlet eeturetion with injection in engine combuetion chamber. Altitude, eea level; etmoepheric reletive humidity, 50 percent.

EXPERIMENTAL INVESTIGATION OF THRUST AUGMENTATION BY WATER-ALCOHOL INJECTION

By Bruce T. Lundin

Lewis Flight Propulsion Laboratory

INTRODUCTION

Experimental investigations of thrust augmentation by water-alcohol injection were first conducted at the NACA Cleveland laboratory in 1943 and subsequent investigations of various applications of this method of augmentation on different types of turbojet engine have been continued to the present. The material presented in this paper constitutes a brief summary of the salient features of these experimental investigations, all of which were conducted at zero-ram, sea-level-pressure conditions.

RESULTS AND DISCUSSION

Compressor-Inlet Injection with Centrifugal-Flow-Type Engine

Among the first of these experimental research programs was an investigation of the injection of water and water-alcohol mixtures at the compressor inlets of a centrifugal-flow-type turbojet engine (references 1 and 2). A schematic diagram of a turbojet engine equipped for injection at the compressor inlets is shown in figure 1. In addition to the tanks and pumps necessary for an aircraft installation, the augmentation equipment consists of a water-alcohol manifold connected to several commercial spray nozzles equally spaced around the circumference of each compressor inlet. The thrust increase attendant with the injection of the water and alcohol is due primarily to cooling of the inlet air by evaporation of the injected liquids, both before reaching the compressor and during the compression process. This cooling effect results in an increase in compressor pressure ratio that, in turn, increases the total mass flow through the engine and the jet velocity, both of which contribute to increased engine thrust.

Normal air temperature. - The thrust augmentation obtained by injection at the compressor inlets at normal inlet-air temperatures with a 4000-pound-thrust centrifugal-flow-type engine is summarized in figure 2, in which the ratio of augmented to normal thrust is plotted against the total liquid consumption for various mixtures

[redacted]

of water and alcohol. These data are based on the results of over 100 runs and summarize the performance obtained at maximum rated engine speed. The engine was equipped with a standard fixed-area exhaust nozzle and the inlet-air temperatures for these tests ranged from 45° to 70° F. The total liquid consumption, used as the abscissa scale, includes the fuel flow to the engine combustion chambers and the flow of injected water and alcohol.

Operation of the engine with pure water injection at rates of total liquid consumption over 4 pounds per second was not possible because the engine fuel system had insufficient capacity to maintain rated engine speed at these injection rates. Operation with injected mixtures containing 60-percent (by weight) alcohol was limited to rates of total liquid consumption of about 5 pounds per second because of excessive tail-pipe gas temperatures and large glowing hot spots in the vicinity of the turbine. For all the water-alcohol mixtures used, the thrust augmentation increased almost linearly with total liquid consumption up to a liquid consumption of $5\frac{1}{2}$ to 6 pounds per second and tended to level off at high rates of liquid consumption. A maximum thrust ratio of 1.26 was obtained at a total liquid consumption of slightly over 7 pounds per second for an injected mixture containing 40-percent alcohol by weight. At this point, the injected flow of water and alcohol was about 6 pounds per second. Because of the leveling of the thrust curves at high injection rates, thrust augmentation only slightly less than the maximum possible augmentation can be obtained at considerably reduced injection rates. For example, a thrust ratio of 1.22 was obtained at a total liquid consumption of about 5.5 pounds per second, which corresponds to a rate of water-alcohol injection of slightly over 4 pounds per second.

A comparison of the curves for various water-alcohol mixtures shows that for the same total liquid consumption the thrust augmentation is increased slightly as the alcohol content of the injected mixture is increased. This improvement in engine performance with increased alcohol injection is a result of a replacement of the engine primary fuel by the injected alcohol, as is illustrated later. One advantage of including alcohol in the injected mixture, therefore, is that the alcohol decreases the primary fuel requirements of the engine and thus permits operation at higher injection rates than are possible with water alone and slightly reduces the total liquid consumption for a given thrust augmentation. An additional advantage is the low freezing temperature of water-alcohol mixtures; the freezing point of a 40-percent-alcohol mixture is about -22° F.

The variation of compressor pressure ratio, air flow, and total gas flow with injection rate for various water-alcohol mixtures is shown in figure 3. The compressor pressure ratio increases fairly rapidly with liquid injection up to a flow of about 4 pounds per second and levels off for higher injection rates. A maximum pressure ratio of slightly over 4.5 was obtained for an injection rate of about 5 pounds per second, compared with the normal pressure ratio of slightly over 4.0. The effect of the amount of alcohol in the injected mixtures is relatively slight. The total mass flow through the engine, which is limited by the capacity of the turbine nozzles, is shown by the dashed line in figure 3. This increase in total mass flow with increased injection rate is approximately proportional to the increase in compressor-outlet pressure because the turbine-inlet temperature was nearly constant over the range of injection rates used (the flow rate being controlled by conditions at the turbine nozzle). The total mass flow increased from a normal value of slightly less than 82 pounds per second to a maximum of over 91 pounds per second at an injection rate of 5 pounds per second, which represents an increase of about 12 percent. Thus, about half of the maximum thrust augmentation of 26 percent, which was shown in figure 2, is a result of the increase in total mass flow through the engine and the remaining half is due to the increased jet velocity provided by the higher pressure ratio. The engine air flow increased from a normal value of slightly over 80 pounds per second to a maximum of about 85.5 pounds per second for an injection rate of 4 pounds per second. Because the total mass flow remained nearly constant in the region of high injection rates, an increase in liquid injection beyond 4 pounds per second was accompanied by a decrease in engine air flow from its maximum value.

The effect of water-alcohol injection on the engine primary fuel flow is shown in figure 4 in which the fuel flow is plotted against the injection rate for the various water-alcohol mixtures. Because of the extra fuel necessary to vaporize and heat the injected water, the fuel required to maintain rated engine speed increases with injection rate for the mixtures containing 0- and 20-percent alcohol. However, because the alcohol burns in the combustion chambers and thus serves as a fuel itself, the engine primary fuel requirements are decreased as the injection of mixtures containing 40- and 60-percent alcohol is increased. An evaluation of the amount of this fuel replacement by increased alcohol content in the injected mixtures showed that about 40 percent of the heat of combustion of the alcohol is liberated in the combustion chambers. The horizontal dashed line drawn through the point of normal engine fuel flow indicates the mixtures of water and alcohol that may be injected without a change in fuel flow and hence without a change in the throttle setting. These

constant-throttle mixtures vary from about 40-percent alcohol at the lowest injection rates to about 32-percent alcohol at the highest injection rates.

Elevated air temperature. - As previously stated, all these results are restricted to inlet-air temperatures (between 45° and 70° F) that prevailed during the time of the tests. Many applications of thrust augmentation are, however, those of high-speed flight at moderate altitudes, where the ram temperature rise of the inlet air is appreciable. Because variations in the temperature of the inlet air may be expected to have an important part in the evaporation process of the injected liquids and hence in the thrust augmentation produced, an investigation has been conducted to determine experimentally the effect of inlet-air temperature on the thrust augmentation produced by injection of water-alcohol mixtures at the compressor inlets. This investigation also served the secondary purpose of providing data for an experimental evaluation of the applicability of the analysis presented in the preceding paper over a range of both liquid injection rates and inlet-air temperatures.

The high inlet-air temperatures required for this investigation were obtained by an exhaust-gas bleedback system in which part of the engine exhaust gases were ducted to the engine inlet and suitably mixed with the cooler air from the normal inlet-air system. The maximum inlet-air temperatures used in this investigation were about 200° F, which required an exhaust-gas bleedback of about 10 percent and resulted in a reduction of the oxygen content of the engine-inlet air from the normal value of 23.2 percent to 22.6 percent by weight. Satisfactory correlation of data from several standard engine tests without injection showed that this reduction in oxygen content of the engine-inlet air did not alter the engine performance. This investigation was also conducted on a 4000-pound-thrust centrifugal-flow-type engine with a standard fixed-area exhaust nozzle and with a variable-area exhaust nozzle.

The results of the investigation with the fixed-area exhaust nozzle are summarized in figure 5, in which the engine thrust is plotted against the inlet-air temperature for the normal (unaugmented) performance and for the augmented operation with total liquid consumptions from 2.25 to 4.25 pounds per second. These tests were restricted to the injection of water alone and the engine was operated at either the maximum rated speed or at the maximum operable speed as limited by allowable tail-pipe gas temperatures. The specific humidity of the inlet air was very nearly constant at a value of about 50 grains per pound of air.

For complete ranges of normal engine performance and of augmented operation at high inlet-air temperatures, it was necessary to continually reduce the engine speed as the inlet-air temperature was increased to order to prevent exceeding the maximum rated tail-pipe gas temperature. In fact, operation of the engine without water injection was limited to an inlet-air temperature of 140° F because further reductions in tail-pipe gas temperature by reducing the engine speed were not possible. This necessary reduction of engine speed, together with the decrease in compressor Mach number attendant with the increased air temperature, is responsible for the large reduction in thrust with increased inlet-air temperature. This decrease in thrust with increased air temperature is much greater for normal engine operation and at low rates of water injection than for the high rates of injection, because for these conditions the necessary reduction in engine speed is greatest. The increase in thrust obtained by water injection is therefore much greater at high inlet-air temperatures than it is at low inlet-air temperatures. For example, with a total liquid consumption of 4.25 pounds per second a thrust increase of about 700 pounds was obtained at 80° F as compared with a thrust increase of about twice this amount, or 1400 pounds, at an inlet-air temperature of 140° F.

The data of figure 5 are replotted in figure 6, where the ratio of augmented to normal engine thrust is shown as a function of inlet-air temperature for the various values of total liquid consumption. The thrust augmentation increases very rapidly with increased inlet-air temperature, particularly for high values of total liquid consumption. For the total liquid consumption of 4.25 pounds per second, which results from the injection of about 2.7 pounds per second of water, the augmented thrust ratio increases from about 1.25 at an inlet-air temperature of 80° F to over 1.70 at an inlet-air temperature of about 140° F.

The results obtained with the variable-area exhaust nozzle on the engine are summarized in figure 7, in which the engine thrust is plotted against the inlet-air temperature for various rates of total liquid consumption. For these runs, the engine was operated at maximum rated speed and the tail-pipe gas temperatures were maintained constant at the maximum rated value by adjustment of the exhaust-nozzle area. As for the previous runs, the specific humidity of the inlet air was fairly constant, varying between 40 and 60 grains per pound. These runs included the injection of mixtures of water and alcohol varying from pure water to 60-percent alcohol but, because no systematic trend with alcohol misture could be detected in the data, the data points are coded for various total liquid consumptions

only. The two dashed lines show, for comparison, the performance with the fixed-area exhaust nozzle on the engine at zero injection and at a total liquid consumption of 4.25 pounds per second, as obtained from the data of figure 5.

The thrust of the engine with the variable-area nozzle is about the same as that obtained with the fixed-area nozzle for inlet-air temperatures varying from about 60° F for unaugmented operation to about 140° F at a total liquid consumption of 4.25 pounds per second. The thrust with the two types of exhaust nozzle is the same because the variable-area nozzle, which was controlled to maintain limiting tail-pipe gas temperatures, had about the same area as the standard fixed-area nozzle at these operating conditions. The thrust with the variable-area nozzle at both higher and lower inlet-air temperatures, however, was greater than that obtained with the fixed-area nozzle because, at the high inlet-air temperatures, the exhaust-nozzle area could be increased to maintain limiting tail-pipe gas temperature instead of reducing the engine speed and, at low inlet-air temperature, slight reductions in the exhaust-nozzle area below the standard size were possible. With the variable-area nozzle, therefore, the decrease in engine thrust with increased inlet-air temperature is less than for the fixed-area nozzle and, moreover, satisfactory operation is possible at higher inlet-air temperatures. The thrust increase obtained by the water-alcohol injection is greater at higher inlet-air temperatures than it is at normal inlet-air temperatures. For example, at a total liquid consumption of 5.25 pounds per second, which resulted from the injection of 4.0 pounds per second of water and alcohol, the thrust augmentation was about 800 pounds at normal inlet-air temperatures and increased to about 1300 pounds at an inlet-air temperature of 200° F.

The data of figure 7 are replotted in figure 8 to show the ratio of augmented to normal thrust for the same range of inlet-air temperatures and total liquid consumptions. The experimental thrust augmentation increases fairly rapidly with both increased inlet-air temperature and increased total liquid consumption and reaches a value of about 1.65 for a total liquid consumption of 5.25 pounds per second at an inlet-air temperature of 200° F. Although the thrust augmentation obtained with the fixed-area nozzle was greater than these values for the variable-area nozzle, especially at high inlet-air temperatures, it is recalled that the actual augmented thrust produced was slightly higher with the variable-area nozzle.

Also included in figure 8 is a series of dashed lines that represent the results of a theoretical analysis of the wet-compression process. The calculations of the theoretical thrust augmentation

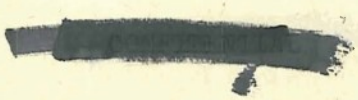

arc, as in the method of the preceding paper, based on the assumptions that the air is completely saturated before entering the compressor and is in equilibrium with the water throughout the compression process. For these calculations, however, the values of compressor efficiency and slip factor used were the same as the values obtained without injection at the various inlet-air temperatures. Adjustments to the compressor efficiency such as were mentioned in the preceding paper were not attempted for these calculations because the effects of liquid injection on compressor performance of this engine are still under study. The theoretical values of the augmented thrust ratio are from 5 to 25 percent higher than the experimental values, the difference increasing with increasing inlet-air temperature, and, moreover, the lines are of somewhat different shape. This difference between the theoretical calculations and experimental performance therefore indicates the degree to which the actual vaporization process departs from the idealized one and the influence of possible changes in compressor performance affected by the water injection.

Compressor-Inlet Injection with Axial-Flow-Type Engine

In addition to the previously discussed investigations on centrifugal-flow-type engines, an investigation has been conducted to determine the performance of an axial-flow-type engine with water-alcohol injection at the compressor inlets (reference 3). A 4000-pound-thrust engine equipped with a variable-area exhaust nozzle was used. Different injection systems were tried in an effort to obtain the best atomization and distribution of the injected liquids. The results obtained with the different systems were all about the same, however, and, for brevity, the results of a typical run with only one of the systems is presented.

In figure 9 the ratio of augmented to normal engine thrust is shown for various total liquid consumptions. For the highest total liquid consumption shown (6.0 lb/sec), the injection rate was about 4.5 pounds per second. The use of this injection rate, however, resulted in damage to the engine in the form of compressor-blade rubbing, and cracking and warping of the blades of the turbine nozzle box. Satisfactory engine operation accordingly limited the injection rate to about 3 pounds per second, resulting in a total liquid consumption of about 4.5 pounds per second and a thrust ratio of 1.15. This limit to the possible thrust augmentation is considerably lower than the value of 1.26 obtained with the centrifugal-flow-type engine and was found to be the result of centrifugal separation

of the injected liquid and air in the compressor and the attendant failure of a large portion of the injected liquid to evaporate in the compressor.

Evidence of this separation of the injected liquid and air is obtained from temperature surveys at the compressor outlet as shown in figure 10 in which the compressor-outlet temperature is plotted against the radial distance across the compressor-outlet annulus for various rates of water injection. Without injection, the temperature profile was fairly even, whereas for all injected flows the air remained relatively uncooled in the region of the blade roots, and decreased to a lower temperature only in the region between the center of the outlet annulus and the blade tips. The maximum temperature difference across the compressor outlet was about 150° F, which indicates considerable centrifugal separation of the injected liquid and air. It is therefore likely that water-alcohol injection at the compressor inlets of an axial-flow-type engine can be used to best advantage only when the engine inlet-air temperature is high enough and the initial relative humidity low enough to provide for evaporation of the largest part of the injected liquid before compression.

Interstage Injection with Axial-Flow-Type Engine

In order to obtain maximum usefulness of water-alcohol injection in an axial-flow engine, some means must be found to avoid the centrifugal separation of the injected liquids and air in the compressor. One method of injection that would avoid the centrifugal separation would be to inject only enough liquid to saturate the air at various stages of the compression process. An experimental investigation is now in progress to determine the performance of an axial-flow engine with interstage injection of water and alcohol.

Before the engine testing phase was started, the characteristics of many different types of injection nozzle were studied in a chamber in which the compressor air-flow conditions were simulated. The principal problem of nozzle design and selection was to obtain an injection nozzle that, with reasonable injection pressures, would give sufficient penetration for the injected liquids to reach the region of the blade roots. This placing of the injected liquid in the region of the blade roots was considered desirable to offset, as much as possible, the centrifugal effects of the rotating compressor blades. It was found that a jet of high penetration could only be obtained with injection nozzles of fairly large diameter, which was incompatable with the requirement of a large number of nozzles to provide even stagewise and circumferential distribution of the injected liquids.

The type of injection nozzle finally chosen and the general arrangement of their installation in the compressor is shown in figure 11. The injection nozzles, which are shown in detail in the insert, were installed in the end of 1/8-inch steel tubes that extended approximately halfway across the compressor annulus. These extension tubes were necessary to enable the injected liquids to reach the region of the blade roots. These tubes were located between the stator blades, near the leading edge, of the third, sixth, and ninth stages, and 20 tubes were installed at each stage. In addition to these 60 interstage tubes arranged at three stages of compression, conventional spray nozzles were installed at the compressor inlet to provide injection for the first three stages of compression. The presence of these injection tubes caused a decrease in normal engine thrust of about 1.5 percent; this disadvantage could, however, conceivably be overcome by incorporating the water passages in the stator blades.

At the present time, the investigation of interstage injection is in progress on a 4000-pound-thrust axial-flow-type engine equipped with a variable-area exhaust nozzle. The program is not yet complete, but sufficient data have been obtained to illustrate the principal features and the usefulness of this system of water-alcohol injection. A summary of some of the results is given in figure 12, in which the ratio of augmented to normal engine thrust at maximum rated engine speed and tail-pipe gas temperatures is plotted against the total liquid consumption for the various water-alcohol mixtures used. Because these data were obtained for inlet-air temperatures that varied considerably between runs, all results have been corrected to constant inlet-air temperature of 88° F, which was a good average of the temperature of the various runs and is the temperature that prevailed for the compressor-inlet injection runs. For all these data the total flow of injected liquids was equally divided among the four injection stations.

As previously noted for the centrifugal-flow-type engine, the thrust augmentation for an axial-flow engine at a given total liquid consumption increases slightly as the alcohol content of the injected mixtures is increased (fig. 12). The thrust augmentation also increases continuously with increased total liquid consumption and reaches a value of about 1.24 for a total liquid consumption of 6 to 7 pounds per second. This amount of thrust augmentation is in close agreement with the performance obtained with the centrifugal-flow engine previously discussed, which indicates satisfactory mixing of the air and the liquids throughout the compression process. To date no compressor-blade rubbing or other harmful effects have occurred such as were experienced with compressor-inlet injection

[redacted]

at high injection rates. For comparison, the performance obtained by injection at the compressor inlet is reproduced in figure 12 as the lower dashed line. Although the thrust augmentation of the inlet-injection system appears higher than that of interstage injection for low injection rates, the difference is largely the result of a shifting of the curve for inlet injection to the left because of a lower unaugmented liquid consumption, or normal engine fuel flow, for the inlet-injection engine. Therefore, for total liquid consumptions from normal to about 3 pounds per second, the performance with inlet injection is about the same as with interstage injection, whereas for higher rates of liquid consumption the interstage injection system gives higher thrust augmentations.

The results of theoretical calculations of thrust augmentation, based on the same compressor efficiency and slip factor for both normal and augmented operation, is shown by the upper dashed line in figure 12. Although the maximum calculated thrust augmentation is only slightly greater than that obtained experimentally, the theoretical liquid consumptions are only about half as great as actually required. At a total liquid consumption of 4 pounds per second, the theoretical augmented thrust ratio is 8 percent greater than the experimental, which illustrates the degree of departure of the actual vaporization process from the idealized one and possibly changes in compressor performance caused by the water injection.

Some typical temperature surveys at the compressor outlet are shown in figure 13, where the compressor-outlet temperature is plotted against the radial distance across the compressor-outlet annulus. The solid lines represent the normal engine performance without injection and with interstage injection at two flow rates. It is apparent that the air was evenly cooled by the evaporation of the injected liquids with, in fact, an even flatter temperature distribution with injection than for normal operation. The typical temperature distribution obtained with compressor-inlet injection (fig. 10) is also included for comparison. In addition to the runs with the extended interstage nozzles, a set of runs was conducted with the interstage injection nozzles flush with the outer wall of the compressor casing. The use of injection nozzles at this location would be obviously desirable in order to avoid the 1.5 percent decrease in unaugmented engine performance. The thrust was considerably reduced for these runs, however, and the compressor-outlet temperature distribution was similar to that obtained with inlet injection, as shown by the upper dashed line in figure 12. This type of temperature distribution, together with reduced thrust augmentation, has also been obtained in several recent tests with

[redacted]

the extended nozzles when the injection pressure was below 200 pounds per square inch. The necessity of placing the injected liquids in the region of the blade roots for this type of installation is therefore evident.

Combustion-Chamber Injection with Axial-Flow-Type Engine

The application of interstage injection to an axial-flow engine, while providing satisfactory augmentation performance, has the disadvantage of complexity of installation, at least for engines already in the production stage. Accordingly, an experimental investigation of injection into the combustion chamber has been conducted in an effort to obtain reasonable thrust increase with a system that retains the advantage of simplicity of installation.

The injection of water into the combustion chambers of a turbojet engine tends to decrease the air flow through the turbine nozzles because the total mass flow cannot increase unless the turbine-inlet pressure is increased. A reduction in the engine air flow, however, shifts the compressor operating point to a higher pressure ratio which, in turn, permits an increase in the mass flow through the engine. A new equilibrium operating point of the engine, having a lower compressor air flow, a higher compressor pressure ratio, and a higher total mass flow, is obtained. The thrust augmentation produced, therefore, depends on the operating characteristics of the compressor and is a result of both the increased mass flow and higher jet velocity provided by the increased pressure ratio. In addition to these effects, the increased gas constant and specific heat of the water-air mixture also contribute, to a smaller degree, to an increase in the turbine-outlet pressure and hence in the jet velocity.

This investigation of thrust augmentation by combustion-chamber injection was conducted with a 4000-pound-thrust axial-flow-type engine equipped with a variable-area exhaust nozzle and operated at maximum rated rotor speed and tail-pipe gas temperature. On the basis of results obtained from preliminary investigations conducted on a single combustion chamber, the liquids were introduced at approximately the midpoint of the combustion chamber as shown in the upper part of figure 14. Separate nozzles were used for the water and alcohol injection and were installed through holes in the inner liner to spray into the primary combustion zone. Four different injection systems were used and the principal characteristics of each system are summarized in the table of figure 14. These four injection systems, which are designated as systems A, B, C, and D, differed in the type of spray (for example, hollow-cone or solid-jet), the number of nozzles per combustion chamber, and the size of the nozzle orifice.

In the lower part of figure 14 is plotted the ratio of augmented to normal engine thrust over a range of total liquid consumptions for all the injection systems and for various combinations of water and alcohol injection. All the data obtained for combustion-chamber injection fall on a single line indicating that, at least for the range of this investigation, the engine performance is not affected by the penetration of the type of the spray used or the mixture of water-alcohol injected. The temperature distributions at the turbine outlet for all the data were also generally similar to that for increased engine operation. The augmented thrust ratio increases almost linearly with increased total liquid consumption and reaches a value of about 1.18 for a total liquid consumption of 6.25 pounds per second. The performance with interstage injection and compressor-inlet injection is shown by the two dashed lines for comparison. The augmentation provided by combustion-chamber injection with this engine is only about three-fourths of that provided by interstage injection throughout the range of injected flows and is slightly higher than that obtained by inlet injection at the highest total liquid consumption.

The effect of combustion-chamber injection rate on the compressor pressure ratio, the total gas flow rate, and the compressor air flow is shown in figure 15. Because of the steep characteristics of the compressor of the engine used, the increase in pressure ratio with increased combustion-chamber injection was accompanied by only a slight decrease in the air flow. With the injection of about 5 pounds per second of water and alcohol into the combustion chambers, the pressure ratio was increased from a normal value of about 3.75 to nearly 4.1, which resulted in a linear increase in the total gas flow from 72 pounds per second to about 77 pounds per second. An analysis of this augmentation cycle, using the measured compressor pressure ratio and air flow and constant values of compressor and turbine efficiency, showed that about 40 percent of the augmentation produced is due to the increased mass flow rate, slightly over 40 percent due to the increased jet velocity arising from the higher compressor pressure ratio, and the remaining 15 to 20 percent due to the change in thermodynamic properties of the turbine and exhaust-nozzle working fluids.

SUMMARY OF RESULTS

The results of the experimental investigations of thrust augmentation by water-alcohol injection, all of which were conducted at zero-ram, sea-level-pressure conditions, show that for the centrifugal-flow-type turbojet engine, the injection of water-alcohol mixtures at the compressor inlets provides a simple and satisfactory

form of thrust augmentation. For normal inlet-air temperatures, augmented thrust ratios of the order of 1.26 are possible for total liquid consumptions of about 7 pounds per second for a 4000-pound-thrust engine. At high inlet-air temperatures, the thrust augmentation produced increases considerably.

For an axial-flow-type engine, the injection of water at the compressor inlets was satisfactory only for low injection rates, producing thrust augmentation ratios of less than 1.15, because of centrifugal separation of the injected liquid and air by the rotating compressor blades. By the use of interstage injection, however, this centrifugal separation was avoided provided the injected liquid was placed in the region of the blade roots. The augmented thrust ratio produced by this method was very nearly the same as provided by compressor-inlet injection in a centrifugal-flow engine, being for a 4000-pound-thrust engine about 1.24 for a total liquid consumption of about 6 to 7 pounds per second. With combustion-chamber injection in the axial-flow engine, the thrust augmentation produced was only about three-fourths of that obtained with interstage injection but this system has the advantage of greater mechanical simplicity.

REFERENCES

1. Jones, William L., and Dowman, Harry W.: Experimental Investigation of Thrust Augmentation of a 1600-Pound-Thrust Centrifugal-Flow-Type Turbojet Engine by Injection of Refrigerants at Compressor Inlets. NACA RM No. E7G23, 1947.

2. Jones, William L., and Engelman, Helmuth W.: Experimental Investigation of Thrust Augmentation of 4000-Pound-Thrust Centrifugal-Flow-Type Turbojet Engine by Injection of Water and Alcohol at Compressor Inlets. NACA RM No. E7J19, 1948.

3. Baron, Burnett, Dowman, Harry W., and Dackis, William C.: Experimental Investigation of Thrust Augmentation of Axial-Flow-Type 4000-Pound-Thrust Turbojet Engine by Water and Alcohol Injection at Compressor Inlet. NACA RM No. E7K14, 1948.

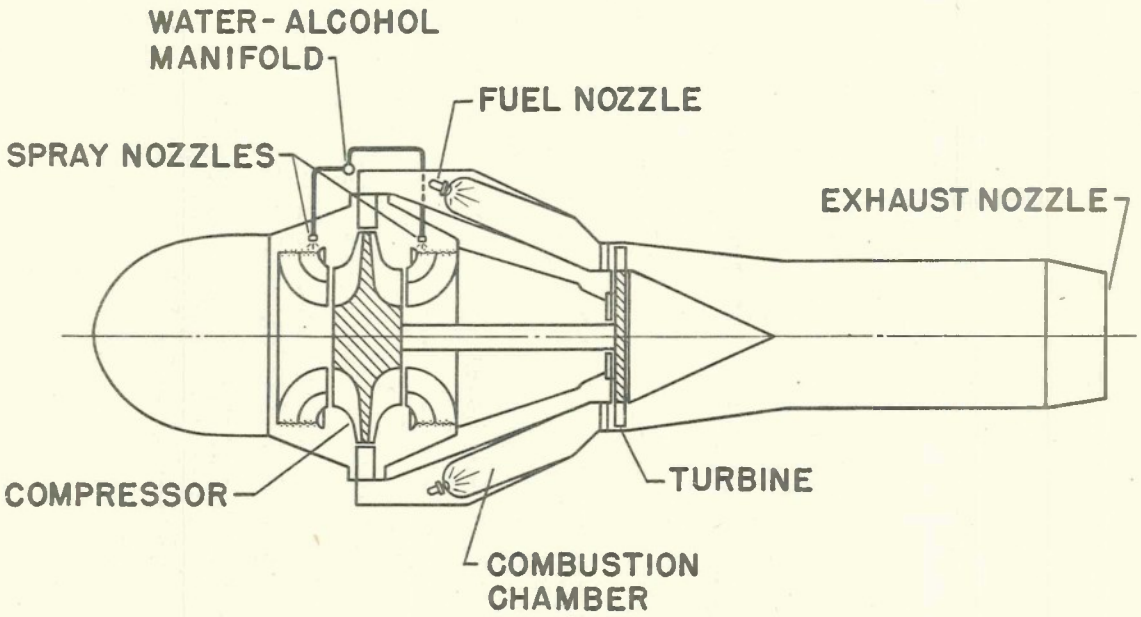

Figure 1. - Schematic diagram of turbojet engine equipped for water-alcohol injection at the compressor inlets.

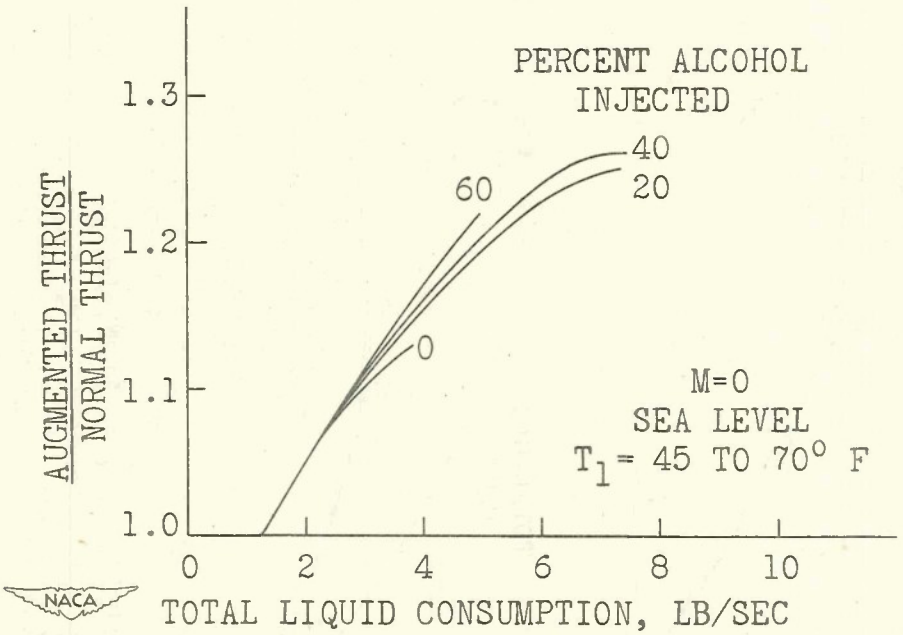

Figure 2. - Variation of ratio of augmented to normal engine thrust with total liquid consumption for various water-alcohol mixtures. Injection at compressor inlets of centrifugal-flow-type engine with fixed-area exhaust nozzle.

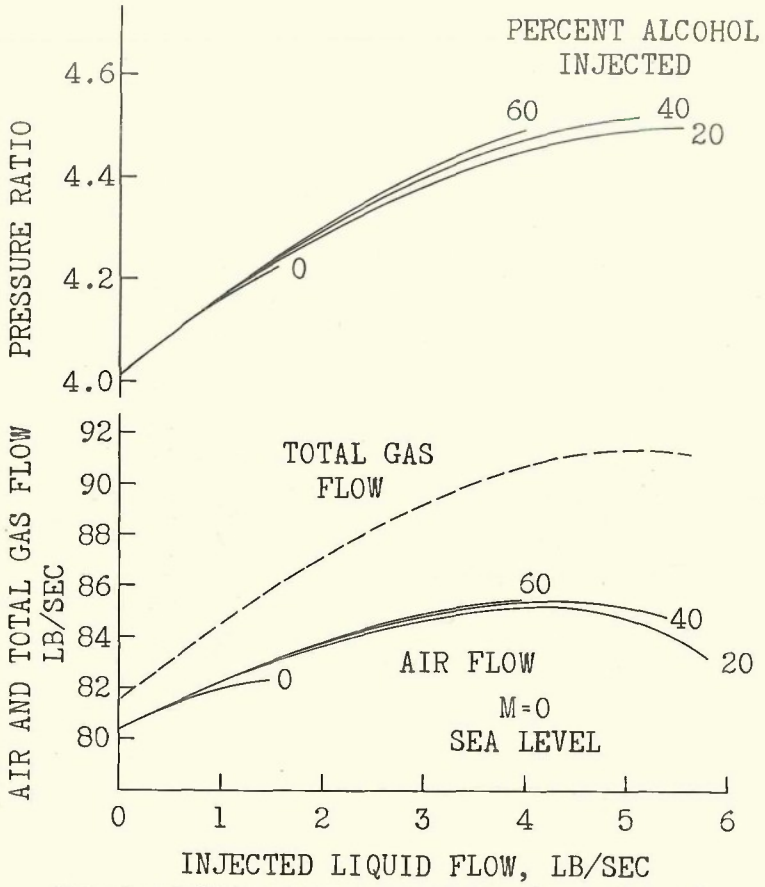

Figure 3. - Variation of compressor pressure ratio, air flow, and total gas flow with injected liquid flow for various mixtures of water and alcohol. Injection at compressor inlets of centrifugal-flow-type engine with fixed-area exhaust nozzle.

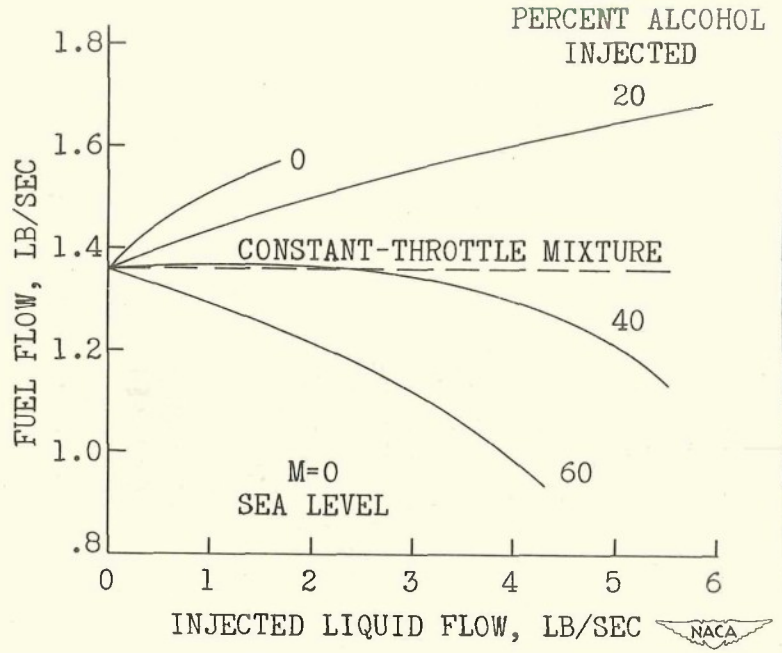

COMPRESSOR INLET INJECTION. CENTRIFUGAL FLOW ENGINE WITH FIXED EXHAUST NOZZLE.

Figure 4. - Variation of normal engine fuel flow with injected liquid flow for various mixtures of water and alcohol. Injection at compressor inlets of centrifugal-flow-type engine with fixed-area exhaust nozzle.

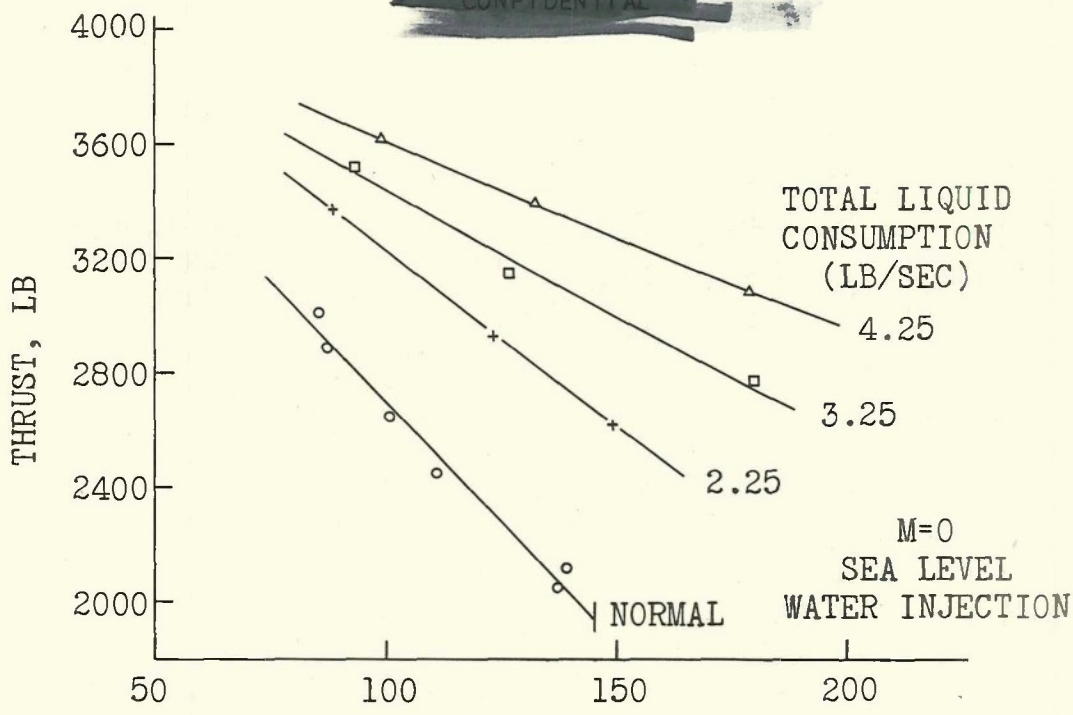

Figure 5. - Variation of engine thrust with compressor-inlet air temperature for various rates of total liquid consumption. Injection at compressor inlets of centrifugal-flow-type engine with fixed-area exhaust nozzle.

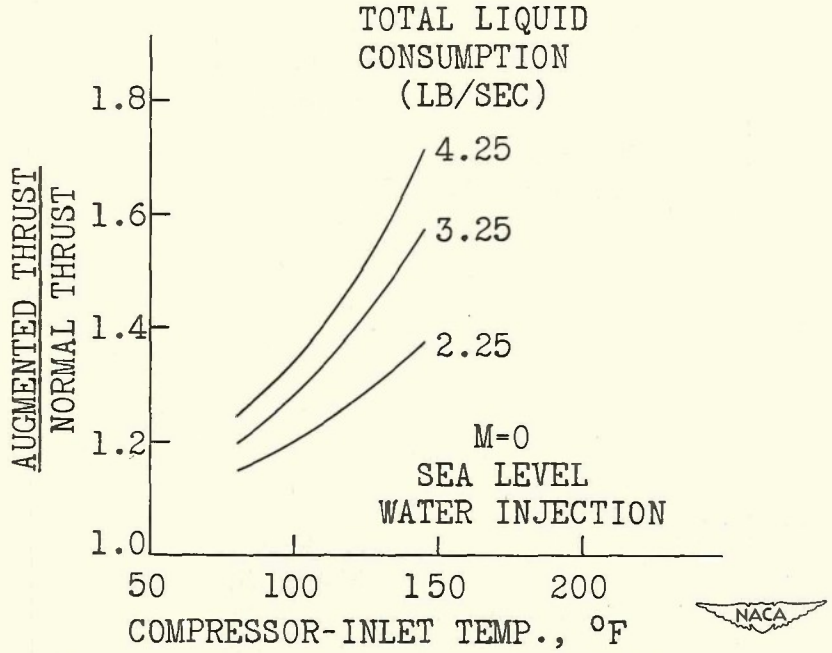

Figure 6. - Variation of ratio of augmented to normal engine thrust with compressor-inlet air temperature for various rates of total liquid consumption. Injection at compressor inlets of centrifugal-flow-type engine with fixed-area exhaust nozzle.

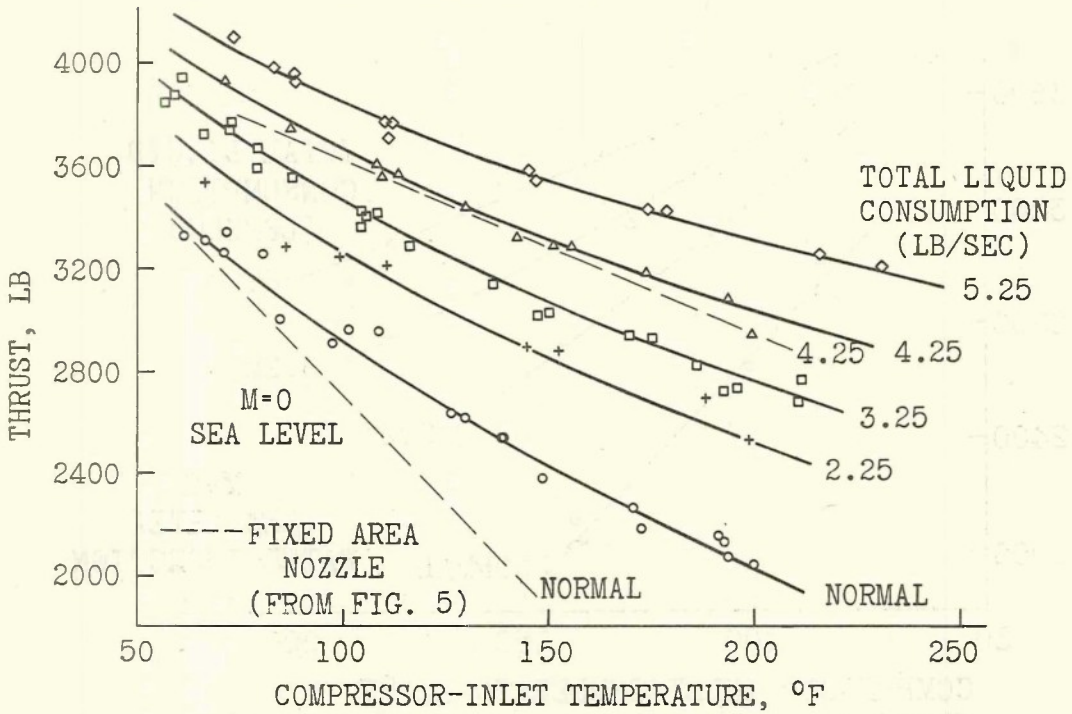

Figure 7. - Variation of thrust with compressor-inlet air temperature for various rates of total liquid consumption. Injection at compressor inlets of centrifugal-flow-type engine with variable-area exhaust nozzle.

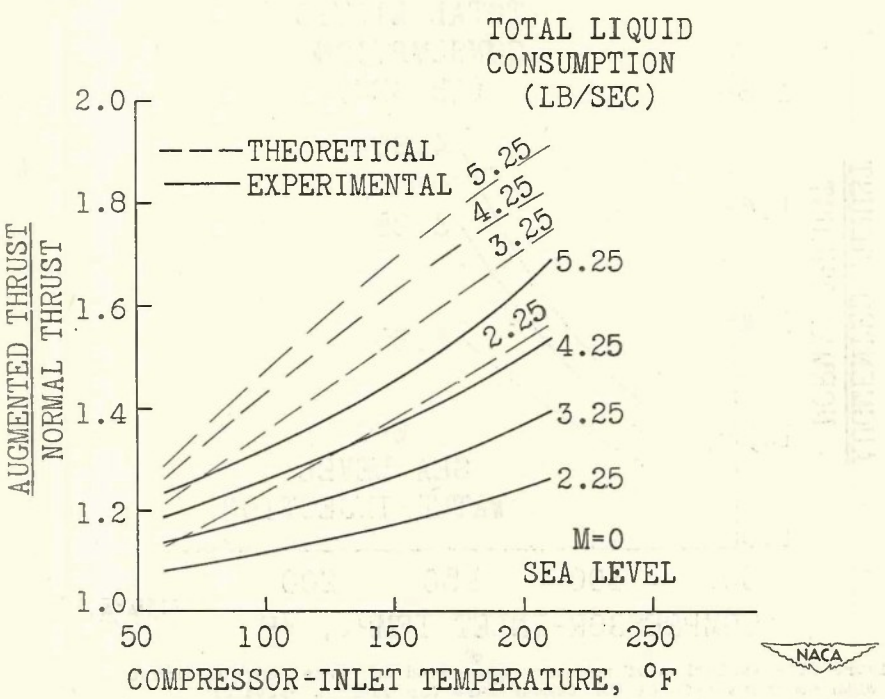

Figure 8. - Variation of ratio of augmented to normal engine thrust with compressor-inlet air temperature for various rates of total liquid consumption. Injection at compressor inlets of centrifugal-flow-type engine with variable-area exhaust nozzle.

Figure 9. - Variation of ratio of augmented to normal engine thrust with total liquid consumption. Injection at compressor inlet of axial-flow-type engine with variable-area exhaust nozzle.

Figure 10. - Compressor-outlet temperature surveys for various rates of water injection at compressor inlet of axial-flow-type engine with variable-area exhaust nozzle.

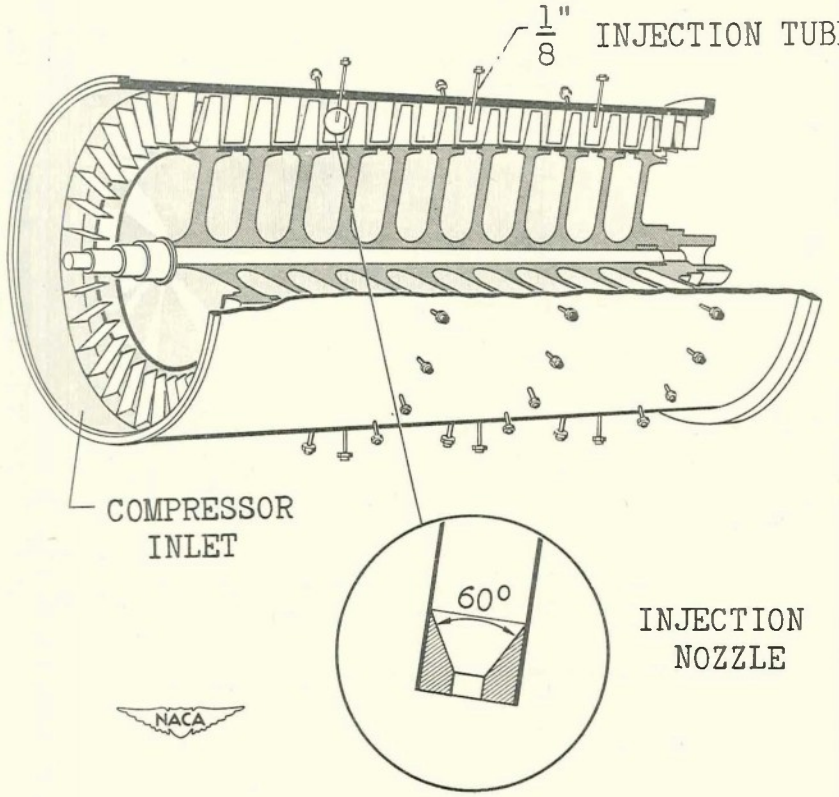

Figure 11. - Diagrammatic sketch of installation of interstage injection nozzles in axial-flow compressor.

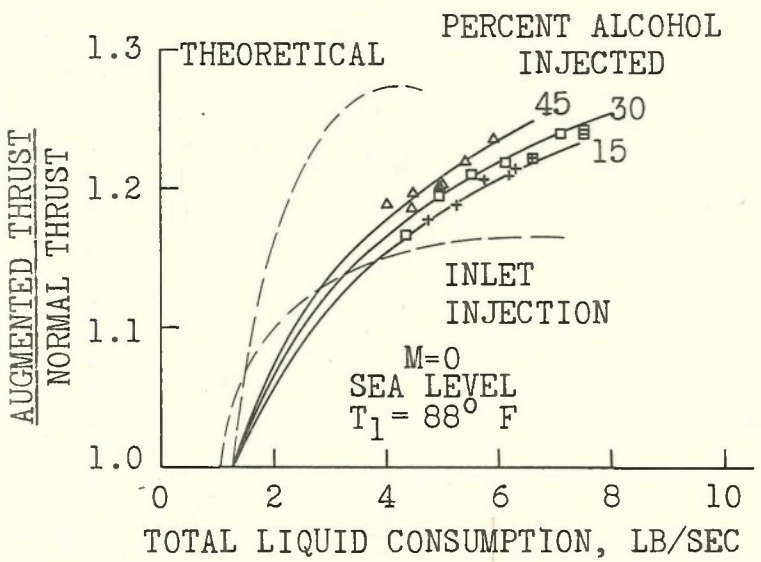

Figure 12. - Variation of ratio of augmented to normal engine thrust with total liquid consumption for various water-alcohol mixtures. Interstage injection in axial-flow-type engine with variable-area exhaust nozzle.

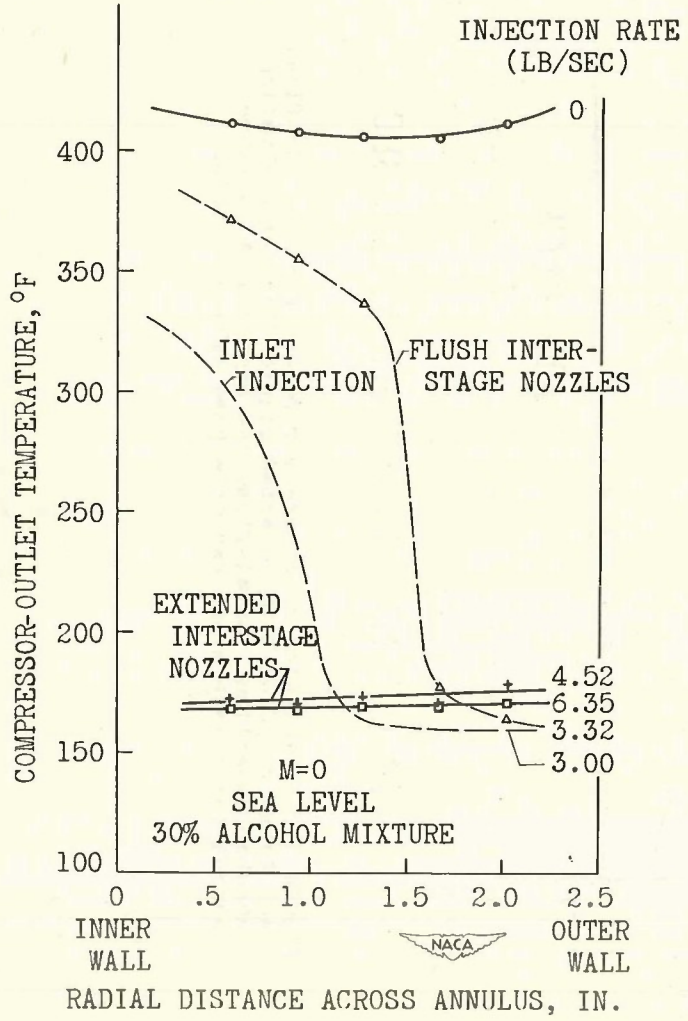

Figura 13. - Compressor-outlet temperature surveys for interstage injection in axial-flow-type engine with variable-area exhaust nozzle.

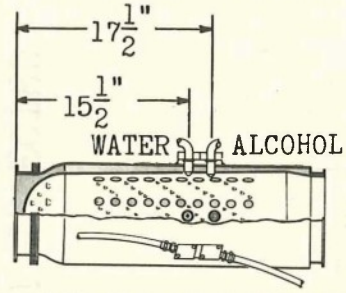

SYSTEM	SPRAY	NOZZLE PAIRS PER COMBUSTOR	ORIFICE SIZE (IN.)	
			WATER	ALCOHOL
A	HOLLOW CONE	2	0.182	0.089
B	" "	3	.149	.073
C	" "	3	.073	.055
D	SOLID JET	3	.073	.055

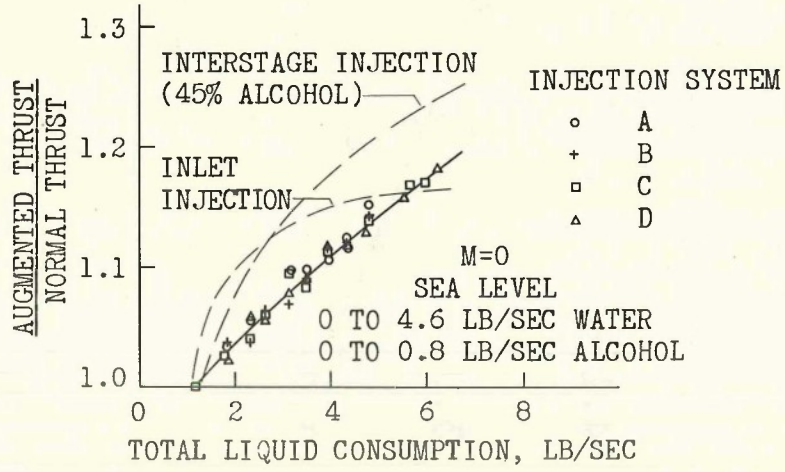

Figura 14. - Variation of ratio of augmented to normal engine thrust with total liquid consumption for combustion-chamber injection. Axial-flow-type engine with can-type combustion chambers and variable-area exhaust nozzle.

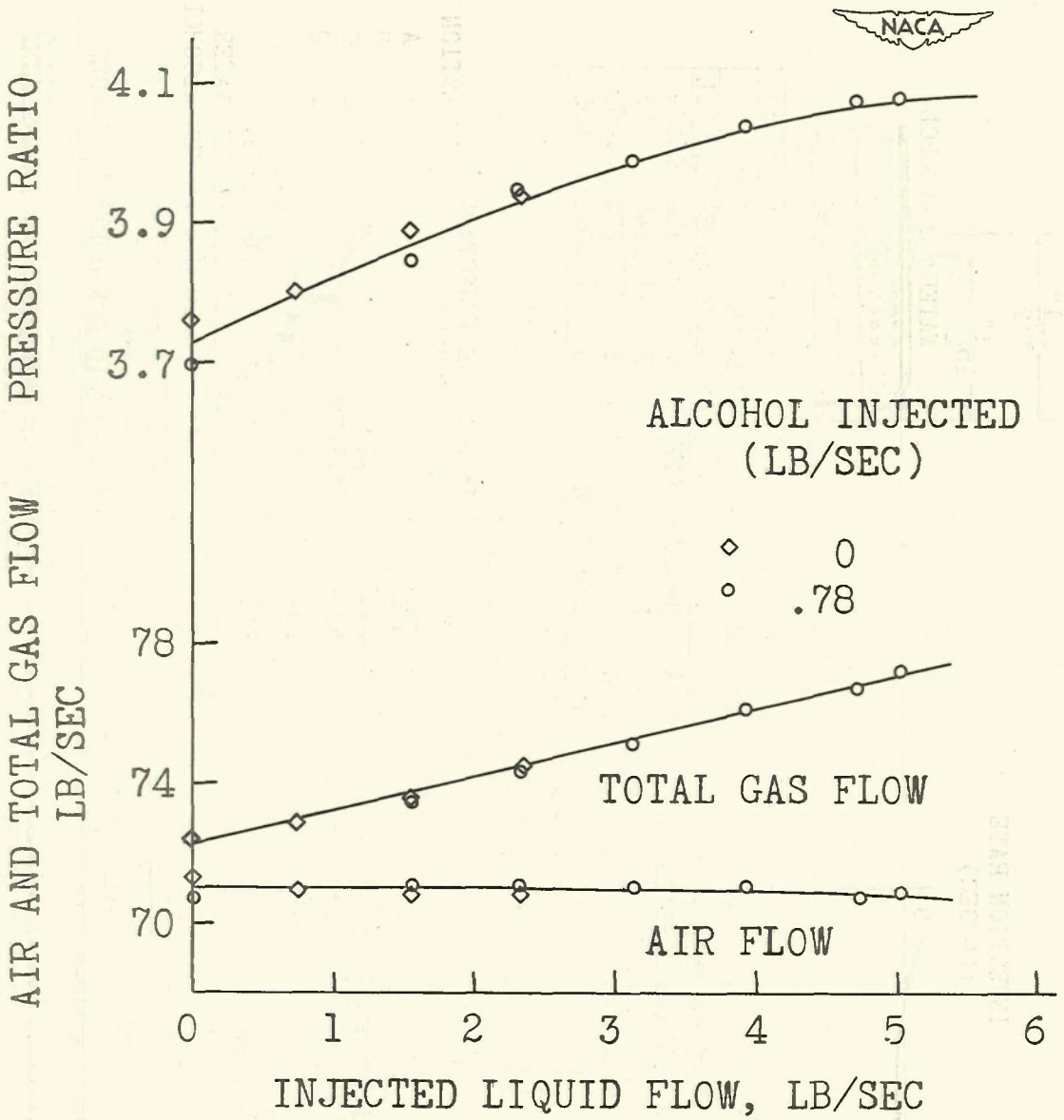

1041F

Figure 15. - Variation of compressor pressure ratio, air flow, and total gas flow with injected liquid flow for combustion-chamber injection. Axial-flow-type engine with can-type combustion chambers and variable-area exhaust nozzle.

INVESTIGATION OF BLEEDOFF METHOD OF THRUST AUGMENTATION

By David S. Gabriel and William L. Jones

Lewis Flight Propulsion Laboratory

INTRODUCTION

Among the several methods of thrust augmentation of turbojet engines considered in this series of papers, the method that provides the greatest take-off thrust increase is the air bleedoff cycle. The permissible turbine-inlet temperature of present turbojet engines limits the amount of fuel that may be burned in the engine combustion chambers. As a result of this temperature limit, the gases passing through the turbine contain a large quantity of dilution air or unburned oxygen. The air bleedoff cycle takes advantage of this excess air by removing it before it passes through the turbine and by using this high-pressure air supply, after burning it in a combustion chamber, for an auxiliary jet. The air that is removed from the normal engine is replaced with water which vaporizes in the engine combustion chamber and passes through the turbine as steam. It is, of course, necessary to increase the fuel flow to the combustion chamber to vaporize this water. Water is used for the replacement fluid primarily because of the low pumping work required. Thus in essence the dilution air is replaced with steam without greatly altering the performance of the engine and at the same time a high-pressure air supply for an auxiliary jet is made available. Compressor-inlet injection is incorporated to take advantage of the additional augmentation that is obtained by the increased compressor-outlet pressures and mass flow.

RESULTS AND DISCUSSION

Figure 1 schematically illustrates a turbojet engine equipped for air bleedoff. The air-bleedoff engine consists of two main components, the ordinary turbojet engine and the auxiliary combustion chamber, which are hereinafter referred to as the primary and secondary engines, respectively. The primary engine is provided with water- and alcohol-injection nozzles at the compressor inlets. A manifold is installed at the inlet of the primary-engine combustion chambers through which compressor-outlet air may be bled to the secondary-engine combustion chamber. Water-injection nozzles are installed in the primary combustion chamber through which water may be injected into the primary combustion zone to replace the bleedoff air.

The bleedoff air is burned at fuel-air ratios up to stoichiometric in the secondary-engine combustion chamber and is ejected through a nozzle. A shutoff valve is installed at the secondary-combustion-chamber inlet. The shutoff valve was necessary to return the engine to normal operating condition but was always in the wide-open position during bleedoff operation.

The original work on air bleedoff, which was reported in reference 1, consisted of a brief investigation on a J31 engine, the results of which are summarized in figure 2. The results were obtained at sea-level, zero flight Mach number conditions. The ratio of augmented thrust to normal thrust is plotted against the ratio of total liquid flow to normal-engine fuel flow. The total liquid flow includes fuel flow to both the primary and secondary engines and all injected water and alcohol flows. The experimental results are shown by the circles and the line is the result of a cycle analysis in which component efficiencies typical of present engines were used. A maximum thrust ratio of 1.65 was obtained experimentally at a liquid flow ratio of about 11.8. This result is about 10 percent lower than the thrust increase predicted by the analysis.

Because of the promising results shown in the preliminary runs, a more complete investigation was conducted on a J33 engine in which an effort was made to establish the effects of some of the operating variables on engine performance. The runs were all made at sea-level, zero flight Mach number conditions. The corrected engine speed was nearly constant at 11,600 rpm and the data were adjusted to a constant speed of 11,600 rpm (military rated speed, 11,500 rpm). The primary-engine nozzle diameter was constant at 19.5 inches and the tail-pipe temperature was held as close as possible to 1225° F by regulation of the amount of water injected into the primary combustion chambers. After a study of water- and alcohol-injection results at the compressor inlet of a J33 engine, the inlet-injection rates of water and alcohol were fixed at 2.0 and 2.2 pounds per second, respectively, corresponding to the condition that produced the best combination of thrust augmentation and liquid consumption.

The water flow to the primary combustion chambers varied from 0 to 9 pounds per second corresponding to a range of bleedoff gas flows from 0 to 24 pounds per second. The bleedoff flow varied with the secondary-engine nozzle diameter and secondary-combustion-chamber fuel-air ratio. The secondary-engine nozzle diameter was varied from 4.5 to 7.0 inches and the fuel-air ratio in the secondary combustion chamber was varied from 0.03 to 0.08.

Because the primary-engine tail-pipe temperature was fixed, the amount of water injected into the primary combustion chambers was a function of the bleedoff flow. Figure 3 shows the variation of water flow to the primary combustion chambers with bleedoff gas flow. There is a linear relation between these variables but only about 0.37 pound of water is required to replace each pound of bleedoff gas flow and to maintain the constant tail-pipe temperature. With a bleedoff flow of 24 pounds per second, about 9 pounds per second of water must be injected.

In order to vaporize and superheat the injected water, additional fuel must be burned in the primary combustion chamber. A part of this fuel is supplied by the alcohol injected into the compressor inlet but additional kerosene must be supplied through the primary-combustion-chamber fuel nozzles. Figure 4 shows the relation of fuel flow into the primary combustion chambers to the bleedoff gas flow. The fuel flow does not include the alcohol flow injected at the compressor inlet. The fuel flow increases from about 0.8 pound per second to 2.25 pounds per second as the bleedoff flow increases from 0 to 24 pounds per second.

Further increases in bleedoff flow above the maximum of 24 pounds per second shown on the curve resulted in combustion failure in the primary combustion chambers. At this bleedoff flow, the over-all fuel-air ratio in the primary combustion chambers, including the alcohol, was about 0.043. Although this over-all fuel-air ratio is considerably below over-all stoichiometric fuel-air ratio, the fuel-air ratio in the primary burning zone was of course, much richer and the combustion failure was probably the result of rich blow-out. Further increases in bleedoff flow, therefore will depend on design changes in the primary combustion chambers.

Figure 5 shows the individual liquid flows to the primary engine as a function of bleedoff flow. As bleedoff flow is increased, water flow to the primary combustion chamber increases, fuel flow to the primary combustion chamber increases and the water and alcohol flow to the compressor inlet is constant. The net result is an increase in total liquid flow as shown by the top curve. The total liquid flow to the primary engine increases from 5 to 15 pounds per second as the bleedoff flow increases from 0 to 24 pounds per second. Because the increase in total liquid flow to the primary engine is less than the increase in bleedoff flow, the net result is a decrease in total flow through the turbine and primary jet and consequently a reduction in augmented primary-engine thrust shown by the curve at the top of the figure. The ratio of augmented primary-engine thrust to normal-engine thrust

decreases from about 1.26 for the engine with inlet injection but no bleedoff to about 1.12 for bleedoff flow of 24 pounds per second.

The performance of the secondary engine may be analyzed in two parts, the thrust and the air flow. In order to provide a better understanding of the effects of the operating variables on performance, the air flow and thrust have been plotted in the form of parameters derived from the fundamental flow equations. Because the combustion-chamber-inlet pressure was sufficiently close to the combustion-chamber-outlet pressure, it was considered reasonable to use the inlet pressure in the correlation. It is a well known relation that for a convergent nozzle operating at greater than critical pressure ratio the mass flow is equal to a constant times the product of the nozzle area and inlet pressure divided by the square root of the inlet temperature.

$$M_b = K_1 \frac{AP_b}{\sqrt{T_b}} \tag{1}$$

M_b mass flow of gas through secondary engine

K_1 constant

A area of nozzle outlet

P_b pressure at secondary-combustion-chamber outlet or nozzle inlet

T_b temperature at secondary-combustion-chamber outlet or nozzle inlet

When equation (1) is divided through by P_bA,

$$\frac{M_b}{P_bA} = \frac{K_1}{\sqrt{T_b}} \tag{2}$$

When $1/\sqrt{T_b}$ is replaced by a function of the fuel-air ratio

$$\frac{M_b}{P_bA} = K_1, F(f/A) \tag{3}$$

This factor is also a function of compressor-outlet temperature which was eliminated from consideration because it is constant for this investigation.

The factor $M_b/(P_bA)$ is plotted against fuel-air ratio in figure 6. The mass flow ratio decreases rapidly from a fuel-air ratio of 0.03 to a fuel-air ratio of 0.05 and then becomes nearly constant with further increase in fuel-air ratio. A curve derived from fluid-flow theory has been plotted in the figure as a dashed line. For this calculation a combustion efficiency of 100 percent and a flow coefficient of 1 was assumed. A greater mass flow was obtained experimentally for a given fuel-air ratio than the theoretical curve predicts because of the lower combustion-chamber temperatures due to the combustion inefficiency; lower nozzle-inlet temperatures, of course, permit the passage of a larger mass flow of gas through a given-size nozzle. The bleedoff flow can be found from this correlation curve for any bleedoff pressure, nozzle area, and secondary fuel-air ratio.

The following additional symbols are used in the analysis of the secondary-engine thrust: P_b' the nozzle-outlet pressure, P_0 the ambient pressure, and F_b the thrust.

The thrust of a convergent nozzle operating at supercritical pressure ratio may be expressed as the product of the mass flow and the critical jet velocity plus the difference between nozzle-outlet pressure and ambient pressure times the nozzle area.

$$F_b = M_bV_b + (P_b' - P_0)A \tag{4}$$

Dividing through by $P_b'A$ and rearranging yields

$$\frac{F_b}{P_b'A} + \frac{P_0}{P_b'} = \frac{M_bV_b}{P_b'A} + 1 \tag{5}$$

For a convergent nozzle operating at supercritical pressure ratio, the nozzle-inlet pressure is equal to a constant times the outlet pressure

$$K_2P_b' = P_b \tag{6}$$

where K_2 is a constant. Replacing P_b' with $\frac{P_b}{K_2}$ yields

$$\frac{F_b}{P_bA} + \frac{P_0}{P_b} = \frac{M_bV_b}{P_bA} + \frac{1}{K_2} \tag{7}$$

but from equation (2)

$$\frac{M_b}{P_b A} = \frac{K_1}{\sqrt{T_b}}$$

also

$$V_b = \sqrt{2g \frac{\gamma}{\gamma+1} RT_b}$$

where V_b is the critical velocity at the nozzle throat; therefore

$$\frac{F_b}{P_b A} + \frac{P_0}{P_b} = \frac{K_1}{\sqrt{T_b}} \sqrt{2g \frac{\gamma}{\gamma+1} RT_b} + \frac{1}{K_2} \tag{8}$$

Consequently

$$\frac{F_b}{P_b A} + \frac{P_0}{P_b} = \text{constant} \tag{9}$$

The values of the parameter of equation (9) as calculated from the experimental data are plotted against secondary-engine nozzle area in figure 7. The thrust factor is constant at a value of 1.1 for secondary nozzle sizes from 4.5 to 7.0 inches. With the constant value of this factor, the thrust of the secondary engine may be calculated for any value of inlet pressure and nozzle area.

The dashed lines at the bottom of figure 8 are the ratio of secondary-engine thrust to normal-engine thrust calculated from the correlation curves shown in figures 6 and 7. These curves are plotted against bleedoff flow for values of secondary-engine fuel-air ratio of 0.03, 0.045, and 0.08. The experimental data are shown by the symbols. The secondary nozzle diameter for these experimental points varied from 4.5 to 7.0 inches.

The calculations from the correlation curves resulted in separate lines for different fuel-air ratios and the test data fall upon those lines (fig. 8). If the analysis had not been made, a single curve probably would have been drawn through the test data and would have obscured the effect of fuel-air ratio.

Also plotted in figure 8 is the ratio of primary-engine thrust to normal-engine thrust previously presented in figure 5. The thrust of the primary and secondary engines combine to produce a maximum total augmented thrust ratio of about 1.7 shown by the data points at the top of the figure. Here again the data points

represent the experimental data and the lines are calculated from the curves of experimental primary-engine thrust and calculated secondary-engine thrust shown at the bottom of figure 8. Without bleedoff, a thrust ratio of 1.26 is obtained because of inlet injection. With maximum bleedoff a secondary-engine-thrust ratio of 1.54 is obtained but the primary-engine-thrust ratio is reduced to 1.16, as previously discussed, resulting in a net thrust ratio of about 1.7 for the bleedoff engine.

In figure 9 the thrust ratio of the bleedoff engine is replotted against the ratio of total liquid flow to normal-engine fuel flow. Lines calculated from the correlation curves are drawn for fuel-air ratios of 0.03, 0.045, and 0.08. Points are plotted from the measured thrust data for fuel-air ratios of 0.03, 0.045, and 0.08. The experimental results agree within 4 percent with the values calculated from the correlation. For a given thrust ratio it is desirable to operate near stoichiometric fuel-air ratio to give the minimum liquid flow ratio and bleedoff flow, although there is little difference between operation at fuel-air ratios of 0.045 and 0.08. Operation at low bleedoff flows is desirable because of better performance of the primary combustion chambers. Operation at the secondary-engine fuel-air ratio of 0.03 in the higher range of the curves with the same secondary-nozzle size as in the low range would probably be impossible because of the high bleedoff flows that would be required.

The dashed line on figure 9 is calculated from the correlation curve for 100 percent combustion efficiency and stoichiometric mixture in the secondary combustion chamber. For equal thrust ratios, the theoretical curve gives 10 percent less liquid flow than the experimental results. The maximum thrust ratio obtained experimentally was about 1.7 at a liquid flow ratio of 12.9. If this thrust ratio is applied to a normal 4000-pound-thrust engine, the augmented take-off thrust would be 6800 pounds with a liquid consumption of about 16.1 pounds per second.

Further increases in thrust augmentation by air bleedoff may be obtained by continued improvement in the secondary combustion-chamber efficiency and by development of a primary-engine combustion chamber that will permit operation at higher bleedoff flows. For most production engines, higher fuel-air ratios in the primary combustion chamber than those shown will require increased fuel-handling capacity for the fuel system.

Particular attention must be paid in the design of the bleedoff system and the water-injection system for the primary combustion chamber in order to minimize changes in the turbine-inlet temperature gradients. The adverse effects of bleedoff and

combustion-chamber injection on the turbine-outlet temperature gradient are shown in figure 10 in which representative radial temperature distributions across the turbine-outlet annulus are plotted for normal operation and for bleedoff operation with 11 pounds per second of bleedoff flow and 4 pounds per second of water flow to the primary combustion chambers. The radial temperature gradient is about 200° F in normal operation with the lowest temperatures occurring at the roots but it increases with bleedoff operation to 500° F with the highest temperatures occurring at the blade roots. These distributions are representative of the gradients with the latest injection and bleedoff configurations and are a considerable improvement over the earlier designs.

SUMMARY

A thrust ratio of 1.7 was obtained at the condition of sea-level take-off in an experimental investigation on a turbojet engine with a bleedoff augmentation system incorporating liquid injection into the compressor inlet. This performance was obtained at the expense of high liquid consumption.

REFERENCE

1. Hall, Eldon W.: Thrust-Augmentation Tests of Type I-16 Jet-Propulsion Engine by Bleedoff and Water and Alcohol Injection. NACA MR No. E5H24, Army Air Forces, 1945.

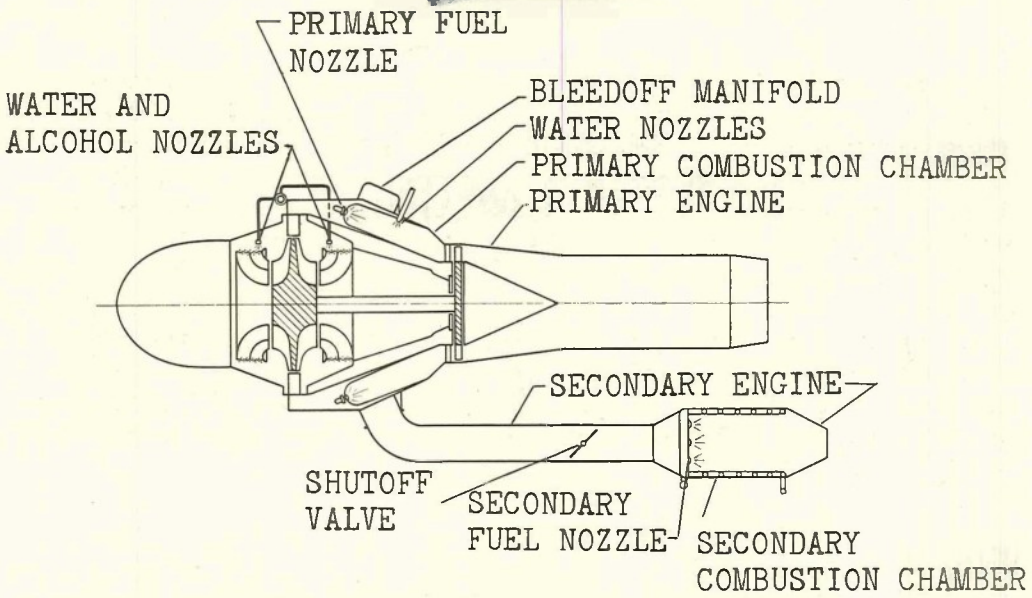

Figure 1. - Schematic diagram of bleedoff engine.

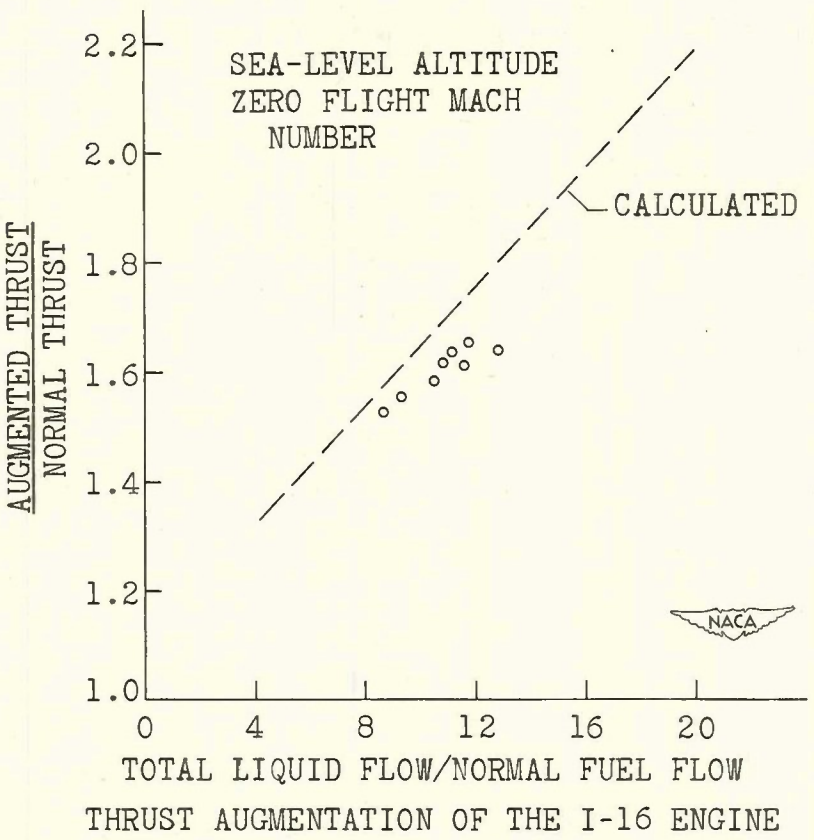

Figure 2. - Variation of ratio of augmented to normal thrust with ratio of total liquid flow to normal-engine fuel flow for J31 engine.

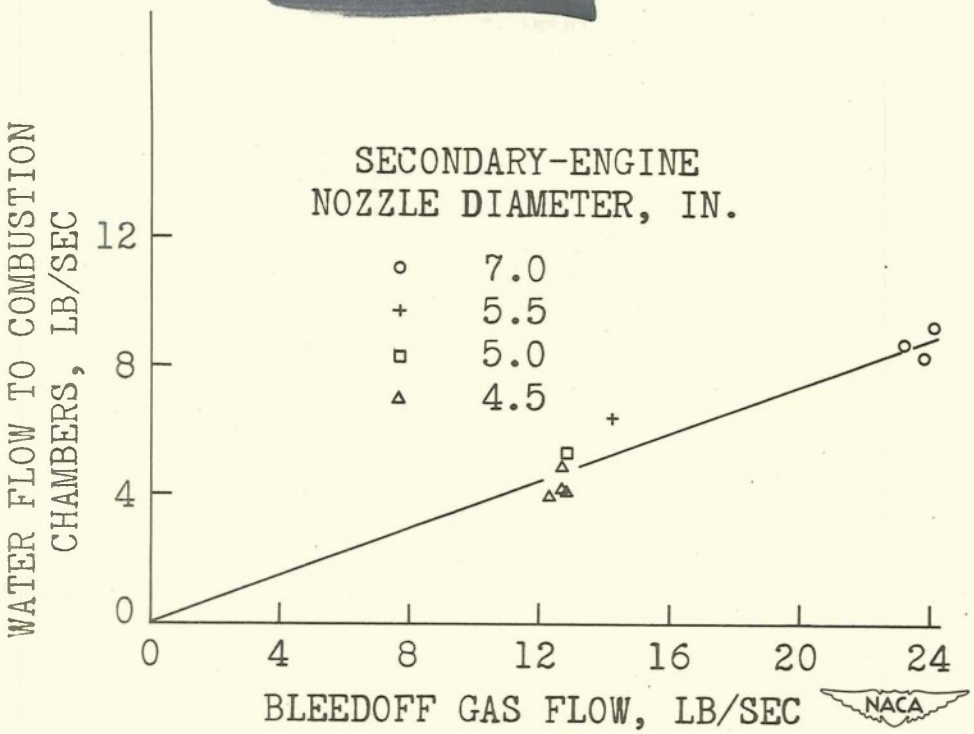

Figure 3. - Variation of water flow to primary-engine combustion chambers with bleedoff gas flow.

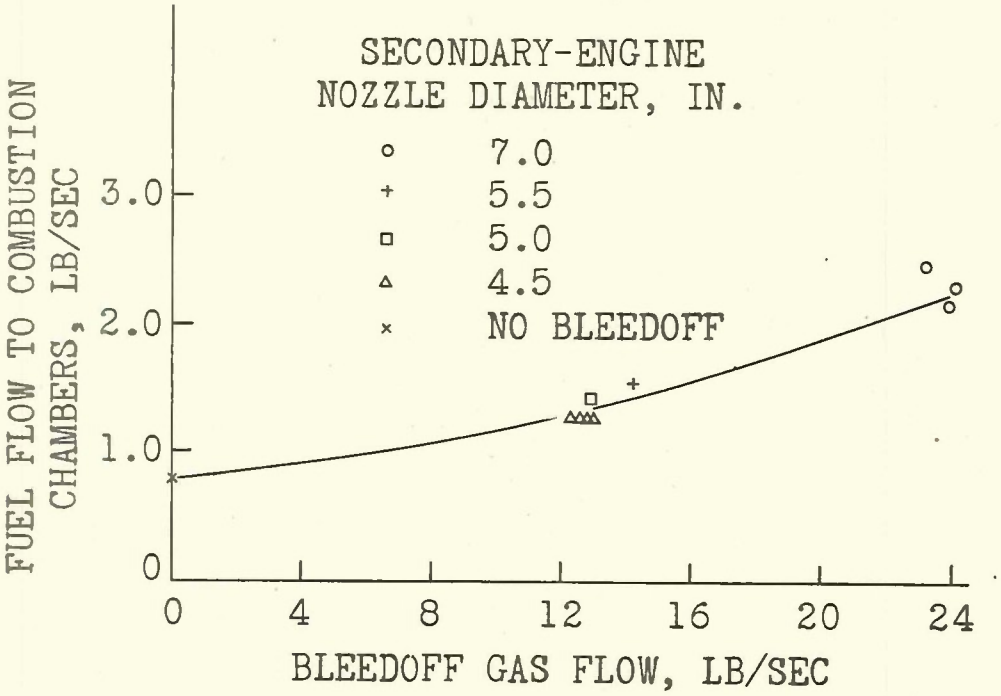

Figure 4. - Variation of fuel flow to primary-engine combustion chambers with bleedoff flow.

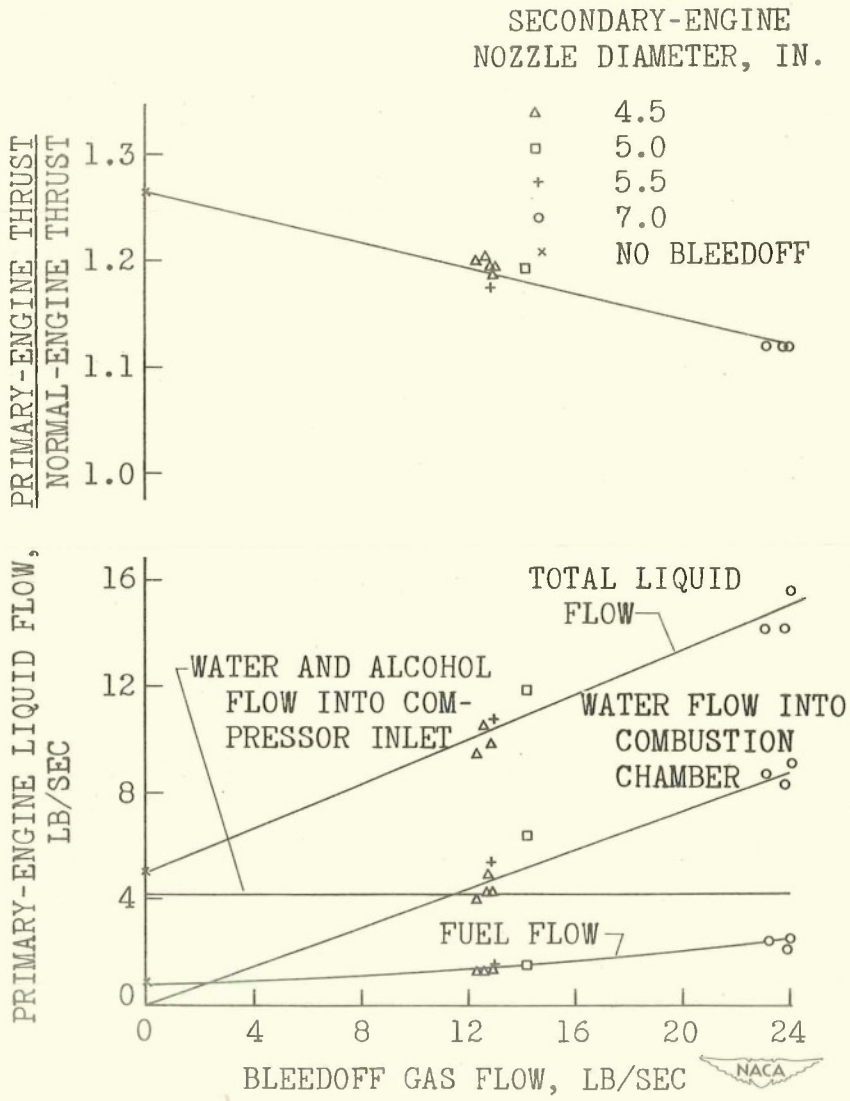

Figure 5. - Variation of individuel liquid flow end thrust of primary engine with bleedoff flow.

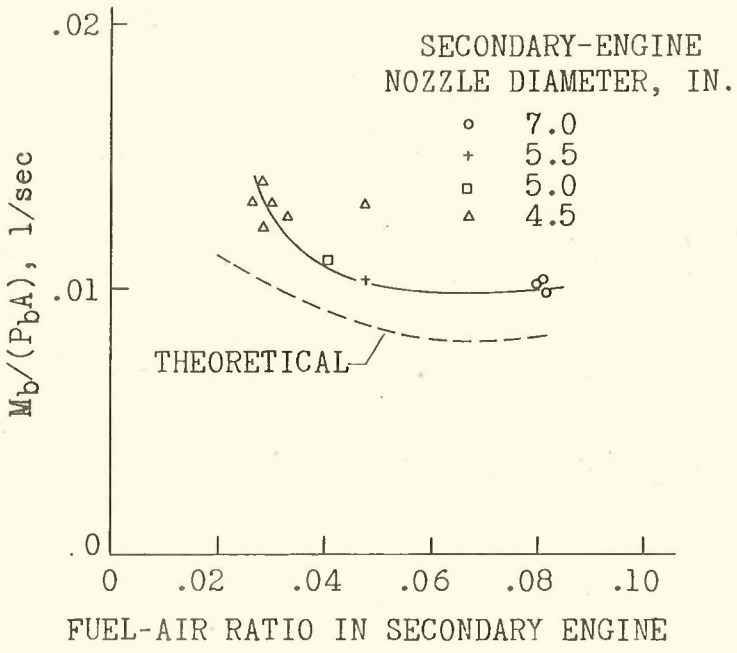

Figure 6. - Air-flow factor for secondary engine as function of secondery-engine fual-air retio.

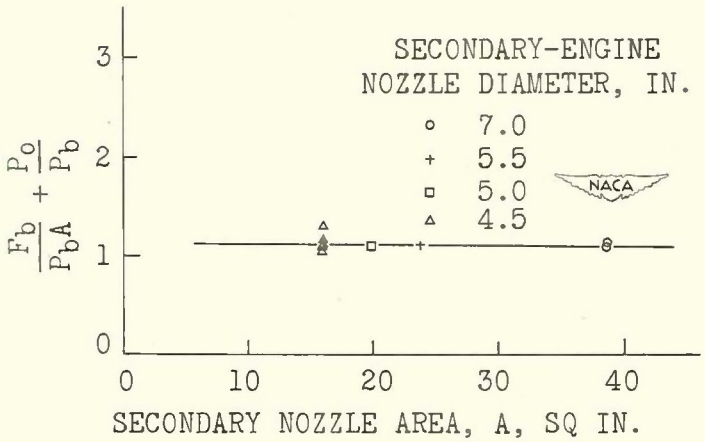

Figura 7. - Variation of thrust of secondery engine with secondary-engine nozzle eree.

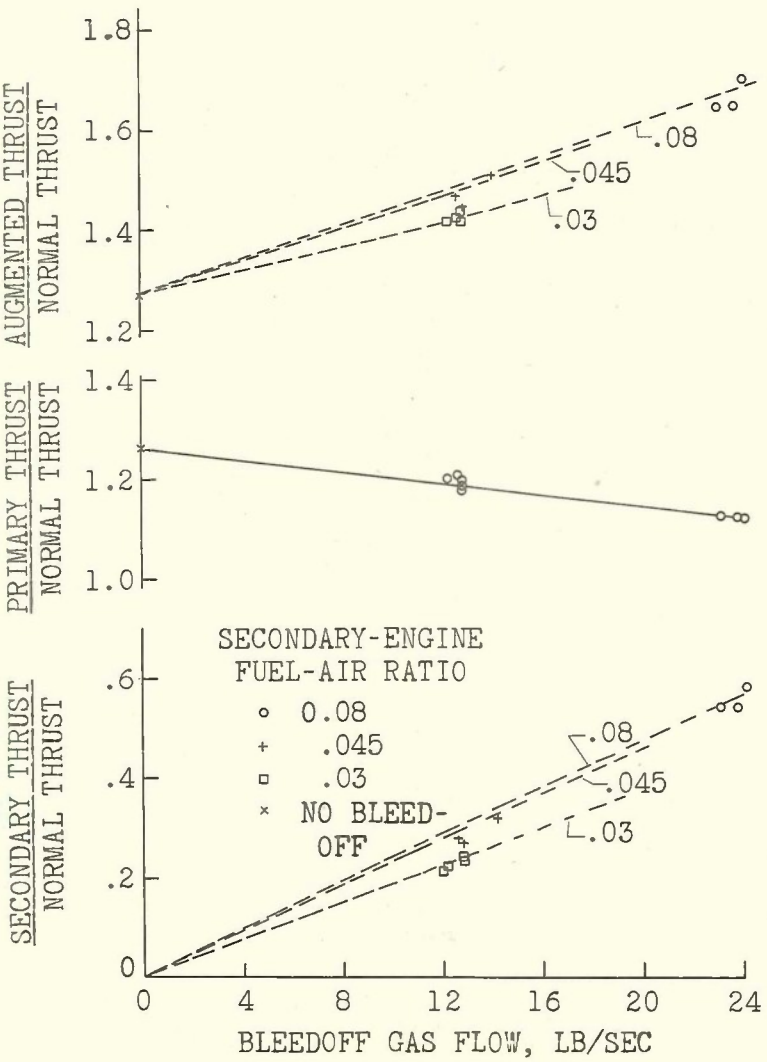

Figure 8. - Thrust of sacondery end primary anginas as function of fuel-air ratio.

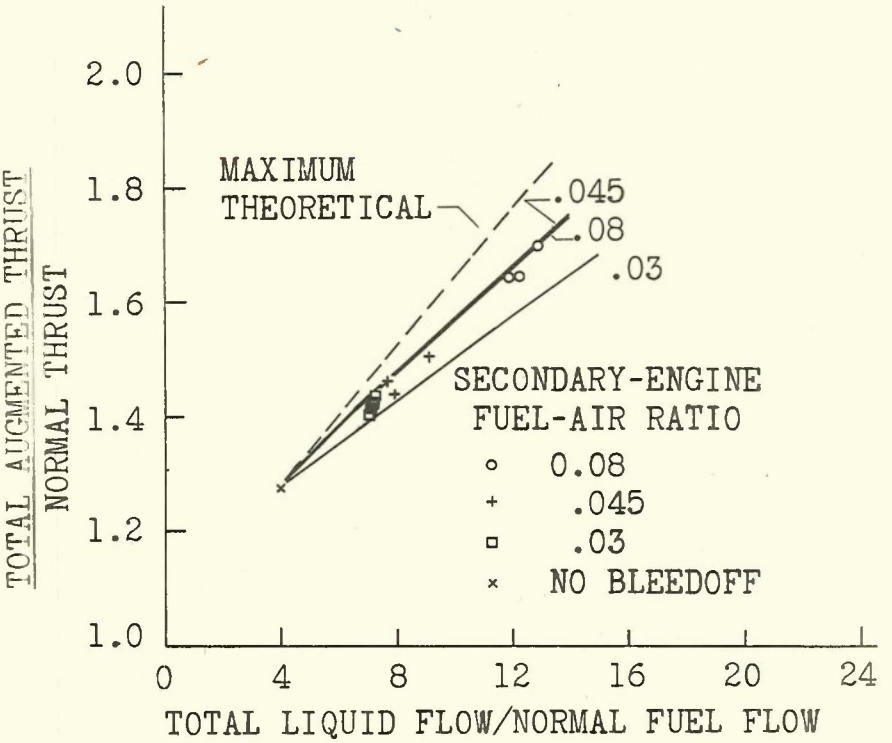

Figure 9. - Variation of ratio of augmented to normal thrust with ratio of total augmented liquid flow to normal-engine fuel flow.

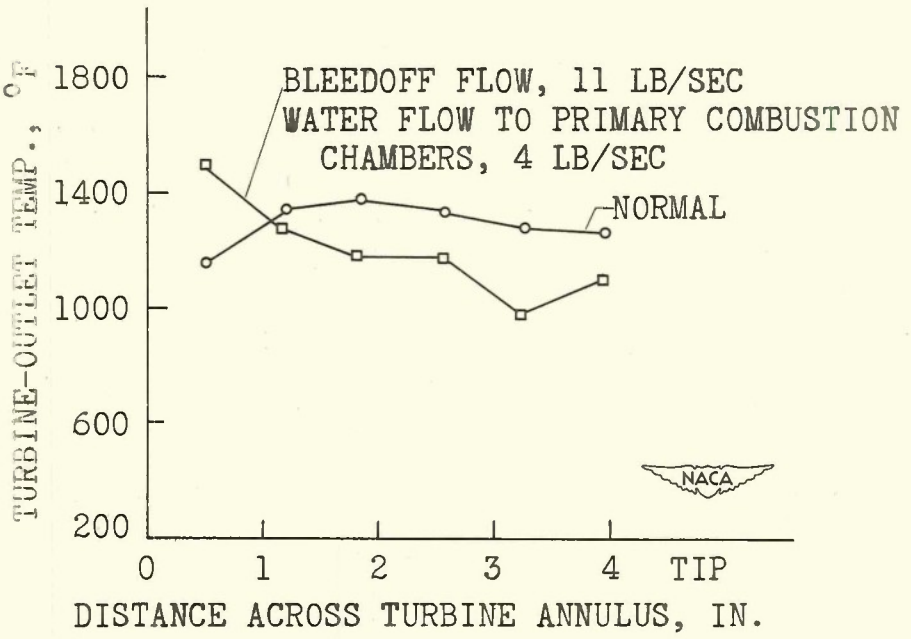

Figure 10. - Radial temperature distributions at turbine outlet for normal operation and for bleedoff operation.

COMPARISON OF VARIOUS METHODS OF THRUST AUGMENTATION

By Eldon W. Hall

Lewis Flight Propulsion Laboratory

INTRODUCTION

The previous papers covered both theoretical and experimental results on the performance of various thrust-augmentation methods. Computations, guided by the experimental results, are used to compare the relative efficiency, additional weight, and applicability of each thrust-augmentation method over a range of flight conditions. The methods considered are tail-pipe burning, water injection at the compressor inlet, a combination of tail-pipe burning plus water injection, and bleedoff with water injection. The tail-pipe-burning plus water-injection method, although not previously discussed, is also considered to be of interest and is included to show what might be expected of this method. Because rocket-assist units have been used to a large extent in assisting the take-off of conventional aircraft, their performance is compared with that of the other methods on the basis of liquid consumption. A more complete description of the systems, methods of analysis, and results are presented in reference 1.

THRUST-AUGMENTATION ANALYSIS

The comparison of augmentation methods was made for altitudes of sea level and 35,000 feet and for flight Mach numbers of 0, 0.85, 1.50, and 2.50. The thrust augmentation of the engine was determined from step-by-step calculations of the performance of both the normal and the augmented engine. The efficiencies chosen were polytropic and are for the compressor, 0.80; for the turbine, 0.85; for the exhaust nozzle, 0.95; and for the inlet diffuser, 1.00, 0.85, 0.80, and 0.70 for flight Mach numbers of 0, 0.85, 1.50, and 2.50, respectively. The primary combustion-chamber total-pressure loss was assumed to be 3 percent of the combustion-chamber-inlet total pressure. The drag coefficient of the tail-pipe burner (ratio of total-pressure loss to inlet velocity head) was assumed to be 0.5. Two fixed engines, one having a constant compressor work input of 85 Btu per pound of air and the other having twice the work input or 170 Btu per pound of air, were assumed to operate over the entire range of altitudes and flight speeds. These values of work input give compressor pressure ratios at sea-level static conditions of

about 4 and 11 and correspond to one- and two-stage centrifugal compressors, respectively. The exhaust-nozzle area was assumed to be adjusted for all cases to give tail-pipe temperatures of 1650° R for the engine with the low-pressure-ratio compressor and 1500° R for the engine with the high-pressure-ratio compressor. These values give turbine-inlet temperatures of about 1960 and 2100° R, respectively.

With tail-pipe burning, the tail-pipe area was assumed to be double the normal tail-pipe area in order to establish a reasonable burner-inlet velocity; charts, which account for the effects of dissociation, were used to calculate the temperatures for various tail-pipe fuel-air ratios. Calculations were made for fuel-air ratios up to stoichiometric.

For the water-injection calculations, the component efficiencies were altered to bring agreement between theoretical and experimental results by the same methods as previously discussed in the fifth paper on the analysis of water injection. For each flight condition, calculations were made with varying amounts of water injected at the compressor inlet to the point where the compressor-outlet air was saturated.

With bleedoff the amount of augmentation for a given liquid injection increases rapidly with an increase in the amount of air bled off. Bleeding off large quantities, however, increases the mass flow of air through the compressor and also the pressure ratio across the turbine and may result in large decreases in the efficiencies of these components. It was found from theoretical considerations that by maintaining the area of the primary-engine exhaust nozzle the same as for normal engine operation at sea-level static conditions the change in the operating conditions of these components was very small (less than the change with only water injection at the compressor inlet. For each flight condition, bleedoff was considered for the case where just sufficient water was injected at the compressor inlet to saturate the air at the compressor outlet. In all cases, the turbine-outlet temperature was maintained at the assumed value by adjusting the amount of air bled off for each amount of water injected in the combustion chamber. The ratios of water flow injected in the primary combustion chamber to bleedoff flow were calculated theoretically. The values obtained gave lower values of the bleedoff flow for a given liquid flow than were obtained experimentally. The bleedoff or auxiliary burner was assumed to operate with a stoichiometric fuel-air ratio in all cases.

The rockets were assumed to have a specific impulse of 190 pounds-seconds per pound for all conditions of altitude and flight speed.

Based upon these assumptions, the values of augmentation to be presented are somewhat higher than the values obtained experimentally at the present time from the various methods. The relative values of the maximums are, however, believed to be indicative of what may be expected in actual practice.

RESULTS AND DISCUSSION

Thrust Augmentation

On the basis of the given assumptions and methods of analysis, figure 1 shows a comparison of the thrust-augmentation methods. The ratio of augmented thrust to normal thrust is plotted against the ratio of total liquid consumption of the augmented engine to fuel consumption of the normal engine. The results are for the engine with the low-pressure-ratio compressor. Because the engine was assumed to operate at a constant rotor speed, the compressor pressure ratio changes with change in flight conditions and with the injection of water. The range of pressure ratios obtained with the low-pressure-ratio compressor (fig. 1(a)) is from 4.3 to 5.0 at sea-level static conditions. The pressure ratio of 4.3 is obtained with the normal engine and the pressure ratio of 5.0 is obtained with water injection.

With water injection, a thrust ratio of 1.32 can be obtained at a liquid ratio of 5.0 when injecting sufficient water to saturate the air at the compressor outlet. The condition for which just sufficient water is injected to saturate the air at the compressor inlet is represented by the lowest cross (fig. 1(a)). The most economical method is tail-pipe burning, which can provide a maximum thrust ratio of 1.55 at a liquid ratio of 4.0; this thrust ratio is comparable to 1.32 with water injection at this liquid ratio. The circle (on the tail-pipe-burning curve fig. 1(a)) represents a stoichiometric fuel-air ratio and is the maximum thrust ratio that can be obtained with tail-pipe burning. Large increases in thrust can be obtained by adding water injection to the tail-pipe-burning method when the over-all fuel-air ratio remains at stoichiometric. A thrust ratio of 2.05 at a liquid ratio of 8.0 can be obtained by this method when saturating the air at the compressor outlet. The cross on the water-injection curve (fig. 1(a)) represents the condition for which just sufficient water is injected to saturate the air at the compressor inlet.

Bleedoff is less efficient than tail-pipe burning or the combination of tail-pipe burning and water injection, inasmuch as a

higher liquid ratio is required for the same thrust ratio. A higher ratio is possible, however, with bleedoff. For example, a thrust ratio of 2.60 can be obtained with bleedoff as compared to a maximum of 2.05 for the combination of tail-pipe burning and water injection. Higher values of the thrust ratio are not possible with bleedoff because stoichiometric fuel-air ratio was reached in the primary combustion chamber. If the amount of water injected at the compressor inlet is limited to that amount required to saturate the air at the compressor inlet instead of the outlet, the maximum thrust ratio of 2.20 is represented by the cross below the curve for bleedoff (fig. 1(a)).

The rocket-assist method is the least efficient inasmuch as it requires the highest liquid ratio for a given thrust ratio. The rocket-assist method, however, has no theoretical limit. The specific impulse of 190 assumed for the rockets is an average value for current rockets. Values as high as 220 are obtained on some commercially available units and values of 350 can be obtained theoretically with liquid oxygen and hydrogen. The specific fuel consumption is inversely proportional to the specific impulse. For a thrust ratio of 2.05, which can be obtained by the combination of tail-pipe burning and water injection, the bleedoff and rocket-assist methods require from 2 to 2.5 times the liquid ratio.

The results for the same conditions, except at a flight Mach number of 0.85, are shown in figure 1(b). The compressor pressure ratio was reduced to 3.7 at a flight Mach number of 0.85 as compared to 4.3 at a flight Mach number of 0 because of the higher air temperature at the compressor inlet. The curves obtained are similar to those for a flight Mach number of zero except that greater values of the thrust ratio are obtained for the same values of the liquid ratio. For example, at a liquid ratio of 8.0, a thrust ratio of 2.90 can be obtained with the combination of tail-pipe burning plus water injection as compared to 2.05 at a flight Mach number of zero. Water injection with saturation at the compressor inlet is more effective because of the higher compressor-inlet temperature at the higher flight Mach number. A maximum thrust ratio of 3.70 at a liquid ratio of 31.5 can be obtained with bleedoff.

In order to show the comparison of the various methods at high altitudes, figure 1(c) presents the results for an altitude of 35,000 feet. The flight Mach number for this case is 0.85. The trends are similar to those for sea level. Both the maximum thrust ratio and the thrust ratio for a given liquid ratio are, however, less for each method. A maximum thrust ratio of 1.32 can be obtained with water injection at a liquid ratio of 4.5. Water injection with only sufficient water to saturate the air at the compressor inlet is

much less effective at the higher altitudes because of the lower inlet-air temperature. With tail-pipe burning, the maximum thrust ratio is 1.92 at a liquid ratio of 3.5. Adding water injection to tail-pipe burning increases the maximum thrust ratio to 2.36 at a liquid ratio of 7.0. Bleedoff can provide a maximum thrust ratio of 2.88 at a liquid ratio of 26.0.

The results for a flight Mach number of 2.50 at 35,000 feet are given in figure 1(d). With an increase in flight Mach number from 0.85 to 2.50, the maximum thrust augmentation obtained from each method is increased about five times. The effectiveness of water injection is more rapidly increased than the effectiveness of the other methods by an increase in flight Mach number. Saturating the air at the compressor inlet gives a thrust ratio of 2.4 with water injection at a liquid ratio of 9.6. The maximum thrust ratio obtained with water injection is 3.5 at a liquid ratio of 18.6. With tail-pipe burning, the maximum thrust ratio is 5.5 at a liquid ratio of 6.0. Adding water injection to tail-pipe burning until the compressor-inlet air is saturated results in a thrust ratio of 8.2 at a liquid ratio of 15.0 and increasing the water-injection rate results in a maximum thrust ratio of 9.3 at a liquid ratio of 22. The maximum thrust ratio with bleedoff is 10.4 at a liquid ratio of 58. It should be noted that the high thrust ratios at a flight Mach number of 2.50 are primarily due to the low thrust of the normal engine. The high liquid ratios for the methods involving the injection of water are due to the large quantities of water that can be evaporated at the high Mach numbers because of the high inlet-air temperature.

The effect of altitude on the maximum thrust ratio is more clearly shown in figure 2. The maximum thrust ratio of each method is plotted against altitude for a flight Mach number of 0.85. All methods show a moderate decrease in maximum thrust ratio as the altitude is increased to 35,000 feet. Because of the constant air temperature above the tropopause (approximately 35,000 feet), the augmentation remains about constant. The maximum thrust ratio with water injection decreases from 1.59 to 1.32 as the altitude is increased for sea level to 35,000 feet. Tail-pipe burning is affected to a smaller extent by altitude than any of the other methods; the maximum thrust ratio decreases from 2.12 to 1.92. The combination tail-pipe burning plus water injection decreases from 2.90 to 2.36 and bleedoff decreases from 3.70 to 2.88 as the altitude increases from sea level to 35,000 feet.

In order to show the effect of flight Mach number on the augmentation more clearly, the maximum thrust ratio of each method is plotted against flight Mach number in figure 3 for an altitude of 35,000 feet. The flight Mach number ranges from 0.85 to 2.50. All

methods show an increase in the maximum thrust ratio as the flight Mach number is increased; although, as shown in figure 1, the increased thrust ratios are obtained at the expense of large increases in the liquid ratios. Increasing the flight Mach number from 0.85 to 2.50 increases the thrust ratio with bleedoff from 2.88 to 10.4 and with the combination of tail-pipe burning plus water injection from 2.34 to 9.3. At a flight Mach number of 2.50, the liquid ratio with bleedoff is about ten times that for tail-pipe burning, and with tail-pipe burning plus water injection, the liquid ratio is about four times that for tail-pipe burning.

The preceeding results are all for an engine having the low-pressure-ratio compressor. The performance of the high-pressure-ratio-compressor engine is presented in figure 4 along with the performance of the low-pressure-ratio-compressor engine for comparison. The thrust ratio is plotted against the liquid ratio for sea level and a flight Mach number of 0.85. For these flight conditions the high-pressure-ratio compressor has a normal pressure ratio of 9.9, which is increased to 14.3 with water injection. In the range of liquid ratios covered by the low-pressure-ratio-compressor engine, there is little difference between values of the thrust ratio for a given liquid ratio for the low- and high-pressure-ratio-compressor engines. Higher values of the thrust ratios are possible with the high-pressure-ratio-compressor engine, but at higher values of the liquid ratio. The greatest increase in thrust ratio is obtained with the methods involving water injection. For example, the maximum thrust ratio with the combination of tail-pipe burning plus water injection increases from 2.90 to 4.36, whereas with tail-pipe burning alone the maximum increases from 2.12 to 2.26. The maximum thrust ratio with bleedoff increases from 3.70 to 4.98.

Weight Analysis

In addition to the weight of the liquid consumed by each method, the weight of the added equipment required by each method is also of importance. Figure 5 shows a comparison of the additional weight of equipment required by the thrust-augmentation methods. The additional weight of equipment divided by the additional thrust or the specific weight of augmentation equipment is plotted against the thrust ratio. The values of the additional thrust and the thrust ratio are for sea-level static conditions. The increased weight is the weight of equipment only and does not include any additional liquids. The equipment weight was estimated from the weight of existing experimental equipment by taking into account any modifications required for airplane installation. For all the methods,

the specific weight decreases as the thrust ratio increases. The minimum specific weight is approximately the same for all methods (0.05 to 0.07) at the maximum values of thrust ratio. When all the methods are considered at a constant thrust ratio, the water-injection method entails the least additional weight followed by the tail-pipe burning method. The specific weights of bleedoff and of the combination of tail-pipe burning plus water injection are about equal and have the highest values. The specific weight of an average normal engine is included for reference. It is apparent, however, that adding the additional augmentation equipment to an engine is equivalent to adding an additional engine having a very low specific weight, except for the additional liquid consumed.

Both the weight of the liquids consumed and the weight of equipment of the various methods have been compared. Neither of these comparisons is adequate inasmuch as the weight of the liquids consumed is a function of the time of operation and the equipment weight is fixed. Calculations were therefore made of the total propulsive weight (weight of engine, liquid consumed, and auxiliary equipment) for each method. Figure 6 shows the ratio of the total propulsive weight of an augmented engine to the total propulsive weight of a larger unaugmented or normal engine (both engines producing the same thrust) plotted against the thrust ratio of the augmented engine. The ratio shown is for 5 minutes of operation of each engine at an altitude of 35,000 feet and a flight Mach number of 0.85. The normal engine total propulsive weight is 1. Values less than 1 indicate a reduction in the weight of the augmented engine, equipment, and liquids from that of a normal engine for the same value of thrust. For the tail-pipe-burning method the total weight of the augmented engine decreases as the thrust ratio increases and reaches a value of less than seven-tenths the normal engine total weight. For the water-injection and the tail-pipe-burning plus water-injection methods, the total weight first decreases to a minimum and then increases as the thrust ratio increases. With bleedoff for 5 minutes of operation the least total weight occurs at the lowest thrust ratio and is approximately equal to the total weight of a normal engine. For shorter periods of operation with bleedoff, 3 minutes for example, the lowest total weight occurs at the maximum thrust ratio and is about 0.85 times the normal engine total weight.

Load-Range Characteristics

Because of the high thrusts for a given engine size and weight, engines equipped with the thrust-augmentation methods may be desirable for high-speed flight in spite of their high liquid consumption.

A study was therefore made of the performance of the complete airplane for a flight Mach number of 1.50 at which the engine was assumed to be operating in the augmented configuration for the entire time of flight. The details of this study and method of analysis are similar to those in reference 2 in which various engine types are compared in terms of airplane load-range characteristics.

In figure 7 the airplane disposable load per pound of gross weight is plotted against the liquid rate per mile per ton of gross weight. This comparison is for an altitude of 35,000 feet and a flight Mach number of 1.50. The performance is calculated for level flight only and does not include the take-off and climb requirements. The disposable load is equal to the gross weight less the weight of the airplane structure and the engine and may consist of liquid weight or liquid and cargo weight. A wing lift-drag ratio of 7 was assumed and the airplane structure weight was assumed to be 30 percent of the gross weight. The normal engine specific weight at sea-level static conditions was assumed to be 0.45 and the weight of the additional equipment was the same as that presented in figure 5. The engines were assumed to be installed in nacelles. The nacelle and fuselage drag and the drag of the additional equipment were deducted from the engine thrust in calculating the gross weight from the lift-drag ratio. All calculations were based on an engine having a normal thrust at sea-level static conditions of 10,000 pounds and weighing 4500 pounds. The engine frontal area was taken as $12\frac{1}{2}$ square feet. Each point on the curves in figure 7, therefore, represents a different airplane, because the airplane becomes larger as the augmentation and the thrust increase.

Operation with the normal engine is shown by the cross in the lower left corner. The various lines represent the different methods with varying amounts of augmentation. The numbers on the curves are values of the thrust ratio. The ratio of ordinate to abscissa and, therefore, the slope of the slanting lines connecting the points on the curves with the origin represent the maximum range of the airplane when all the disposable load is fuel. These slopes have been labeled directly in terms of range on the outer scale. The normal engine, for example, has a maximum range of 233 miles. The initial point for tail-pipe burning at a thrust ratio of 1 is at a lower disposable load and range than the normal engine because of the loss in thrust and the increase in drag when the engine is equipped for tail-pipe burning. As the augmentation by tail-pipe burning is increased to stoichiometric, the ratio of disposable load to gross weight and the range are increased without much increase in liquid rate per unit gross weight. The liquid rate per ton mile remains nearly constant with augmentation by tail-pipe

burning in spite of the increase in specific fuel consumption for the following reason: One of the important factors that affects this quantity is the liquid rate per hour per pound of net thrust where the net thrust is defined as the difference between the engine thrust and the engine nacelle drag. By augmentation the engine thrust is increased without an increase in nacelle drag and hence the percentage increase in net thrust is greater than the percentage increase in engine thrust. This effect tends to offset the increase in fuel rate per pound of engine thrust to give an approximately constant liquid rate per pound of net thrust (and hence gross weight) with increase in augmentation by tail-pipe burning.

At the point of maximum augmentation by tail-pipe burning the gross weight is approximately 3.5 times the gross weight for normal operation. The decrease in range that is obtained with tail-pipe burning by decreasing the gross weight to the same value as for normal operation is also shown (fig. 7). Although the range is decreased about 100 miles by decreasing the gross weight, the range is still considerably greater than with the normal engine. The maximum range with tail-pipe burning is 590 miles. Adding water injection to tail-pipe burning increases the disposable load but the increase in liquid rate per unit gross weight results in a slightly shorter maximum range than with tail-pipe burning alone. Water injection alone results in about the same maximum range as the normal engine. The principal effect of bleedoff is to increase the disposable load per unit gross weight with an increase in liquid rate per unit gross weight and some decrease in maximum range. From these curves, it may be concluded that for a flight Mach number of 1.50, tail-pipe burning is the only method when used for the entire flight that will increase the range over that of a normal engine.

These results are based on rather conservative estimates of engine performance. In order to determine whether the tail-pipe-burning or the tail-pipe-burning plus water-injection method increases the range of a normal engine when the engine is much more efficient, these methods are compared for two different engines in figure 8. The results for engine A are the same as those presented in figure 7. For engine B both the compressor and turbine efficiencies were increased 5 percent and the inlet-diffuser efficiency was increased from 0.80 to 0.965. Somewhat lower values for the engine weight and frontal area were also assumed. The maximum range of the engine B without tail-pipe burning is 750 miles. As the augmentation increases, the maximum range increases to 1000 miles. Maintaining the same gross weight for the augmented engine as for the normal engine gives a maximum range of 940 miles for engine B with augmentation.

Although this increase in range with the addition of tail-pipe burning is not as great as for engine A, it appears safe to conclude that even with a highly efficient engine the addition of tail-pipe burning increases the maximum range.

SUMMARY OF RESULTS

From a theoretical comparison of various methods of thrust augmentation, it may be stated that either bleedoff or rocket assist offers the possibility of large thrust increases at the expense of high values of specific liquid consumption. For small increases in thrust, water injection offers the advantage of extreme simplicity and light weight. Tail-pipe burning offers the advantages of light weight with thrust increases intermediate between those for water injection and bleedoff and of the lowest values of specific liquid consumption. Tail-pipe burning may, however, involve some loss of thrust during unaugmented operation. The combination of tail-pipe burning plus water injection permits a flexible system, either providing large amounts of augmentation with a moderate specific liquid consumption or smaller amounts with a low specific liquid consumption. For continued operation at supersonic speeds, tail-pipe burning appears to be the only augmentation method of those considered that increases the maximum range over that obtained with the normal engine.

REFERENCES

1. Hall, Eldon W., and Wilcox, E. Clinton: Theoretical Comparison of Several Methods of Thrust Augmentation for Turbojet Engines. NACA RM No. E8H11, 1948.

2. Cleveland Laboratory Staff: Performance Ranges of Application of Various Types of Aircraft-Propulsion System. NACA TN No. 1349, 1947.

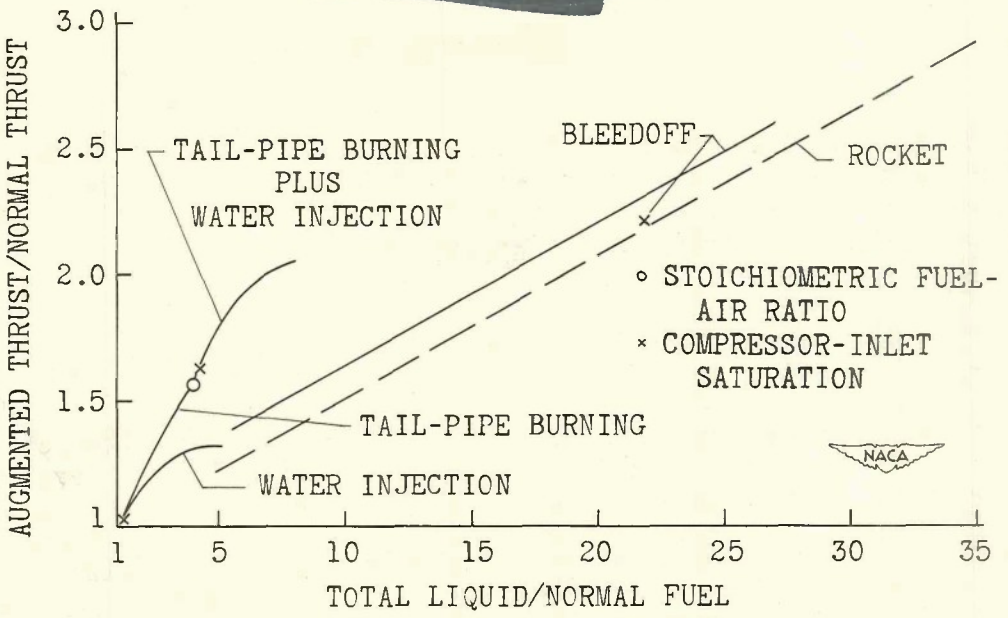

(a) Altituda, sea leval; flight Mach number, 0; low-pressura-ratio compressor (prassure ratio, 4.3 to 5.0).

Figura 1. - Variation of ratio of augmented to normal thrust with ratio of total liquid to normal fuel.

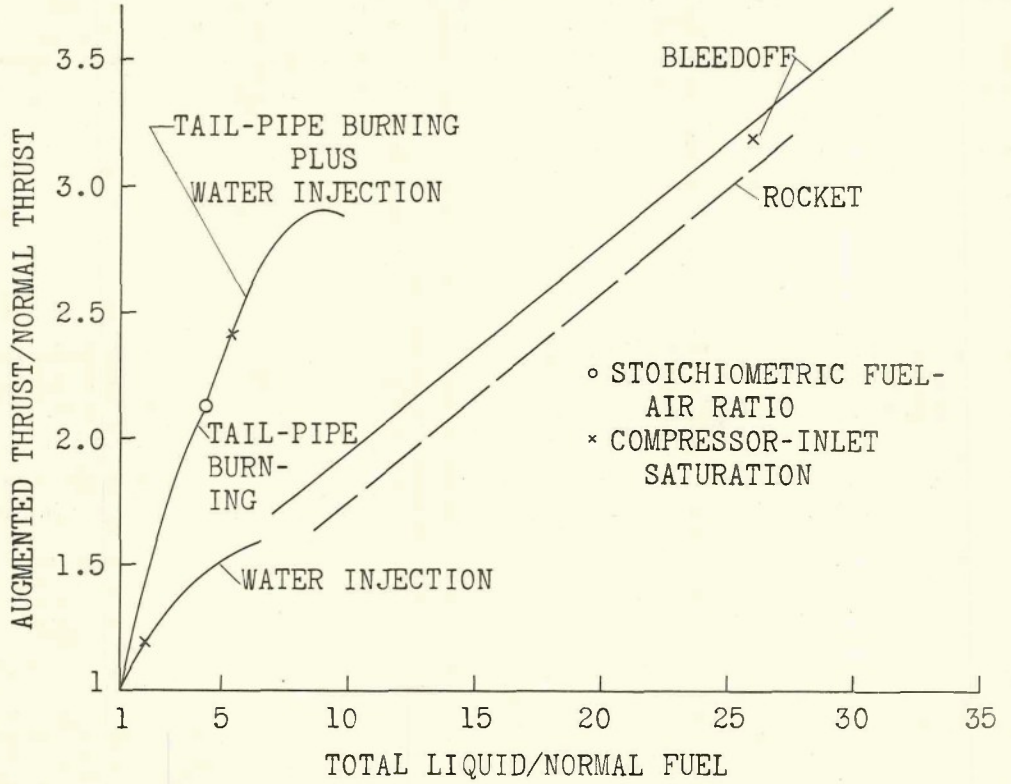

(b) Altitude, sea leval; flight Mach number, 0.85; low-prassure-ratio compressor (pressura ratio, 3.7 to 4.6).

Figure 1. - Continuad. Variation of ratio of augmanted to normal thurst with ratio of total liquid to normal fuel.

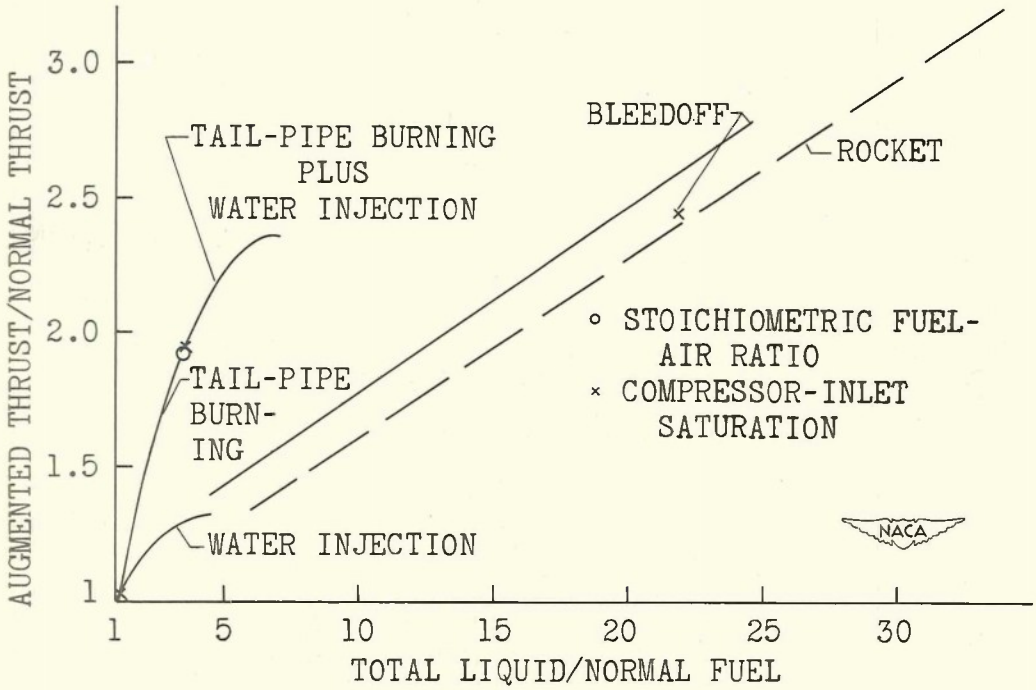

(c) Altitude, 35,000 feet; flight Mach number, 0.85; low-pressure-ratio compressor (pressure ratio, 5.1 to 6.0).

Figura 1. - Continued. Veriation of retio of augmented to normel thrust with ratio of totel liquid to normal fual.

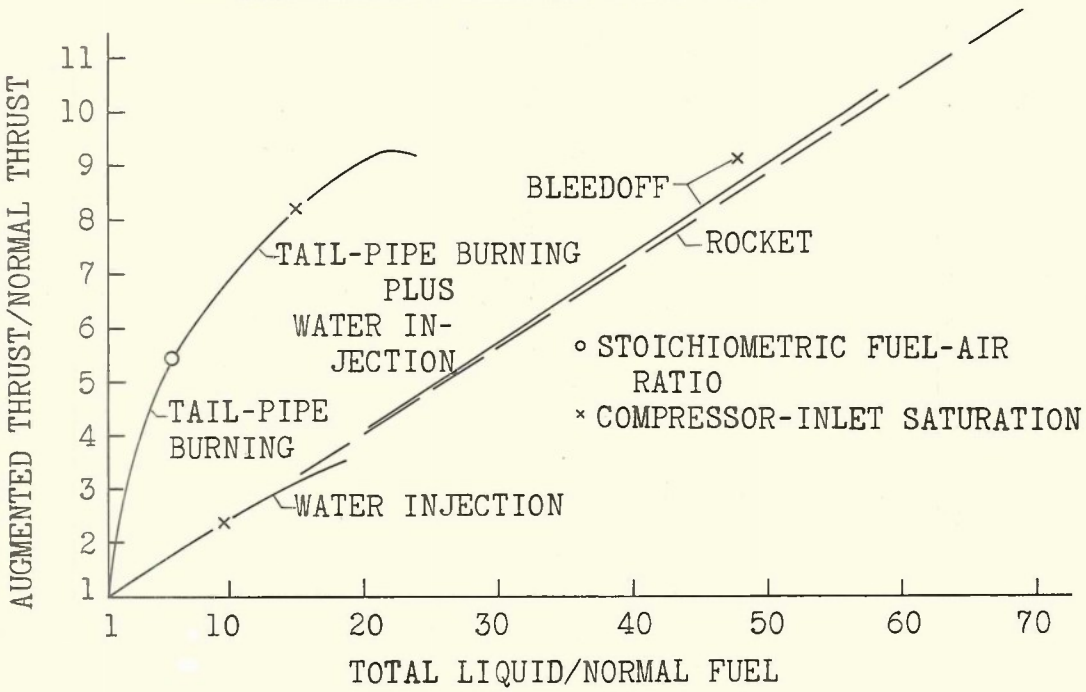

(d) Altitude, 35,000 faat; flight Mech numbar, 2.50; low-pressura-retio compressor (prassure ratio, 2.6 to 4.1).

Figura 1. - Concluded. Variation of ratio of augmented to normal thrust with ratio of total liquid to normal fual.

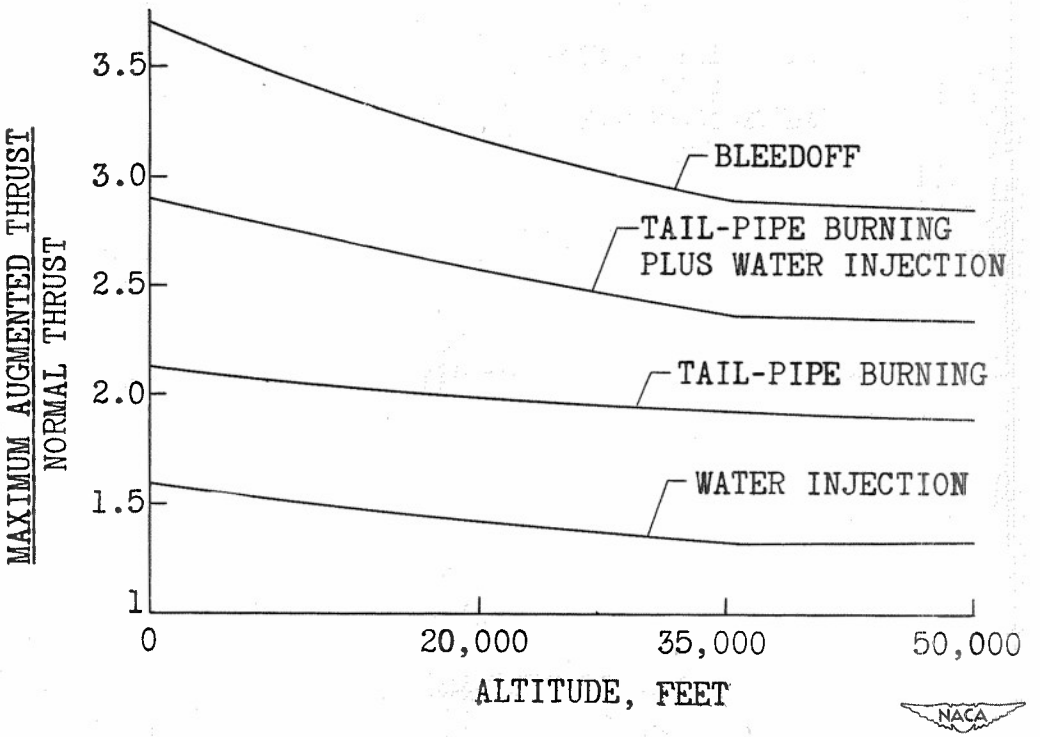

Figure 2. - Effect of altitude on maximum available thrust augmentation. Flight Mach number, 0.85; low-pressure-ratio compressor (pressure ratio, 3.9 to 6.0).

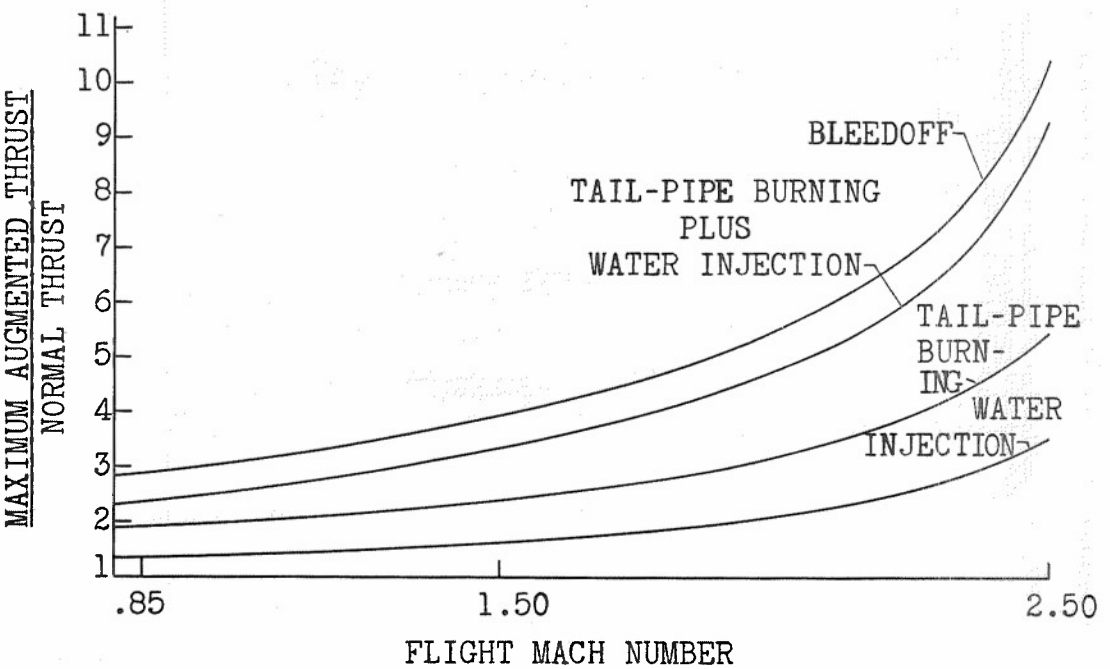

Figure 3. - Effect of flight Mach number on maximum available thrust augmentetion. Altitude, 35,000 feet; low-preesure-retio compressor (preesure ratio, 2.6 to 6.0).

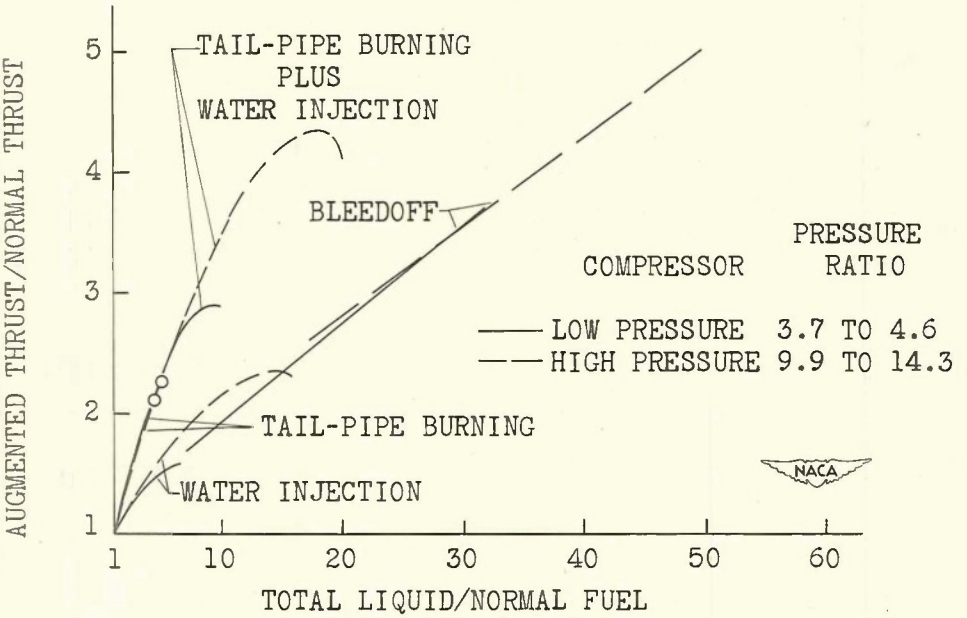

Figure 4. - Effect of compressor pressure ratio on thrust augmentation and ratio of total liquid to normal fuel. Altitude, sea level; flight Mach number, 0.85.

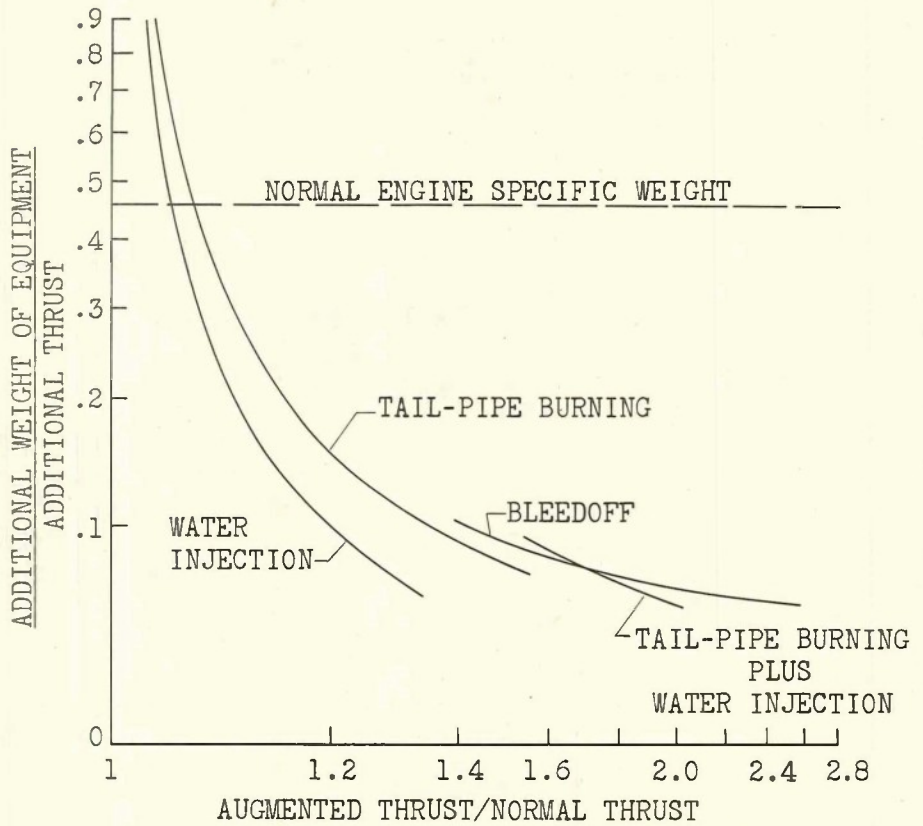

Figure 5. - Variation of specific weight of augmentation equipment with ratio of augmented to normal thrust. Altitude, sea level; flight Mach number, 0; low-pressure-ratio compressor.

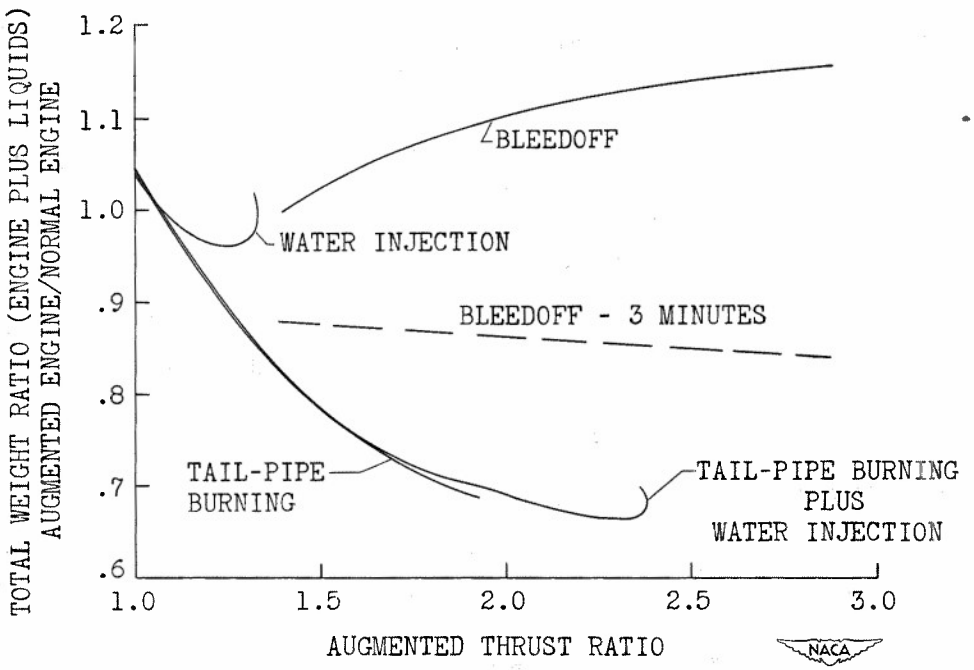

Figure 6. - Effect of thrust ratio on total propulsive weight for given flight time. Altitude, 35,000 feet; flight Mach number, 0.85; time of operation, 5 minutes. (Normal engine with same thrust as augmented engine.)

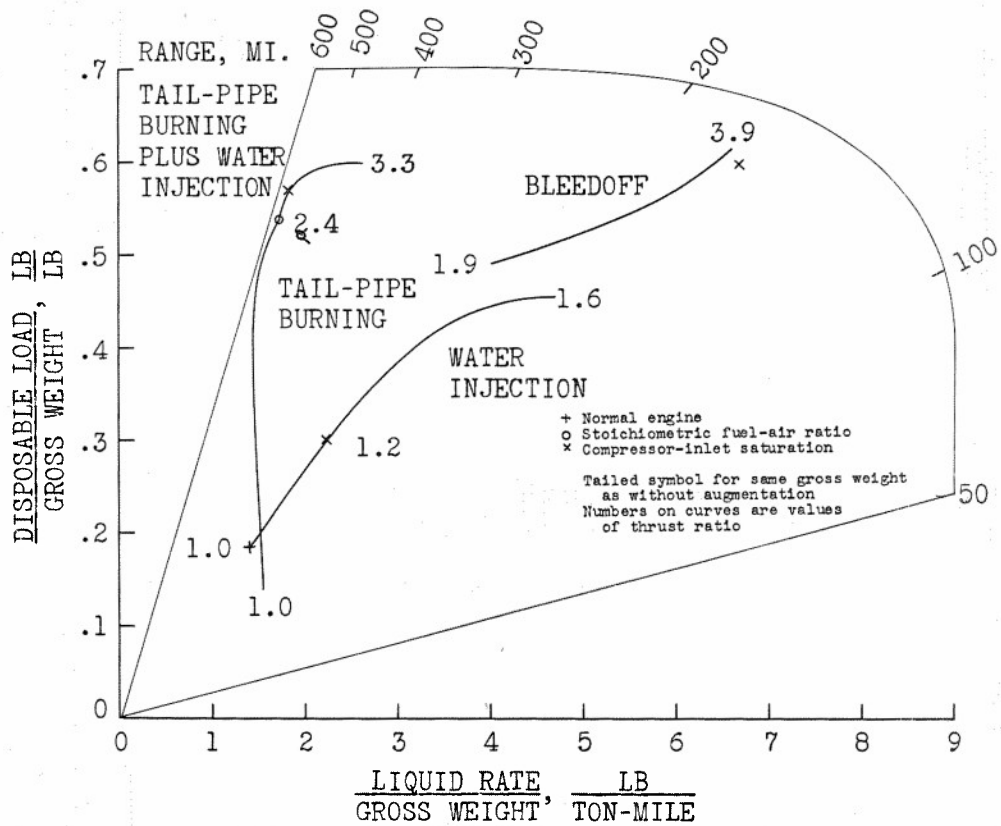

Figure 7. - Load-range characteristics of airplane powered by turbojet engines with various methods of thrust augmentation. Altitude, 35,000 feet; flight Mach number, 1.50.

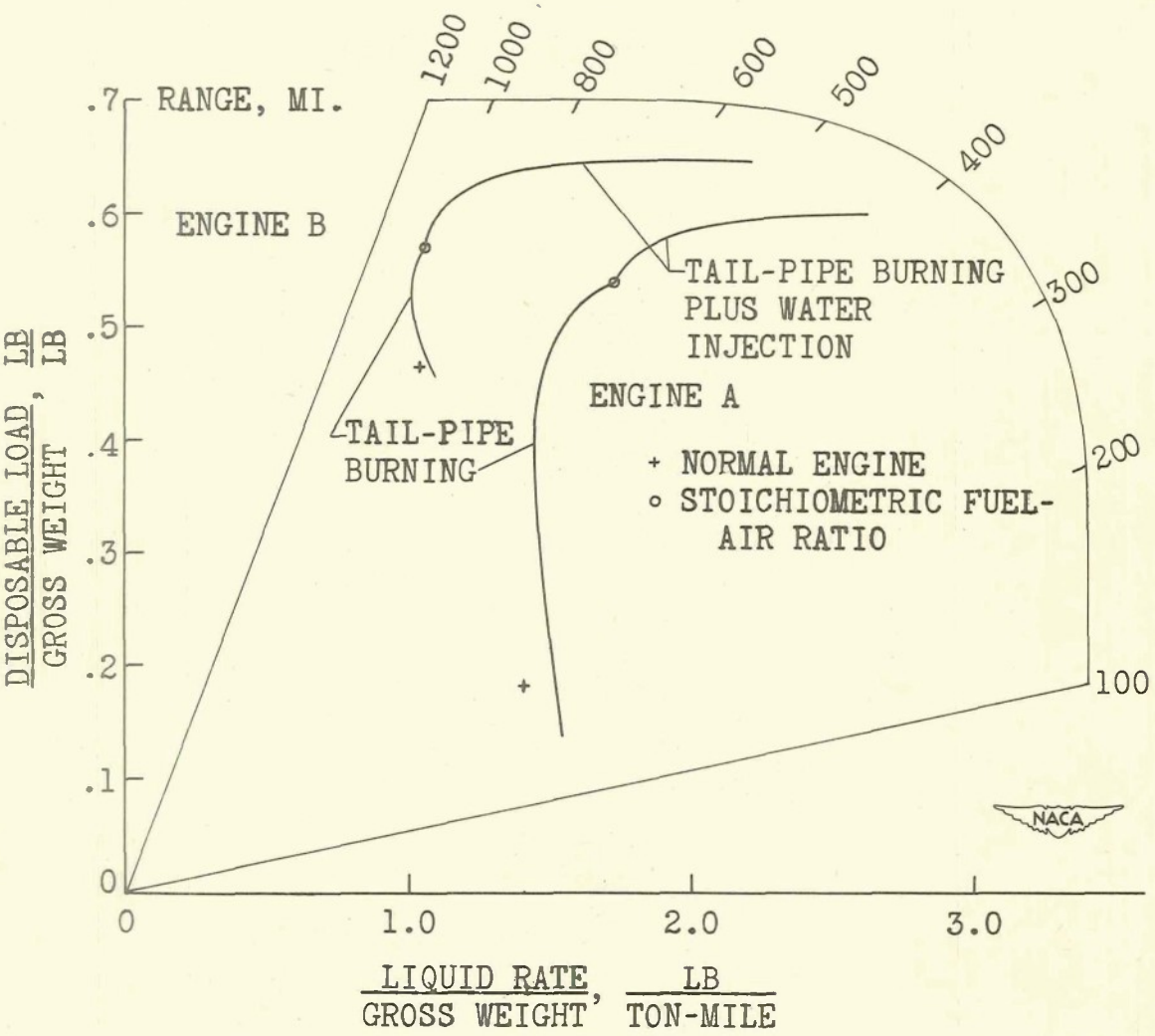

Figure 8. - Comparison of load-range characteristics of airplane with two different engines. Altitude, 35,000 feet; flight Mach number, 1.50.

ATI-71 148

National Advisory Committee for Aeronautics, Lewis Flight Propulsion Lab., Cleveland, O.
NACA CONFERENCE ON TURBOJET-ENGINE THRUST-AUGMENTATION RESEARCH - A COMPILATION OF THE PAPERS PRESENTED BY NACA STAFF MEMBERS, by Eugene J. Manganiello, Alfred W. Young and Clinton E. Wilcox. 28 October 1948. 92 pp. CONFIDENTIAL

(Not abstracted)

DIVISION: Power Plants, Jet and Turbine (5)
SECTION: General (0)
DISTRIBUTION: U. S. Military Organizations request copies from ASTIA-DSC. Others route requests to ASTIA-DSC thru AMC, Wright-Patterson Air Force Base, Dayton, O. Attn: NACA.

SECURITY INFORMATION
CONFIDENTIAL
CRCL

I. Manganiello, Eugene J.
II. Young, Alfred W.
III. Wilcox, Clinton E.

When this card has served its purpose, it may be destroyed in accordance with AFR 205-1, Army Reg. 380-5 & OPNAV Inst. 5510.1.

ARMED SERVICES TECHNICAL INFORMATION AGENCY
DOCUMENT SERVICE CENTER

CONFIDENTIAL CRCL

KS #26 NASA - 3, 4 Feb 69.